

ENERGY BASED SEISMIC PERFORMANCE ASSESSMENT OF  
REINFORCED CONCRETE COLUMNS

A THESIS SUBMITTED TO  
THE GRADUATE SCHOOL OF NATURAL AND APPLIED SCIENCES  
OF  
MIDDLE EAST TECHNICAL UNIVERSITY

BY

BORA ACUN

IN PARTIAL FULFILLMENT OF THE REQUIREMENTS  
FOR  
THE DEGREE OF DOCTOR OF PHILOSOPHY  
IN  
CIVIL ENGINEERING

MARCH 2010

Approval of the thesis:

**ENERGY BASED SEISMIC PERFORMANCE ASSESSMENT OF  
REINFORCED CONCRETE COLUMNS**

submitted by **BORA ACUN** in partial fulfillment of the requirements for the degree  
of **Doctor of Philosophy in Civil Engineering Department, Middle East  
Technical University** by,

Prof. Dr. Canan Özgen \_\_\_\_\_  
Dean, Graduate School of **Natural and Applied Sciences**

Prof. Dr. Güney Özcebe \_\_\_\_\_  
Head of Department, **Civil Engineering**

Prof. Dr. Haluk Sucuoğlu \_\_\_\_\_  
Supervisor, **Civil Engineering Dept., METU**

Assoc. Prof. Dr. M. Altuğ Erberik \_\_\_\_\_  
Co-Supervisor, **Civil Engineering Dept., METU**

**Examining Committee Members:**

Prof. Dr. Güney Özcebe \_\_\_\_\_  
Civil Engineering Dept., METU

Prof. Dr. Haluk Sucuoğlu \_\_\_\_\_  
Civil Engineering Dept., METU

Prof. Dr. Murat Dicleli \_\_\_\_\_  
Department of Engineering Sciences, METU

Prof. Dr. Sinan Altın \_\_\_\_\_  
Dept. of Civil Engineering, Gazi University

Assoc. Prof. Dr. Barış Binici \_\_\_\_\_  
Civil Engineering Dept., METU

**Date:** \_\_\_\_\_ 08.03.2010

**I hereby declare that all information in this document has been obtained and presented in accordance with academic rules and ethical conduct. I also declare that, as required by these rules and conduct, I have fully cited and referenced all material and results that are not original to this work.**

Name, Last Name : Bora ACUN

Signature :

## **ABSTRACT**

### **ENERGY BASED SEISMIC PERFORMANCE ASSESSMENT OF REINFORCED CONCRETE COLUMNS**

Acun, Bora

Ph.D., Department of Civil Engineering

Supervisor: Prof. Dr. Haluk Sucuođlu

March 2010, 214 pages

Severe seismic events in urban regions during the last two decades revealed that the structures constructed before the development of modern seismic codes are the most vulnerable to earthquakes. Sub-standard reinforced concrete buildings constitute an important part of this highly vulnerable urban building stock. There is urgent need for the development and improvement of methods for seismic performance assessment of existing reinforced concrete structures.

As an alternative to current conventional force-based assessment methods, a performance evaluation procedure for structural members, mainly reinforced concrete columns is proposed in this study, by using an energy-based approach combined with the low cycle fatigue concept. An energy-based hysteresis model is further introduced for representing the inelastic response of column members under severe seismic excitations. The shape of the hysteresis loops are controlled by the dissipated cumulative energy whereas the ultimate strength is governed by the low

cycle fatigue behavior. These two basic characteristics are obtained experimentally from full scale specimens tested under constant and variable amplitude displacement cycles.

The first phase of the experimental program presented in the study constitutes of testing sub-standard non-conforming column specimens. The second phase of testing was conducted on standard, code compliant reinforced concrete columns. A total number of 13 specimens were tested. The behavior of these specimens was observed individually and comparatively according to the performance based objectives. The results obtained from the experiments were employed for developing relations between the energy dissipation capacity of specimens, the specimen properties as well as the imposed displacement history. Moreover, the measured rotation capacities at the plastic regions are evaluated comparatively with the limits proposed by modern displacement-based seismic design and assessment provisions.

**Keywords:** Reinforced concrete columns, energy based seismic performance assessment, energy-based hysteresis model, load path effects, plastic rotation capacity

## ÖZ

### BETONARME KOLON ELEMANLARIN ENERJİ ESASLI BİR YÖNTEMLE SİSMİK PERFORMANS DEĞERLENDİRMESİ

Acun, Bora

Doktora, İnşaat Mühendisliği Bölümü

Tez Yöneticisi: Prof. Dr. Halûk Sucuoğlu

Mart 2010, 214 sayfa

Son yirmi yılda kentsel bölgelerde meydana gelen depremler, modern tasarım yönetmeliklerinden önce kullanılan yönetmeliklere bağlı kalınarak inşa edilen yapıların deprem etkilerine karşı önemli zayıflıklar gösterdiğini ortaya koymuştur. Bu durum ışığında, halihazırda kullanımda bulunan pek çok betonarme yapının deprem etkileri altındaki performanslarının değerlendirilmesi için yeni yöntemler önerilmesi ya da varolan yöntemlerin iyileştirilmesi gerekmektedir.

Bu amaçla, özellikle betonarme kolon elemanları için enerji esaslı yöntemlerin düşük çevrimli yorulma kuramları ile bir arada kullanıldığı yeni bir performans değerlendirme yönteminin aşamaları bu çalışmada gösterilmiştir. Betonarme kolon elemanlarının dinamik etkiler altında elastik ötesi davranışını temsil edebilen bir kesit modeli önerilmiştir. Önerilen kesit modelinin oluşturulmasında temel olarak her çevrimde tüketilen enerji değeri ile birlikte, ulaşılan maksimum dayanım ile ilgili öngörüler de düşük çevrimli yorulma kriterleri

göz önünde bulundurularak kullanılmıştır. Enerji ve dayanım ile ilgili bu değerler tam ölçekli betonarme kolon elemanları üzerinde yapılan deneylerden elde edilen verilerden yola çıkılarak hesaplanmıştır. İki tip tam ölçekli kolon elemanı test edilmiştir. İlk grup elemanlar günümüz standartlarına uymayan kolonları temsil ederken, ikinci grup kolonlar modern standartlara göre hazırlanmış kolonları temsil etmektedir. Toplam 13 adet eleman test edilmiştir. Bu elemanların davranışları, tekil olarak ve birbirleri arasında karşılaştırmalı olarak incelenmiştir. Elde edilen sonuçlar, eleman özellikleri ile gözlemlenen enerji tüketme kapasitesinin yanısıra uygulanan yerdeğiştirme protokolü ile enerji tüketme kapasitesi arasında da beklendiği gibi bir ilişki olduğunu göstermektedir. Deney sırasında gözlenen kolon mafsal bölgesi plastik dönme kapasitesi değerleri güncel bazı yönetmelik değerleriyle kıyaslanmıştır.

**Anahtar Kelimeler:** Betonarme kolonlar, enerji esaslı performans değerlendirmesi, enerji esaslı histeresis modelleri, deplasman protokolü, plastik dönme kapasitesi

*To Csipkerózsikám who enlightened my life at my darkest hours*

## ACKNOWLEDGEMENTS

This study was conducted under the supervision of Prof. Dr. Haluk Sucuođlu. I would like to express my appreciation for his support and guidance throughout the study.

I would like to thank to my co-supervisor Assoc. Prof. Dr. M. Altuđ Erberik not only for providing me valuable comments during the course of the study but also for his support and friendship like an elder brother.

Many thanks to Prof. Dr. Guneş Özcebe for his valuable comments and guidance especially during the experimental stage of the study.

I also would like to thank to Prof. Dr. Murat Dicleli, Prof Dr. Yalđın Mengi and Assoc. Prof. Dr. Barıř Binici for their constructive criticism and valuable helps.

I would also like to thank to my lifelong friend Emre Akin who gave his dedicated support and assistance at every stage of this study. We are walking on the same path.

İlker Kazaz, Aliřahin Tařlıgedik, Selim Guneş, Ufuk Yazgan, Hasan Metin, Burhan Avcı, Osman Keskin and Sebay Durul are the ones who deserve my special thanks for their friendship, help and support. I would like to thank all my research assistant friends at the Structural Mechanics Laboratory for their understanding and support as well.

Last but not least, the most special thanks and sincere appreciations of mine go to my “Valide Sultan” Meřkure Acun who dedicated her life, her love and all her understanding to me and to my dad “Babammm” Ali Acun who supported me in every second of this long and complicated experience. My brother Dt. Burak Acun also deserves my deepest thanks for his love and support.

## TABLE OF CONTENTS

ABSTRACT.....	iv
ÖZ.....	vi
DEDICATION.....	viii
ACKNOWLEDGEMENTS.....	ix
TABLE OF CONTENTS.....	x
LIST OF TABLES.....	xiv
LIST OF FIGURES.....	xv
CHAPTER	
1. INTRODUCTION.....	1
1.1 General.....	1
1.2 Objective and Scope.....	2
2. LITERATURE REVIEW.....	5
2.1 Energy in Earthquake Engineering.....	5
2.2 Energy-Based Hysteresis Models.....	8
2.3 Low Cycle Fatigue Behaviour of Concrete Members.....	13
2.4 The Effect of Loading History on Member Response Deterioration....	18
3. EXPERIMENTAL PROGRAM.....	22
3.1 General.....	22
3.2 Test Specimens.....	23
3.3 Material Properties.....	27
3.4 Design of Specimens.....	28
3.5 Construction of Test Specimens.....	30
3.5.1 Formwork.....	31

3.5.2	Instrumentation of Reinforcing Bars.....	31
3.5.3	Preparation of Reinforcing Cages.....	33
3.5.4	Casting and Curing.....	33
3.6	Test Setup.....	35
3.6.1	Lateral and Axial Loading System.....	36
3.7	Instrumentation.....	38
3.7.1	Load, Displacement and Strain Measurements.....	39
3.8	Testing Program.....	42
4.	TEST RESULTS.....	44
4.1	General.....	44
4.2	Test Observations and Response of Column Specimens.....	45
4.2.1	Non-Conforming Specimens (Type-1).....	45
4.2.1.1	Specimen 1P2.....	46
4.2.1.2	Specimen 2P3.....	49
4.2.1.3	Specimen 3P3_N0.4.....	52
4.2.1.4	Specimen 4P4.....	55
4.2.1.5	Specimen 5P5.....	58
4.2.1.6	Specimen 6PV1.....	61
4.2.1.7	Specimen 7P3_U.....	64
4.2.2	Conforming Specimens (Type-2).....	66
4.2.2.1	Specimen 1D2.....	67
4.2.2.2	Specimen 2D3.....	70
4.2.2.3	Specimen 3D4.....	73
4.2.2.4	Specimen 4D5.....	76
4.2.2.5	Specimen 5DV1.....	79
4.2.2.6	Specimen 6DV2.....	82
5.	SEISMIC PERFORMANCE EVALUATION OF THE COLUMN SPECIMENS.....	85
5.1	General.....	85
5.2	Column Database.....	85
5.3	Deformation Capacities of Columns.....	86

5.3.1	Moment-Curvature Analysis.....	87
5.3.2	Limit State Calculations.....	100
5.3.2.1	ASCE/SEI 41-Update Limit States.....	100
5.3.2.2	Eurocode 8 Limit States.....	101
5.3.2.3	TDY (2007) Limit States.....	102
5.3.3	Limit State Comparisons.....	103
5.3.4	ASCE/SEI 41-Update Modeling Parameters.....	105
5.4	The Effect of Displacement History on Target Displacement Demand.....	115
5.5	Limitations of Test Results and Their Implications.....	119
6.	ENERGY DISSIPATION CHARACTERISTICS OF RC COLUMNS UNDER LOW CYCLE FATIGUE LOADING .....	120
6.1	General.....	120
6.2	Capacity Curves.....	123
6.3	Cumulative Cyclic Energy Dissipation Characteristics.....	125
6.4	Normalized Cyclic Energy Dissipation Characteristics.....	128
6.4.1	Normalization with respect to the 1 <sup>st</sup> Full Cycle.....	129
6.4.2	Normalization with respect to the 2 <sup>nd</sup> Full Cycle.....	132
6.5	Prediction of Cyclic Energy Dissipation in Low-Cycle Fatigue.....	134
6.5.1	Dissipated Energy Ratio, $E_1/E_2$ .....	136
6.5.1.1	Low Cycle Fatigue Parameter, $\alpha$ .....	141
6.5.1.2	Low Cycle Fatigue Parameter, $\beta$ .....	145
6.6	The Effect of Axial Load on Energy Dissipation Capacity.....	149
6.7	The Effect of Bond Strength on Energy Dissipation Capacity.....	150
6.8	Strength Degradation Under Low Cycle Fatigue Loading.....	151
6.8.1	The Effect of Axial Load on Strength Degradation.....	155
6.8.2	The Effect of Bond Strength on Strength Degradation.....	156
7.	ENERGY-BASED HYSTERESIS MODEL FOR REINFORCED CONCRETE MEMBERS IN FLEXURE.....	158
7.1	General.....	158
7.2	Influence of Displacement History on Energy Dissipation .....	159

7.3	Dissipated Energy Predictions for Constant Amplitude Loading.....	160
7.3.1	Prediction of Cycle-1.....	162
7.3.2	Prediction of Energy Dissipation in Cycle-2.....	162
7.3.3	Prediction of Dissipated Energy in the Consecutive Cycles.....	163
7.4	Strength Deterioration under Constant Amplitude Loadings.....	166
7.5	Construction of Constant-Amplitude Hysteresis Cycles.....	167
7.6	Direct Prediction of Cumulative Dissipated Energy for Variable Amplitude Displacement Cycles.....	177
7.7	Moment-Rotation Model for Reinforced Concrete Column Sections in Flexure.....	178
7.7.1	Rules for Constructing the Hysteresis Model.....	179
7.7.2	Hysteretic Response Prediction of R/C Column Sections under Variable-Amplitude Loading.....	184
8.	SUMMARY AND CONCLUSIONS.....	189
8.1	Summary.....	189
8.2	Conclusions.....	190
	REFERENCES.....	194
	APPENDIX	
	A. DESIGN OF REFERENCE COLUMN IN 4-STORY BUILDING FRAME.....	203
	CURRICULUM VITAE.....	212

## LIST OF TABLES

### TABLES

Table 3.1	Variables investigated in the experimental program for Type-1 specimens.....	26
Table 3.2	Variables investigated in the experimental program for Type-2 specimens.....	27
Table 3.3	Material properties and reinforcement ratios of test specimens .....	29
Table 3.4	Displacement protocols imposed on the test specimens .....	43
Table 5.1	Material properties of selected test specimens .....	86
Table 5.2	Target drift ratios calculated with equivalent linearization .....	118
Table 6.1	Reinforced concrete column specimen data .....	122
Table 6.2	Energy dissipation characteristics of specimens under low-cycle fatigue.....	137
Table 7.1	Energy dissipated in the 1 <sup>st</sup> and 2 <sup>nd</sup> full cycles .....	164
Table A.1	Design forces for column C01.....	207
Table A.2	Column design – Type-1 columns.....	210
Table A.3	Column design – Type-2 columns.....	211

## LIST OF FIGURES

### FIGURES

Figure 2.1	Piecewise linear energy based hysteresis models proposed by Stojadinovic and Thewalt (1996).....	9
Figure 2.2	Energy based hysteresis model proposed by Sucuoğlu and Erberik (2004).....	10
Figure 2.3	Graphical representation of damage prediction procedure proposed by Erberik and Sucuoğlu (2004).....	13
Figure 2.4	Stress-strain relationship for a concrete specimen showing common points and stability point (Karsan and Jirsa, 1969).....	14
Figure 2.5	(a) Bond fatigue test results, (b) Slip versus number of cycles diagram evaluated from test results, (c) Monotonic bond strength-slip diagram (Balazs, 1991).....	16
Figure 2.6	Bond fatigue curves proposed by Balazs (1991) for reversed cyclic loading .....	17
Figure 2.7	Types of strength deterioration, (a) Cyclic and (b) In-cycle strength deterioration (FEMA P440A, 2009).....	18
Figure 3.1	Typical reinforced concrete column specimen .....	23
Figure 3.2	Dimensions and details of, (a) Type-1 column specimens, (b) Type-2 column specimens.....	25
Figure 3.3	Metal formwork of footing and column before casting .....	32
Figure 3.4	Reinforcing cage of a typical Type-1 specimen .....	34
Figure 3.5	Reinforcing cage of a typical Type-2 specimen .....	34

Figure 3.6	Concrete placing for a Type-2 column with ready-mixed concrete...	36
Figure 3.7	Schematic view of test setup .....	37
Figure 3.8	General view of the test set-up .....	38
Figure 3.9	Instrumentation of test specimen .....	40
Figure 3.10	A ready-to-test specimen .....	41
Figure 4.1	Details of curvature measurements.....	45
Figure 4.2	Displacement history imposed on Specimen 1P2.....	46
Figure 4.3	Lateral load - top displacement response of Specimen 1P2.....	47
Figure 4.4	Base moment-curvature response of Specimen 1P2.....	47
Figure 4.5	Onset of bar buckling, North-West faces of Specimen 1P2.....	48
Figure 4.6	Displacement history imposed on Specimen 2P3.....	49
Figure 4.7	Lateral load - top displacement response of Specimen 2P3.....	50
Figure 4.8	Base moment-curvature response of Specimen 2P3.....	50
Figure 4.9	Buckling of longitudinal bars, North-West faces of Specimen 2P3...	51
Figure 4.10	Displacement history imposed on Specimen 3P3_N0.4.....	52
Figure 4.11	Lateral load - top displacement response of Specimen 3P3_N0.4.....	53
Figure 4.12	Base moment-curvature response of Specimen 3P3_N0.4.....	53
Figure 4.13	View of the specimen at the end of test, North-West faces of Specimen 3P3_N0.4.....	54
Figure 4.14	Displacement history imposed on Specimen 4P4.....	55
Figure 4.15	Lateral load - top displacement response of Specimen 4P4.....	56
Figure 4.16	Base moment-curvature response of Specimen 4P4.....	56
Figure 4.17	The North-East faces of Specimen 4P4 at the end of test .....	57
Figure 4.18	Displacement history imposed on Specimen 5P5.....	58

Figure 4.19	Lateral load - top displacement response of Specimen 5P5.....	59
Figure 4.20	Base moment-curvature response of Specimen 5P5.....	59
Figure 4.21	End of test view of Specimen 5P5 .....	60
Figure 4.22	Displacement history imposed on Specimen 6PV1.....	61
Figure 4.23	Lateral load - top displacement response of Specimen 6PV1.....	62
Figure 4.24	Base moment-curvature response of Specimen 6PV1.....	62
Figure 4.25	North face of Specimen 6PV1 at the last stage of loading.....	63
Figure 4.26	Displacement history imposed on Specimen 7P3_U.....	64
Figure 4.27	Lateral load - top displacement response of Specimen 7P3_U.....	65
Figure 4.28	Base moment-curvature response of Specimen 7P3_U.....	65
Figure 4.29	Crack opening at the East face of Specimen 7P3_U.....	66
Figure 4.30	Displacement history imposed on Specimen 1D2.....	67
Figure 4.31	Lateral load - top displacement response of Specimen 1D2.....	68
Figure 4.32	Base moment-curvature response of Specimen 1D2.....	68
Figure 4.33	Crack pattern after 2 <sup>nd</sup> full cycle, South face of Specimen 1D2.....	69
Figure 4.34	Displacement history imposed on Specimen 2D3.....	70
Figure 4.35	Lateral load - top displacement response of Specimen 2D3.....	71
Figure 4.36	Base moment-curvature response of Specimen 2D3.....	71
Figure 4.37	Crack pattern after 5 <sup>th</sup> cycle at the North face of Specimen 2D3.....	72
Figure 4.38	Displacement history imposed on Specimen 3D4.....	73
Figure 4.39	Lateral load - top displacement response of Specimen 3D4.....	74
Figure 4.40	Base moment-curvature response of Specimen 3D4.....	74
Figure 4.41	Crushing and spalling of concrete at the corners of South-East face of Specimen 3D4.....	75

Figure 4.42	Displacement history imposed on Specimen 4D5.....	76
Figure 4.43	Lateral load - top displacement response of Specimen 4D5.....	77
Figure 4.44	Base moment-curvature response of Specimen 4D5.....	77
Figure 4.45	North face of Specimen 4D5 at the end of test .....	78
Figure 4.46	Displacement history imposed on Specimen 5DV1.....	79
Figure 4.47	Lateral load - top displacement response of Specimen 5DV1.....	80
Figure 4.48	Base moment-curvature response of Specimen 5DV1.....	80
Figure 4.49	Crack pattern after 4 <sup>th</sup> cycle at the South-East faces of Specimen 5DV1.....	81
Figure 4.50	Displacement history imposed on Specimen 6DV2.....	82
Figure 4.51	Lateral load - top displacement response of Specimen 6DV2.....	83
Figure 4.52	Base moment-curvature response of Specimen 6DV2.....	83
Figure 4.53	North face of Specimen 6DV2 at the last stage of loading.....	84
Figure 5.1	Moment-chord rotation relations for Type-1 columns, Specimen 1P2.....	88
Figure 5.2	Moment-chord rotation relations for Type-1 columns, Specimen 2P3.....	89
Figure 5.3	Moment-chord rotation relations for Type-1 columns, Specimen 3P3_N0.4.....	90
Figure 5.4	Moment-chord rotation relations of Type-1 columns, Specimen 4P4.....	91
Figure 5.5	Moment-chord rotation relations for Type-1 columns, Specimen 5P5.....	92
Figure 5.6	Moment-chord rotation relations for Type-1 columns, Specimen 6PV1.....	93
Figure 5.7	Moment-chord rotation relations for Type-2 columns, Specimen 1D2.....	94

Figure 5.8	Moment-chord rotation relations for Type-2 columns, Specimen 2D3.....	95
Figure 5.9	Moment-chord rotation relations for Type-2 columns, Specimen 3D4.....	96
Figure 5.10	Moment-chord rotation relations for Type-2 columns, Specimen 4D5.....	97
Figure 5.11	Moment-chord rotation relations for Type-2 columns, Specimen 5DV1.....	98
Figure 5.12	Moment-chord rotation relations for Type-2 columns, Specimen 6DV2.....	99
Figure 5.13	Comparison of responses of Type-1 specimens with the ASCE41 modeling parameters.....	106
Figure 5.14	Comparison of responses of Type-2 specimens with the ASCE41 modeling parameters.....	108
Figure 5.15	Experimental responses of Type-1 column specimens in terms of base shear-drift ratios .....	110
Figure 5.16	Experimental responses of Type-2 column specimens in terms of base shear-drift ratios .....	112
Figure 5.17	Envelope curves for positive base shear-drift ratio cycles of (a) Type-1 and (b) Type-2 column specimens.....	114
Figure 5.18	(a) Bi-linear capacity curves for Type-1 and Type-2 specimens, (b) design spectrum .....	117
Figure 6.1	Moment-rotation response of column specimens with, (a) flexure (Type-1 and Type-2), (b) shear-flexure (Pujol, Wight and Sozen) failure modes.....	121
Figure 6.2	Base moment-chord rotation capacity curves of Type-1 specimens...124	
Figure 6.3	Base moment-chord rotation capacity curves of Type-2 specimens...124	
Figure 6.4	Base moment-chord rotation capacity curves of (a) Pujol (2002) and (b) Wight and Sozen (1975) specimens.....	125
Figure 6.5	Dissipated energy accumulation of Type-1 specimens with the number of cycles .....	126

Figure 6.6	Dissipated energy accumulation of Type-2 specimens with the number of cycles.....	126
Figure 6.7	Cumulative dissipated energy curves for, (a) Pujol and (b) Wight and Sozen specimens.....	127
Figure 6.8	Force-based cycle definition for, (a) 1 <sup>st</sup> full cycle, (b) 2 <sup>nd</sup> full cycle..	128
Figure 6.9	Variation of cyclic dissipated energy, normalized with respect to the 1 <sup>st</sup> full cycle, with the number of cycles: Type-1 specimens.....	129
Figure 6.10	Variation of cyclic dissipated energy, normalized with respect to the 1 <sup>st</sup> full cycle, with the number of cycles: Type-2 specimens.....	130
Figure 6.11	Variation of cyclic dissipated energy, normalized with respect to the 1 <sup>st</sup> full cycle, with the number of cycles: Pujol specimens.....	131
Figure 6.12	Variation of cyclic dissipated energy, normalized with respect to the 1 <sup>st</sup> full cycle, with the number of cycles: Wight and Sozen specimens.....	131
Figure 6.13	Variation of cyclic dissipated energy, normalized with respect to the 2 <sup>nd</sup> full cycle, with the number of cycles: Type-1 specimens.....	132
Figure 6.14	Variation of cyclic dissipated energy, normalized with respect to the 2 <sup>nd</sup> full cycle, with the number of cycles: Type-2 specimens.....	133
Figure 6.15	Variation of cyclic dissipated energy, normalized with respect to the 2 <sup>nd</sup> full cycle, with the number of cycles: Pujol specimens.....	133
Figure 6.16	Variation of cyclic dissipated energy, normalized with respect to the 2 <sup>nd</sup> full cycle, with the number of cycles: Wight and Sozen specimens.....	134
Figure 6.17	A representative exponential decay in normalized energy dissipation capacity after the second cycle for a typical r/c component .....	135
Figure 6.18	Correlation of $E_1/E_2$ with ductility for test specimens with flexure dominant failure mode .....	138
Figure 6.19	Correlation of $E_1/E_2$ with confinement ratio for test specimens with flexure-shear failure mode .....	139

Figure 6.20	Correlation of $E_1/E_2$ with shear ratio for test specimens with flexure-shear failure mode .....	140
Figure 6.21	Variation of $E_1/E_2$ with rotation ductility for test specimens with flexure-shear failure mode .....	141
Figure 6.22	Correlation of $\alpha$ with ductility for test specimens with flexure dominant failure mode .....	142
Figure 6.23	Correlation of $\alpha$ with confinement ratio for test specimens with flexure-shear failure mode .....	143
Figure 6.24	Correlation of $\alpha$ with shear ratio for test specimens with flexure-shear failure mode .....	144
Figure 6.25	Correlation of $\alpha$ with ductility for test specimens with flexure-shear failure mode .....	145
Figure 6.26	Variation of $\beta$ with rotation ductility for test specimens with flexure dominant failure mode .....	146
Figure 6.27	Correlation of $\beta$ with confinement ratio for test specimens with flexure-shear failure mode .....	147
Figure 6.28	Correlation of $\beta$ with shear ratio for test specimens with flexure-shear failure mode .....	148
Figure 6.29	Correlation of $\beta$ with rotation ductility for column specimens with flexure-shear failure mode .....	149
Figure 6.30	Comparison of the cyclic energy dissipation capacities of two companion columns with different axial load levels. Normalized energy dissipation, (a) w.r.to 1 <sup>st</sup> full cycle, (b) w.r.to 2 <sup>nd</sup> full cycle and (c) Cumulative energy dissipation .....	150
Figure 6.31	Comparison of the cyclic energy dissipation capacities of two companion columns with different bond strength. Normalized energy dissipation, (a) w.r.to 1 <sup>st</sup> full cycle, (b) w.r.to 2 <sup>nd</sup> full cycle and (c) Cumulative energy dissipation .....	151
Figure 6.32	Cyclic strength degradation in low-cycle fatigue .....	152
Figure 6.33	Normalized strength degradation with the number of cycles in Type-1 specimens.....	153

Figure 6.34	Normalized strength degradation with the number of cycles in Type-2 specimens.....	153
Figure 6.35	Normalized strength degradation with the number of cycles in Pujol specimens.....	154
Figure 6.36	Normalized strength degradation with the number of cycles in Wight and Sozen specimens.....	155
Figure 6.37	Comparison of the normalized cyclic strength degradation of two companion columns with different axial load levels.....	156
Figure 6.38	Comparison of the normalized cyclic strength degradation of two companion columns with different bond strength.....	157
Figure 7.1	Effect of the sequence of imposed displacements on the energy dissipation characteristic of column specimens in flexure.....	161
Figure 7.2	Correlation of actual dissipated energy with predicted dissipated energy at the first full cycle.....	163
Figure 7.3	Normalized dissipated energy curves for (a) Type-1 and (b) Type-2 specimens .....	165
Figure 7.4	Comparison of experimental and predicted dissipated energies for typical Type-1 and Type-2 specimens .....	166
Figure 7.5	Normalized strength degradation for, (a) Type-1 and (b) Type-2 column members .....	167
Figure 7.6	A representative analytical cycle with boundary conditions .....	169
Figure 7.7	Predicted and observed responses of Specimen 2P3 for first five cycles .....	170
Figure 7.8	Predicted and observed responses of Specimen 4P4 for first five cycles .....	171
Figure 7.9	Predicted and observed responses of Specimen 5P5 for first five cycles .....	172
Figure 7.10	Predicted and observed responses of Specimen 1D2 for first five cycles.....	173
Figure 7.11	Predicted and observed responses of Specimen 2D3 for first five cycles .....	174

Figure 7.12	Predicted and observed responses of Specimen 3D4 for first five cycles.....	175
Figure 7.13	Predicted and observed responses of Specimen 4D5 for first five cycles .....	176
Figure 7.14	Cumulative dissipated energy predictions for variable-amplitude loadings of, (a) 6PV1, (b) 5DV1 and (c) 6DV2.....	178
Figure 7.15	Phase-2 of analytical hysteresis model .....	180
Figure 7.16	Phase-3 of analytical hysteresis model .....	181
Figure 7.17	Rules for the unloading and reloading branches of proposed moment-rotation hysteresis model .....	183
Figure 7.18	Envelope curves proposed for estimation of hysteretic response of (a) Type-1 specimens and (b) Type-2 specimens .....	184
Figure 7.19	(a) Experimental and predicted response and (b) cumulative dissipated energy histories of specimen 6PV1.....	186
Figure 7.20	(a) Experimental and predicted response and (b) cumulative dissipated energy histories of specimen 5DV1.....	187
Figure 7.21	(a) Experimental and predicted response and (b) cumulative dissipated energy histories of specimen 6DV2.....	188
Figure A.1	Plan view of a 4-story building.....	203
Figure A.2	Elevation view of frame C-C.....	204
Figure A.3	Analysed planar frame.....	206

# **CHAPTER 1**

## **INTRODUCTION**

### **1.1 General**

In current seismic design codes of most countries, structural design is achieved by performing a force-based demand-capacity analysis. Structural demands and capacities are measured in terms of forces and strengths. Typically, force demand is assessed from a linear elastic response spectrum analysis under a code design spectrum, reduced by a factor which indirectly and approximately represents inelastic seismic response. Then demand-capacity analysis is performed for all structural members and their critical sections. A member is accepted as safe or adequate if it is capable of carrying the force demands with the provided capacity. However, considering the cyclic characteristic of earthquake loading, reinforced concrete structural members designed to ultimate levels usually cannot maintain their initial stiffnesses and strengths during seismic response. This true response phenomenon which can not be directly assessed with forced based analysis techniques usually cause damage in members and eventually leads to lower seismic performance.

More recent seismic evaluation procedures employ displacement capacity and demand in seismic assessment. Under seismic action, if the deformation capacity exceeds the associated demand, the structural system is considered capable of surviving the entire earthquake excitation within the accepted performance

limits. However, similar to force-based design philosophy, this procedure also does not consider the effect of time dependent amplitude variation, frequency content and duration of strong ground motions on the performance of structural members.

A more rational seismic design approach is to interpret the loading path effect of earthquake excitation in terms of input energy. The design criterion in energy-based methods is achieved by the comparison of energy absorption capacity of the structure to earthquake energy input. In other words, the energy input should be balanced with the energy dissipated in structure throughout energy absorption or dissipation mechanisms such as damping or inelastic action (hysteretic energy) while the members remain within the expected performance limits. Therefore identification and verification of energy dissipation capacities and mechanisms of structural members become an important issue in performance assessment of reinforced concrete members. Since energy dissipation takes place along with inelastic action such as cracking and plastic hinging of members, the damage attained in turn can also be quantified by the degradation of their energy dissipation capacities which can actually be calculated by the reduction in the area enclosed by the response hysteresis cycles.

Severe seismic events in urban regions during the last two decades revealed that structures constructed before the development of modern seismic codes are the most vulnerable to earthquakes. Sub-standard reinforced concrete buildings constitute an important part of this highly vulnerable urban building stock. Therefore there is an urgent need for the development and improvement of realistic methods for seismic performance assessment of existing reinforced concrete structures. Energy-based seismic evaluation appears as a promising field to fill this gap.

## **1.2 Objective and Scope**

This study is organized to utilize a dual experimental-analytical approach for establishing an energy-based seismic performance assessment procedure for

reinforced concrete column members of frame structures which represent both the existing non-conforming design and the adequate code conforming design. With this objective, the basic low-cycle fatigue characteristics and the consequent deterioration behaviour of concrete column members are obtained under simulated seismic loading. Correlations between the energy dissipation mechanisms and material and sectional properties are derived for full scale column specimens tested under cyclic displacement histories. The effect of imposed displacement path on the hysteretic response, energy dissipation and degradation characteristics of column members is identified and the deterioration characteristics of reinforced concrete column members are assessed through an energy based approach. In the analytical phase of the study, the main effort of the work was put on the realistic prediction of the inelastic response of reinforced concrete members by developing an energy-based sectional model. This model is derived by improving a formerly proposed model which is calibrated and verified by using the gathered information from the conducted experiments.

Throughout the study;

- An extensive literature review on topics such as the concept of energy in earthquake resistant design, experimental studies on performance assessment of reinforced concrete structures, section models for reinforced concrete columns, low-cycle fatigue behaviour of concrete members and the effect of loading history on member response is carried out and a summary of relevant publications are presented in Chapter 2.
- Details of the conducted experiments on real size reinforced concrete column specimens are presented in Chapter 3. Test setup, dimensions and properties of test specimens, instrumentation and testing program are described in this chapter.

- Results of each conducted specimen test are summarized in Chapter 4 in terms of specimen responses. Observations on the response of test specimens throughout the entire testing program are given with supporting visual documents in this chapter.

- Seismic performance evaluation of the tested specimens is carried out in Chapter 5 according to the limit state definitions of the up-to-date design manuals such as Eurocode 8, ASCE/SEI 41-Update and Turkish Earthquake Code (TDY 2007) and comparative discussion of the proposed limit states proposed in these manuals is presented.

- Characteristic of energy dissipation and the effect of deterioration on member response under low-cycle fatigue loading are studied in Chapter 6. For a selected set of column tests, including the tests conducted within the content of this study, hysteretic response envelopes, cyclic energy dissipation and cyclic flexural strength deterioration are investigated in view of low cycle fatigue loading. The effects of some variables such as axial load ratio and bonding conditions between concrete and longitudinal bars are also discussed in this chapter.

- An analytical hysteresis model for the representation of inelastic moment-rotation response of column members in flexure is proposed in Chapter 7. With its features such as long term memory on cumulative dissipated energy, cyclic strength deterioration and combined piecewise linear and quadratic representation of cyclic response, proposed model is utilized for predicting the inelastic response of column members under variable amplitude loading paths.

- A general summary of the study with its main motivation and findings and conclusions reached are itemized in Chapter 8.

## CHAPTER 2

### LITERATURE REVIEW

A literature review on the concept of energy in earthquake resistant design, studies on performance assessment of reinforced concrete structures, section models for reinforced concrete columns, low-cycle fatigue behaviour of concrete members and the effect of loading history on member response is carried out and the summary of this review with comments are presented in this chapter.

#### 2.1 Energy in Earthquake Engineering

Energy in seismic analysis can be expressed in terms of input and dissipated mechanical energy. Therefore it is necessary to introduce the basic energy quantities such as energy input and dissipated or stored energy for a typical structural system under ground excitation.

The equation of motion for a single degree of freedom (SDOF) system under ground excitation can be formulated as given in Equation 2.1;

$$m\ddot{u} + c\dot{u} + f_s(u) = -m\ddot{u}_g \quad (2.1)$$

where  $m$  is the mass,  $c$  is the viscous damping coefficient,  $f_s$  is the restoring force for the SDOF system and  $\ddot{u}_g$  is the ground acceleration.

The energy equation for the system can be derived from the equation of motion by integrating each term with respect to relative displacement  $u$ ;

$$\int_0^u m.\ddot{u}.du + \int_0^u c.\dot{u}.du + \int_0^u f_s(u).du = -\int_0^u m.\ddot{u}_g du \quad (2.2)$$

The right-hand side of Equation 2.2 represents the energy imparted to the system ( $E_I$ ) due to dynamic motion of the ground. This imparted energy should temporarily be stored or be dissipated by the system which is represented by the terms on the left-hand side of the equation, maintaining an energy equilibrium state for the system. The terms on the left-hand side of the Equation 2.2 represents the stored kinetic energy ( $E_K$ ), energy dissipated by damping ( $E_D$ ), temporarily stored elastic strain energy ( $E_S$ ) and dissipated hysteretic energy due to inelastic action ( $E_H$ ), respectively, as given in Equation 2.3. The terms in Equation 2.3 are cumulative at time  $t$ , when the displacement is  $u(t)$ .

$$E_K + E_D + E_S + E_H = E_I \quad (2.3)$$

The idea of using energy in earthquake resistant design was first stated by Housner in 1956. He formulated the basic concept at any instant of dynamic action. The energy imparted to the structure has to be equal to the sum of dissipated and stored energy. Following the general idea, he also proposed an equation for obtaining total input energy from the velocity response spectrum,

$$E_I = \frac{1}{2} m.S_{V,\xi}^2 \quad (2.4)$$

where  $m$  is the total mass of structure and  $S_{V,\xi}$ , is the maximum relative velocity of the mass.

In fact, after Housner's proposal of an energy-based design procedure, this approach in earthquake resistant design was underestimated for a long time.

However in recent years, with advances in seismic design concepts and implementations such as base isolation and energy dissipation systems, the interest in energy based methodologies increased considerably.

After Housner's derivation, several researchers (Akiyama,1985; Kuwamura and Galambos, 1989; Uang and Bertero, 1990; Sucuoğlu and Nurtuğ, 1995) also proposed several formulations related to mainly the ground motion parameters such as peak ground velocity, duration and frequency content of ground motion in order to predict the energy imparted to structures. Zahrah and Hall (1984) studied imparted and absorbed energy in SDOF systems in order to evaluate structural performance. They considered factors such as the type of ground motion and its cyclic effect on performance of the structure. During the following years, several researchers studied the mechanism of energy dissipation and its components such as damping and hysteretic behaviour. Damage models for SDOF systems were constructed by energy based concepts (McCabe and Hall, 1989; Fajfar et. al, 1990; Bruneau and Wang, 1996; Decanini and Mollaioli, 2001). Manfredi (2001) proposed a method for assessment of energy demand to SDOF systems by adopting an equivalent number of plastic cycle definition.

With developments in understanding the energy concepts, studies on SDOF systems extended to MDOF structures. In 1992, Leger and Dussault investigated the influence of models for viscous damping on structural response. Shen and Akbas (1999) proposed a procedure for energy based design and damage prediction for MDOF systems by quantifying the plastic deformations at members of generic moment resisting steel frames. Knowing the fact that the impart energy should be equal to dissipated energy, they estimated the distribution of dissipated energy by hysteretic response and by damping for MDOF systems and stated that the estimations done for MDOF system responses based on SDOF analysis have critical drawbacks and discrepancies. Leelataviwat et al (2002) utilized the energy balance concept for proposing a methodology for design of MDOF systems.

This study focuses on identification of dissipated hysteretic energy term  $E_H$  by proposing a section model for reinforced concrete column members incorporating deterioration behavior under repeated and reversed displacement

cycles. Thus, the effect of loading history on reinforced concrete columns becomes crucial to investigate since it is one of the most influential parameters on the deteriorating behavior of reinforced concrete members. The proposed energy-based hysteresis model particularly employs dissipated energy as the basic parameter controlling the shape of hysteresis loops. Cyclic degradation in strength is another independent control parameter which is obtained experimentally from the low cycle fatigue behavior of reinforced concrete.

## **2.2 Energy-Based Hysteresis Models**

Tembulkar and Nau (1987) carried out an analytical study on inelastic structures modelled as SDOF systems with two different hysteretic models, in order to investigate the role of models on seismic energy dissipation. They have stated that damage attained by a reinforced concrete member under dynamic action can not be predicted adequately by response spectrum concepts. Therefore, a well constructed hysteresis model should be constructed as a tool for the damage assessment of concrete structural members.

Stojadinovic and Thewalt (1996) proposed a pair of energy balanced hysteresis models based on experiments that were conducted previously on knee joint sub-systems by Thewalt in 1995. Both proposed models were piecewise linear and segments on envelope curves were defined by some special points such as first crack, yield and ultimate resistance as shown in Figure 2.1.

They performed a benchmark study and compared their models with well known hysteresis models in view of shape and dissipated energy and reached a conclusion that all piecewise linear hysteresis models have some limitations in predicting the response of reinforced concrete structures. However with well defined parameters, energy based hysteresis models may successfully represent seismic response by considering the deteriorating behaviour of reinforced concrete members.

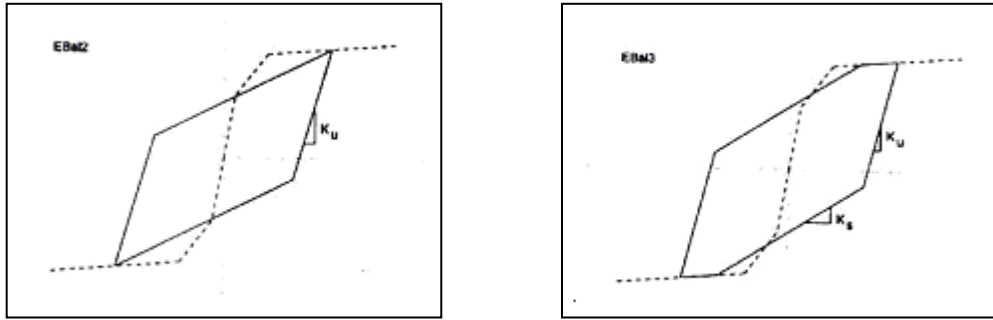


Figure 2.1 Piecewise linear energy based hysteresis models proposed by Stojadinovic and Thewalt (1996)

In 2004 Sucuoğlu and Erberik proposed a piece-wise linear energy based hysteresis model primarily based on Clough's stiffness degrading model (Figure 2.2). The proposed model also has the capability of simulating strength deterioration with its energy based memory for each displacement response cycle. They evaluated the deterioration in strength by quantifying the reduction in energy dissipation capacity for that cycle due to low-cycle fatigue and pinching. They concluded that both the amplitude and number of higher amplitude displacement response cycles increase significantly with the reduction in energy dissipation capacity, which leads to increasing damage.

Structural damage characterization under seismic loading has extensively been studied in recent years and many models with different concepts have been proposed. One of the relatively simplest one was the prediction of damage in terms of ductility demands. Although much effort has been spent on estimation of damage with ductility demand in reinforced concrete frames, there is still a large gap between the ductility demand and actual observed damage in experiments. Eventually, researchers constructed more realistic damage models with different parameters. In the light of these findings, different models have been proposed by researchers using either the classical definition of low-cycle fatigue or energy dissipation of a member during its inelastic response, or stiffness deterioration under reversed cyclic loading.

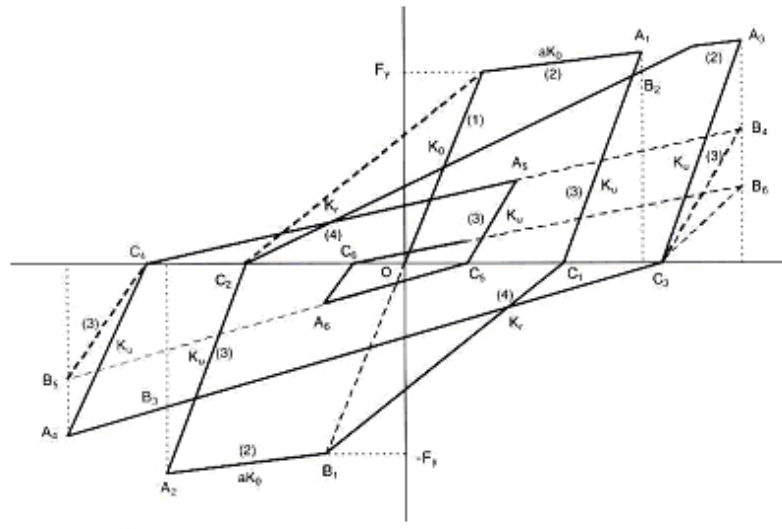


Figure 2.2 Energy based hysteresis model proposed by Sucuoglu and Erberik (2004)

Cumulative damage concept was apparently first used by Palmgren (1924). In 1945, Miner developed a new concept to represent the cumulative damage of aluminium members under high-cycle repeated loading simply based on the work absorbed by a specimen. Basically, the concept held that the damage could be expressed in terms of the number of cycles applied ( $n_n$ ) divided by the number that produce failure at a given stress level ( $N_n$ ). When the summation of these increments of damage at several levels becomes unity, failure occurs.

$$\frac{n_1}{N_1} + \frac{n_2}{N_2} + \frac{n_3}{N_3} + \dots + \frac{n_n}{N_n} = 1 \quad \rightarrow \quad \sum \frac{n_n}{N_n} = 1 \quad \rightarrow \quad \text{Failure}$$

In 1985 Park and Ang proposed a popular linear damage model which was constructed by a combination of damage due to excessive deformation (non-cumulative) and due to a ratio of plastic strain energy (cumulative) as given in Equation 2.5.

$$D_i = \frac{\Delta_m}{\Delta_{um}} + \frac{\beta \cdot E_h}{V_y \cdot \Delta_{um}} \quad (2.5)$$

where  $\Delta_m$  is the maximum displacement,  $\Delta_{um}$  is the maximum displacement at monotonic loading,  $V_y$  is yield strength,  $\beta$  is a parameter defining strength deterioration and  $E_h$  dissipated energy.

In 1995 Chai and Romstad improved Park and Ang model with modification on  $\beta$  and plastic strain energy parameters (Equation 2.6).

$$D_i = \frac{\Delta_m}{\Delta_{um}} + \frac{\beta^* \cdot (E_h - E_{hm})}{V_y \cdot \Delta_{um}} \quad (2.6)$$

where  $\beta^*$  is modified strength deterioration parameter and  $E_{hm}$  is the dissipated strain energy under monotonic loading.

Sucuoğlu and Erberik (2004) also derived an energy based damage formulation composed of two parts.

$$D_n = D_m + \Delta D_m \quad (2.7)$$

The first term on the right hand side of Equation 2.7,  $D_m$  represents the damage due to maximum plastic deformation. The second term,  $\Delta D_m$ , represents the damage accumulated due to low-cycle fatigue behaviour of reinforced concrete member, and proposed as given in Equation 2.8,

$$\Delta D_m = \frac{\mu_m}{\mu_u - 1} \cdot \left( \frac{4}{5 \cdot \bar{E}_{h,n}} - 1 \right) \quad (2.8)$$

where  $\bar{E}_{h,n}$  is the normalized dissipated energy at the  $n$ -th constant amplitude cycle,  $\mu_m$  is maximum ductility demand and  $\mu_u$  is ultimate ductility capacity.

This normalized energy quantity at an  $n$ -th cycle of response was derived by the authors in a companion paper as,

$$\bar{E}_{h,n} = \alpha + (1 - \alpha).e^{\beta(1-n)} \quad (2.9)$$

Here in Equation 2.9,  $(1-\alpha)$  was defined as the loss of energy dissipation capacity and  $\beta$  parameter was defined as the rate of loss.

Performing a series of experiments on scaled beam-column joint elements, Erberik and Sucuoğlu (2004) calibrated the  $\alpha$  and  $\beta$  parameters through a nonlinear regression analysis with the obtained data, concluding that,  $\alpha$  parameter seemed to be influenced by bond between concrete and plain bars, whereas the  $\beta$  parameter seemed to be influenced by concrete strength. By making modifications on proposed energy and damage expressions and introducing “equivalent number of cycles with constant ductility,  $n_{eq}$ ” definition, they expressed a general energy and damage formulation for variable amplitude displacement variations as given in Equation 2.10 and Equation 2.11.

$$\bar{E}_{h,neq} = \alpha + (1 - \alpha).e^{\beta(1-neq)} \quad (2.10)$$

$$D_m = \frac{\mu_{e,m} - 1}{\mu_u - 1} + \frac{\mu_{e,m}}{\mu_u - 1} \left( \frac{4}{5.\bar{E}_{h,neq}} - 1 \right) \quad (2.11)$$

where  $\mu_{e,m}$  was maximum effective ductility and defined as the half of difference between the maxima and minima of the largest displacement cycle. A graphical representation was also given by the authors, where the damage prediction procedure for variable amplitude loading was explained as shown in Figure 2.3.

### 2.3 Low Cycle Fatigue Behaviour of Concrete Members

It was mentioned in Erberik and Sucuoğlu (2004) that deterioration in bond between reinforcing bars and concrete influences the damage of reinforced concrete members significantly. Karsan and Jirsa (1969) carried out an experimental study on plain concrete specimens in order to describe the behaviour of concrete under repeated compressive loading. They tested short rectangular column specimens under various compressive loading (both monotonic and repeated) and derived expressions for the stress-strain behaviour of concrete. In light of test results, they reached the following conclusions:

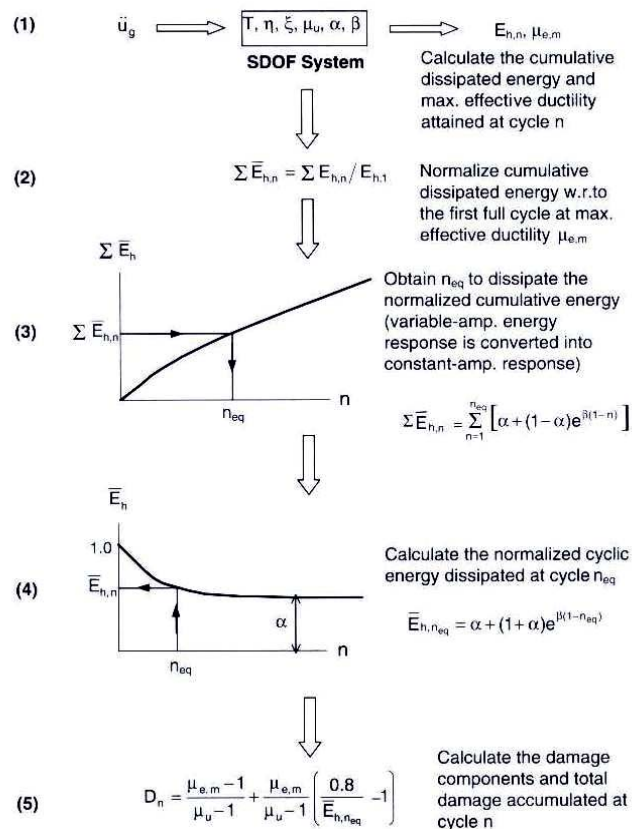


Figure 2.3 Graphical representation of damage prediction procedure proposed by Erberik and Sucuoğlu (2004)

- The stress-strain curves for cyclic loading generally do not exceed a so-called envelope curve which is actually the stress-strain curve of specimens under monotonic loading.
- A specimen can be loaded to its envelope regardless of the strain accumulated until that cycle before failure.
- Under constant amplitude repeated loading, strain accumulation does not produce failure until it reaches the envelope curve.

In spite of the definition of Sinha et al (1964) for common points describing where reloading cycle crosses the unloading cycle and where strains stabilize for subsequent loops, Karsan and Jirsa (1969) revealed that there should be a range for common points instead of a specific point for intersection of reloading and unloading branches as shown in Figure 2.4. As a result, Karsan and Jirsa (1969) concluded that, failure for a specimen under repeated loading can be produced with the accumulation of strains for stress levels greater than the stress level for an estimated stability limit.

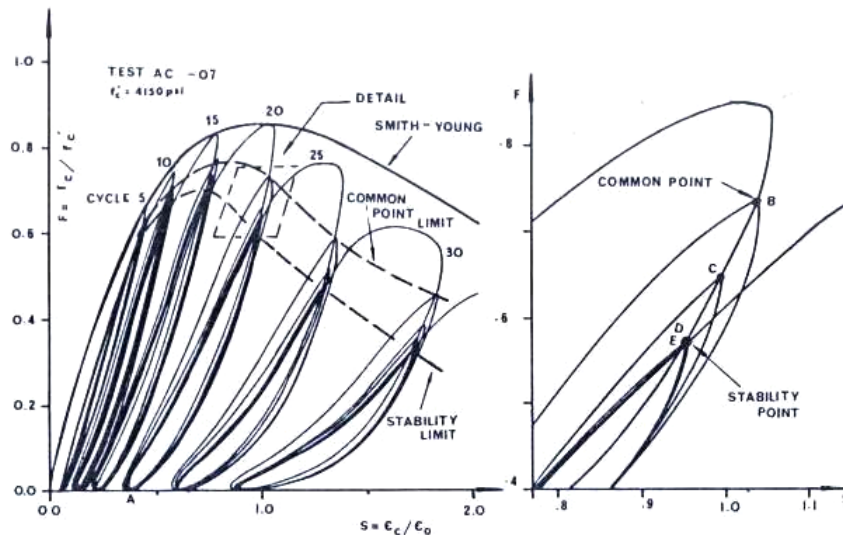


Figure 2.4 Stress-strain relationship for a concrete specimen showing common points and stability point (Karsan and Jirsa ,1969)

Balazs (1991) conducted tests on concrete prism pullout specimens in order to obtain information on the bond behaviour of reinforced concrete elements under both repeated and reversed loadings. As many researchers indicated, he also stated that the most important parameters affecting the bond behaviour of reinforced concrete elements are rib pattern of steel bars (Soretz and Holzenbein, 1979), concrete cover (Kemp and Wilhelm, 1979), concrete strength (CEB, 1982), anchorage length (Lin and Hawkins, 1982) and type of loading (Ismail and Jirsa, 1972; Eligehausen et al., 1983). Considering the main variables for his tests as bar diameter, anchorage length and loading history, Balazs (1991) carried out tests on both unconfined specimens under repeated loading and confined specimens under reversed loading, all having sufficient concrete cover that ensures no longitudinal splitting during experiments. He plotted the repeated loading test results and stress-cycle number (s-N) curves derived from these tests with monotonic test results on the same figure in order to illustrate the bond fatigue phenomenon of concrete specimens under repeated loading as shown in Figure 2.5.

Figure 2.5 clearly shows that the increments in slip decreased in the first stage of loading cycles and then stayed constant up to the slip value that corresponds to ultimate bond strength,  $S_{\tau_{bu}}$  which was observed under monotonic pull-out tests. From that point forward, slip increased progressively up to pull-out failure. In the light of this result, Balazs (1991) underlined the statement that “*a pull-out type bond failure may occur due to cyclic loading without applying the monotonic ultimate pull-out force*”.

Balazs (1991) also investigated the bond behaviour of confined concrete specimens under reversed loading either with slip-controlled or force-controlled cycles. In slip-controlled reversals, bond softening was characterized by decrease in bond stress. On the other hand, in load-controlled cycles, it was shown that the softening in bond will be due to increase in slip. As a result, Balazs (1991) proposed a family of curves in order to represent the bond behaviour under reversed cyclic loading of confined concrete members. As shown in Figure 2.6, Balazs (1991) represented the reductions in both bond strength ( $\tau_u$ , obtained by monotonic

loading) and related slip ( $S_{\tau_u}$ ) for reversed cyclic loading with some modification factors ( $\chi_1$ ,  $\chi_2$  and  $\chi_3$ ). Actually  $\chi_1$  represents the reduction in monotonic envelope curve in secondary loading direction,  $\chi_2$  represents the decrease in bond strength under reversed cyclic loading and  $\chi_3$  represents reduction for slip corresponding to slip at monotonic bond strength.

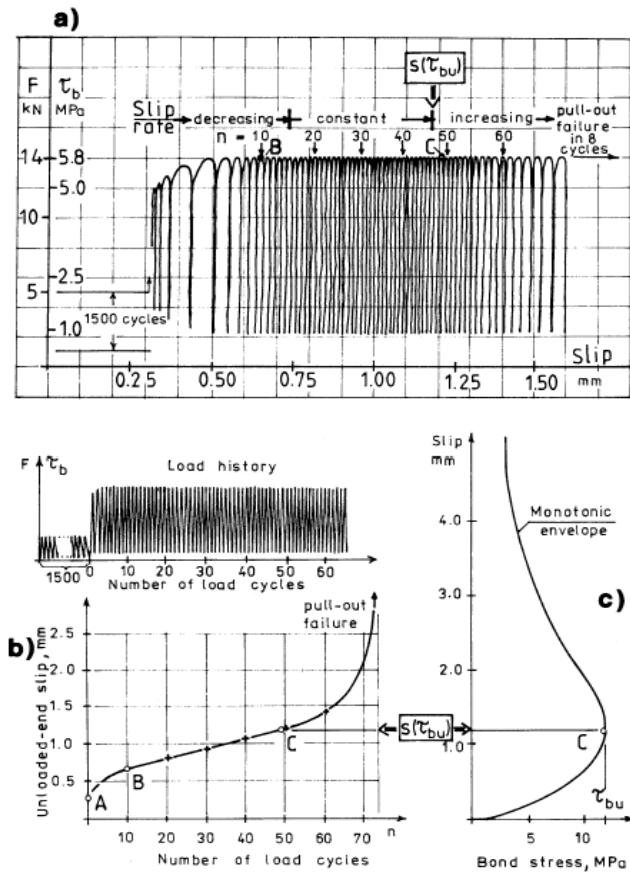


Figure 2.5 (a) Bond fatigue test results, (b) Slip versus number of cycles diagram evaluated from test results, (c) Monotonic bond strength-slip diagram (Balazs, 1991)

The reduction in strength capacity (i.e. bond strength for Balazs's work) due to repeated and/or reversed loading is called strength deterioration in general.

Youssef and Ghobarah (1999) proposed a macro-model element which accounts for strength deterioration due to bond slip and concrete crushing of reinforced concrete columns designed for flexure. Kwak and Kim (2001) introduced a hysteretic moment-curvature relationship for beam members which takes into account the effect of bond slip, fixed-end rotation and pinching effects by modifying the moment-curvature relationship implicitly. Many researchers proposed several sectional models or implemented some new rules to modify an already known model to represent this deteriorating behaviour for reinforced concrete members under cyclic loadings (Sivaselvan and Reinhorn, 1999, 2000; Park et al., 1987; Ibarra et al., 2005; Mostaghel, 1998; Roufaiel and Meyer, 1987).

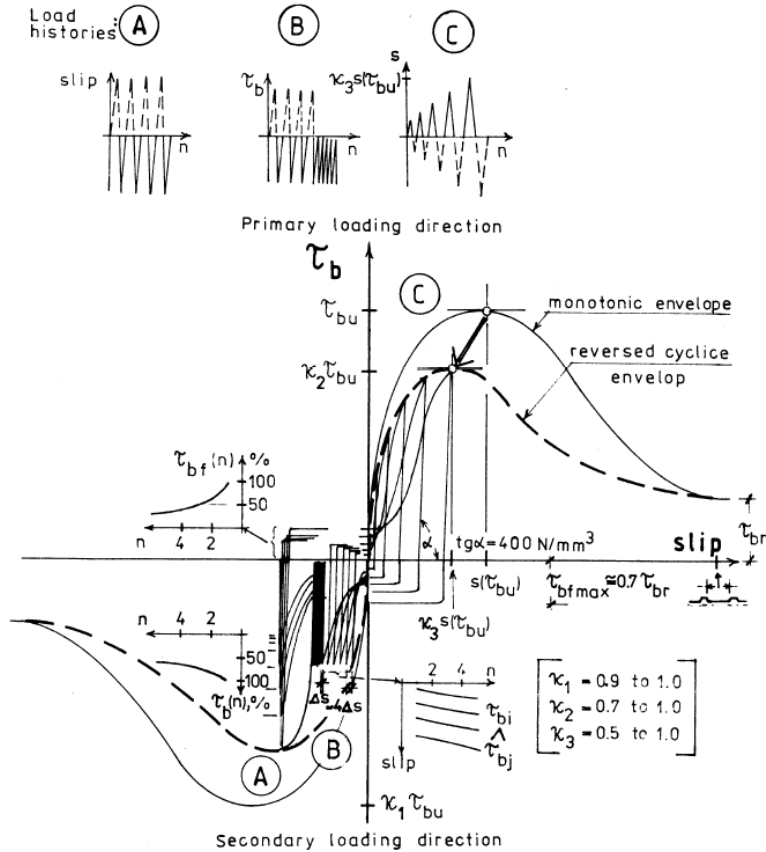


Figure 2.6 Bond fatigue curves proposed by Balazs (1991) for reversed cyclic loading

Deterioration in strength can be classified in two distinct cases depending on the stage where the reduction occurs (FEMA 440, 2005; FEMA P440A, 2009). In the first case, which is called as cyclic strength deterioration, the loss in strength capacity occurs within the subsequent cycles of hysteretic behaviour. In the second case, which is called in-cycle deterioration, reduction in capacity occurs within the same cycle while the deformation increases. The main reason for the drop in capacity in first case is accepted as the amplitude of experienced displacements and the number of excursions with the certain amplitudes, while, for the latter case, P-D effect and the attained damage which leads to degradation in material properties is thought to be effective. The representative hysteretic responses for generic column specimens with two different types of strength deterioration are depicted in Figure 2.7.

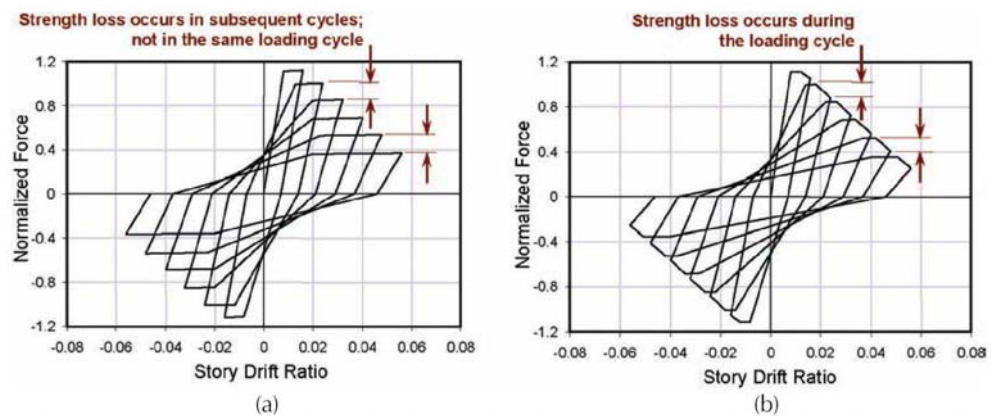


Figure 2.7 Types of strength deterioration, (a) Cyclic and (b) In-cycle strength deterioration (FEMA P440A, 2009)

## 2.4 The Effect of Loading History on Member Response Deterioration

Since the deterioration in member capacity, which can also be quantified with the deterioration in energy absorption and dissipation capacity, is a composition of stiffness degradation, strength degradation and pinching, all relevant parameters

such as axial load ratio, reinforcement ratio, shear span ratio, loading history, concrete strength, bond strength etc. affect the member response under random dynamic excitations. Among all, within the scope of this study, a special emphasis has been given to the effect of loading history as well as the effect of axial load and bond strength on member response deterioration.

Galal and Ghobarah (2003) investigated the effect of variable axial load amplitude and pattern on strength, stiffness and deformation capacity of reinforced concrete members. Knowing the fact that the magnitude of axial load has an effect on sectional moment capacity, they verified that the axial load history should be identified clearly to assess the response of column members. Sezen and Moehle (2006) studied the effect of axial load and lateral load history and magnitude on member response, concluding that a new definition should be done for performance assessment of reinforced concrete columns depending on their axial load level since it is a crucial parameter on failure mode. They also investigated the influence of loading pattern on deformation capacity of columns and concluded that under constant axial load, deformation capacity of tested specimens under monotonic loading are greater than the ones tested under cyclic loading. Bechtoula et al. (2005) tested small-scale and large-scale reinforced concrete specimens designed for flexure to assess the effects of parameters such as axial load and loading pattern (uni-direction, square, circular), finding out that the intensity of applied load has a minor effect on strength deterioration for specimens tested under uni-directional horizontal loading compared to the specimens tested under other loading patterns. They also showed that the equivalent viscous damping has an increasing trend with the increase in axial load. In 1996, Taylor et al. compared the influence of loading protocols commonly used for reinforced concrete testing on member response and damage. Conducting tests either under so-called standard or constant and random amplitude loading protocols, they concluded that there is a limit of  $4\Delta_y$  for stable response before failure. Moreover, considering only the results of tests carried out under constant amplitude loading, they concluded that the cumulative energy is not a good indicator for damage prediction. Perus and Fajfar (2007) investigated the correlations of parameters such as axial load, transverse and longitudinal

reinforcement ratio, shear span and concrete compressive strength with drift limits (i.e. yielding, capping drift and ultimate drift) and constructed a normalized force-displacement envelope for column members. For reinforced concrete columns with light transverse reinforcement, Elwood and Moehle (2006) predicted the limit states of yielding, shear failure and axial load failure by utilizing experimental data and constructed an idealized backbone curve. Comparing their proposed curve with the limit states indicated in FEMA 356, they concluded that the FEMA 356 limit states are overconservative in predicting drift capacities of reinforced concrete column members.

New generation of performance-based seismic rehabilitation and design codes express the flexural performances of column in terms of total or plastic rotation capacities of the critical end regions whereas shear failure is strictly prohibited (ASCE/SEI 41, 2007; Elwood et al., 2007; Eurocode 8, 2005). Shear-flexure failure in columns starts with flexural yielding, but as damage accumulates, failure mode turns into shear due to inadequate seismic detailing. Inclined cracks develop after the formation of flexural cracks since maximum shear exceeds the shear at inclined cracking. Limited deformation capacities of these columns have been recognized accordingly in the performance based codes based on experimental research (Lynn et al, 1996; Sezen and Moehle, 2006; Yoshimura et al, 2004; Quasalem et al, 2004). The deformation capacities of columns which undergo pure flexure failure are related to the reinforcement detailing as well as the imposed displacement history. Repeated number of large amplitude cycles may lead to degradation in lateral strength and stiffness, hence the exhaustion of deformation capacities of columns responding in flexure. Although the effects of longitudinal and lateral reinforcement on the deformation capacity of columns are well understood under standard displacement protocols, information on the effect of repeated severe displacement cycles is limited. Iwasaki et al (1987) tested bridge piers, and Pujol et al (2006) tested small scale columns under displacement reversals and investigated the effect of the number of displacement cycles on column deformation capacity. Columns in both of these tests developed inclined cracking after flexural yielding. Verderame et al. (2008) tested concrete columns with smooth reinforcing bars and

substandard detailing, but failing in pure flexure, in order to investigate the differences in the displacement capacity under monotonic and cyclic loading.

## **CHAPTER 3**

### **EXPERIMENTAL PROGRAM**

#### **3.1 General**

A two-phase experimental program is conducted on full-scale column specimens. Seven sub-standard specimens (Type-1), with plain bars and low concrete strength, were tested in the first phase. These specimens represent the columns of existing buildings constructed before 70's in Turkey with poor detailing and low concrete strength. The aim of the first experimental phase was to obtain information on the deterioration behavior of such structural components. In the second phase of the experimental program, another six column specimens with deformed bars and proper detailing (Type-2) were tested. Normal strength concrete was used for the second type of specimens. It is accepted that the set represents the columns designed and detailed according to the current Turkish Earthquake Code (TDY 1998, 2007).

Throughout this chapter, starting with the selection criteria for specimen type and dimensions, the design of reinforced concrete column members, properties of materials, the details of established test setup, scheme for instrumentation and testing program are given in detail.

### 3.2 Test Specimens

The test specimens represent an isolated part of the columns of an existing building which are extracted from the inflection points. The dimensions of a typical specimen are shown in Figure 3.1.

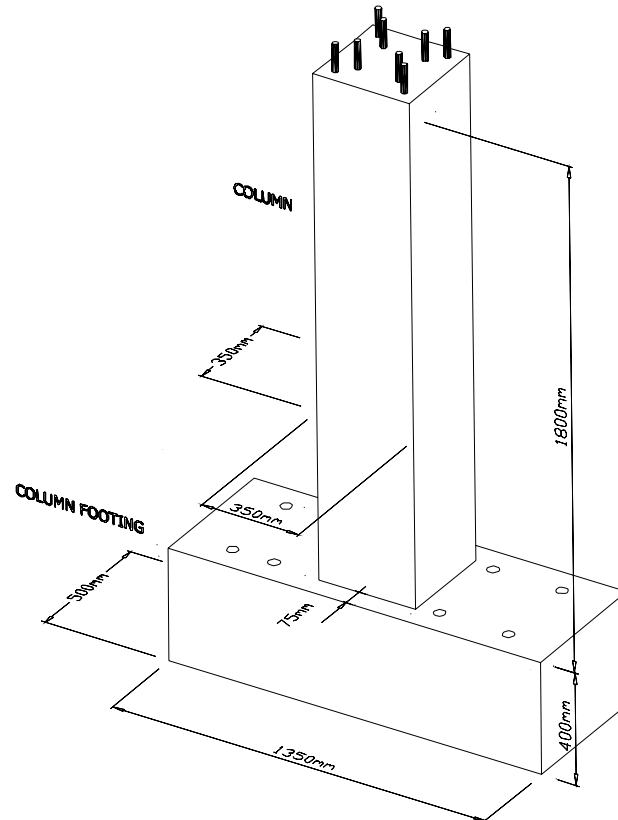


Figure 3.1 Typical reinforced concrete column specimen

The column cross-section dimensions were  $350 \times 350 \text{ mm}^2$  and their clear height was 1800 mm. They were cast vertically with a footing simulating a connection region with a rigid stub at one end so that the inelastic action will only occur on the column face. Footing had dimensions of  $1350 \times 500 \times 400 \text{ mm}$  and it was properly reinforced.

Plain bars were used as longitudinal and transverse reinforcements of Type-1 column specimens. All seven columns were longitudinally reinforced with eight  $\phi$ -14 plain bars ( $\rho_1 = 1.0\%$ ) and transversely reinforced with  $\phi$  8 hoops and ties. A peripheral hoop with  $90^\circ$  hooks and a pair of cross ties with  $135^\circ$  hook at one end and  $90^\circ$  hook at the other hand were used as the set of transverse reinforcement at one layer. The transverse bar sets were spaced at 165 mm from the bottom of column through the  $4/5$  of the clear height. The spacing was then reduced to 50 mm at the top cap of the columns where stress concentration was expected since lateral and axial loads are transmitted to the specimens at this region. Dimensions and reinforcement details of a Type-1 specimen are shown in Figure 3.2. No stirrups were placed within the column-footing joint region. As an exception within the group, one of the specimens was built with its longitudinal bars coated with a thin layer of silicone and covered with grease from the level of column-footing intersection to the top of column (except the hooks at the upper end of the column) in order to reduce/prevent the bond between longitudinal bars and concrete. This specimen represents a column with unbonded longitudinal reinforcement.

A simple notation was used for the designation of test specimens. The first numeral indicates the number of specimen within the group. The second character represents the bar type used as longitudinal reinforcement (**P** = Plain bars, **D** = Deformed bars). The third numeral indicates the amplitude of imposed drift ratio in the first constant displacement stage of the loading history where the drift ratio is rounded to the nearest integer, and the last character after underscore, if any exists, indicates the state of exception. Hence the specimen name “**3P3\_N0.4**” indicates the third column specimen with plain bars, tested under constant amplitude tip displacement cycles (in the first stage of loading) with a drift ratio of approximately 3% and the applied axial load level was higher than the other specimens in the group where N=0.4 indicates an axial load ratio of 40%. For variable amplitude loadings, the third character is replaced by two characters starting with **V** and a number representing the type of variable amplitude displacement protocol. The variable amplitude protocols are presented in the later sections of this chapter in detail.

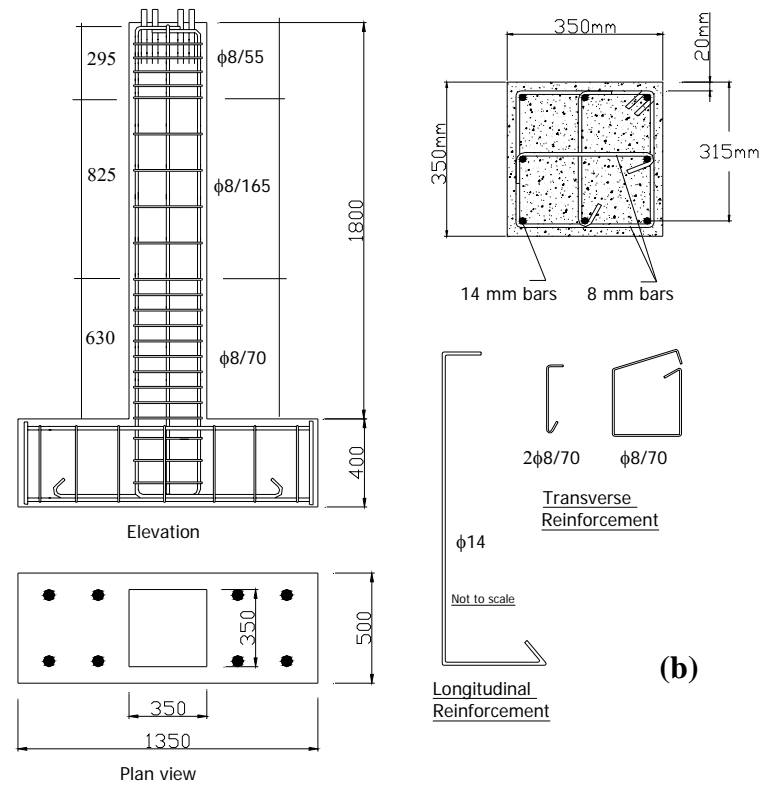
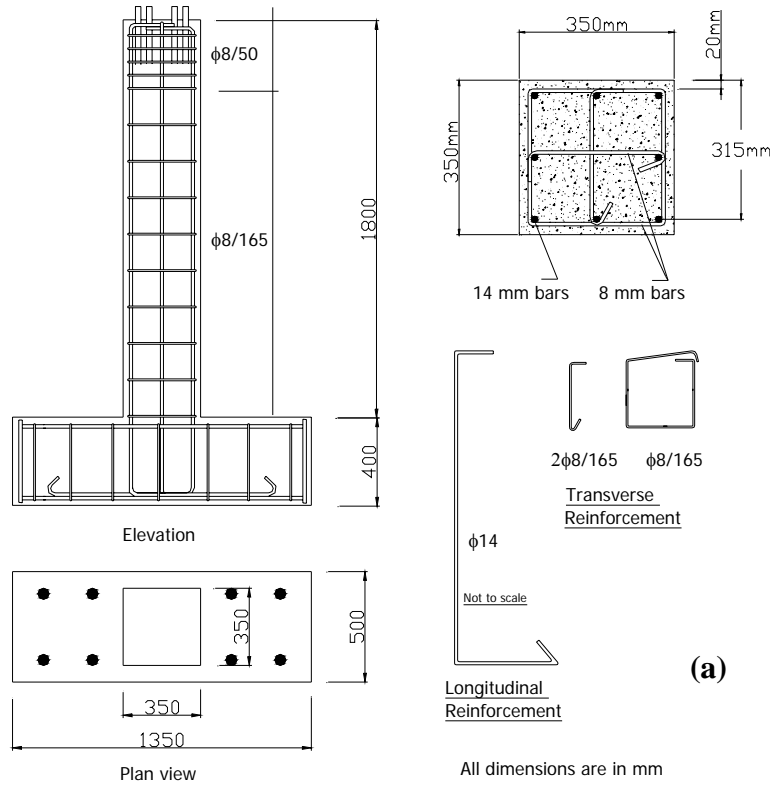


Figure 3.2 Dimensions and details of, (a) Type-1 column specimens, (b) Type-2 column specimens

The test variables which are expected to have a significant effect on the deterioration behaviour of column members are presented in Table 3.1 for Type-1 specimens, with the associated specimen names. Main variables are the type of loading (constant or variable amplitude loading), axial load ratio ( $N/N_0 = 0.2$  or  $N/N_0 = 0.4$ ) and the bonding conditions for longitudinal bars.

Table 3.1 Variables investigated in the experimental program for Type-1 specimens.

Specimen No	Specimen Code	Long. Bar Type	Axial Load Ratio	Drift Ratio	Loading Type	Long. Bar Bond
1	1P2	Plain	0.2	1.75	Constant Amp.	Bonded
2	2P3			2.50		
3	3P3_N0.4		0.4	2.50		
4	4P4		0.2	3.50	Variable Amp. (VI- Random)	
5	5P5			5.25		
6	6PV1		N/A			
7	7P3_U		2.50	Constant Amp	Reduced Bond	

For Type-2 specimens, the same amount ( $\rho_1 = 1.0\%$ ) and the same configuration of longitudinal reinforcements as of Type-1 specimens was used, however with deformed bars. The set of transverse reinforcement at one level of cross section was provided as a peripheral hoop with  $135^\circ$  hooks at its ends and two cross ties, all of which were  $\phi 8$  deformed bars. However, the spacing of the transverse bar sets were different for Type-2 specimens where it was 70 mm within the plastic hinging region (up to 630 mm from the level of footing) and 165 mm along the rest of the column height to the last 300 mm cap region at the top. Spacing of transverse reinforcement was reduced in this region to 55 mm in order to

reinforce the region properly so that premature failure due to the application of lateral load and axial load can be prevented. Three sets of transverse reinforcement within the footing for the joint region with a spacing of 100 mm were also provided in conformance to the Turkish Earthquake Code (TDY 1998).

The only test parameter for Type-2 specimens was the amplitude of imposed tip displacement. Four specimens were tested under constant amplitude displacement reversals and the remaining two were tested under variable amplitude displacement cycles. For all Type-2 specimens, the same axial load ratio ( $N/A_g \cdot f_{ck} = 0.2$ ) was applied. The details of test variables with the associated specimen labels are summarized in Table 3.2.

Table 3.2 Variables investigated in the experimental program for Type-2 specimens

Specimen No	Specimen Code	Long. Bar Type	Axial Load Ratio	Drift Ratio	Loading Type	Long. Bar Bond
1	1D2	Deformed	0.2	1.75	Constant Amp.	Bonded
2	2D3			2.50		
3	3D4			3.50		
4	4D5			5.25		
5	5DV1			N/A	Variable Amp. (V1-Random)	
6	6DV2			N/A	Variable Amp. (V2-LinearInc)	

### 3.3 Material Properties

Reinforcements of the concrete specimens were purchased as 12 m steel bars for four different types of bars ( $\phi$  14 deformed and plain bars,  $\phi$  8 deformed and

plain bars). They were cut down to desired lengths in the laboratory. Three sample coupons were taken and tested from each batch. The yield strengths and ultimate strengths of reinforcing bars used in both types of specimens are given in Table 3.3.

The mix design and concrete casting for Type-1 specimens were prepared and held in the laboratory. Each specimen of this group was cast separately one at a time. For Type-2 specimens, ready-mixed concrete was used. During casting of each specimen for both groups, nine standard cylinder specimens were taken and these cylinders were tested on the 7<sup>th</sup>, 28<sup>th</sup> and on the testing day of column specimen in order to monitor through out the curing period and to obtain the compressive strength of concrete of test specimens at the day of testing. The average compressive strengths of each specimen at the day of testing are given in Table 3.3.

### **3.4 Design of Specimens**

For realistic simulation of the inelastic actions in the critical regions of an actual building member under seismic loading, it is decided to use full scale test specimens representing an internal column of a reinforced concrete building frame. In determining the geometry of selected test specimens;

- a) Minimum requirements for dimensions and detailing of column members according to Turkish Earthquake Code and TS-500-2000,
- b) Laboratory conditions and loading system limitations,
- c) Compatibility with ongoing and future experimental programs on column specimens, were considered.

For this purpose, an internal column of a 4-story 3-bay reinforced concrete building frame was designed according to the requirements outlined in TS-500-2000 and Turkish Earthquake Code (1998, 2007). The building was a modified version of a generic building that is mainly used as an example in Ersoy and Özcebe (2001) for the implementation of design concepts in reinforced concrete structures.

Table 3.3 Material properties and reinforcement ratios of test specimens

Specimen Type	Specimen Code	Concrete	Longitudinal Reinforcement			Transverse Reinforcement		
			Compressive Strength $f'_c$ MPa	Yield Strength $f_y$ MPa	Ultimate Strength $f_u$ MPa	Reinforcement Ratio $\rho_l$ $A_s / b_w \cdot h$	Yield Strength, $f_{yw}$ MPa	Ultimate Strength, $f_{uw}$ MPa
Type -1	1P2	13.5						
	2P3	12.2						
	3P3_N0.4	13.1						
	4P4	12.4	315	448	0.01	368	487	0.0026
	5P5	11.4						
	6PV1	12.5						
	7P3_U	13.2						
Type - 2	1D2	25.8						
	2D3	25.9						
	3D4	27.6						
	4D5	24.6	454	604	0.01	469	685	0.0061
	5DV1	25.0						
	6DV2	25.3						

Although prohibited by TEC (1998, 2007), the selected column member was designed nominally with 13 MPa compressive strength concrete and by using plain bars as longitudinal and transverse reinforcement in order to represent an existing non-conforming column. Moreover, it is assumed that there is no confined region provided for this column and the maximum stirrup spacing allowed for unconfined regions was used all along the column height. This column member was treated as the reference for the first group of specimens (Type-1), where the other members are the variants of this reference specimen by means of changes in testing parameters. The same member was designed and detailed by using deformed bars and 25 MPa concrete strength, and treated as the reference member of the second group of column specimens (Type-2). The nominal design procedure of the internal column of the generic frame that was selected as the basic test specimen is given in Appendix A.

### **3.5 Construction of Test Specimens**

All column specimens were prepared in the METU Structural Mechanics Laboratory. Steel bars for longitudinal and transverse reinforcements of column specimens were purchased as 12 meter bars and were cut and bent for desired lengths accordingly. Some of these bars were instrumented after being bent and were assembled to form the reinforcing cage of the testing specimens. For Type -1 specimens, concrete mixture was prepared in the laboratory with a concrete mixer of 400 kilograms capacity. For Type-2 specimens, ready-mixed concrete was purchased from a local company. All specimens were cast within specially fabricated modular metal formworks and were cured under the same standard curing conditions. The details for construction of specimens are given in the following sections.

### **3.5.1 Formwork**

For concrete casting, specially manufactured modular metal formworks were purchased. The pieces of formwork were manufactured precisely to match with the exact dimensions of the test specimens when they are assembled. All pieces were fabricated from 2 mm thick galvanized metal sheets, strengthened and stiffened with belts and braces at certain places in order not to let the formwork deform during the concrete placing. Each piece had a unique layout of holes at their edges of connection with other pieces so that only the matching couples were connected. Hence assemblage of whole formwork was done with sequences from bottom to top. The pieces of formwork for footing were assembled at first and the reinforcing cage of specimen was put in afterwards. After making the alignments for clear cover spacing and putting the metal pipes for anchorage holes, the mid part of the formwork was assembled and attached to the formwork of footing. At this stage, the specimen was ready for concrete casting. After placing the concrete up to this level and consolidated by vibrators, the top part of formwork was assembled and connected to the body and the rest of the concrete was placed immediately not to let a cold-joint to form due to sequential concrete casting. All connections for formwork pieces were done by screws. A typical specimen with assembled formwork before concrete casting is given in Figure 3.3.

### **3.5.2 Instrumentation of Reinforcing Bars**

For measurements of strains on reinforcing bars, the corner bars of the longitudinal reinforcements and the stirrups within the critical hinging region were instrumented with strain gages. Three strain gages were installed on each instrumented longitudinal bar. The first gage was installed at a location on the bar where it corresponds to the 75 mm level below the column-footing intersection in order to measure the strain penetration within the footing. The second strain gage was installed exactly at the level of column-footing intersection to be able to

monitor internal strain and stress at this level since this is the most critical section of the specimen. The third strain gage was mounted on the bar at a level of 300 mm above the column–footing intersection to depict the average strain profile on longitudinal bars within the plastic hinging region.



Figure 3.3 Metal formwork of footing and column before casting

Two strain gages were installed on two opposite legs of two stirrups each, where these stirrups were placed within the plastic hinging region. The first instrumented stirrup was placed at the cross-section of column-footing intersection and the second one was placed at approximately 165 mm above the first instrumented one.

After installation of each strain gage, all gages were cabled and coated with special protective coating against moisture and afterwards they were covered with a thick layer of silicon coating to have protection during concrete placing.

### **3.5.3 Preparation of Reinforcing Cages**

Reinforcing cages of column specimens for both types were prepared in two stages. For a typical test specimen, the cage of footing was prepared first. 4 $\phi$ 20 deformed bars were used as both for the tension and compression reinforcement.  $\phi$ 8 hoops were used as transverse reinforcement.

Longitudinal reinforcing bars of the columns were then assembled with the footing cage. 8 $\phi$ 14 bars were connected to the footing cage one by one, and the stirrups and cross-ties were placed on the column longitudinal reinforcement to form the reinforcing cage of specimen. The ends of the longitudinal bars were bent to provide anchorage for these bars. At the top end, steel bars were bent 90° with an anchorage length of 240 mm and at the bottom end the anchorage length was kept as 1500 mm with a 135° hook at the very end. The peripheral hoops for Type-1 specimens were prepared from  $\phi$ 8 plain bars with 90° hooks. For Type-2 specimens, deformed bars were used and the ends of hoops were bent 135°. An assembled footing and column reinforcement are shown in Figure 3.4 and Figure 3.5 for Type-1 and Type-2 specimens, respectively.

### **3.5.4 Casting and Curing**

Two different methods of concrete casting were put into practice for two different types of specimens. Since it is assumed that the Type-1 specimens are representing the actual columns of buildings which are not complying with the Turkish Earthquake Code criteria in terms of low concrete strength and poor detailing, their concrete mixture was prepared in the lab with a concrete mixer and placed into the formwork manually for producing low strength concrete with deficiencies of poor workmanship in concrete placing. Due to the capacity of concrete mixer, all specimens of this group were cast one by one with three batches

at each casting. For Type-2 specimens, ready-mixed concrete was purchased from a local company and three specimens were cast in parallel at each casting session.



Figure 3.4 Reinforcing cage of a typical Type-1 specimen



Figure 3.5 Reinforcing cage of a typical Type-2 specimen

All specimens were cast vertically. Before the concrete placement, inner surfaces of metal formwork were covered with a thin layer of oil. Eight steel pipes were put in the footing perpendicular to the upper surface in order to create holes through which the specimens will be fixed to the mat foundation with high strength bolts. During the concrete placement, nine standard cylinders were taken from each batch as samples of cast concrete. 8 $\phi$ 24 high strength connection bolts were embedded perpendicularly to the top surface of the column specimens while the concrete was still fresh. The steel head of the loading apparatus was attached and fixed to the specimens by the help of these high strength bolts when the specimens are ready to put on the test setup.

Formworks were not removed at least for seven days. At the seventh day, the pieces at the upper part of the formwork were removed and the specimens were started to be cured by covering them with wet burlap. Type-1 specimens were kept in curing conditions only for fourteen days. On the other hand, Type-2 specimens were cured up to their twenty first day. All specimens were queued for testing after curing. A concrete casting session for Type-2 column specimens with ready-mixed concrete is shown in Figure 3.6.

### **3.6 Test Setup**

With its upgraded facilities, a new set-up for testing the real size reinforced concrete column specimens has been established in METU Structural Mechanics Laboratory and prototype column specimens were tested on this set-up. Loading and the support conditions for specimens on the set-up are shown in Figure 3.7 schematically.



Figure 3.6 Concrete placing for a Type-2 column with ready-mixed concrete

### 3.6.1 Lateral and Axial Loading System

Specimens were placed and tested on a mat foundation fixed to the strong floor with post tensioned bars. A steel head was placed on top of the columns and lateral load was applied by an actuator with hinges attached at both ends, at the level of this steel head. Two steel beams were placed on either side of the specimen parallel to the loading direction and a set of rollers were attached to the upper part of columns in order to prevent the out-of-plane movement of specimens.

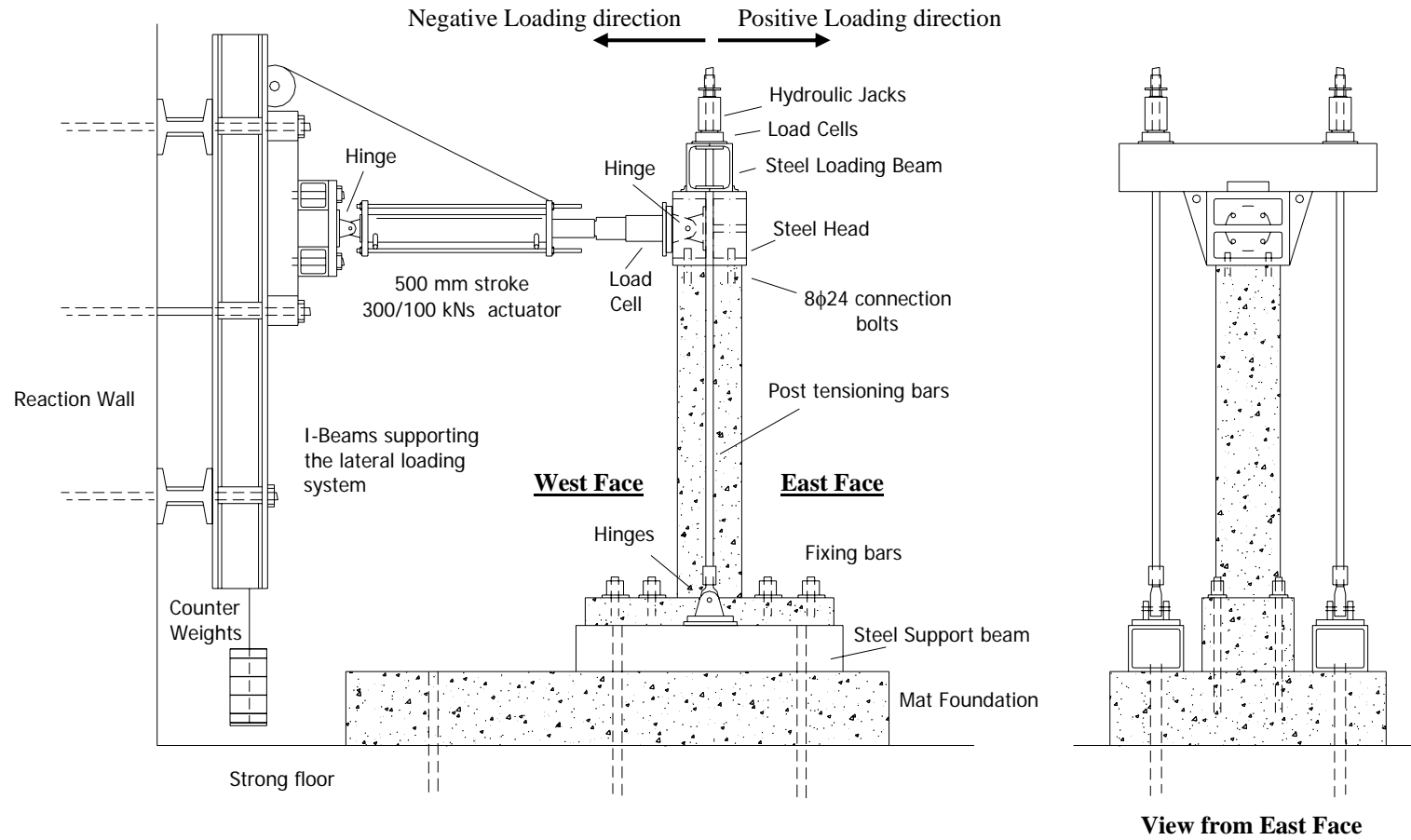


Figure 3.7 Schematic view of test setup

Axial load was applied by a steel loading beam placed horizontally on the steel head, perpendicular to the loading direction. Two high strength steel rods with hinges at footing level were connected both to the steel loading beam and mat foundation and load was applied by post-tensioning of these rods. Axial load level was kept constant during the tests. The general view of test setup is shown in Figure 3.8.



Figure 3.8 General view of the test set-up

### **3.7 Instrumentation**

The response of test specimens under cyclic loading was monitored by using continuously operating instruments and data acquisition system. Applied cyclic lateral load and axial load were measured by calibrated load cells. The deformations

at the tip and within the critical region of column members, and resulting rotations, curvatures and strains in longitudinal reinforcement were also monitored by use of installed dial gages, LVDT's and strain gages.

Nominal locations of instruments and the types of gages are shown in Figure 3.9 and a ready-to-test specimen with all instruments mounted and connected to the data acquisition system is also given in Figure 3.10.

### **3.7.1 Load, Displacement and Strain Measurements**

For lateral load measurements, a 300 kN compression-tension load cell, attached in between the steel head and the actuator, was used. The axial load was monitored and recorded by two separate load cells with capacities of 500 kN's each, placed at both ends of steel loading beam on top of the specimen, with equal distances to the specimen centerline.

Four dial gages on both faces of column specimen along with the loading direction and 350 mm above the surface of footing were attached to measure the rotations and crack openings within the plastic hinging region. Another dial gage with a capacity of 10 mm was also used to measure the rigid body motion of mat foundation. No significant readings were taken from this gage.

Four LVDT's with capacities of 200 mm each were mounted on four corners of the steel head on top of the column to measure the tip displacement of specimen. The reasons for attaching four transducers were to put one reserve gage on each side in case of interruption at any of the primary gages and at the same time to monitor whether there is a twisting or not during the imposition of severe displacement cycles. No significant differences at readings of LVDT couples were measured. More LVDT's with capacities of 200 mm were installed to several levels of specimen to picture the deformation gradient along the height of the specimen.

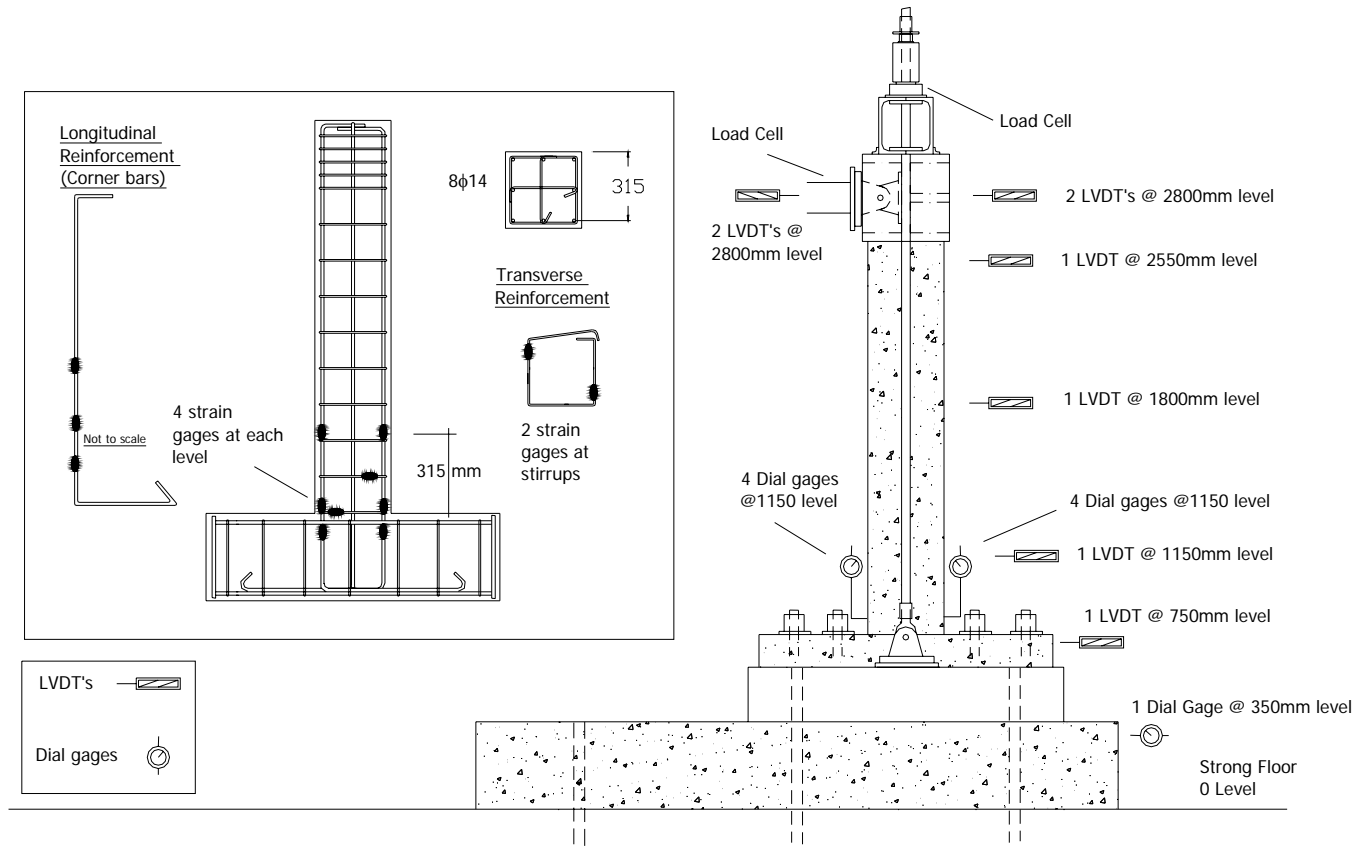


Figure 3.9 Instrumentation of test specimen

Three strain gages were installed on each corner longitudinal bars at different levels to measure the strains in reinforcing bars. Within the plastic hinging zone, two of the stirrups were instrumented with 2 strain gages on each opposite legs. The details and the locations of the installed strain gages were already given in former sections of this chapter.



Figure 3.10 A ready-to-test specimen

### 3.8 Testing Program

Test specimens were placed and fixed on a mat foundation with eight high strength Dywidag bars in front of a reaction wall where an actuator was attached from one end for applying the lateral loads. A massive steel loading head was fixed on top of the specimen to connect this actuator and the high strength rods for applying the lateral and axial load, respectively. All specimens were whitewashed before the installation of instruments so that minor cracks and their propagations would be monitored easily during the tests especially at low amplitude loading levels. After installation of all instruments at different locations of the specimen, they were cabled and connected to the data acquisition system. Calibration checks were done for all these instruments before each test.

Tests were started with the application of axial load on specimens where the level of load was decided from the results of cylinder tests conducted just before the execution of experiments. When the desired axial load level was attained, it was kept constant and lateral load application procedure was initiated. Specimens were tested under displacement controlled loading. Either two-staged constant-amplitude cyclic displacement patterns or multi-staged variable-amplitude loading schemes were imposed on specimens. After imposition of each half cycle, tests were halted for a short period in order to investigate the crack openings and propagations, visible damages such as concrete spalling, crushing, hoop opening or bar buckling, taking pictures of the damaged locations and making notes about the events observed during that half cycle. The imposed displacement protocols for each member of both types of column specimens are given in Table 3.4 in terms of both tip displacements and the corresponding drift ratios.

Tests were terminated either when the end of displacement protocols was reached or a failure was occurred where failure is defined as bar buckling, hoop opening or severe core concrete crushing.

Table 3.4 Displacement protocols imposed on the test specimens

Cycle No	SPECIMENS												
	Type 1						Type 2						
	1P2	2P3	3P3_N0.4	4P4	5P5	6PV1	7P3_U	1D2	2D3	3D4	4D5	5DV1	6DV2
1	35 (1.75)	50 (2.5)	50 (2.5)	70 (3.5)	105 (5.25)	10 (0.5)	50 (2.5)	35 (1.75)	50 (2.5)	70 (3.5)	105 (5.25)	10 (0.5)	17.5 (0.87)
2	35 (1.75)	50 (2.5)	50 (2.5)	70 (3.5)	105 (5.25)	10 (0.5)	50 (2.5)	35 (1.75)	50 (2.5)	70 (3.5)	105 (5.25)	10 (0.5)	17.5 (0.87)
3	35 (1.75)	50 (2.5)	50 (2.5)	70 (3.5)	105 (5.25)	10 (0.5)	50 (2.5)	35 (1.75)	50 (2.5)	70 (3.5)	105 (5.25)	10 (0.5)	17.5 (0.87)
4	35 (1.75)	50 (2.5)	50 (2.5)	70 (3.5)	105 (5.25)	50 (2.5)	50 (2.5)	35 (1.75)	50 (2.5)	70 (3.5)	105 (5.25)	50 (2.5)	35 (1.75)
5	35 (1.75)	50 (2.5)	50 (2.5)	70 (3.5)	105 (5.25)	50 (2.5)	50 (2.5)	35 (1.75)	50 (2.5)	70 (3.5)	105 (5.25)	50 (2.5)	35 (1.75)
6	35 (1.75)	70 (3.5)	70 (3.5)	105 (5.25)	70 (3.5)	50 (2.5)	70 (3.5)	35 (1.75)	50 (2.5)	105 (5.25)	70 (3.5)	50 (2.5)	35 (1.75)
7	35 (1.75)	70 (3.5)	70 (3.5)	105 (5.25)	70 (3.5)	35 (1.75)	70 (3.5)	35 (1.75)	50 (2.5)	105 (5.25)	70 (3.5)	35 (1.75)	50 (2.5)
8	70 (3.5)	70 (3.5)	70 (3.5)	105 (5.25)	70 (3.5)	35 (1.75)	70 (3.5)	70 (3.5)	70 (3.5)	105 (5.25)	70 (3.5)	35 (1.75)	50 (2.5)
9	70 (3.5)	70 (3.5)	70 (3.5)	105 (5.25)	70 (3.5)	35 (1.75)	70 (3.5)	70 (3.5)	70 (3.5)	105 (5.25)	70 (3.5)	35 (1.75)	50 (2.5)
10	70 (3.5)	70 (3.5)	70 (3.5)	105 (5.25)	70 (3.5)	70 (3.5)	150 (7.5)	70 (3.5)	70 (3.5)	70 (3.5)	70 (3.5)	70 (3.5)	70 (3.5)
11	70 (3.5)	105 (5.25)				70 (3.5)	150 (7.5)	70 (3.5)	70 (3.5)			70 (3.5)	70 (3.5)
12	70 (3.5)	105 (5.25)				70 (3.5)		70 (3.5)	70 (3.5)			70 (3.5)	70 (3.5)
13	105 (5.25)	105 (5.25)				35 (1.75)		105 (5.25)	105 (5.25)			35 (1.75)	105 (5.25)
14						35 (1.75)		105 (5.25)	105 (5.25)			35 (1.75)	105 (5.25)
15						35 (1.75)		105 (5.25)	105 (5.25)			35 (1.75)	105 (5.25)
16						105 (5.25)						105 (5.25)	
17						105 (5.25)						105 (5.25)	
18						105 (5.25)						105 (5.25)	

## **CHAPTER 4**

### **TEST RESULTS**

#### **4.1 General**

The results of the conducted tests are presented in detail in this chapter. The response of each test specimen to the imposed displacement histories are given in terms of both lateral (piston) load – tip deflection and base moment – curvature hysteresis curves for non-conforming and conforming column specimens in Section 4.2, respectively. Note that the piston load is not equal to the lateral load acting on the specimen. Lateral load is obtained from piston load after correcting it for the lateral component of the tension in the steel-rod used for applying the axial force. The corrected lateral force-displacement relations are shown in the next chapter. The history of each test with its crucial stages such as first cracking, spalling of cover concrete, bar buckling etc. are summarized and the state of column at an instant of testing is illustrated by a picture of the specimen.

Curvatures at a section 350 mm above the base of column were measured by four dial gages installed on East and West faces (see Figure 3.7) of each column specimen. Average of readings of these dial gages on each surface were used for the calculation of curvatures. Nominal locations of the gages are depicted in Figure 4.1.

Base moments were simply calculated by multiplying the applied lateral load by the distance between the base and tip of specimens.

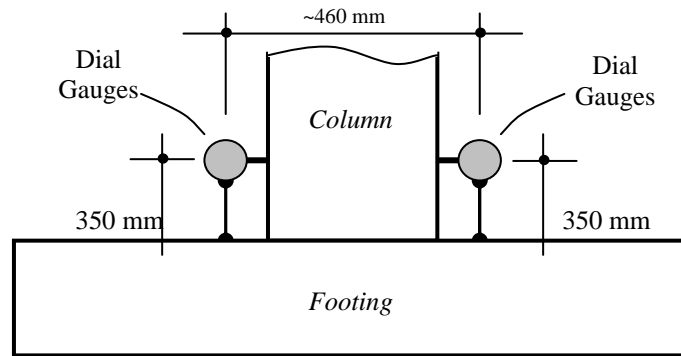


Figure 4.1 Details of curvature measurements

## 4.2 Test Observations and Response of Column Specimens

Hysteretic responses of reinforced concrete column specimens to the imposed displacement protocols are presented in this section. The applied lateral load-top displacement responses of each specimen are given along with the base moment-curvature response of the same specimen. Imposed displacement histories with their pattern and sequence are also explained in detail for both types of specimens. With their high  $a/d$  ratios, flexure dominant failure modes were observed for all tested specimens of both types.

### 4.2.1 Non-Conforming Specimens (Type-1)

All Type-1 specimens were subjected to different cyclic displacement histories in order to observe the effect of low cycle fatigue on strength and energy dissipation capacity, except specimens 7P3\_U and 3P3\_N0.4. These specimens were tested under the same displacement protocol with specimen 2P3 in order to compare their responses for different variables such as higher axial load ratio and lack of bond between longitudinal bars and concrete. Since all Type-1 specimens were poorly detailed and cast with low strength concrete, severe damage was observed especially at their critical regions at the end of tests.

#### 4.2.1.1 Specimen 1P2

The first specimen of the non-conforming columns was tested under a displacement protocol shown in Figure 4.2. The compressive strength of concrete on the day of testing was 13.5 MPa. The column specimen was subjected to a constant axial load of 340 kN which corresponds to an axial load ratio of  $0.206A_g f_{ck}$ .

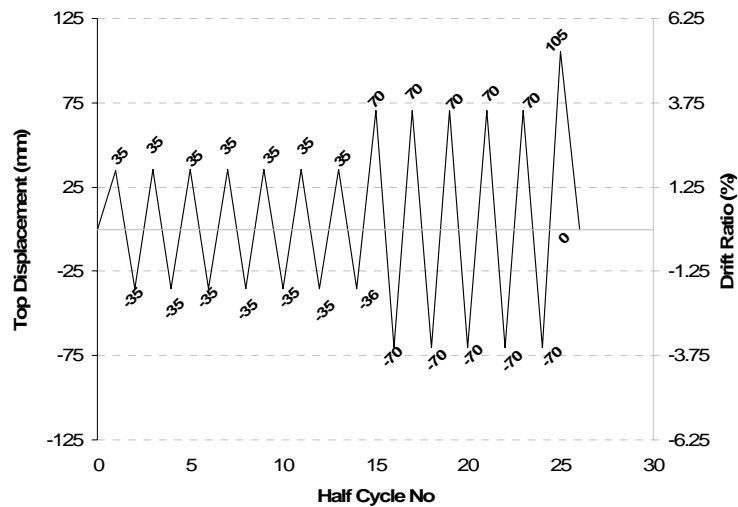


Figure 4.2 Displacement history imposed on Specimen 1P2

At the first stage of loading, seven cycles of top displacement reversals with amplitude of 35 mm (1.75% of drift ratio) were imposed on the specimen. At the second stage, the amplitude of imposed displacement was increased to 70 mm (3.5% of drift ratio) and 5 full cycles were applied. At the last stage, it was planned to impose 105 mm (5.25% of drift ratio) amplitude cycles but after the first positive half cycle, the acquisition system has failed so the test was terminated.

Lateral load versus top displacement graphics of specimen 1P2 is given in Figure 4.3. The response of specimen 1P2 in terms of base moment versus curvature is also given in Figure 4.4.

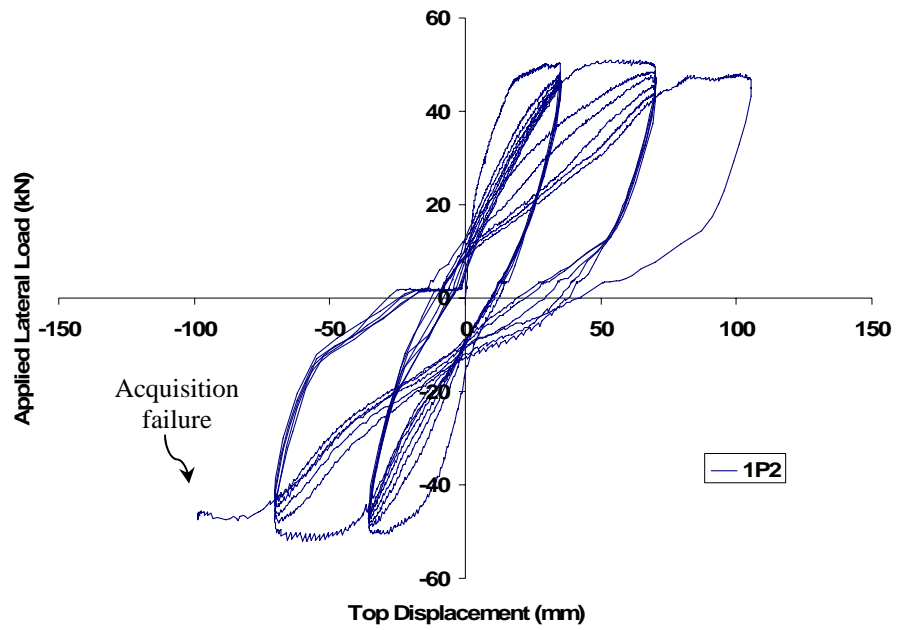


Figure 4.3 Lateral load - top displacement response of Specimen 1P2

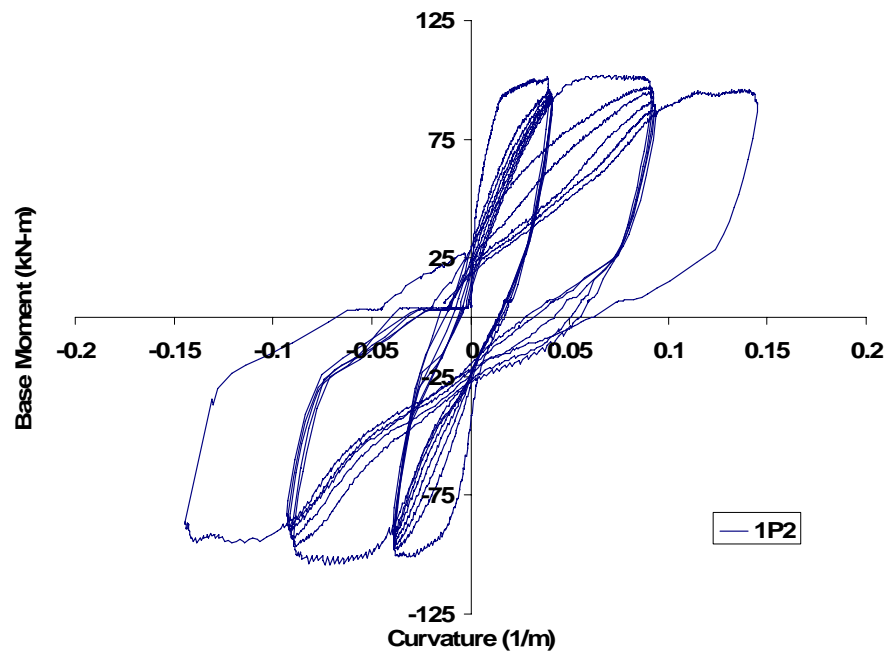


Figure 4.4 Base moment-curvature response of Specimen 1P2

First cracking of concrete was observed during the first positive cycle at 2 cm above the column-footing intersection on the West face of specimen when the applied lateral load was about 25 kN. Additional flexural cracks formed at several locations extending 45-50 cm above from the bottom of column during this cycle. In the proceeding cycles, these cracks propagated to the North and South faces of column reaching almost mid section. At the fourth negative half cycle, the concrete cover at the West corners of column started crushing and spalling. At the eighth positive half cycle, crushing of cover concrete at East face was observed. Spalling of concrete initiated on this face at the eighth negative half cycle making the longitudinal reinforcement visible. At the ninth negative half cycle, the cover concrete on West face crushed and spalled totally up to the level of 20 cm from the footing face. The picture of the specimen at this stage of testing is shown in Figure 4.5. At the tenth positive half cycle, the buckling of longitudinal bars was observed. The test was terminated due to an acquisition failure after conducting three more cycles.

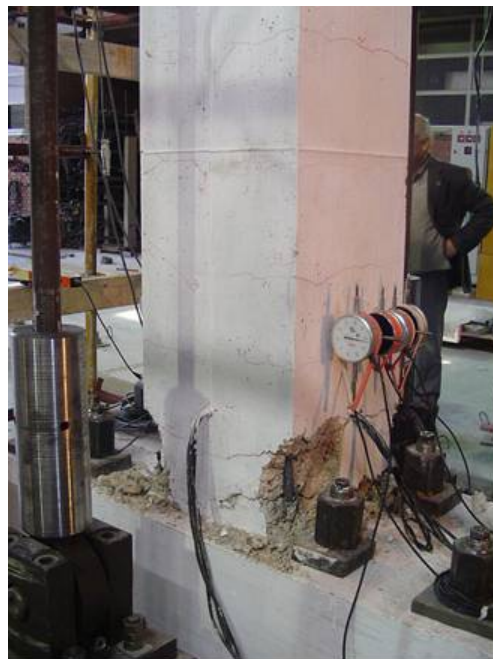


Figure 4.5 Onset of bar buckling, North-West faces of Specimen 1P2

### 4.2.1.2 Specimen 2P3

The second specimen of the non-conforming columns was tested under a displacement protocol shown in Figure 4.5. The compressive strength of concrete on the day of testing was 12.2 MPa. Column specimen was subjected to a constant axial load of 302 kN which corresponds to an axial load ratio of  $0.202A_g f_{ck}$ .

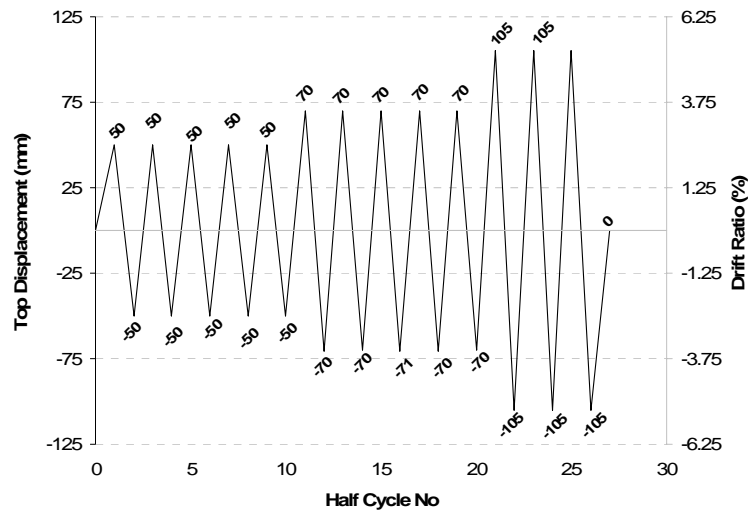


Figure 4.6 Displacement history imposed on Specimen 2P3

The specimen was initially subjected to 5 cycles of displacement reversals at an amplitude of 50 mm at top (2.5% of drift ratio). After the initial stage, test was continued with top displacement reversals of 70 mm (3.5% of drift ratio) for 5 full cycles. At the last stage, the specimen was subjected to top displacement amplitude of 105 mm (5.25 drift ratio) until failure which occurred at the end of the third cycle of this stage.

Applied lateral load versus top displacement graphics of specimen 2P3 is shown in Figure 4.7. The response of specimen 2P3 in terms of base moment versus curvature is also given in Figure 4.8.

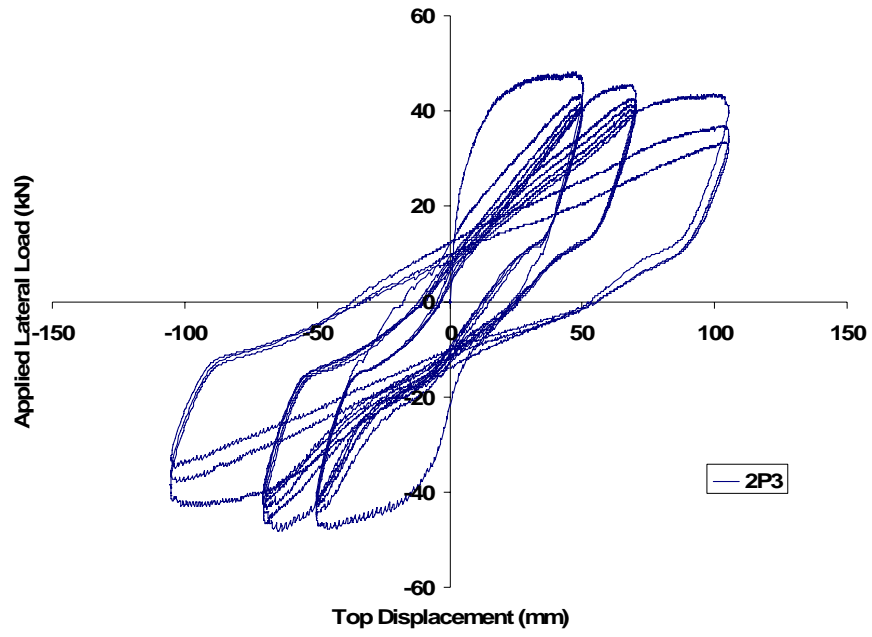


Figure 4.7 Lateral load - top displacement response of Specimen 2P3

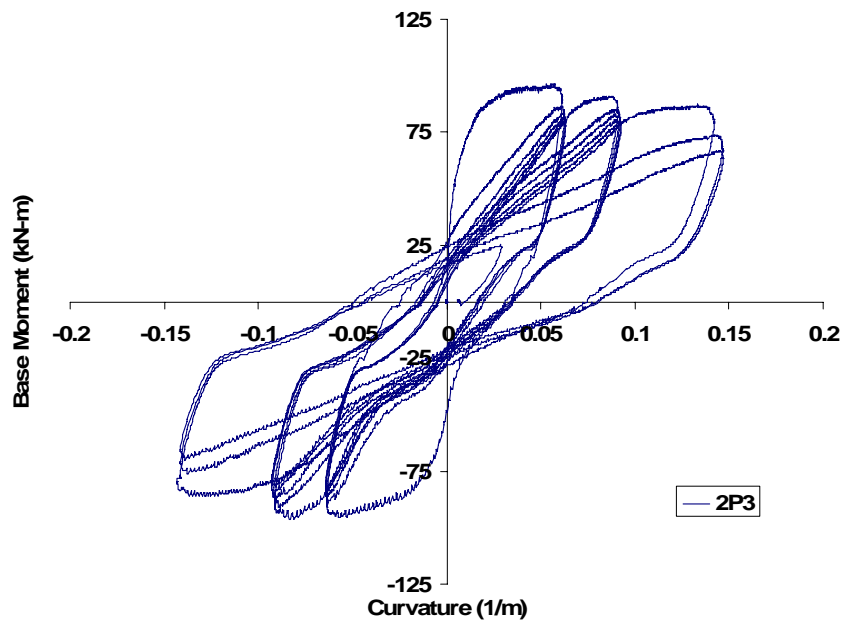


Figure 4.8 Base moment-curvature response of Specimen 2P3

First tensile crack was observed at the base of the column when the applied lateral load was about 24 kN. Horizontal flexural cracks were spread to a level of 700 mm from the column base at almost every tie level during the cycle. The measured crack width when maximum top displacement was attained at the first positive half cycle (50 mm) was approximately 5 mm. At the second cycle crushing of cover concrete at corners were initiated. Vertical cracks along with the corner longitudinal bars appeared at the third cycle and spalling of concrete was observed at corners. Cracks at the base of column widened and longitudinal reinforcement at the base was visible at the seventh cycle. At the eighth cycle, bar buckling on corner longitudinal bars was observed. The view of the specimen at this cycle of the test is shown in Figure 4.9.



Figure 4.9 Buckling of longitudinal bars, North-West faces of Specimen 2P3

### 4.2.1.3 Specimen 3P3\_N0.4

The third specimen of non-conforming columns was tested under a displacement protocol shown in Figure 4.10 which is identical with Specimen 2P3 for the first two stages of displacement reversals. The compressive strength of concrete on the day of testing was 13.1 MPa. The column specimen was subjected to a constant axial load of 640 kN which corresponds to an axial load ratio of  $0.40A_g f_{ck}$ .

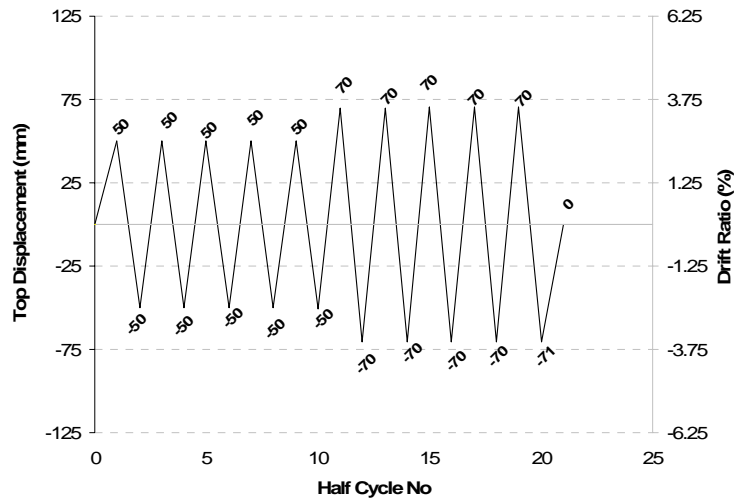


Figure 4.10 Displacement history imposed on Specimen 3P3\_N0.4

Lateral load versus top displacement graph of specimen 3P3\_N0.4 is given in Figure 4.11. The response of specimen 3P3\_N0.4 in terms of base moment versus curvature is also shown in Figure 4.12.

First tensile crack was observed at the column base when the applied lateral load was about 43 kN and the top displacement was 15 mm. Cracks were spread up to a level of 450 mm above the column base with approximately 10-15 cm spacing. Crushing at cover concrete for a region of 200 mm above the column base occurred when the maximum top displacement of this cycle attained.

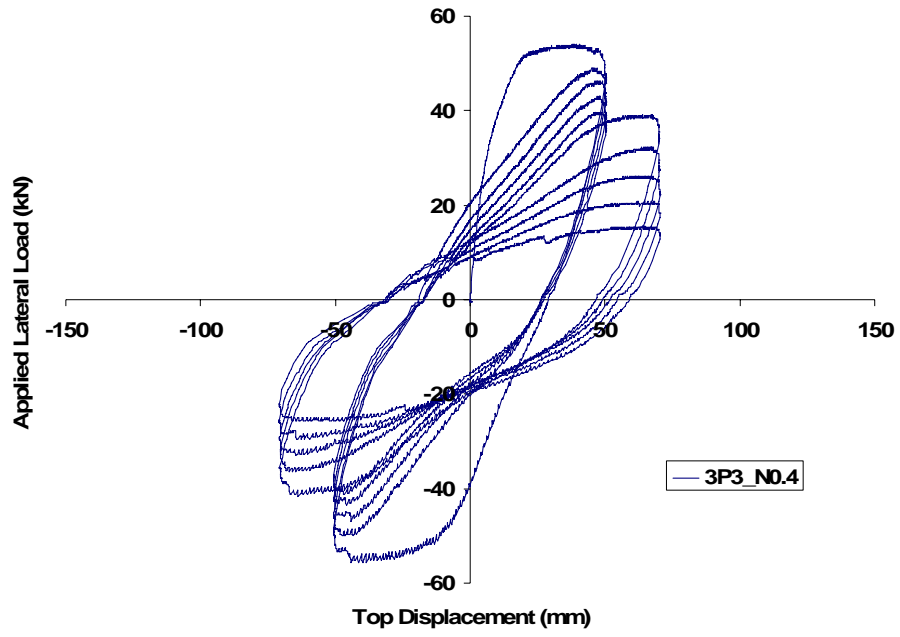


Figure 4.11 Lateral load - top displacement curve of Specimen 3P3\_N0.4

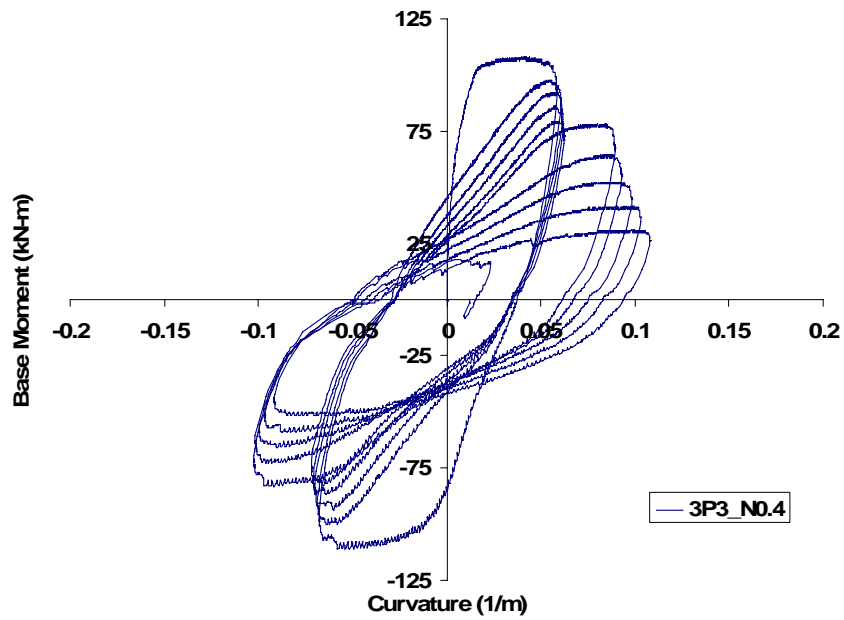


Figure 4.12 Base moment-curvature response of Specimen 3P3\_N0.4

At the second cycle, crack widths increased and some new cracks formed, starting from 45-50 cm above column base up to 80-90 cm along the column height. Spalling of cover concrete occurred where crushing in the former half cycle initiated. Within the same cycle, vertical cracks formed and after spalling of cover concrete at corners, longitudinal bars became visible. Buckling of longitudinal reinforcement also observed at the second negative half cycle. At the fifth cycle, cover concrete from the level of column base up above the second tie is totally spalled and all three longitudinal bars on compression side buckled. At the sixth cycle, buckling of longitudinal bars increased and core concrete crushed. After spalling of loose concrete at the ninth cycle, tie opening is observed. Test was terminated at this stage after one more cycle. The view of specimen at the end of test 3P3\_N0.4 is shown in Figure 4.13.



Figure 4.13 View of the specimen at the end of test, North-West faces of Specimen 3P3\_N0.4

#### 4.2.1.4 Specimen 4P4

The fourth specimen of non-conforming columns was tested under a displacement protocol shown in Figure 4.14. The compressive strength of concrete on the day of testing was 12.4 MPa. Column specimen was subjected to a constant axial load of 308 kN which corresponds to an axial load ratio of  $0.20A_g f_{ck}$ .

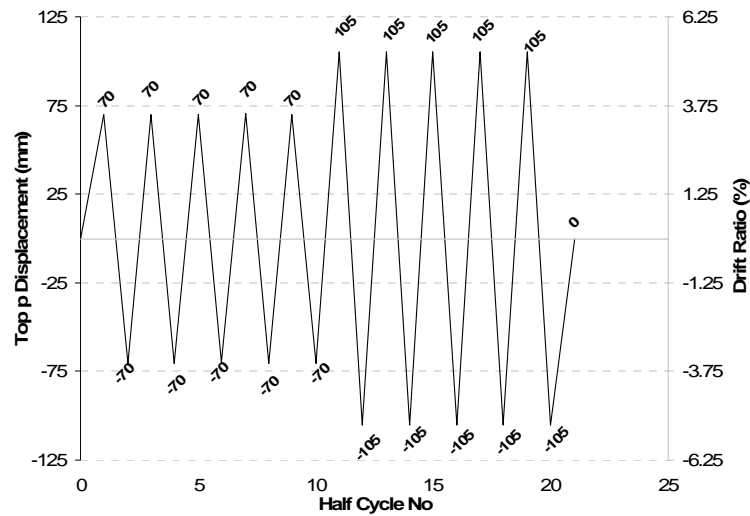


Figure 4.14 Displacement history imposed on Specimen 4P4

The testing was started with 5 full cycles at amplitude of 70 mm (3.5% of drift ratio). At the second stage, the amplitude of displacement cycles was increased to 105 mm (5.25% of drift ratio) and 5 full cycles of loading was conducted which lead to the failure of specimen.

Lateral load versus top displacement graphics of specimen 4P4 is given in Figure 4.15. The response of specimen 4P4 in terms of base moment versus curvature is shown in Figure 4.16.

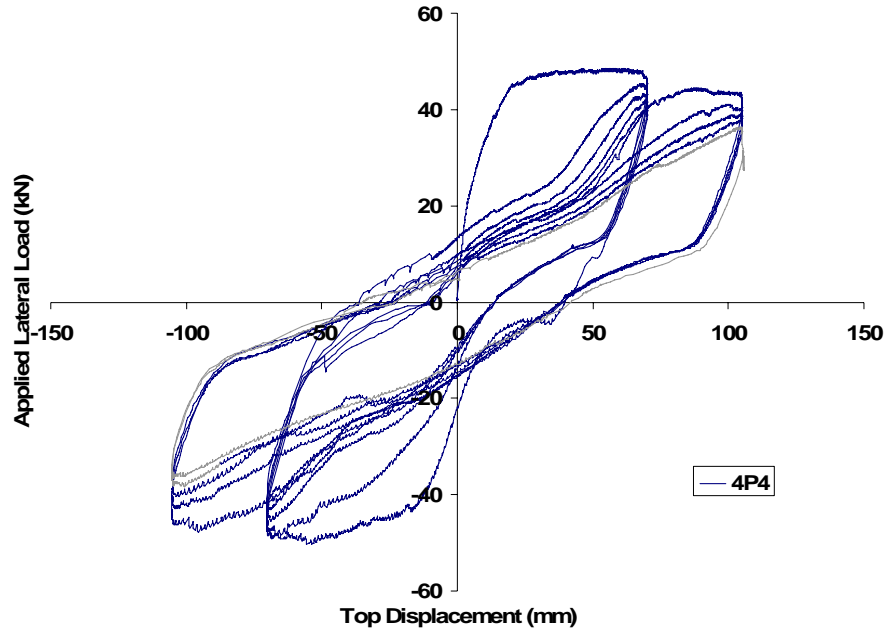


Figure 4.15 Lateral load - top displacement relation of Specimen 4P4

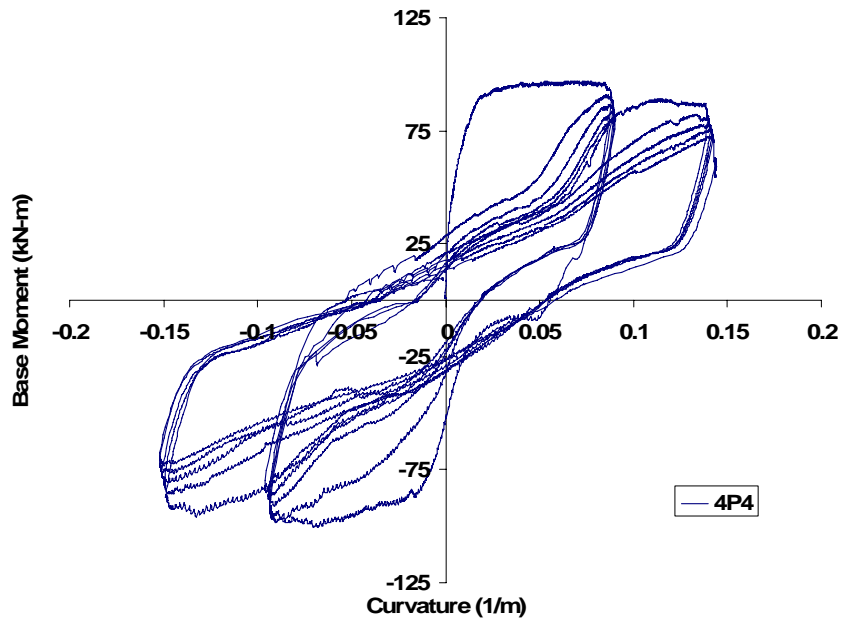


Figure 4.16 Base moment-curvature response of Specimen 4P4

First tensile crack was observed at the base of column when the applied lateral load was 22 kN. Horizontal flexural cracks formed and spread up to a level of 80 cm from the column base at almost every tie level during this first cycle. Crack width at the base was measured as approximately 7 mm when the maximum top displacement (70 mm) was attained. At the second cycle, crushing of cover concrete at corners was initiated and vertical cracks along the corner longitudinal bars appeared. Spalling of concrete at corners was also observed in this cycle. Cracks at the base of column became wider and longitudinal reinforcement at the base was visible at the third cycle. Bar buckling on corner longitudinal reinforcement was observed when the maximum displacement of this cycle was attained within this cycle. View of the specimen at the end of test is shown in Figure 4.17.

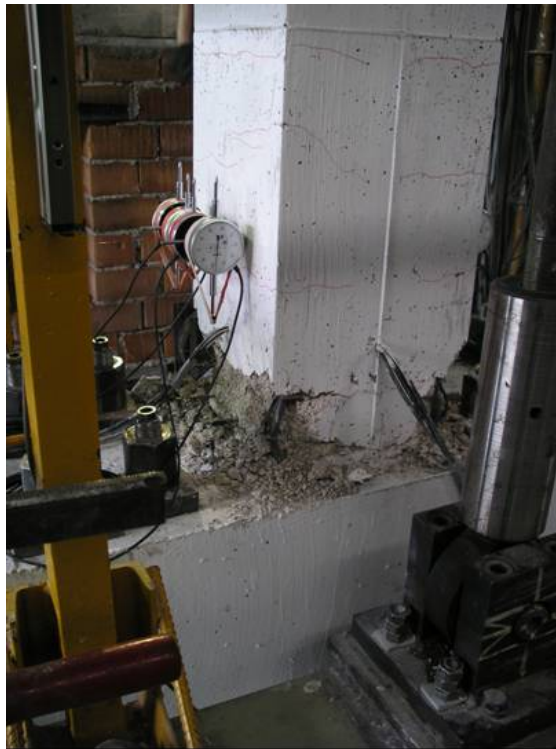


Figure 4.17 The North-East faces of Specimen 4P4 at the end of test

#### 4.2.1.5 Specimen 5P5

The fifth specimen of non-conforming columns was tested under a displacement protocol shown in Figure 4.18. The compressive strength of concrete on the day of testing was 11.4 MPa. Column specimen was subjected to a constant axial load of 300 kN which corresponds to an axial load ratio of  $0.21A_g f_{ck}$ .

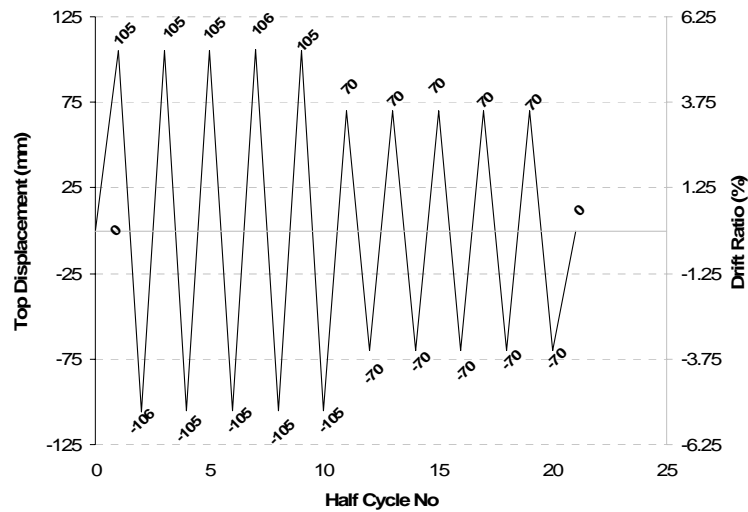


Figure 4.18 Displacement history imposed on Specimen 5P5

The specimen was loaded with top displacement reversals of 105 mm (5.25% of drift ratio) at the initial stage of testing. After 5 full cycles, the specimen was further subjected to 5 more cycles of displacement reversals with lowered amplitude of 70 mm (3.5% of drift ratio). This pattern of displacement history was derived by changing the sequence of first two stages of imposed displacement protocol of Specimen 4P4.

Lateral load versus top displacement graphics of specimen 5P5 is given in Figure 4.19. The response of specimen 5P5 in terms of base moment versus curvature is shown in Figure 4.20.

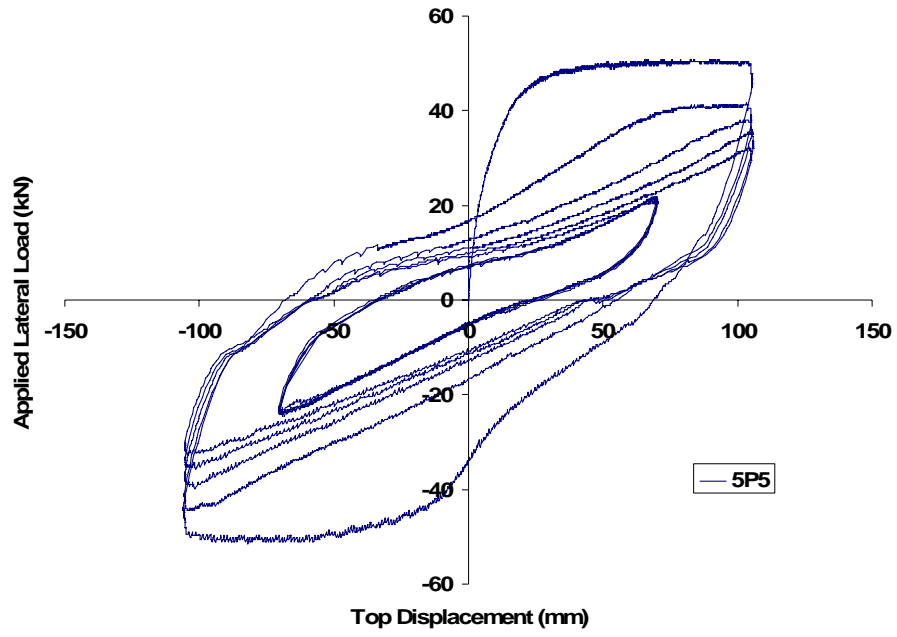


Figure 4.19 Lateral load - top displacement response of Specimen 5P5

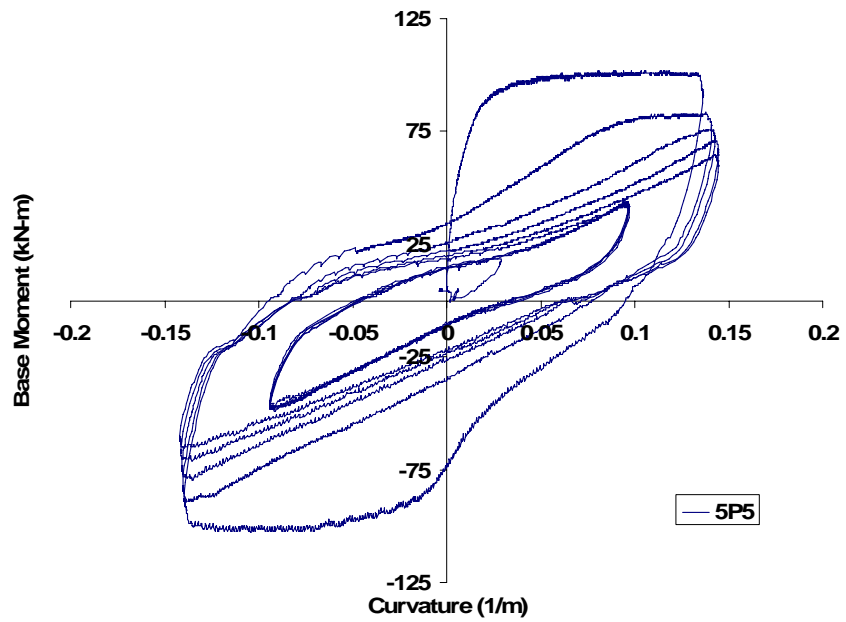


Figure 4.20 Base moment-curvature response of Specimen 5P5

Since it is the most severe loading scheme throughout the testing program with the imposed displacement amplitude of 105 mm (5.25% of drift ratio) at the initial loading stage, all important observations for specimen response starting with first tensile crack till buckling of longitudinal bars were observed during the 1<sup>st</sup> and 2<sup>nd</sup> full cycles. At the end of first full cycle, wide cracks at the column base were formed and cover concrete crushed. The crack width at base of column when maximum top displacement attained was measured as approximately 10 mm. Spalling of cover concrete and buckling of longitudinal bars followed at the end of second full cycle. The view of Specimen 5P5 at the end of the test is shown in Figure 4.21.



Figure 4.21 End of test view of Specimen 5P5

#### 4.2.1.6 Specimen 6PV1

The sixth specimen of non-conforming columns was tested under a displacement protocol with variable amplitudes shown in Figure 4.22. The compressive strength of concrete on the day of testing was 12.5 MPa. Column specimen was subjected to a constant axial load of 304 kN which corresponds to an axial load ratio of  $0.20A_g f_{ck}$ .

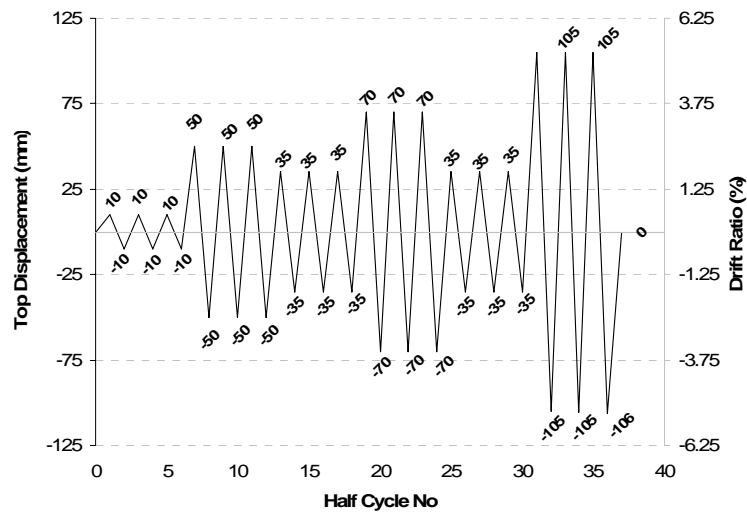


Figure 4.22 Displacement history imposed on Specimen 6PV1

The test was initiated by imposing three elastic cycles at top displacement amplitude of 10 mm (0.5% of drift ratio). The sequence for the rest of the displacement protocol was constituted by randomly composing the initial stages of displacement histories of the previously tested specimens. Hence it is considered as a variable-amplitude displacement history. At each stage of loading, 3 full cycles were imposed on the specimen.

Lateral load versus top displacement graphics of specimen 6PV1 is given in Figure 4.23. The response of specimen 6PV1 in terms of base moment versus curvature is shown in Figure 4.24.

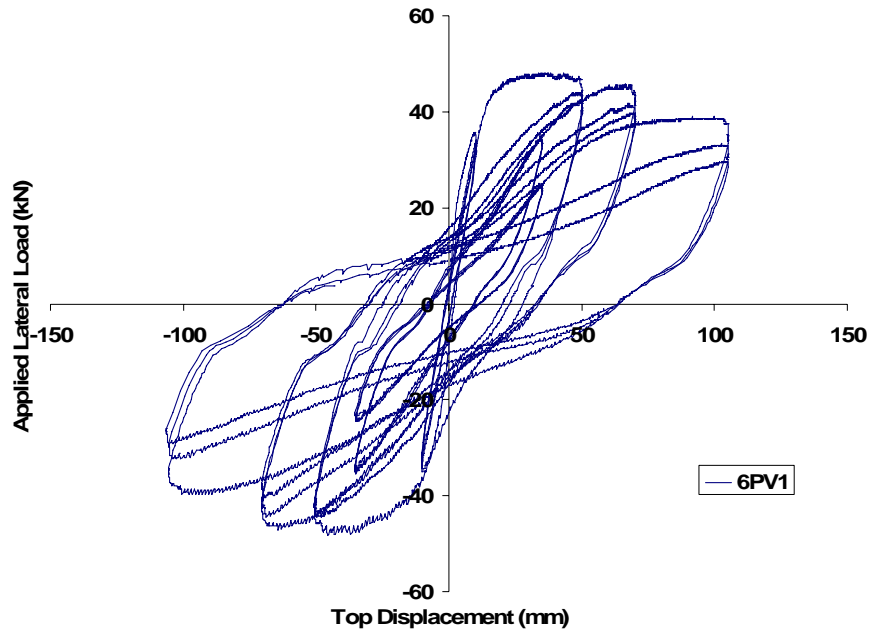


Figure 4.23 Lateral load - top displacement response of Specimen 6PV1

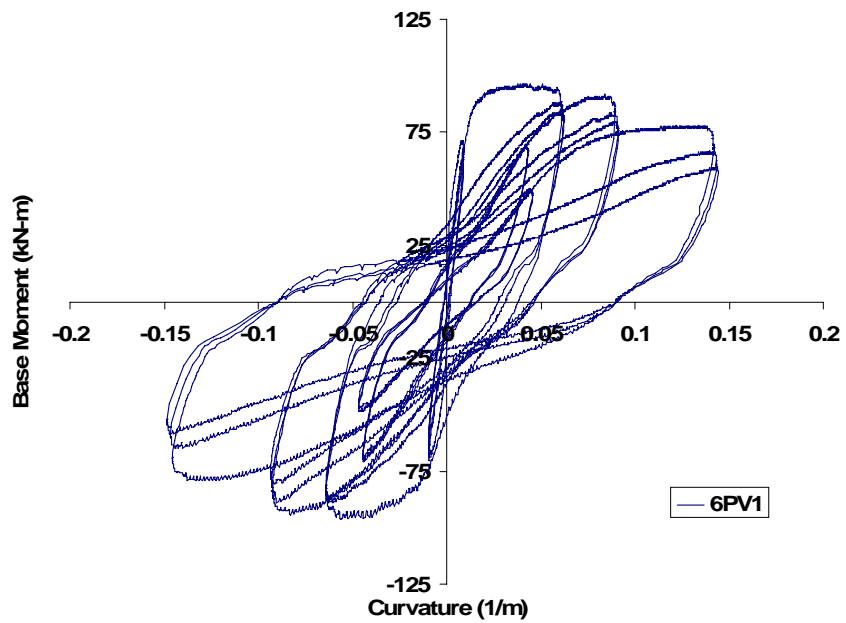


Figure 4.24 Base moment-curvature response of Specimen 6PV1

First cracking of concrete was observed at the first positive cycle when the applied lateral load was about 22 kN. Additional hairline-like flexural cracks formed at several locations up to 45-50 cm above the bottom of column during the elastic cycles of the first stage. In the following cycles, these cracks propagated to the North and South faces of column. At the second stage, the concrete cover at column corners started crushing and spalling. At the third stage where the amplitude of imposed displacement was decreased, no significant event observed on the specimen behavior. At the fourth stage, the cover concrete spalled totally up to the level of 20 cm from the footing face and bar buckling initiated. At the fifth reduced stage, no significant new event was observed. At the last and most severe stage core concrete crushed and bar buckling occurred. The picture of the specimen at the last stage of testing is shown in Figure 4.25.



Figure 4.25 North face of Specimen 6PV1 at the last stage of loading

#### 4.2.1.7 Specimen 7P3\_U

The seventh specimen of non-conforming columns was tested under the displacement protocol shown in Figure 4.26. The compressive strength of concrete on the day of testing was 13.2 MPa. Column specimen was subjected to a constant axial load of 322 kN which corresponds to an axial load ratio of  $0.20A_g f_{ck}$ .

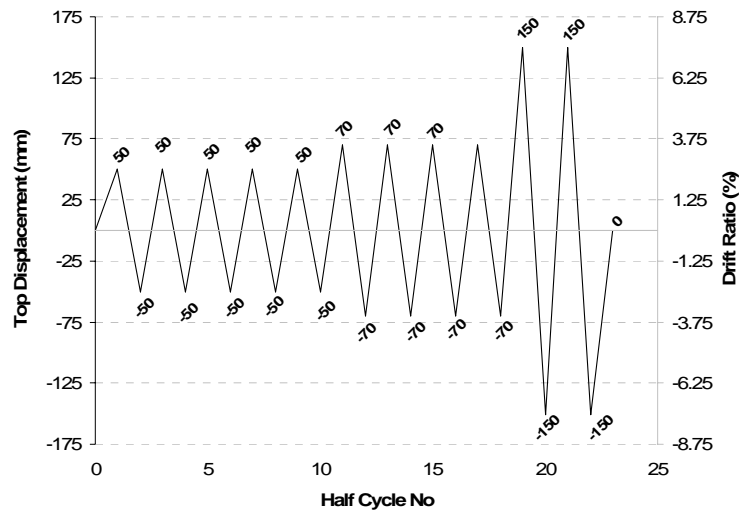


Figure 4.26 Displacement history imposed on Specimen 7P3\_U

This special unbonded specimen was tested under the same displacement protocol of Specimen 2P3 for the first two stages of displacement reversals in order to compare the responses of these two pair of specimens with different bonding conditions. At the third and last stage of loading, the amplitude of imposed displacements was increased to 150 mm (7.5% of drift ratio) for observing the specimen behavior under severe displacement demand.

Lateral load versus top displacement graphics of specimen 7P3\_U is given in Figure 4.27. The response of specimen 7P3\_U in terms of base moment versus curvature is shown in Figure 4.28.

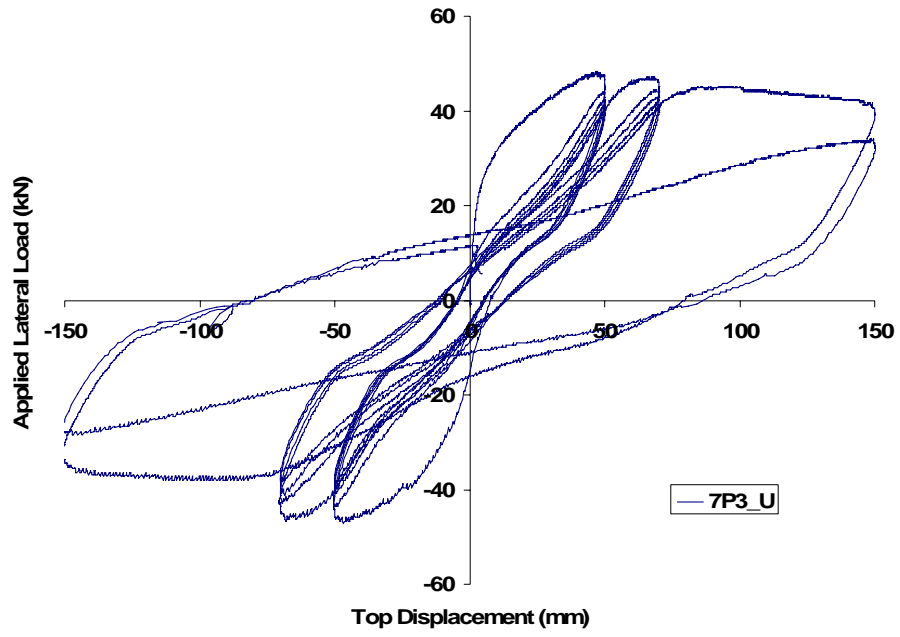


Figure 4.27 Lateral load - top displacement curve of Specimen 7P3\_U

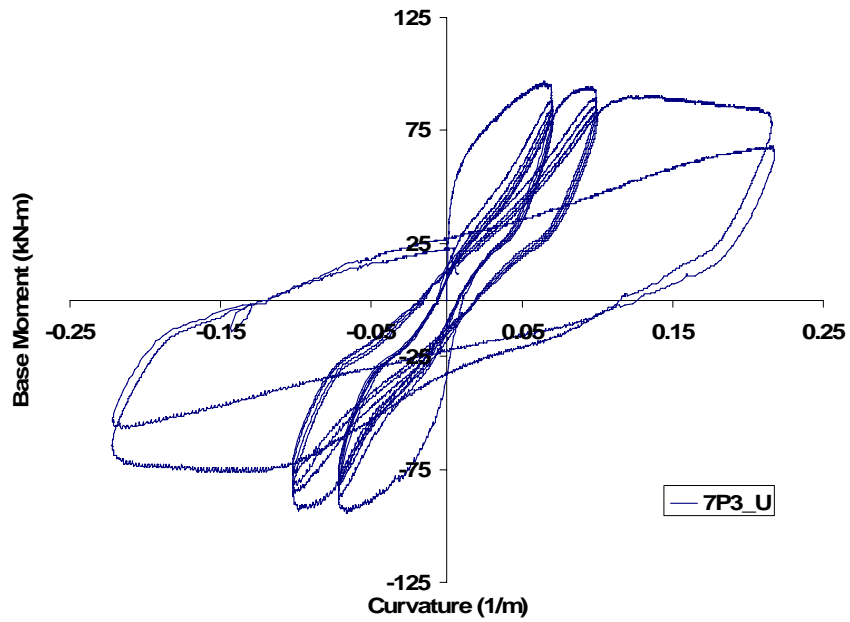


Figure 4.28 Base moment-curvature response of Specimen 7P3\_U

Since the bond between concrete and longitudinal reinforcement is prevented along the column height for Specimens 7P3\_U, only one single crack was formed at about 5 cm above the base and this crack was extended to full depth during the first stage of loading. No other flexural cracks were observed on the specimen. The crack width was measure as approximately 6-8 mm when maximum top displacement was attained at the first positive cycle. The single crack opening on East face of specimen after the 1<sup>st</sup> full cycle is shown in Figure 4.29. At the 2<sup>nd</sup> cycle, vertical cracks were formed along the longitudinal reinforcement at the column base at corners and crushing of concrete initiated during the following cycles. At the 7<sup>th</sup> cycle, crushing and spalling of cover concrete extended up to 25 cm from the column base which initiated bar buckling at the following cycles.



Figure 4.29 Crack opening at the East face of Specimen 7P3\_U

#### **4.2.2 Conforming Specimens (Type-2)**

Type-2 column specimens were tested under similar displacement protocols applied to Type-1 columns in order to form pairs of specimens with common testing



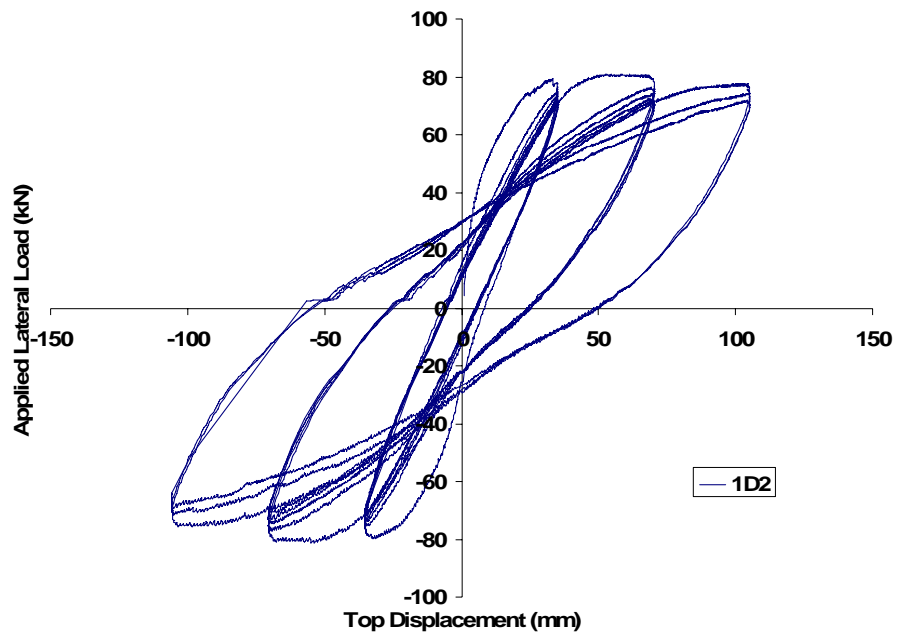


Figure 4.31 Lateral load - top displacement response of Specimen 1D2

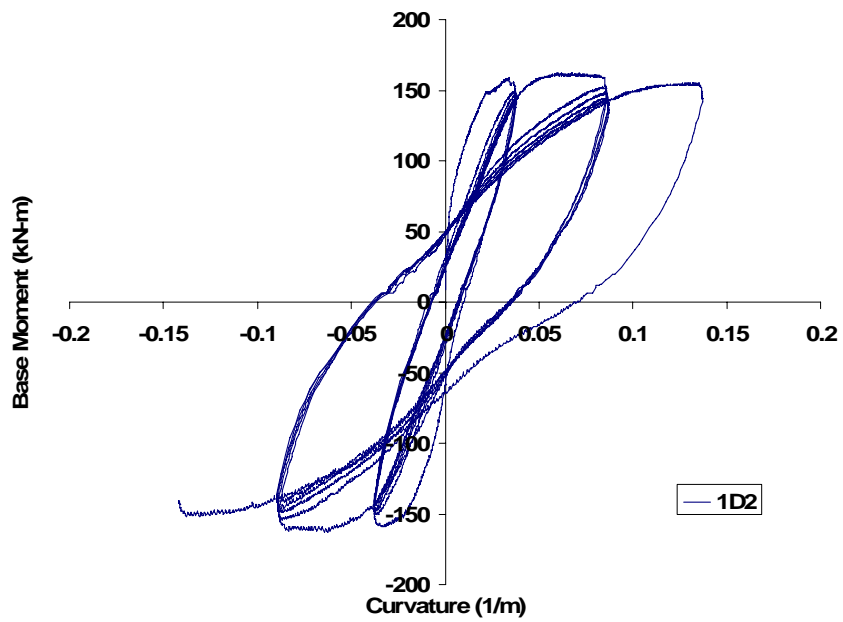


Figure 4.32 Base moment-curvature response of Specimen 1D2

First tension crack appeared during the first positive half cycle at the column-footing intersection when the applied lateral load was about 45 kN. Several flexural cracks formed along the column height up to a level of 70-80 cm from the base and these cracks propagated on the North and South faces during the cycle. A few additional flexural cracks were formed and the former ones were widened during the following cycle. The crack pattern after the 2<sup>nd</sup> cycle is shown in Figure 4.33. At the third negative cycle, crushing at cover concrete was observed at the column base in the North-West corner. At the fourth cycle, the cracks were spread up to a level of 120 cm. At the fifth positive cycle, concrete at East face started to crush and spall. By the start of second stage at the eighth cycle, the crushing and spalling at cover concrete became more severe. At the eighth negative cycle, a vertical crack along the corner longitudinal reinforcement at the North-West side was observed. Longitudinal reinforcement became visible at the ninth cycle at the bottom of column. Spalling of cover concrete extended up to 20 cm from the base at the corners. Buckling of longitudinal bars was initiated at the 13<sup>th</sup> cycle of the last stage and all corner bars buckled during the following cycles.

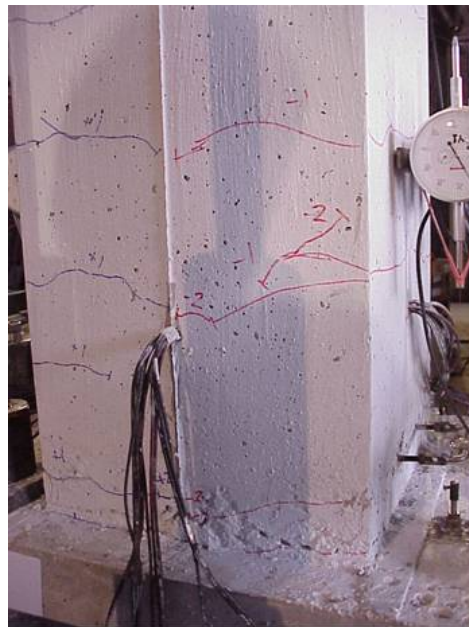


Figure 4.33 Crack pattern after the 2<sup>nd</sup> full cycle, South face of Specimen 1D2

#### 4.2.2.2 Specimen 2D3

The second specimen of the Type-2 conforming columns was tested under a displacement protocol shown in Figure 4.34. The compressive strength of concrete on the day of testing was 25.9 MPa. Column specimen was subjected to a constant axial load of 632 kN which corresponds to an axial load ratio of  $0.20A_g f_{ck}$ .

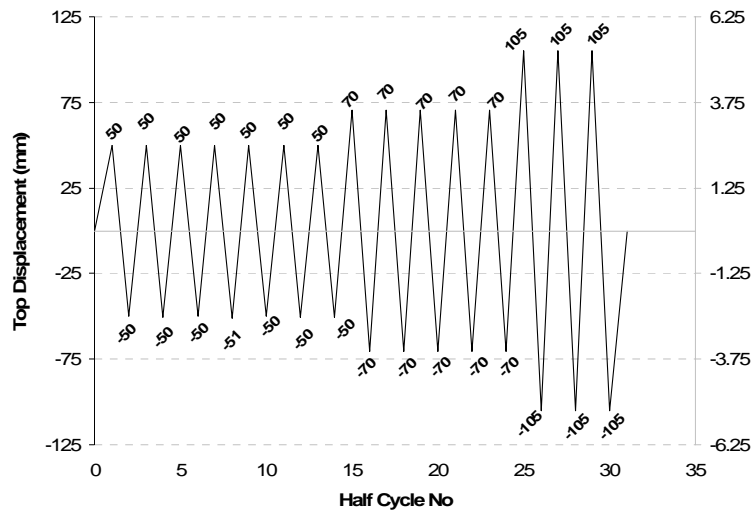


Figure 4.34 Displacement history imposed on Specimen 2D3

Seven cycles of displacement reversals with amplitude of 50 mm (2.5% of drift ratio) were imposed on the specimen at the first stage.

Lateral load versus top displacement graphics of specimen 2D3 is given in Figure 4.35. The response of specimen 2D3 in terms of base moment versus curvature is shown in Figure 4.36.

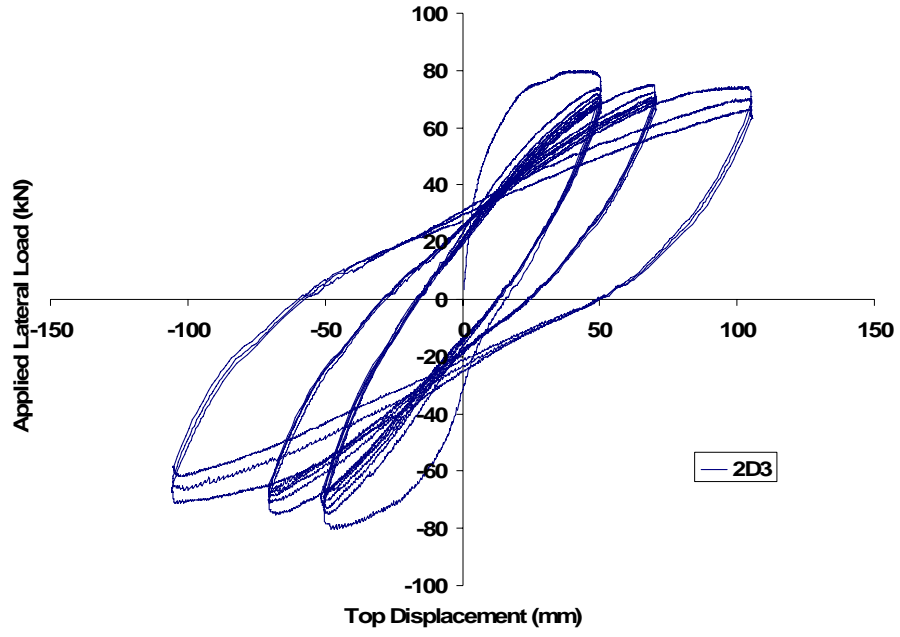


Figure 4.35 Lateral load - top displacement curves of Specimen 2D3

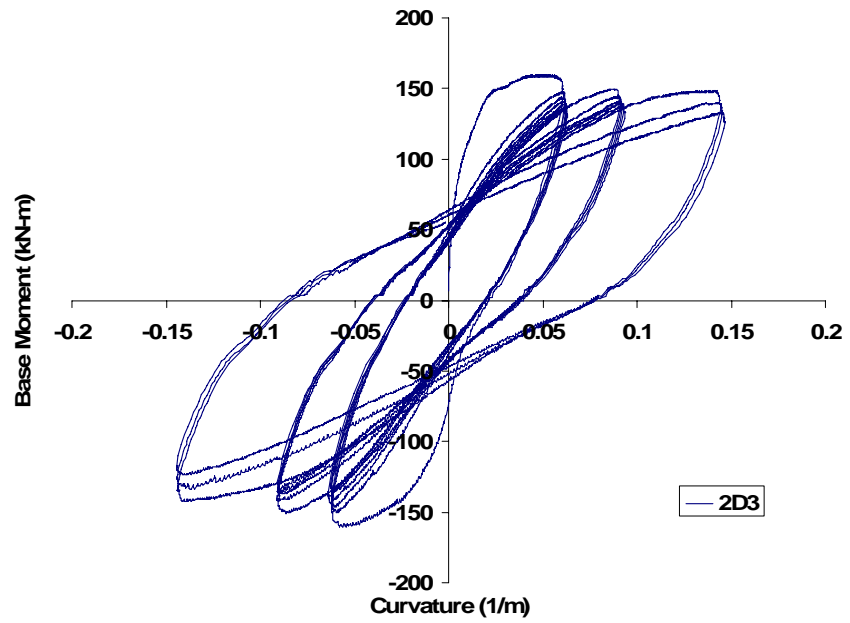


Figure 4.36 Base moment-curvature response of Specimen 2D3

First tension crack appeared during the first positive half cycle at column-footing intersection when top displacement was about 10 mm. Several flexural cracks were formed along the column height up to a level of 60 cm from the bottom at almost every tie level and these cracks propagated on the North and South faces during the cycle. At the second positive cycle, crushing of cover concrete was observed at the column base. At the third cycle, concrete at the East face started to crush and spall and ties were exposed. Crack pattern of specimen at the 5<sup>th</sup> cycle is given in Figure 4.37. With the start of second stage at the eighth cycle, crushing and spalling of cover concrete became more severe. Longitudinal reinforcement buckled at the ninth cycle.

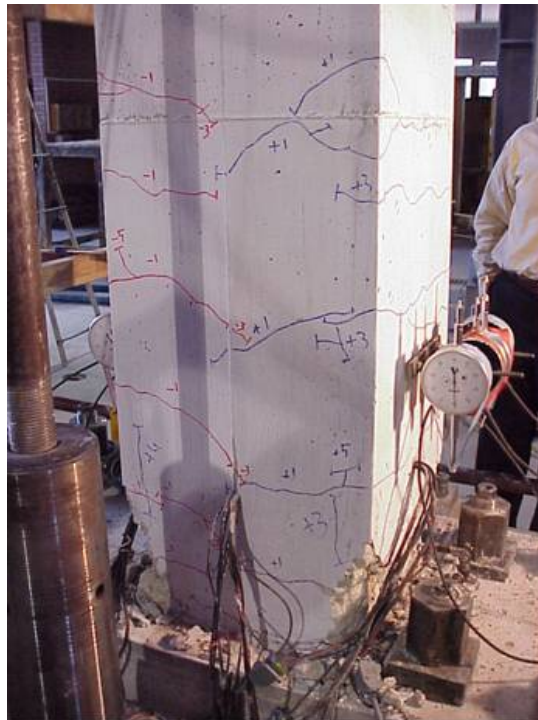


Figure 4.37 Crack pattern after the 5<sup>th</sup> cycle at the North face of Specimen 2D3

### 4.2.2.3 Specimen 3D4

The third specimen of the conforming columns was tested under a displacement protocol shown in Figure 4.38. The compressive strength of concrete on the day of testing was 27.6 MPa. Column specimen was subjected to a constant axial load of 674 kN which corresponds to an axial load ratio of  $0.20A_g f_{ck}$ .

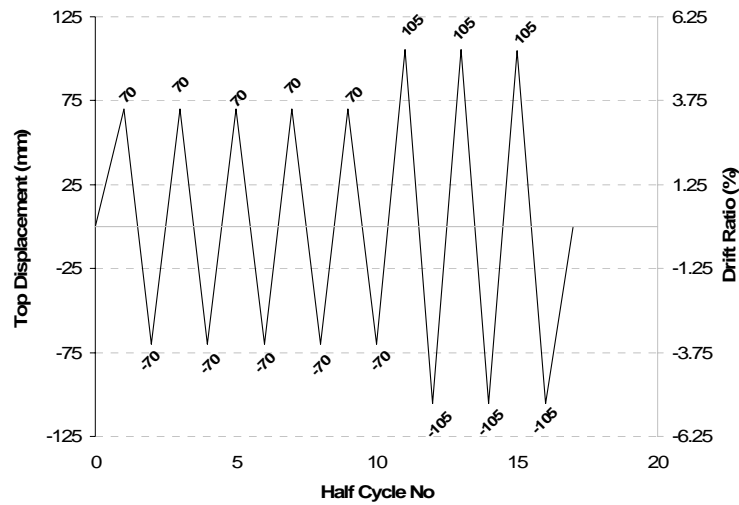


Figure 4.38 Displacement history imposed on Specimen 3D4

At the initial stage, the specimen was subjected to 5 cycles with top displacement amplitude of 70 mm (3.5% of drift ratio). The testing was planned to continue with another 5 cycles at 105 mm amplitude (5.25% drift ratio) at the second stage. But at the end of eighth full cycle, due to a problem in the loading system, the test was terminated when the specimen was almost at the onset of failure with its degraded load carrying capacity down to 75% of initial.

Lateral load versus top displacement graphics of specimen 3D4 is given in Figure 4.39. The response of specimen 3D4 in terms of base moment versus curvature is shown in Figure 4.40.

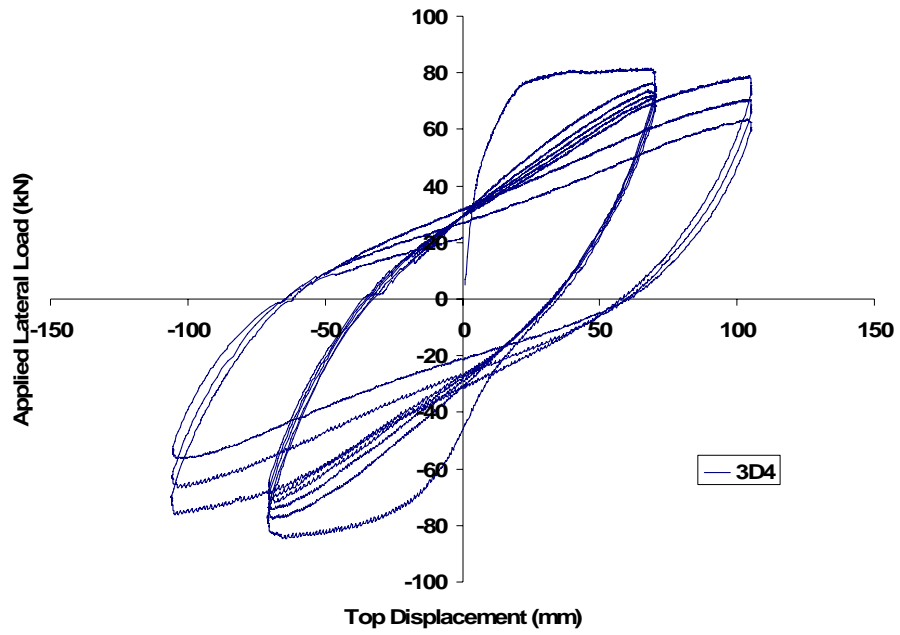


Figure 4.39 Lateral load - top displacement response of Specimen 3D4

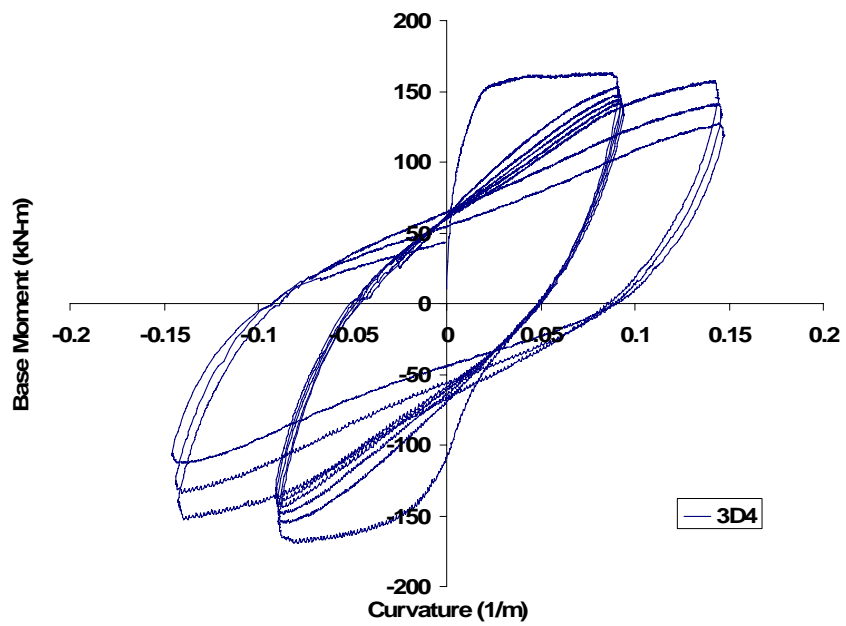


Figure 4.40 Base moment-curvature response of Specimen 3D4

Several flexural cracks formed during the first cycle along the column height up to a level of 100 cm from the bottom and these cracks propagated on the North and South faces during this cycle. A few additional flexural cracks were formed and the former ones widened during the following cycle. Crushing of cover concrete and spalling at corners was observed in this cycle. At the second positive cycle, crushing of cover concrete become severe and longitudinal bars and ties at column base were exposed. Crack pattern of specimen at this cycle is given in Figure 4.41. Bar buckling was initiated at the 4<sup>th</sup> cycle. After the 7<sup>th</sup> cycle where the amplitude of top displacement was increased to 105 mm, core concrete crushing was observed.



Figure 4.41 Crushing and spalling of concrete at the corners of the South-East face of Specimen 3D4

#### 4.2.2.4 Specimen 4D5

The fourth specimen of the conforming columns was tested under a displacement protocol shown in Figure 4.42. The compressive strength of concrete on the day of testing was 24.6 MPa. Column specimen was subjected to a constant axial load of 610 kN which corresponds to an axial load ratio of  $0.20A_g f_{ck}$ .

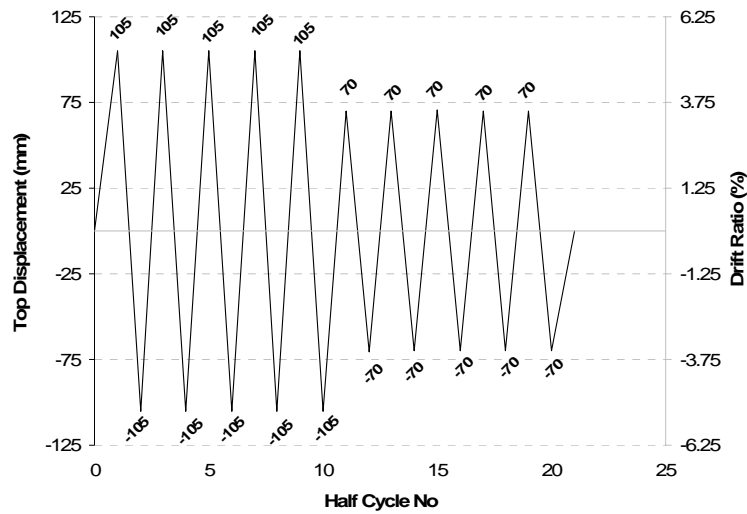


Figure 4.42 Displacement history imposed on Specimen 4D5

The imposed displacement history in terms of amplitudes, number of cycles and the sequence of applied cycles was exactly the same with the displacement protocol of Type-1 specimen 5P5 where the testing was started with a high amplitude of 105 mm top displacement (5.25% drift ratio) and then lowered down to an amplitude of 70 mm (3.5% drift ratio).

Load versus top displacement graphics of specimen 4D5 is given in Figure 4.43. The response of specimen 4D5 in terms of base moment versus curvature is shown in Figure 4.44.

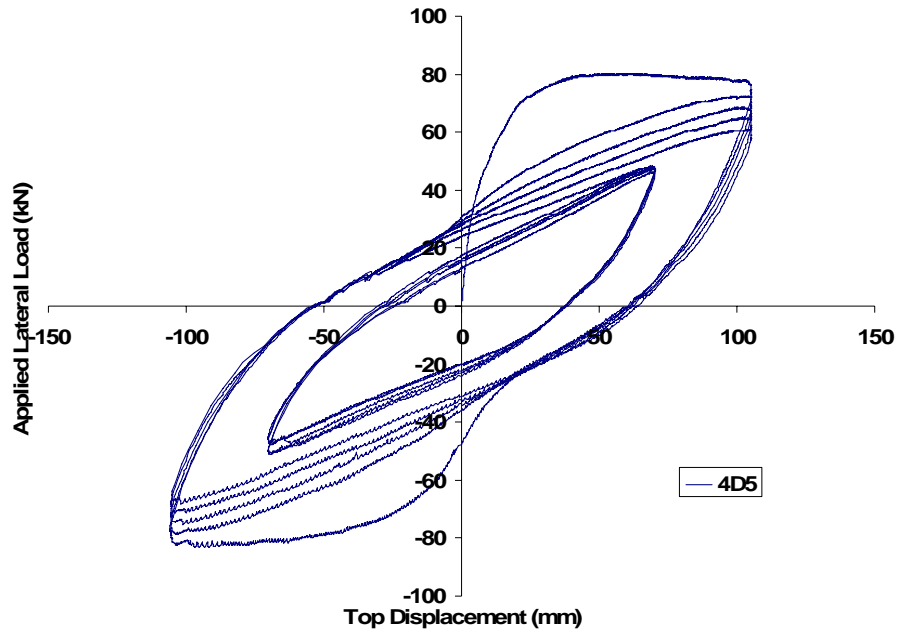


Figure 4.43 Lateral load - top displacement response of Specimen 4D5

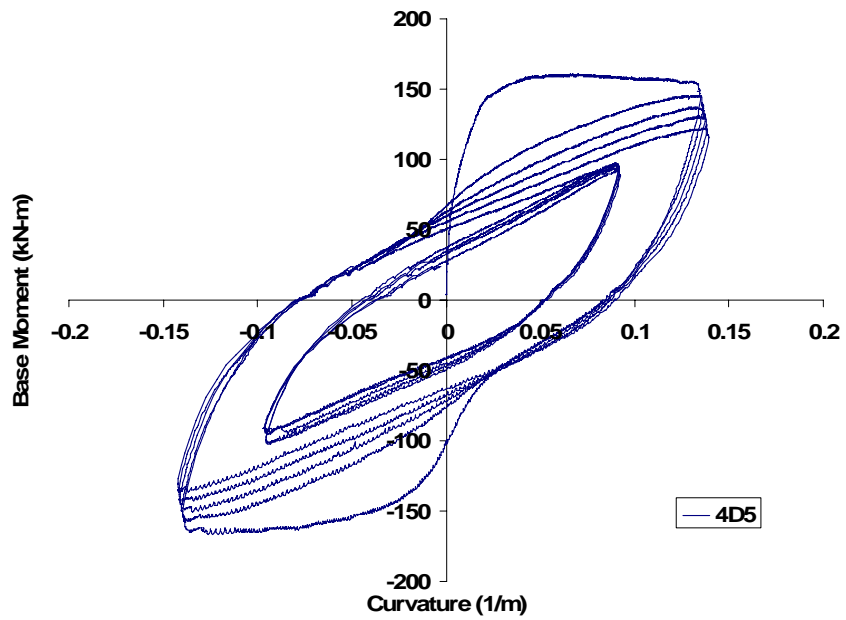


Figure 4.44 Base moment-curvature response of Specimen 4D5

Similar to its pair from Type-1 specimens with its severe displacement protocol, all important observations for the specimen response starting with the first tensile crack until buckling of longitudinal bars were observed during the first stage of loading. First cracking was observed when the top displacement was 8 mm. At the end of first full cycle, wide cracks at the column base were formed and crushing of cover concrete occurred. Spalling of concrete became severe and longitudinal bars were exposed at the column base at the end of second full cycle. Buckling occurred during the 4th cycle. During the second stage where the amplitude of displacement reversals was decreased, no significant observations were made on the specimen response. The view of plastic hinge region at the end of the test is shown in Figure 4.45.



Figure 4.45 North face of Specimen 4D5 at the end of test

#### 4.2.2.5 Specimen 5DV1

The fifth specimen of the conforming columns was tested under a displacement protocol given in Figure 4.46. The compressive strength of concrete on the day of testing was 25 MPa. Column specimen was subjected to a constant axial load of 608 kN which corresponds to an axial load ratio of  $0.20A_g f_{ck}$ .

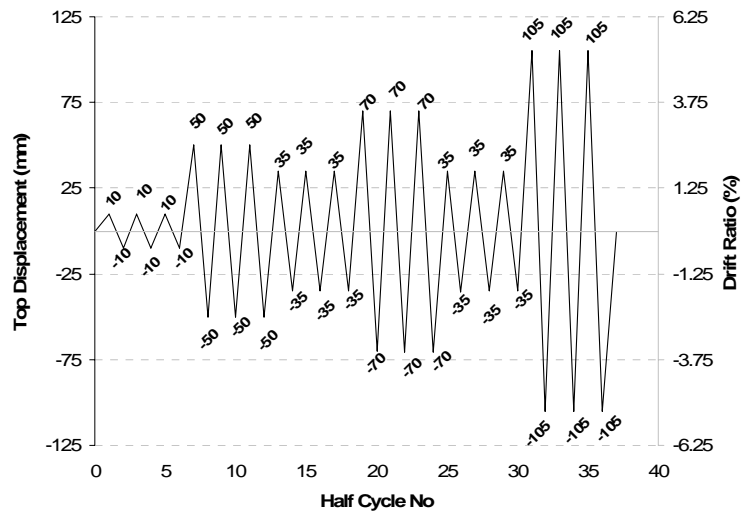


Figure 4.46 Displacement history imposed on Specimen 5DV1

Starting with elastic cycles, the specimen was tested under randomly constituted displacement protocol which is identical to the displacement protocol of the Type-1 specimen 6PV1.

Load versus top displacement graphics of specimen 5DV1 is given in Figure 4.47. The response of specimen 5DV1 in terms of base moment versus curvature is shown in Figure 4.48.

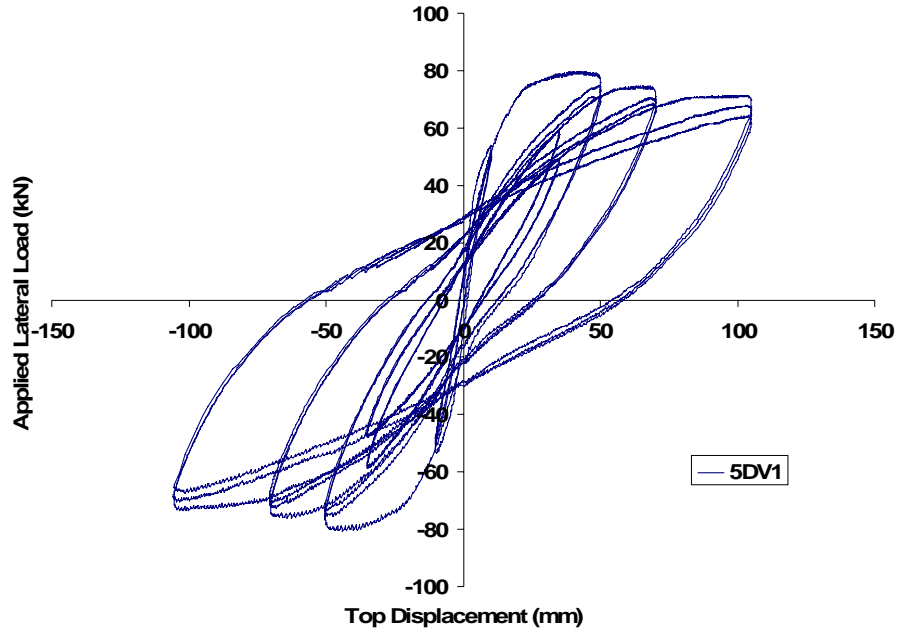


Figure 4.47 Lateral load - top displacement curves of Specimen 5DV1

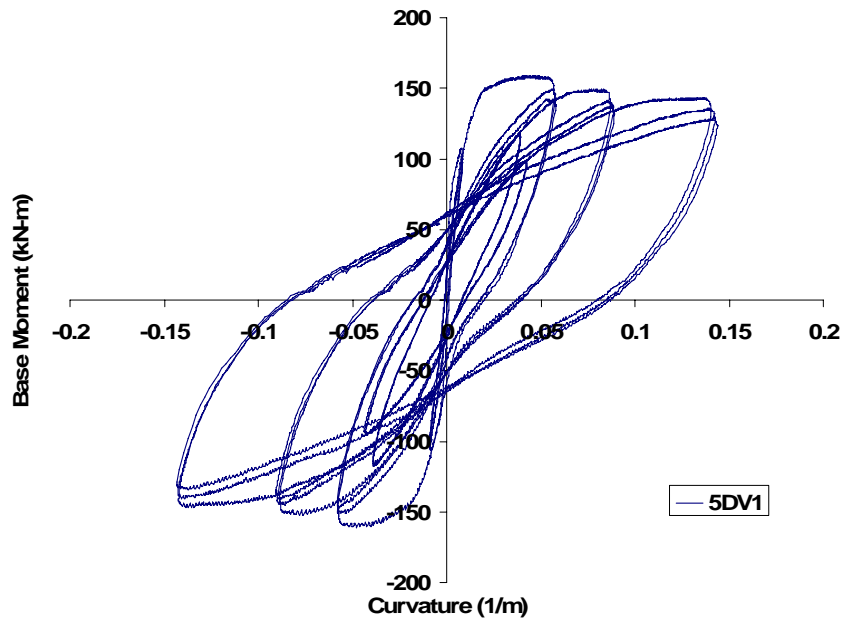


Figure 4.48 Base moment-curvature response of Specimen 5DV1

First cracking of concrete was observed at the first positive cycle when the applied lateral load was about 42 kN. Additional flexural cracks were formed at several locations up to 75-80 cm above the bottom of column during the elastic cycles of the first stage. In the following cycles, these cracks propagated at the North and South faces of column through the mid section. At the second stage, concrete cover at the corners of column started crushing and spalling. The crack pattern of specimen at this stage is given in Figure 4.49. At the third stage where the amplitude of imposed displacement decreased, no significant events were observed on the specimen behavior. At the fourth stage, spalling of cover concrete extended up to the level of approximately 20 cm from the footing face and horizontal cracks were observed along the longitudinal bars. At the fifth stage, hoops at the column base level became visible. During the last and most severe stage, bar buckling initiated and a cross tie opened at the column base level.

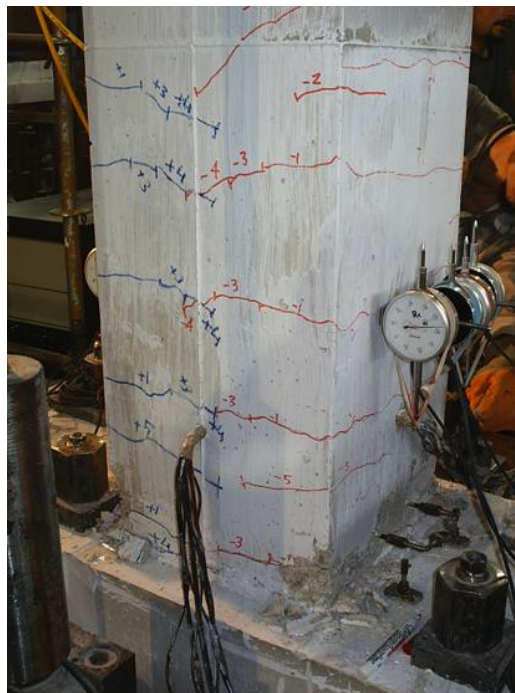


Figure 4.49 Crack pattern after the 4<sup>th</sup> cycle at the South-East faces of Specimen 5DV1

#### 4.2.2.6 Specimen 6DV2

The sixth specimen of the conforming columns was tested under a displacement protocol given in Figure 4.50. The compressive strength of concrete on the day of testing was 25.3 MPa. Column specimen was subjected to a constant axial load of 616 kN which corresponds to an axial load ratio of  $0.199A_g f_{ck}$ .

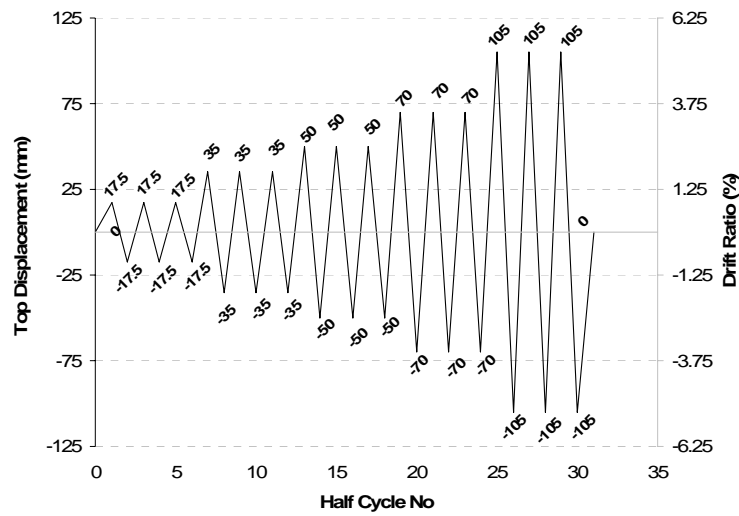


Figure 4.50 Displacement history imposed on Specimen 6DV2

Starting with elastic cycles of imposed displacements, the specimen was tested under the displacement protocol with constantly increasing stages of top displacement amplitudes. At each stage of loading, three full cycles were imposed on the specimen.

Lateral load versus top displacement graphics of specimen 6DV2 is presented in Figure 4.51. The response of specimen 6DV2 in terms of base moment versus curvature is shown in Figure 4.52.

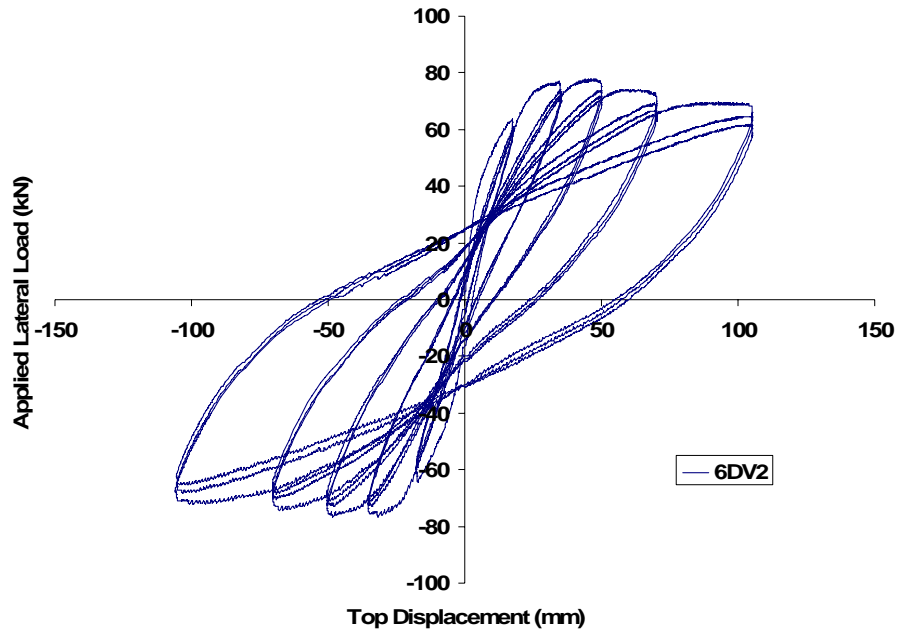


Figure 4.51 Lateral load - top displacement response of Specimen 6DV2

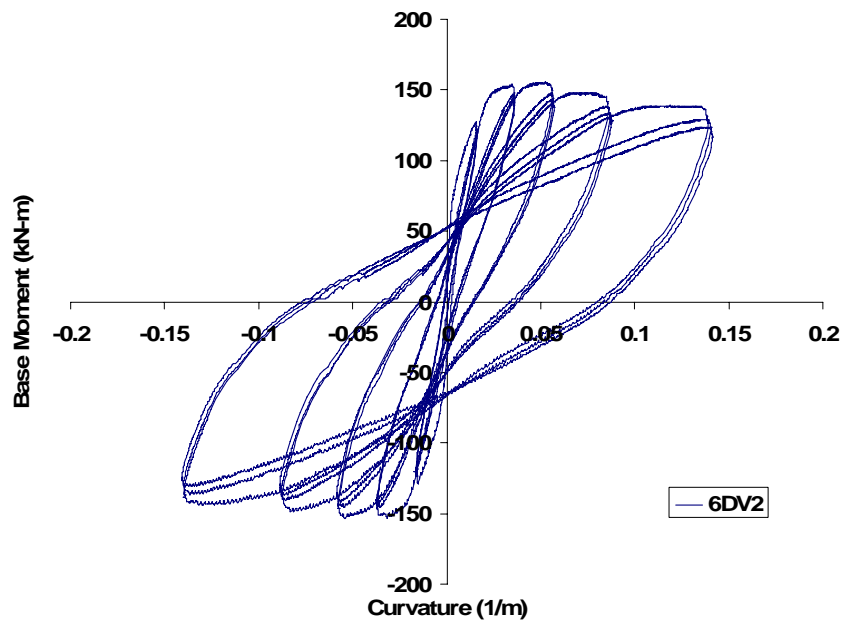


Figure 4.52 Base moment-curvature response of Specimen 6DV2

Similar to the former variable amplitude testing of Type-2 specimens, flexural cracks formed at several locations up to 75-80 cm above the bottom of column during the elastic cycles of first stage. At the second stage, these cracks were propagated and the crack openings were broadened. Concrete cover at the corners of column started crushing. At the third stage, crushing of cover concrete became more severe and spalling initiated. At the fourth stage, ties were exposed and spalling extended up to a level of 20 cm. At the last cycle of this stage, longitudinal bars became visible. At the fifth stage bar buckling initiated. The North view of specimen at this stage when the maximum top displacement was attained is shown in Figure 4.53

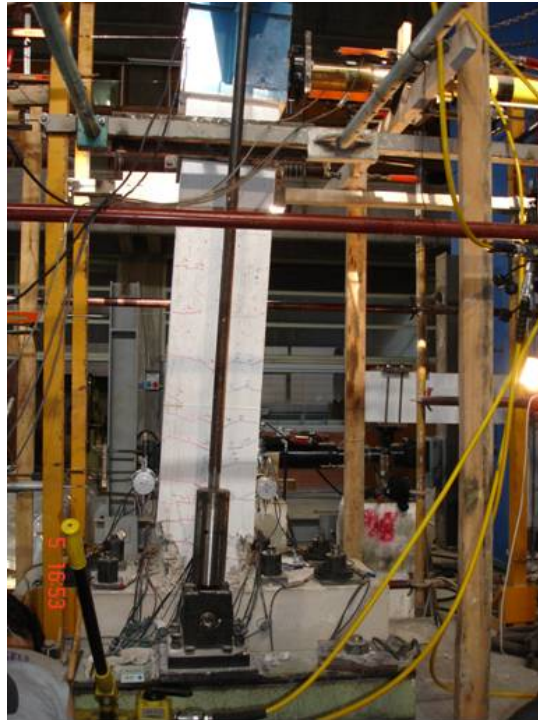


Figure 4.53 North face of Specimen 6DV2 at the last stage of loading

## **CHAPTER 5**

### **SEISMIC PERFORMANCE EVALUATION OF THE COLUMN SPECIMENS**

#### **5.1 General**

The effect of displacement history on the deformation response of concrete columns controlled by flexure is investigated in this chapter. The results obtained are expected to improve the displacement-based criteria developed for modeling and seismic performance assessment of reinforced concrete columns.

#### **5.2 Column database**

In this chapter, the test results of twelve full scale column specimens designed for pure flexure failure, reported in Chapter 4 are utilized. Six members of Type-1 specimens except the one prepared with reduced bond in between concrete and longitudinal reinforcement (3P3\_U) and all members of Type-2 specimens were utilized for the seismic performance evaluation of reinforced concrete column members. General properties of these specimens are summarized in Table 5.1.

Observed rotations at the plastic hinge region are evaluated comparatively with the limits proposed by ASCE/SEI 41-Update (2007), Eurocode 8 (2005) and the Turkish Earthquake Code, TDY (2007), and the observed moment-chord

rotation and lateral force-displacement behavior is assessed in view of the modeling criteria in ASCE/SEI 41-Update.

Table 5.1- Material properties of the selected test specimens

Specimen Type	Concrete	Longitudinal Reinforcement			Transverse Reinforcement		
		Compressive Strength $f'_c$ (MPa)	Yield Strength $f_y$ (MPa)	Ultimate Strength $f_u$ (MPa)	Reinforcement Ratio $\rho_l$ ( $A_s / b_w \cdot h$ )	Yield Strength $f_{yw}$ (MPa)	Ultimate Strength $f_{uw}$ (MPa)
<b>Type-1</b>	13	315	448	0.01	368	487	0.0026
<b>Type-2</b>	25	454	604	0.01	469	685	0.0061

### 5.3 Deformation Capacities of Columns

The first set of test results are presented for the moment-chord rotation relationships for the bottom ends of column specimens. Chord rotation at the bottom end is equal to the drift angle, i.e. top displacement divided by the specimen height, and it represents total rotation of the plastic hinge region including the elastic and plastic components. The results are shown in Figure 5.1 to Figure 5.12 for the Type-1 and Type-2 specimens, respectively. The test results are repeated three times in each figure in order to indicate the limit states of three codes at three performance levels. Analytical moment-chord rotation relations calculated under monotonously increasing moments, obtained from moment-curvature relations along the column height are marked on each figure. Plastic curvatures of the plastic hinge region at the column base are converted to plastic rotations by assuming a plastic hinge length in obtaining the analytical moment-chord rotation relations. Details of analytical moment-curvature analysis and plastic hinge length calculations are presented in the following section. A picture of the plastic hinge

region at the end of the test for all tested column specimen are also given at the inset of each moment-chord rotation diagram.

### 5.3.1 Moment-Curvature Analysis.

Analytical moment-curvature analyses were carried out by using a computer program CUMBIA (Montejo and Kowalsky, 2007) which is a compilation of several *Matlab* codes. These codes were modified and recompiled accordingly to perform the moment-curvature analysis of tested column specimens. As provided default by computer program CUMBIA, the model proposed by Mander et.al. (1988) was utilized for confined and unconfined concrete. Reinforcing steel stress-strain relationship was adopted from the model proposed by King et al. (1986).

Calculated moment-curvature relations were bi-linearized by using the equal area method for simplicity and for specifying a distinct yield point with the associated yield curvature and yield strength. Buckling limit state was selected as the ultimate point for moment-curvature analysis.

Conversions from curvatures to plastic rotations were done by multiplying the calculated curvatures by a plastic hinge length expressed in terms of two components defined by Priestley et al (2007) given in Equation 5.1.

$$L_p = 0.2 \left( \frac{f_u}{f_y} - 1 \right) L_C + L_{SP} \geq 2.L_{SP} \quad (5.1)$$

Here  $f_u$  and  $f_y$  are ultimate and yield strength of reinforcing bars, respectively.  $L_C$  is the length from the critical section to the point of contra-flexure.  $L_{SP}$  is the strain penetration length and defined as;

$$L_{SP} = 0.022.f_y.d_l \text{ (MPa)} \quad (5.2)$$

where  $d_l$  is the diameter of longitudinal reinforcement.

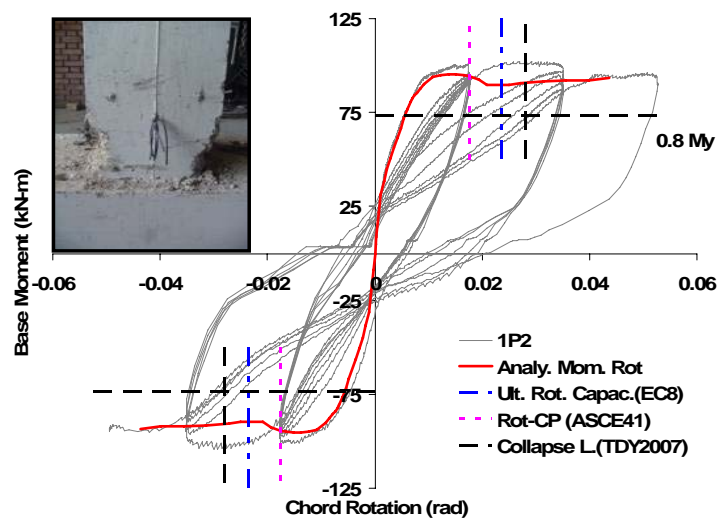
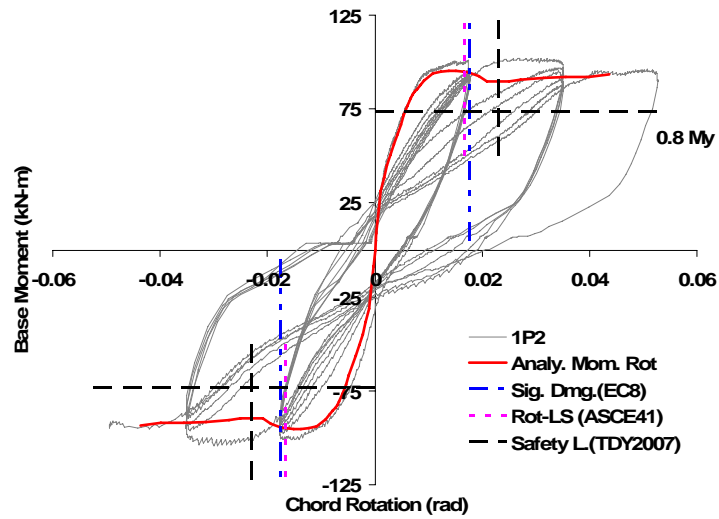
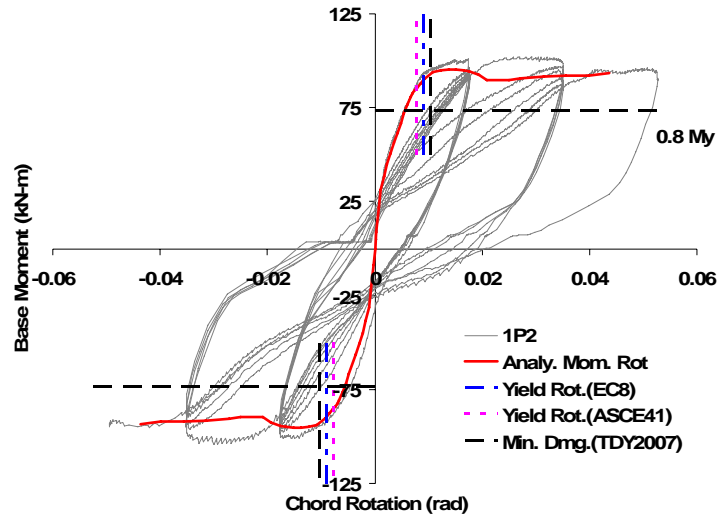


Figure 5.1 Moment-chord rotation relations for Type-1 columns, Specimen 1P2

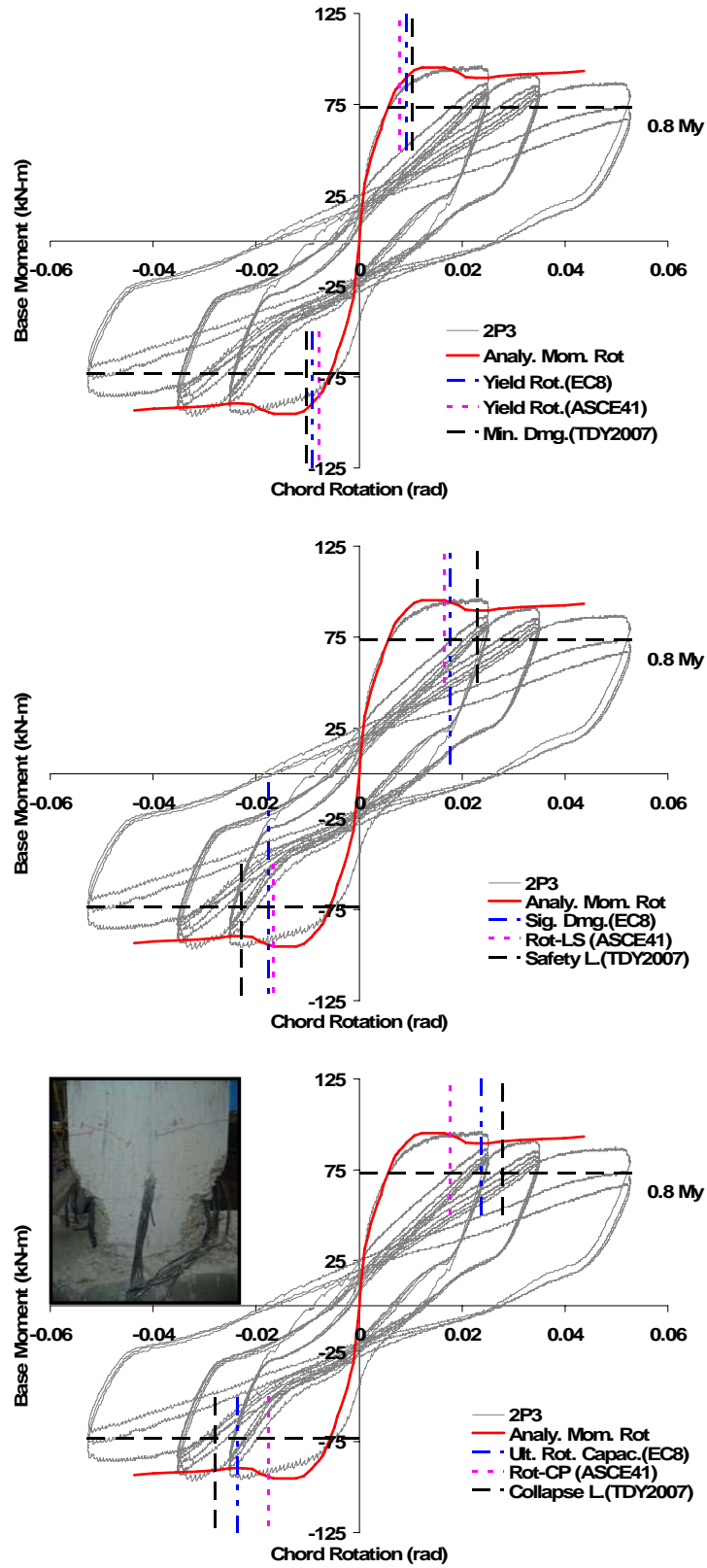


Figure 5.2 Moment-chord rotation relations for Type-1 columns, Specimen 2P3

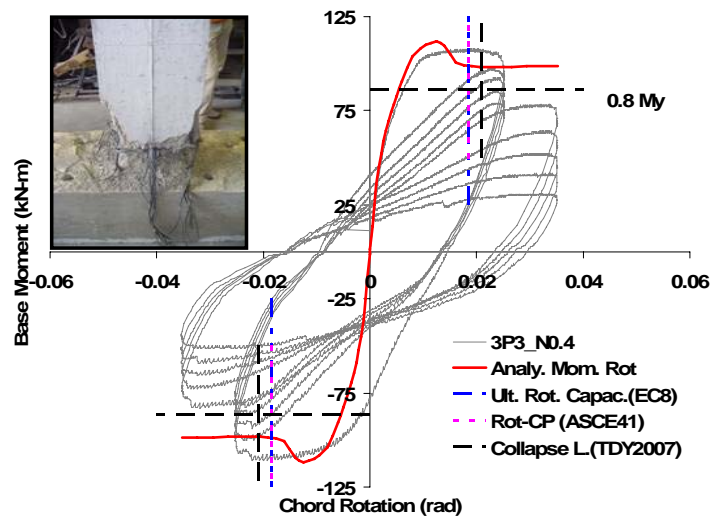
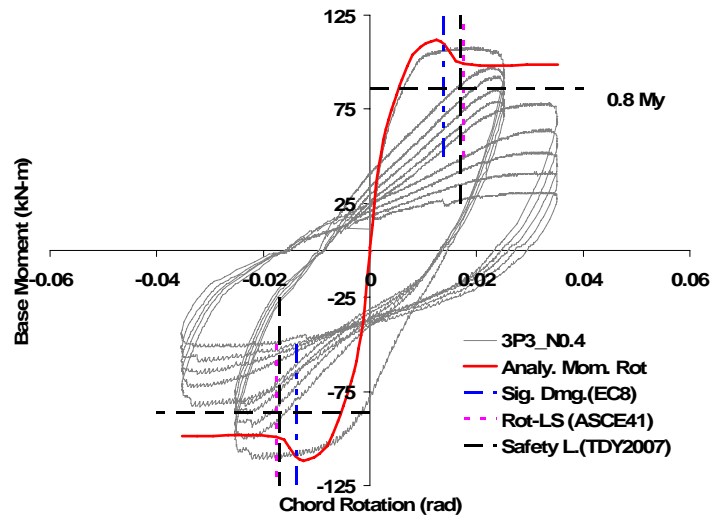
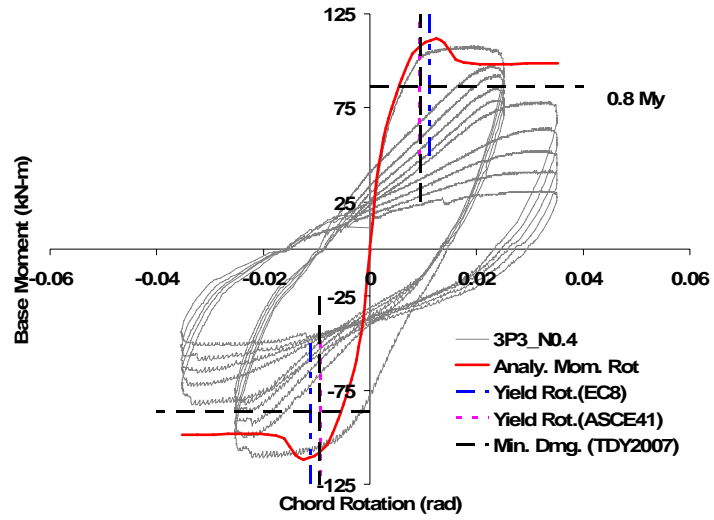


Figure 5.3 Moment-chord rotation relations for Type-1 columns, Specimen 3P3\_N04

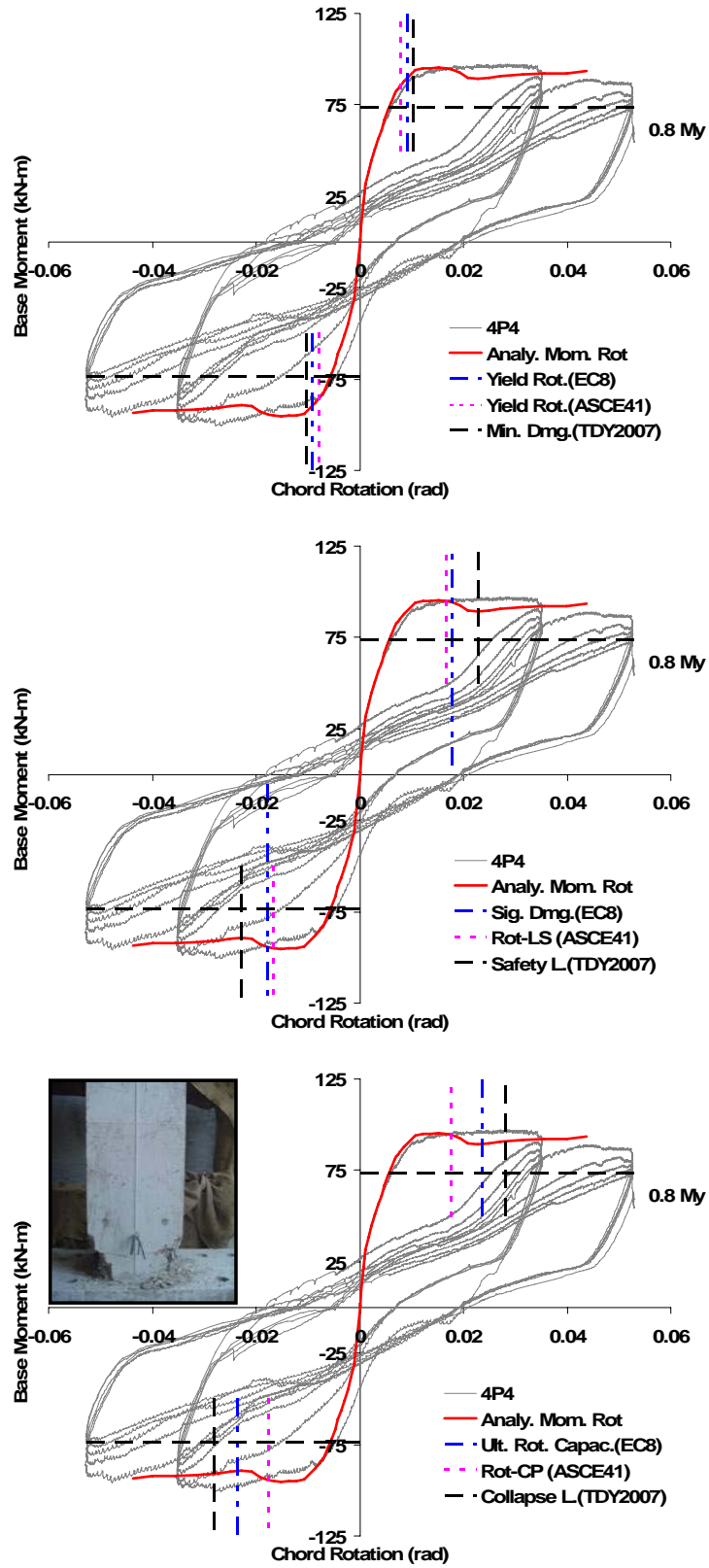


Figure 5.4 Moment-chord rotation relations for Type-1 columns, Specimen 4P4

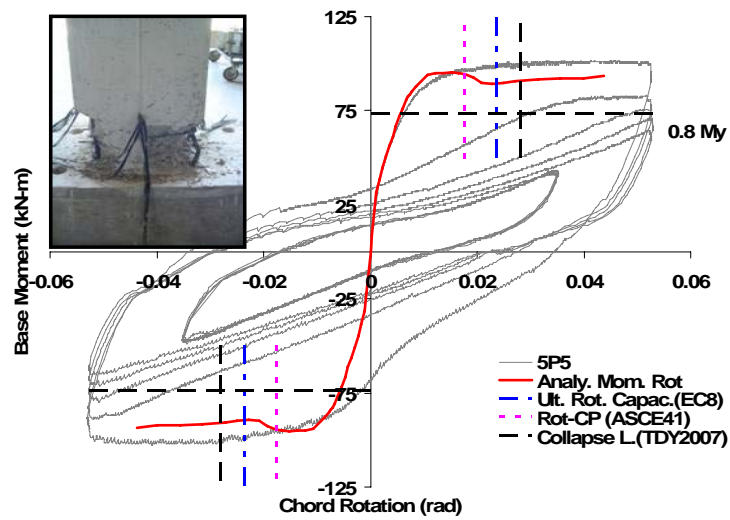
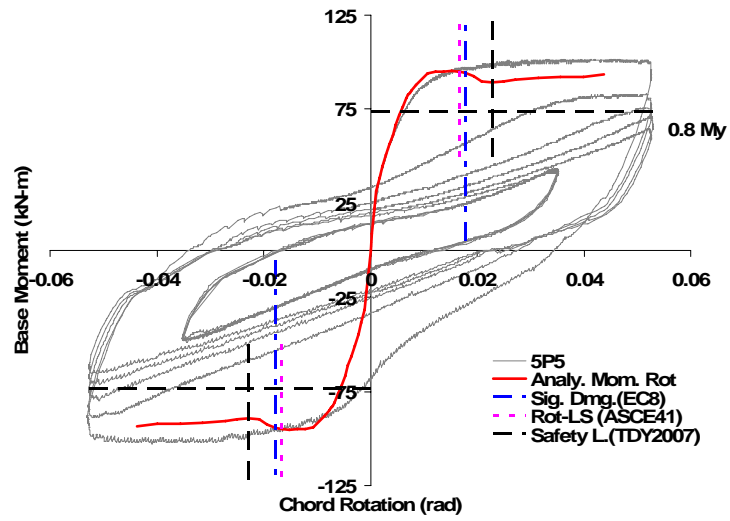
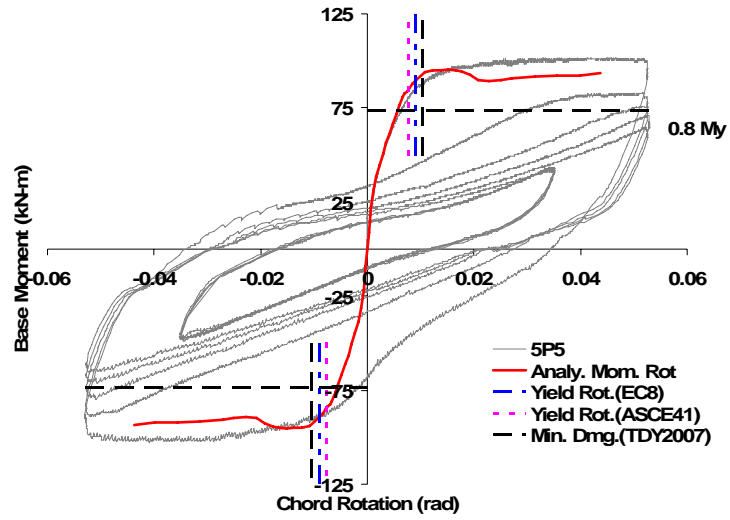


Figure 5.5 Moment-chord rotation relations for Type-1 columns, Specimen 5P5

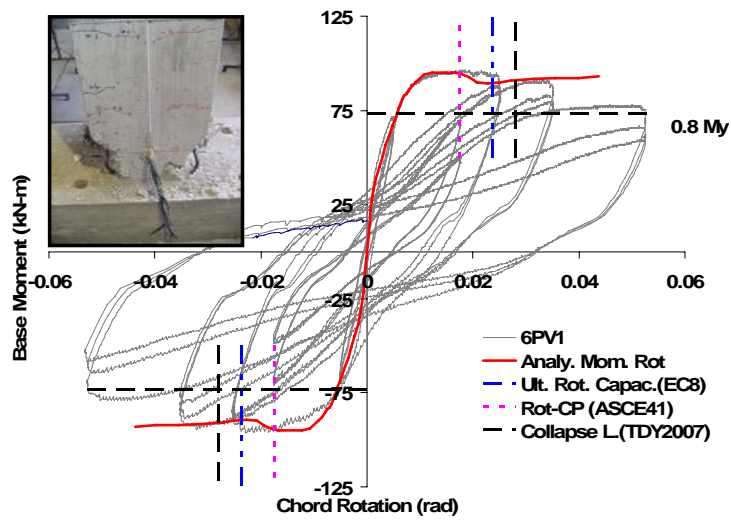
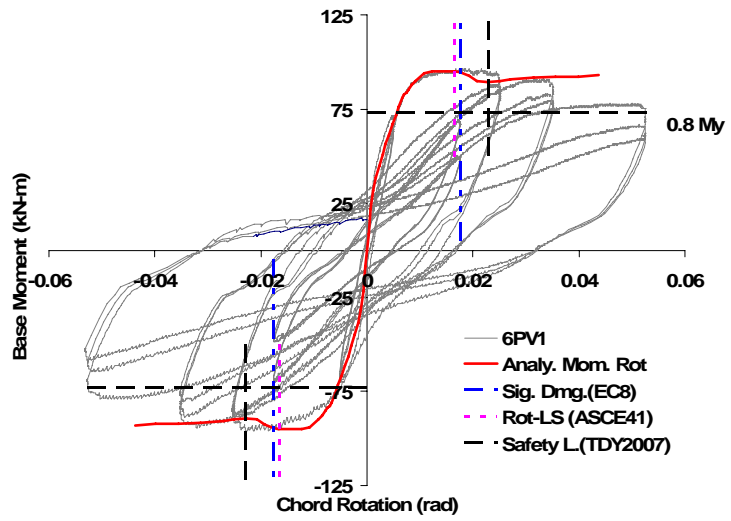
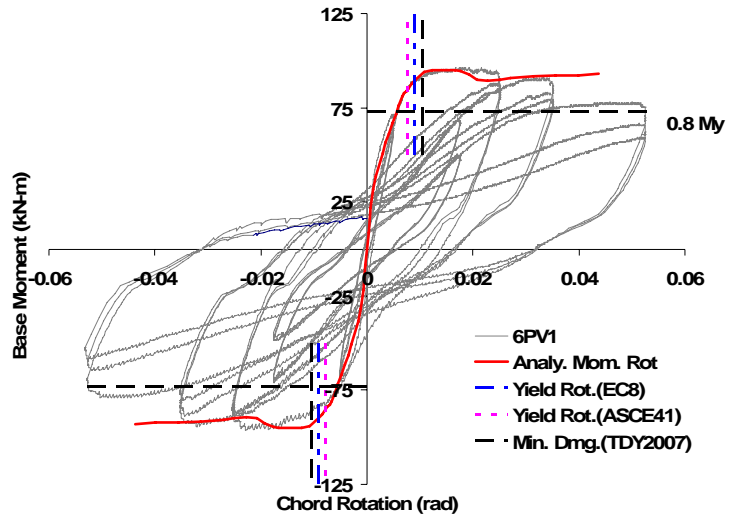


Figure 5.6 Moment-chord rotation relations for Type-1 columns, Specimen 6PV1

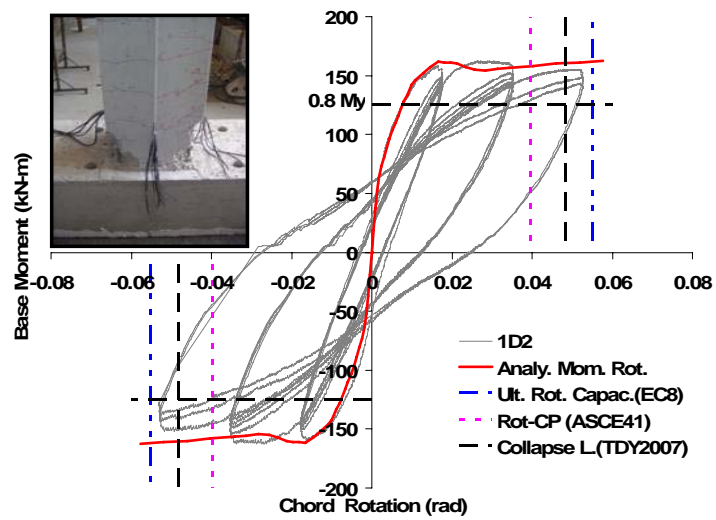
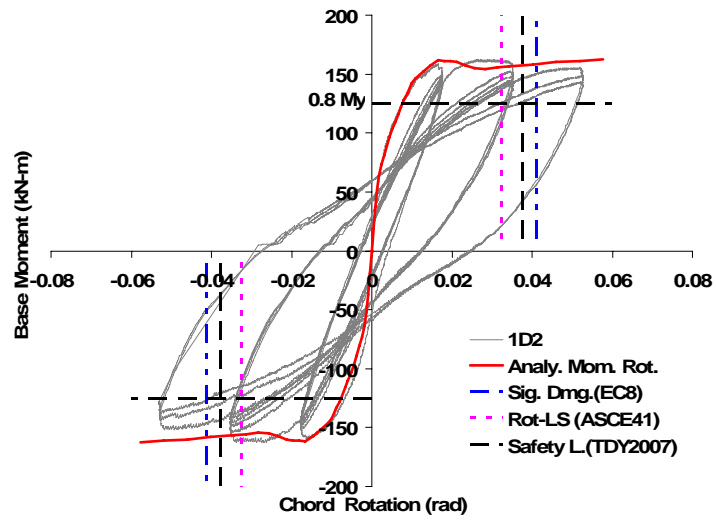
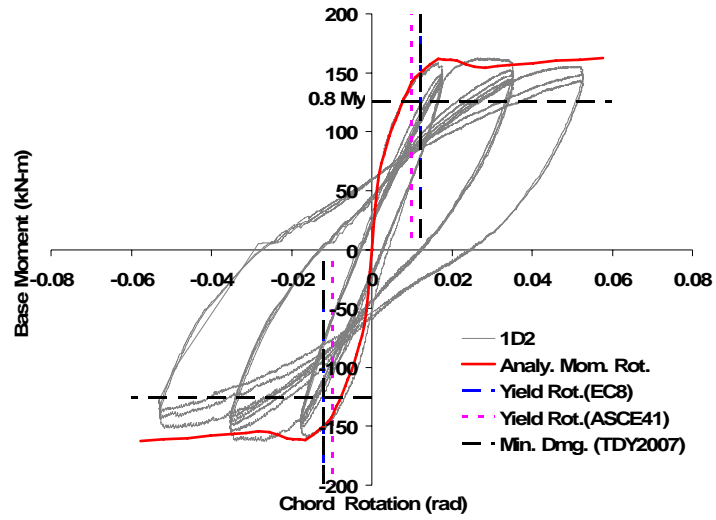


Figure 5.7 Moment-chord rotation relations for Type-2 columns, Specimen 1D2

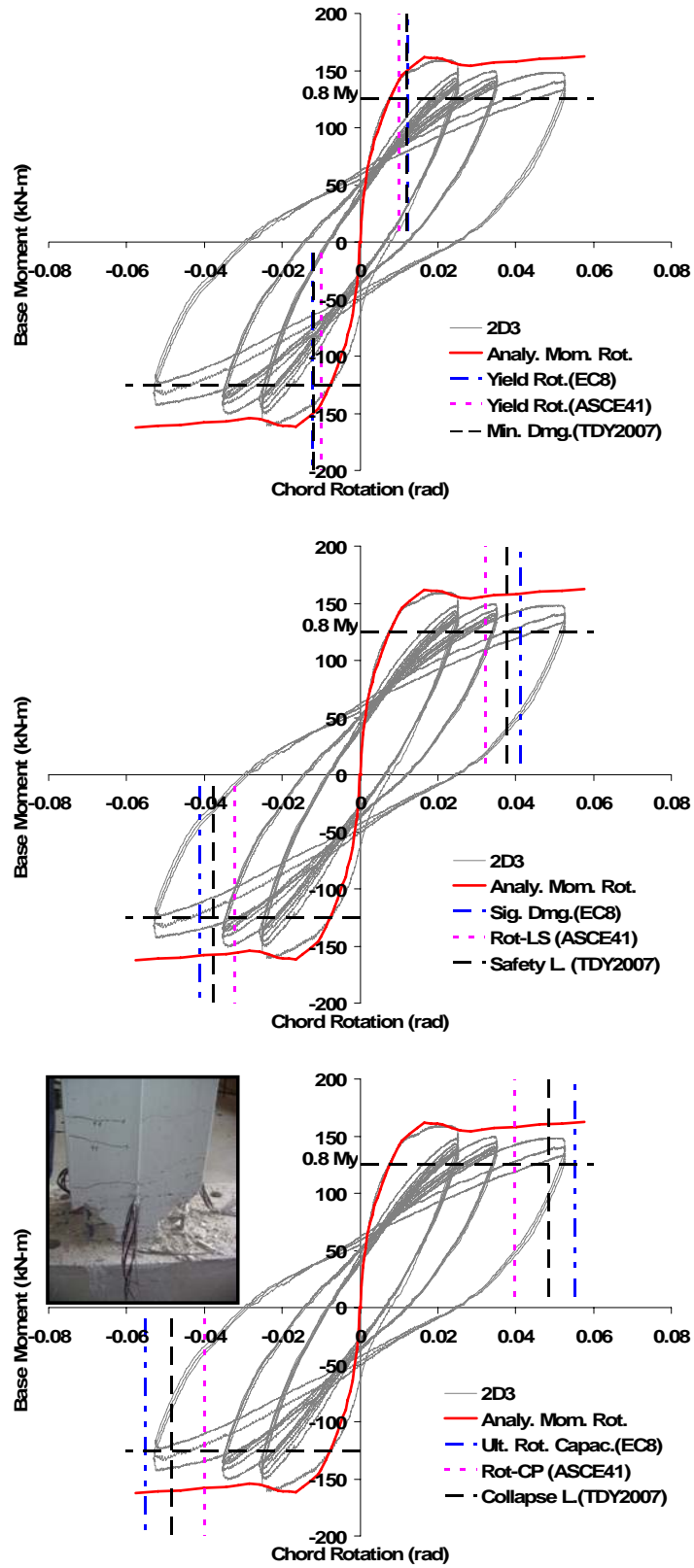


Figure 5.8 Moment-chord rotation relations for Type-2 columns, Specimen 2D3

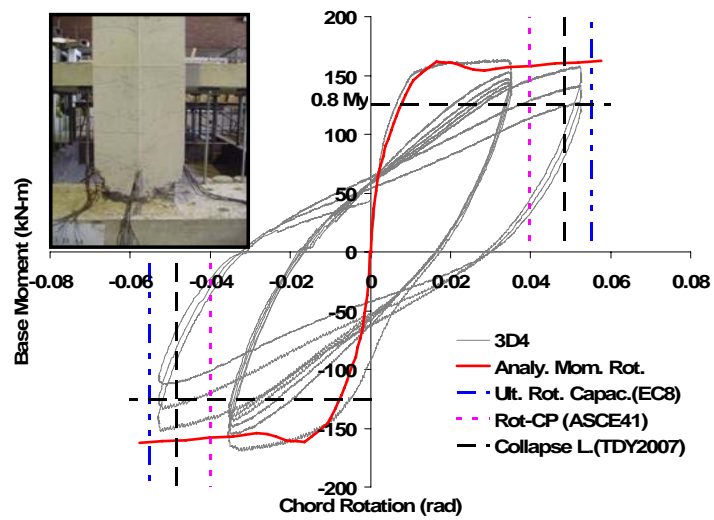
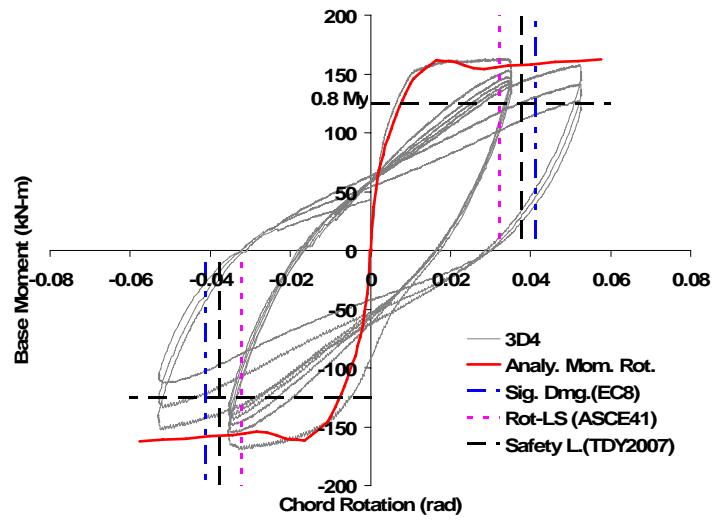
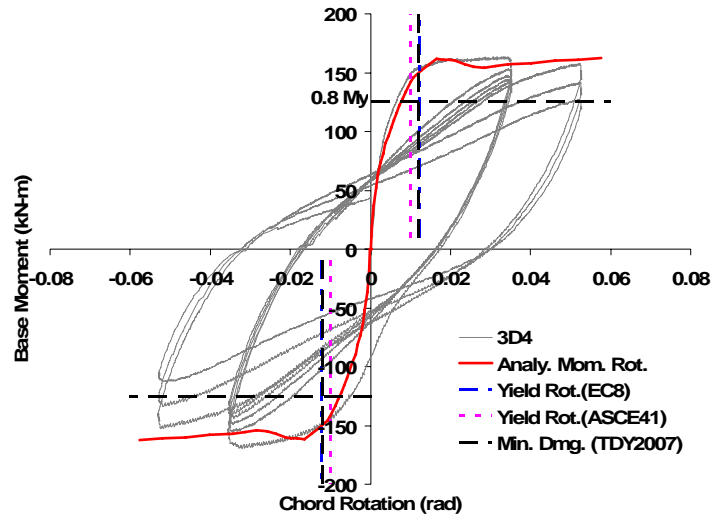


Figure 5.9 Moment-chord rotation relations for Type-2 columns, Specimen 3D4

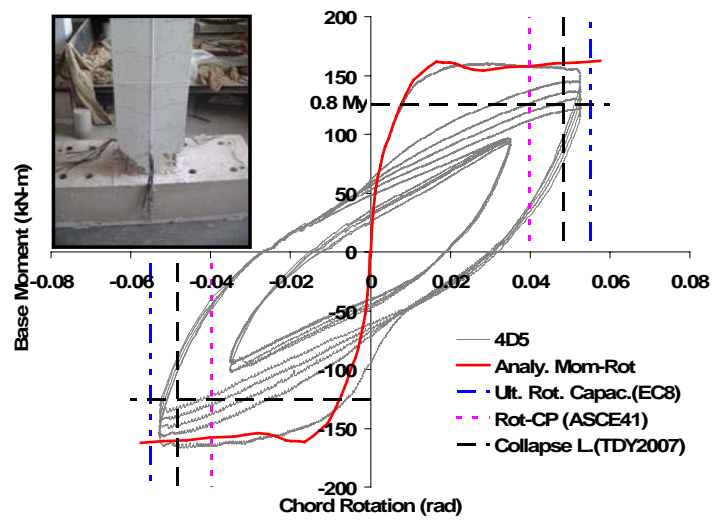
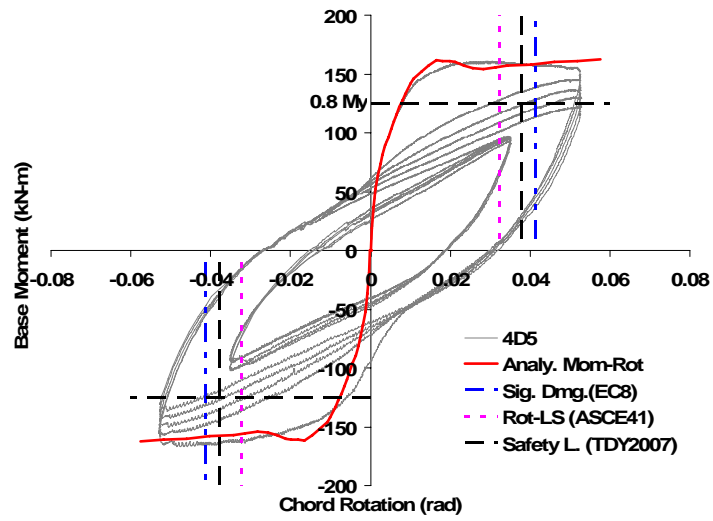
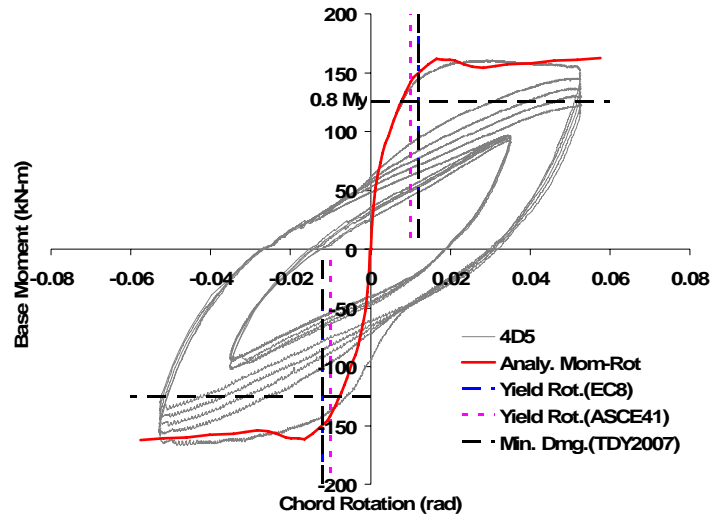


Figure 5.10 Moment-chord rotation relations for Type-2 columns, Specimen 4D5

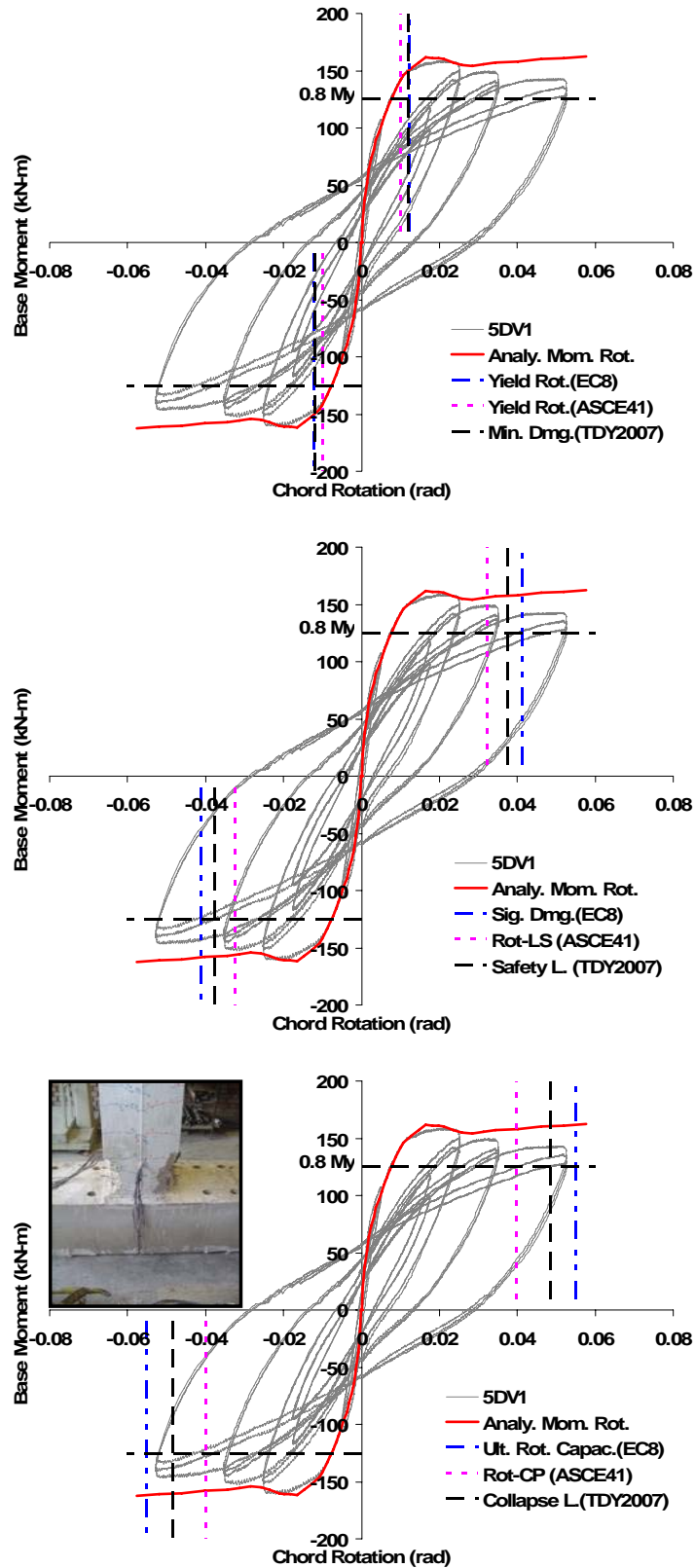


Figure 5.11 Moment-chord rotation relations for Type-2 columns, Specimen 5DV1

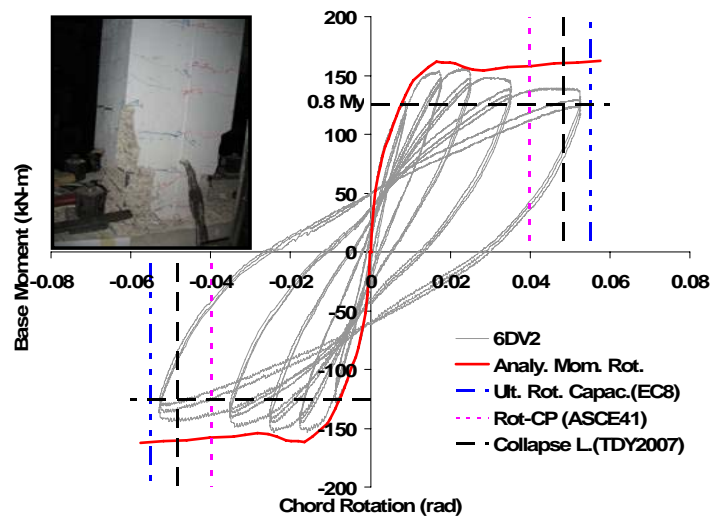
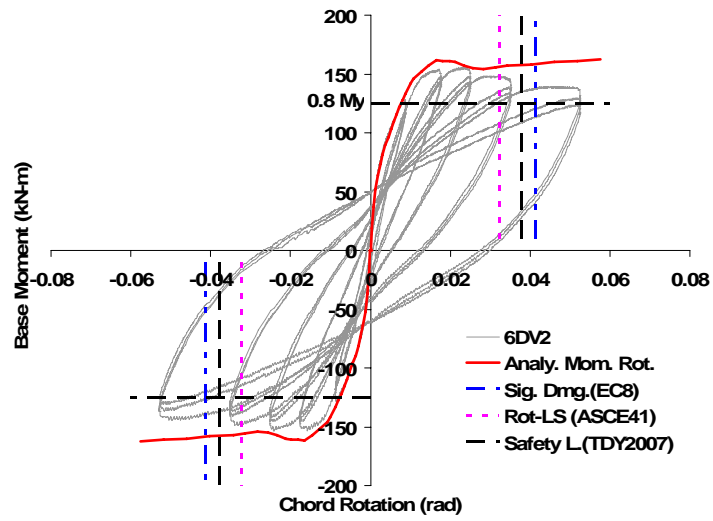
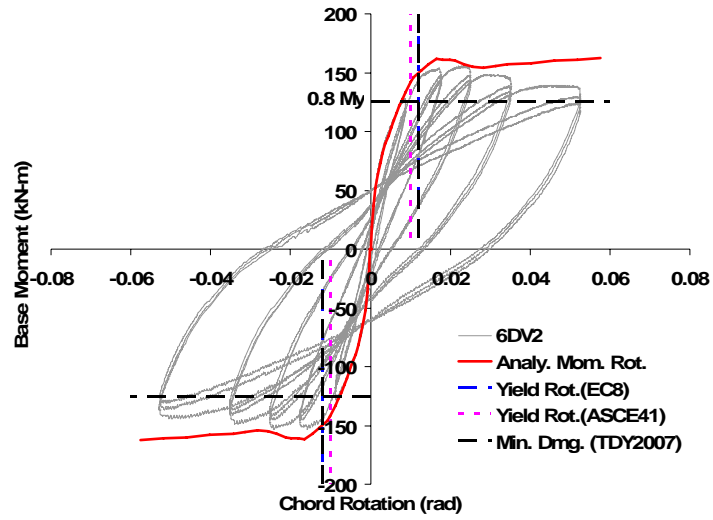


Figure 5.12 Moment-chord rotation relations for Type-2 columns, Specimen 6DV2

### 5.3.2 Limit State Calculations

Three deformation limit states corresponding to yield rotation, significant damage and ultimate rotation capacity according to Eurocode 8, yield rotation, life safety and collapse prevention according to ASCE/SEI 41-Update (2007) and minimum damage, safety limit and collapse limit according to TDY (2007) are marked respectively on each diagram in both loading directions in Figures 5.1-5.12. 80% levels of the positive and negative yield moments ( $0.8 M_y$ ) are also indicated on the vertical axis.

#### 5.3.2.1 ASCE/SEI 41-Update Limit States

Type-1 specimens are classified as Condition (ii) by ASCE/SEI 41-Update although flexure failure is ensured by a low  $V_p/V_n$  ratio.  $V_p/V_n$  ratios for Type-1 and Type-2 specimens are 0.32 and 0.20, respectively, except for the column specimen with high axial load where it is 0.34. The reason for Condition (ii) classification is the transverse reinforcement with  $90^\circ$  hooks and spacing-to-depth ratio exceeding 0.5 (it is 0.52 for the Type-1 specimens). There are three more cases of Condition (ii) in ASCE/SEI 41-Update where the first two are for flexure-shear failure and the third is for the lap spliced transverse reinforcement. Plastic rotations corresponding to limit states “Life Safety” (LS) and “Collapse Prevention” (CP) are interpolated from the values given in the related Table 6-8 of ASCE/SEI 41-Update in accordance with the calculated axial load, transverse reinforcement and shear ratio of this type of specimens. For calculation of yield rotation, effective stiffness of the column specimens is estimated based on the axial load ratio and the yield moments are extracted from the bi-linearized moment-curvature curves.

### 5.3.2.2 Eurocode 8 Limit States

Eurocode 8 accounts for plain longitudinal bars and transverse reinforcement with 90° hooks in calculating the deformation-based performance levels of concrete columns (Fardis and Kosmopoulos, 2007). Spacing-to-depth ratio is considered as a variable parameter. The ultimate chord rotation values are defined in Eurocode 8 by Equation 5.3;

$$\theta_{um} = \frac{1}{\gamma_{el}} 0.016 \cdot (0.3^v) \left[ \frac{\max(0.01; \omega')}{\max(0.01; \omega)} f_c \right]^{0.225} \left( \frac{L_v}{h} \right)^{0.35} 25^{\left( \alpha \rho_{xx} \frac{f_{yw}}{f_c} \right)} (1.25^{100 \rho_d}) \quad (5.3)$$

where  $\gamma_{el}$  is taken as 1.0 and the contribution of transverse reinforcement with 90° hooks to the rotation capacity of columns is also taken into account.  $v$  is the axial load ratio calculated by  $N/b \cdot h \cdot f_c$ . The variable  $L_v$  is shear span (M/V),  $h$  is section depth,  $f_c$  is concrete compressive strength,  $\omega$  and  $\omega'$  are mechanical reinforcement ratio of tension and compression reinforcements,  $\alpha$  is confinement effectiveness factor,  $\rho_{xx}$  is ratio of transverse reinforcement parallel to the direction of loading,  $\rho_d$  is the steel ratio of diagonal reinforcement. Since the Type-1 specimens were constructed with smooth longitudinal bars and inadequate transverse reinforcement detailing at the plastic hinging zone, ultimate chord rotation values are reduced by 0.575. Chord rotations for significant damage limit state are taken as the ¾ of the ultimate chord rotation (near collapse) as indicated by Eurocode 8. Chord rotations at yielding are calculated with Equation 5.4 given below by considering three different components of rotation due to flexure, shear and anchorage slip, respectively;

$$\theta_y = \phi_y \cdot \frac{L_s}{3} + 0.0013 \cdot \left( 1 + 1.5 \frac{h}{L_s} \right) + \frac{0.13 \cdot \phi_y \cdot d_{bL} \cdot f_y}{\sqrt{f_c}} \quad (5.4)$$

where  $\theta_y$  is the yield curvature of the section,  $d_{bL}$  is diameter of longitudinal (tension) reinforcement,  $f_y$  is the yield strength of reinforcement and

### 5.3.2.3 TDY (2007) Limit States

In TDY 2007, the performance limit states for reinforced concrete columns are defined in terms of maximum strain values for each state, either controlled by tensile strain of reinforcing steel or compressive strain at extreme fiber of concrete section, or outermost fiber of core concrete. These limit states of “Minimum Damage” (MN), “Safety Limit” (GV) and “Collapse Limit” (GÇ) are given in Equations 5.5, 5.6 and 5.7, respectively.

$$(\varepsilon_{cu})_{MN} = 0.0035 \quad ; \quad (\varepsilon_s)_{MN} = 0.010 \quad (5.5)$$

$$(\varepsilon_{cg})_{GV} = 0.0035 + 0.01 (\rho_s / \rho_{sm}) \leq 0.0135 \quad ; \quad (\varepsilon_s)_{GV} = 0.040 \quad (5.6)$$

$$(\varepsilon_{cg})_{GC} = 0.004 + 0.014 (\rho_s / \rho_{sm}) \leq 0.018 \quad ; \quad (\varepsilon_s)_{GC} = 0.060 \quad (5.7)$$

Here,  $\varepsilon_s$  is steel strain,  $\varepsilon_{cu}$  is the compressive strain at the outmost fiber of the concrete section,  $\varepsilon_{cg}$  is compressive strain at the outermost fiber of the core concrete,  $\rho_s$  is the volumetric ratio of transverse reinforcement and  $\rho_{sm}$  is the volumetric ratio of minimum transverse reinforcement.

Although the procedure for calculating the limit states in TDY 2007 is proposed in terms of strains, the drift ratios which can be calculated accordingly are limited by some upper bound values for each limit state. Knowing the fact that, for a cantilever column specimen, chord rotation exactly corresponds to drift ratio, proposed drift limits of TDY 2007 are calculated but not considered during the limit state assessment to keep the focus on rotations rather than drift ratios.

Moment-curvature analyses (CUMBIA) of column sections with their defined material and sectional properties under specific axial load were carried out for each type of specimen and the strain profiles over the section were calculated. For the locations defined at TDY 2007 (for concrete; MN- at cover; GV, GÇ- in the core; for steel; tension reinforcement) the plastic curvature values corresponding to the limit state strain values were calculated. These plastic curvatures were then multiplied by the plastic hinge length defined as  $l_p = h/2$  in the TDY 2007 in order to calculate the plastic rotations. Each plastic rotation was finally added to the chord rotation value at yielding for calculating the total chord rotation beyond the elastic limit.

Since the limit state strain values were only sensitive to the ratio of transverse reinforcement in TDY 2007, the differences in the limit state values of Type-1 and Type-2 columns arise from the curvature values calculated from the corresponding moment-curvature analysis associated with the transverse reinforcement.

### **5.3.3 Limit State Comparisons**

The results given in Figure 5.1 to Figure 5.6 reveal that the deformation-based performance limits proposed for non-conforming (Type-1) columns by Eurocode 8 and TDY 2007 are more tolerant compared to ASCE/SEI 41-Update. Nevertheless, all codes are very conservative in setting the two related performance limits of life safety (significant damage, safety limit) and collapse prevention (near collapse, collapse limit) in terms of plastic rotations in view of the test results. Type-1 specimens exhibit total deformation capacities of at least twice of the code acceptance criteria under severe displacement cycles yet they maintain more than 80% of their yield moment capacities. The performance of the specimen 3P3 with an axial load ratio of 0.4 however conforms better with the code performance criteria. Accordingly, it may be stated that non-conforming columns under moderate

axial loads and with ensured flexure failure mode have significantly larger deformation capacities than those specified by the current performance based seismic codes. This conclusion was also confirmed by Verderame et al. (2008). It should also be kept in mind that although Type-1 columns are classified as non-conforming columns in this study, they are not the exact representatives of the actual on-site non-conforming columns which were built with lower concrete strength, with lower transverse reinforcement ratios and with worse reinforcement detailing.

Type-2 specimens are classified as Condition (i) by ASCE/SEI 41-Update. Eurocode 8 accounts for the enhanced seismic performance of these columns with deformed longitudinal bars, low shear and axial force and proper confinement at the plastic hinge region in specifying their deformation-based performance criteria. The same expressions for Type-1 specimens (Equation 5.3 and 5.4) are also utilized for Type-2 specimens. No reduction for calculated ultimate chord rotations is carried out since the Type-2 column specimens were detailed according to seismic code provisions. On the other hand, TDY 2007 considers implicitly the effect of axial load, deformed bars and detailing of transverse reinforcement by including it in the moment-curvature analysis and explicitly the transverse reinforcement ratio in calculating the limit state strain values as given in Equations 5.5, 5.6 and 5.7. The type of reinforcing bars (plain or deformed) and the shear ratio is not considered as parameters for limit state calculation in TDY 2007. It is observed from Figure 5.7 to 5.12 that the performance limit states proposed in terms of rotations by all three codes are quite close to each other for the yield limit state (minimum damage), however they are quite different for the other limit states. Significant damage and ultimate capacity deformation limits of Eurocode 8 are 27% and 39% larger than the life safety and collapse prevention limits of the ASCE/SEI 41-Update, respectively, although these different performance limit definitions in the two codes actually indicate similar performance levels. Moreover, the safety limit (GV) and collapse limit (GÇ) of TDY 2007 are 17% and 22% larger than the ASCE/SEI 41-Update limits, and 10% and 14% smaller than the EC8 limits, respectively. The results presented in Figure 5.7 to Figure 5.12 confirm the limit state predictions of

Eurocode 8 and TDY 2007 meanwhile demonstrate that ASCE/SEI 41-Update limit state definitions with the proposed plastic rotation values are too conservative for such columns, even when the columns are subjected to severe displacement cycles.

It should be noted that TDY 2007 does not account for flexure-shear behavior in classifying the performance of columns. Since the columns tested in this study do not exhibit such behavior, such a possible shortcoming is not displayed in the code prediction. This shortcoming is discussed in detail by Ergüner (2009).

#### **5.3.4 ASCE/SEI 41-Update Modeling Parameters**

Two parameters  $a$  and  $b$  are proposed in the ASCE/SEI 41-Update for modeling the plastic hinge behavior of flexural members where  $a$  is the plastic rotation at significant loss of plastic rotation capacity, and  $b$  is the plastic rotation at axial load failure. These two parameters are mainly employed in the nonlinear static analysis of concrete structures for constructing the capacity curves. Moment-chord rotation envelope relations obtained by employing the associated values of the two parameters for Type-1 and Type-2 specimens are calculated and compared with the results obtained from the experiments in Figure 5.13 and Figure 5.14, respectively.

It can be observed from Figure 5.13 and Figure 5.14 that the plastic hinges of both types of column specimens are capable of sustaining larger plastic deformations before significant loss of plastic rotation capacity. The modeling parameter  $a$  seems to be very conservative for defining the rotation capacity of column plastic hinges when the axial load ratio is around 0.20 whereas the suggested  $a$  values may be more reasonable at higher axial loads.

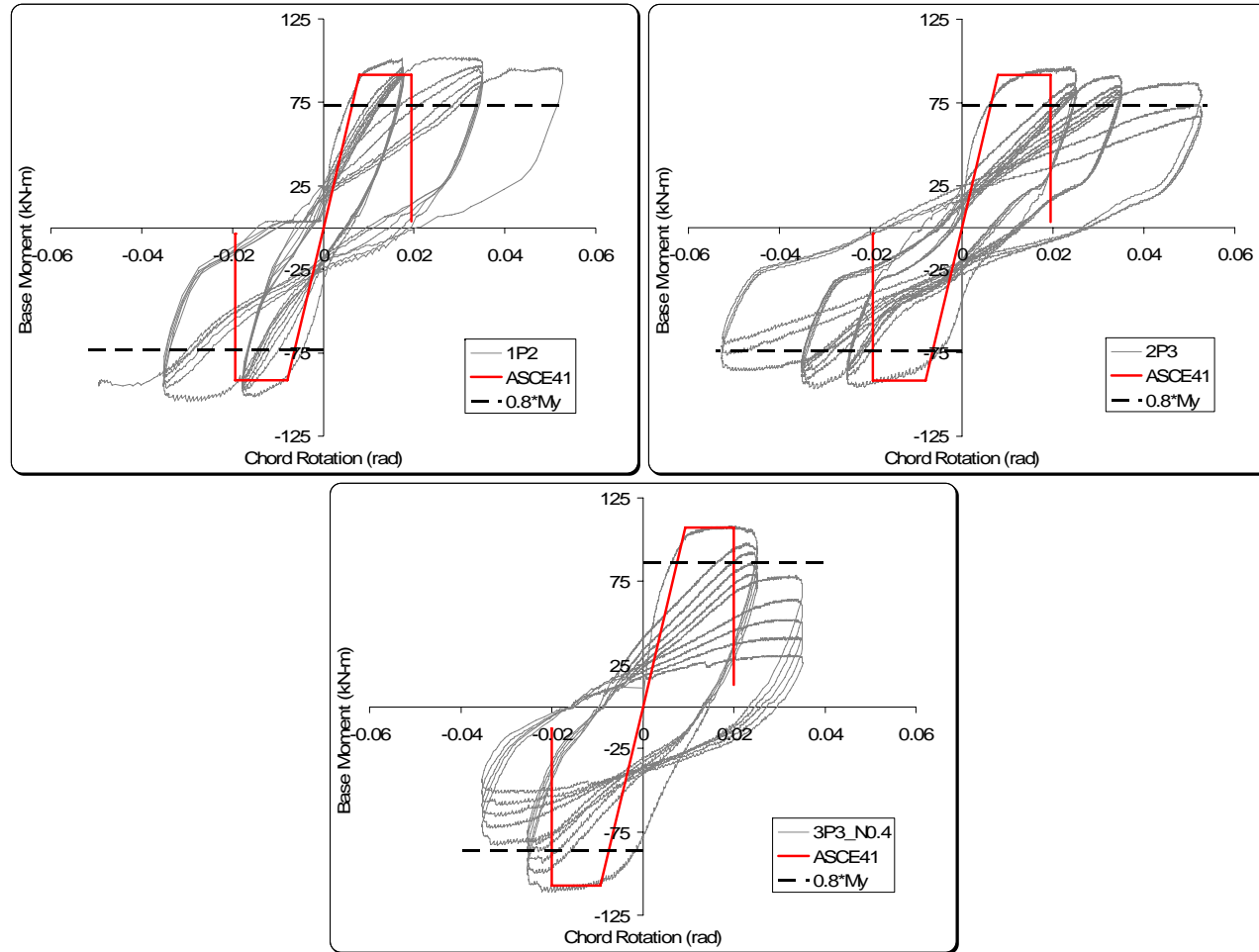


Figure 5.13 Comparison of responses of Type-1 specimens with the ASCE41 modeling parameters

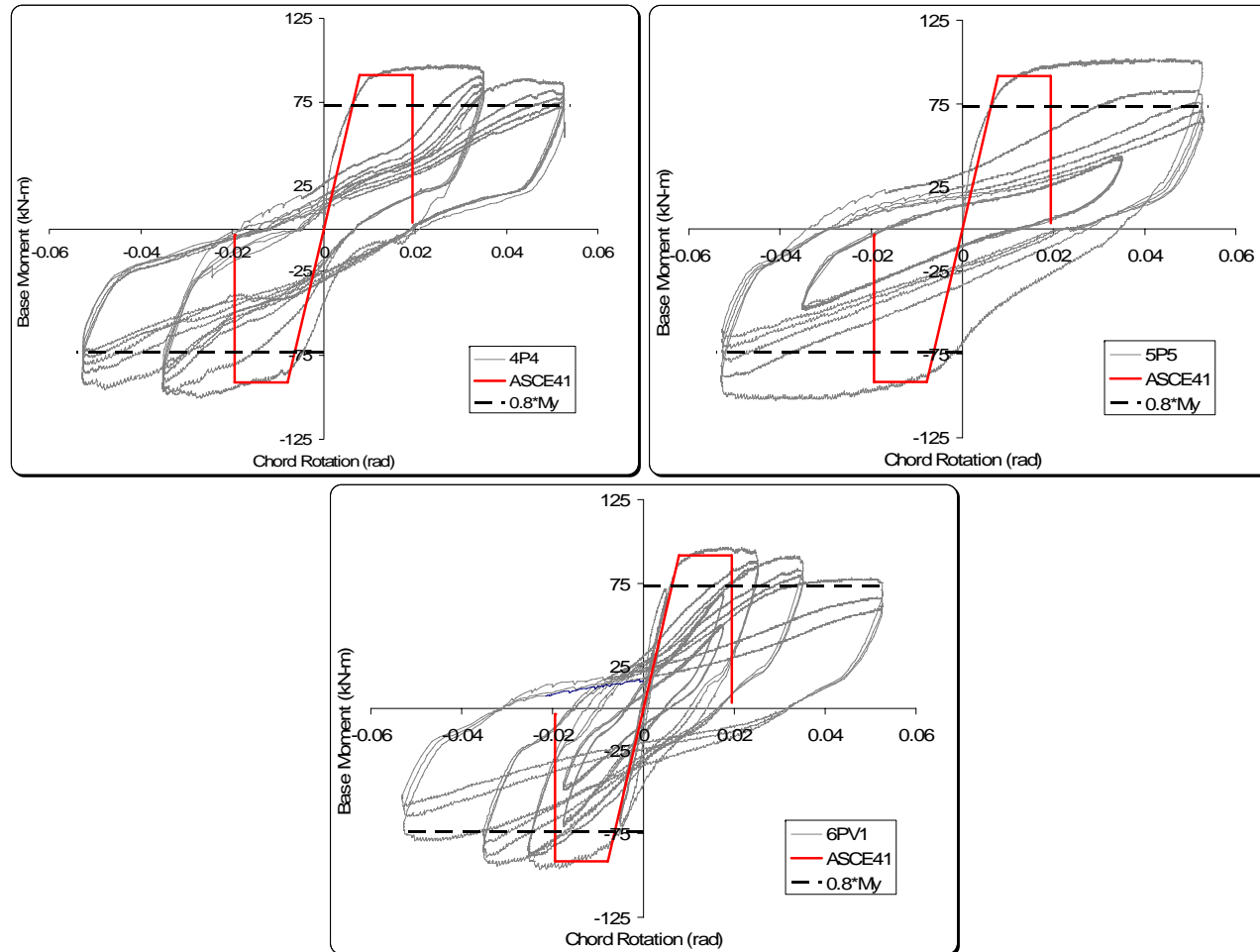


Figure 5.13 (cont'd) Comparison of responses of Type-1 specimens with the ASCE41 modeling parameters

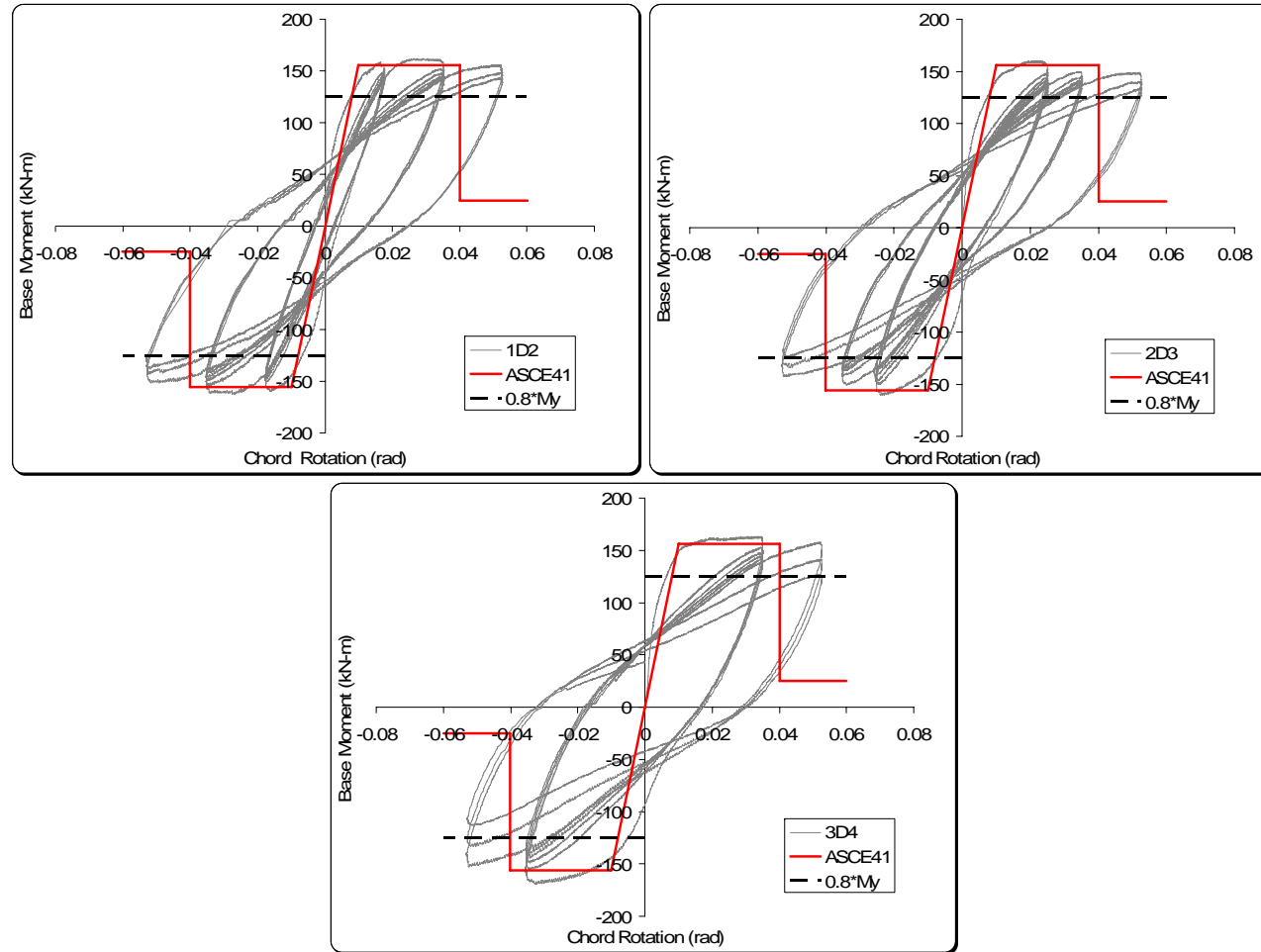


Figure 5.14 Comparison of responses of Type-2 specimens with the ASCE41 modeling parameters

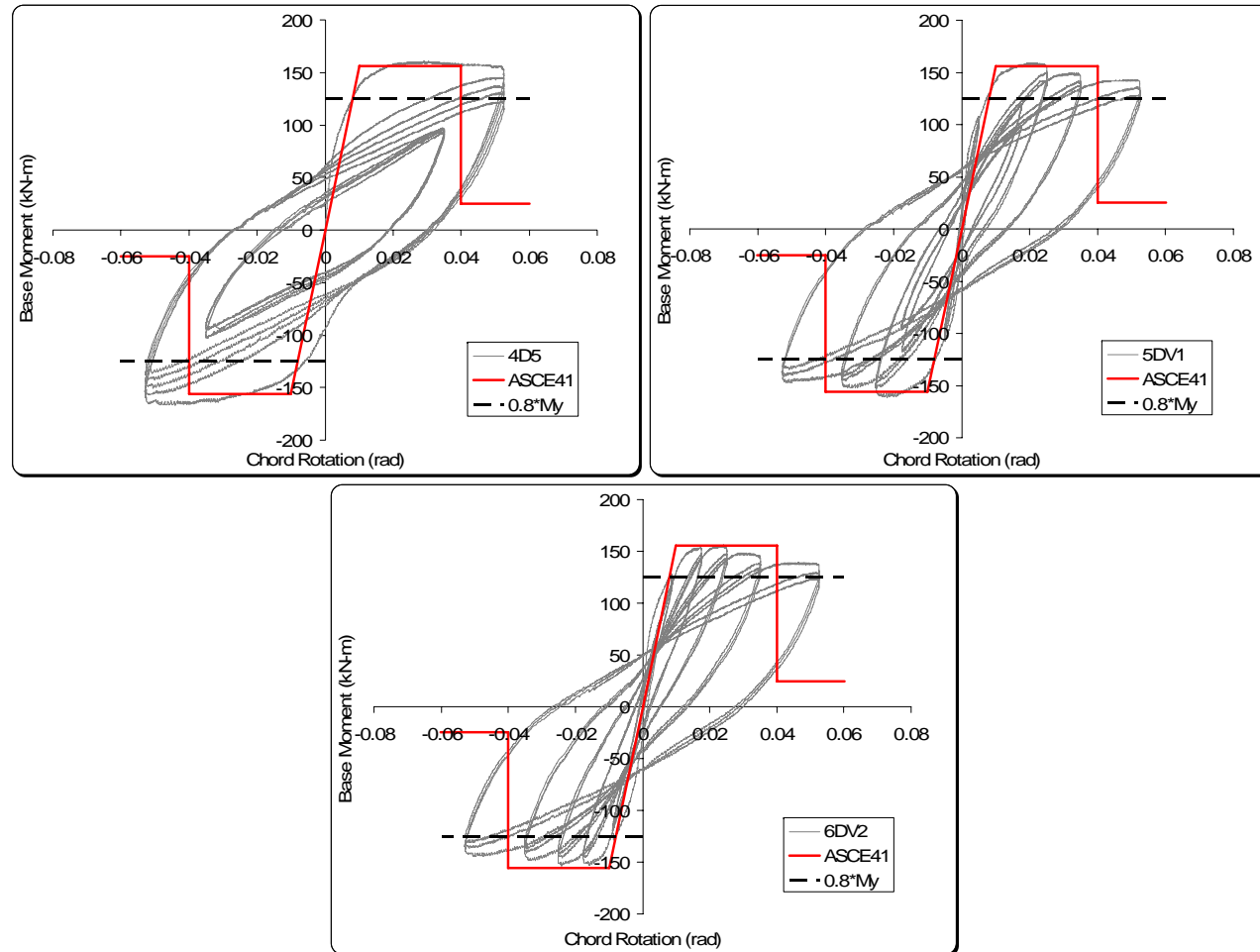


Figure 5.14 (cont'd) Comparison of responses of Type-2 specimens with the ASCE41 modeling parameters

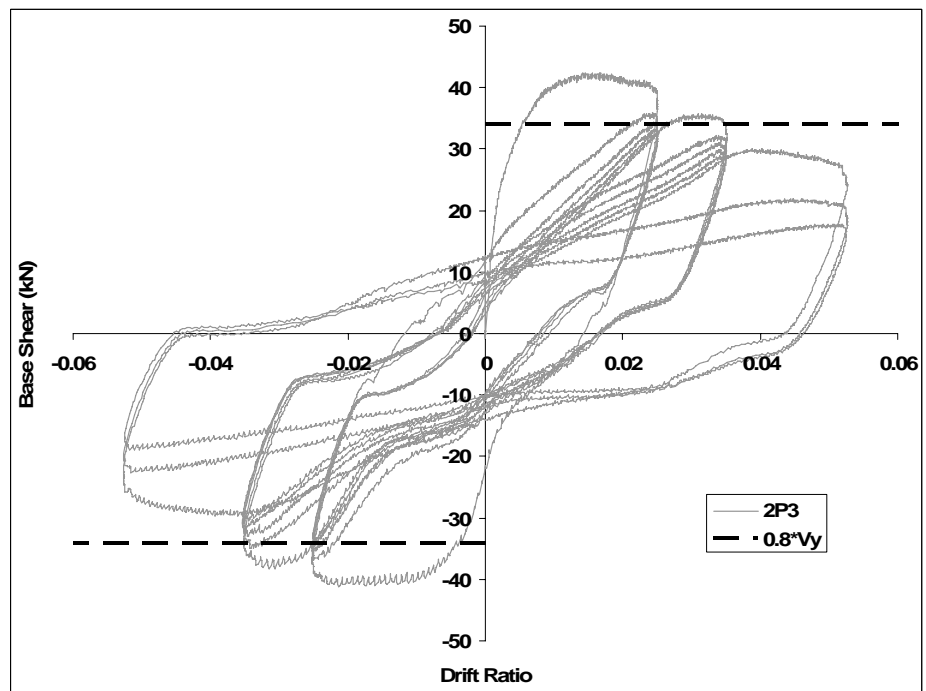
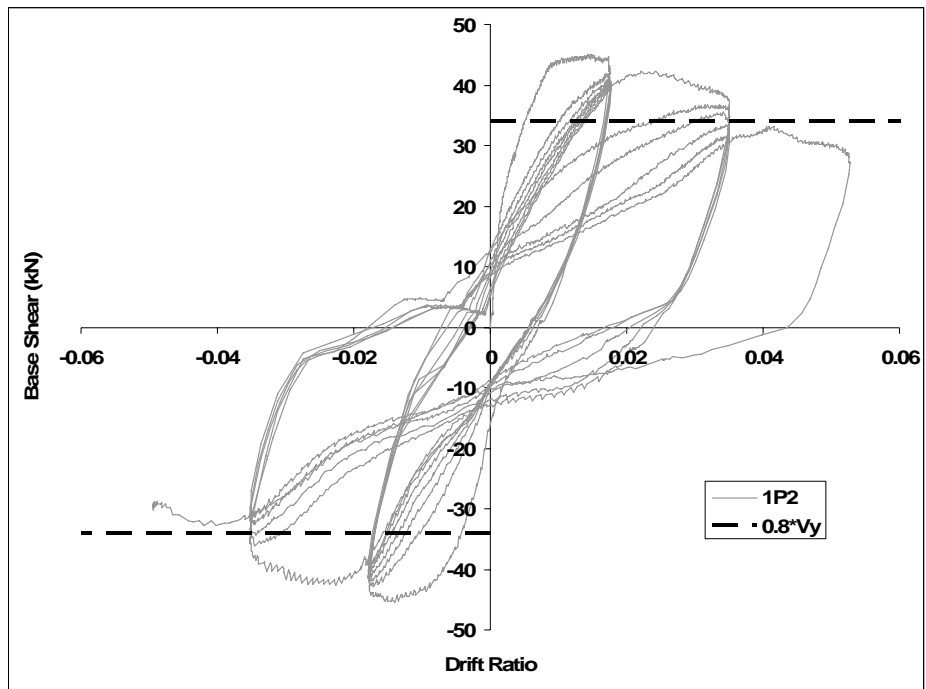


Figure 5.15 Experimental responses of Type-1 column specimens in terms of base shear-drift ratios

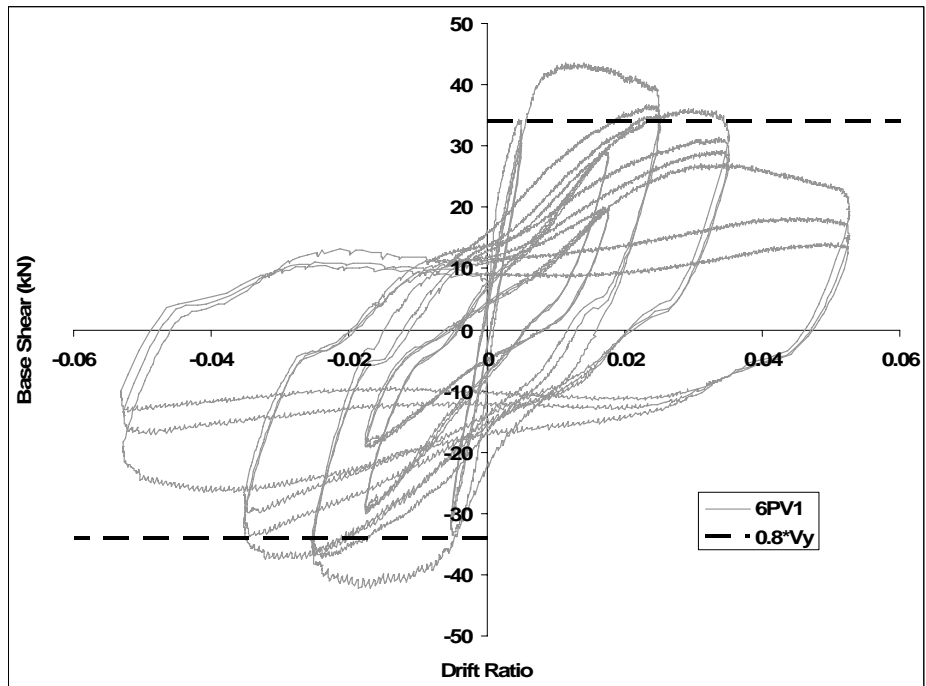
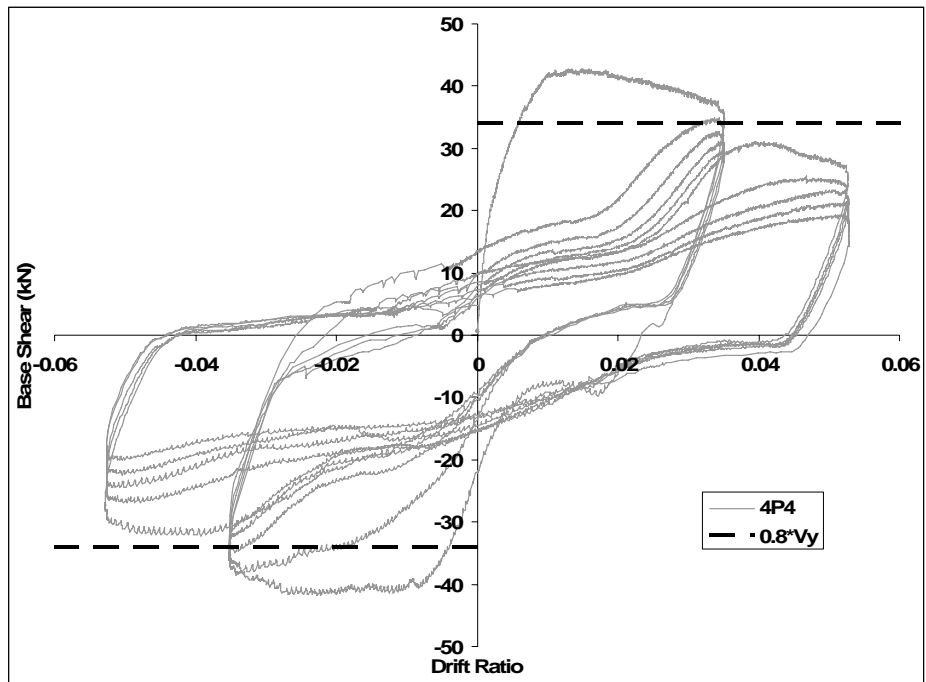


Figure 5.15 (cont'd) Experimental responses of Type-1 column specimens in terms of base shear-drift ratios

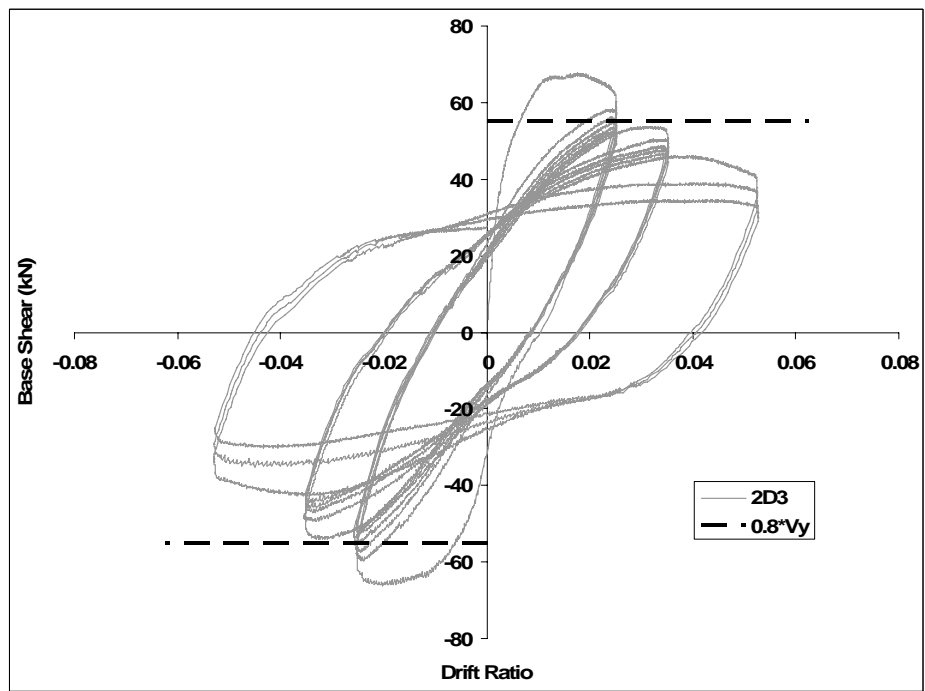
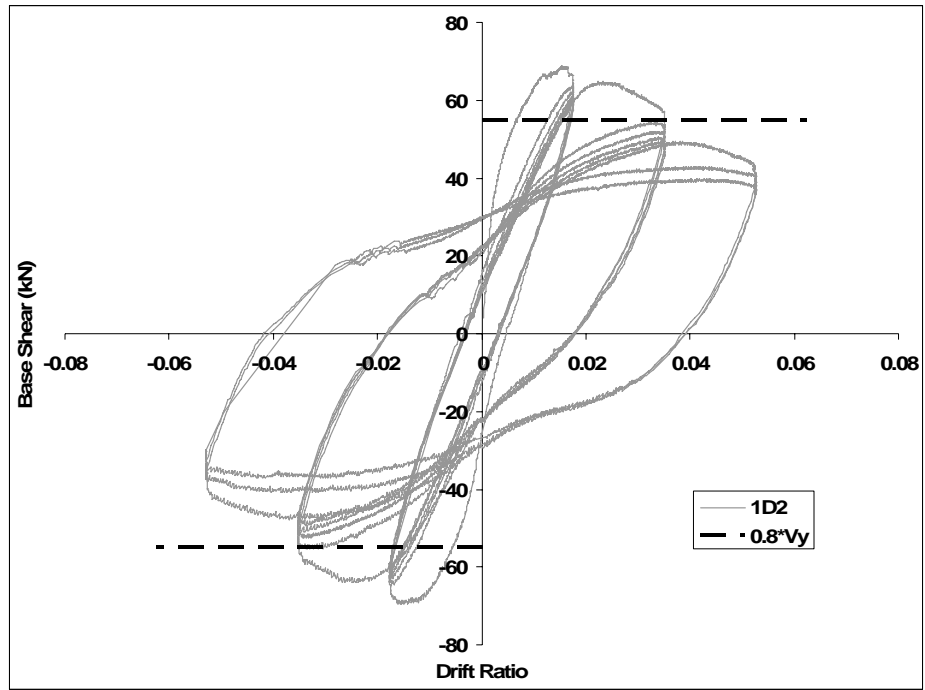


Figure 5.16 Experimental responses of Type-2 column specimens in terms of base shear-drift ratios

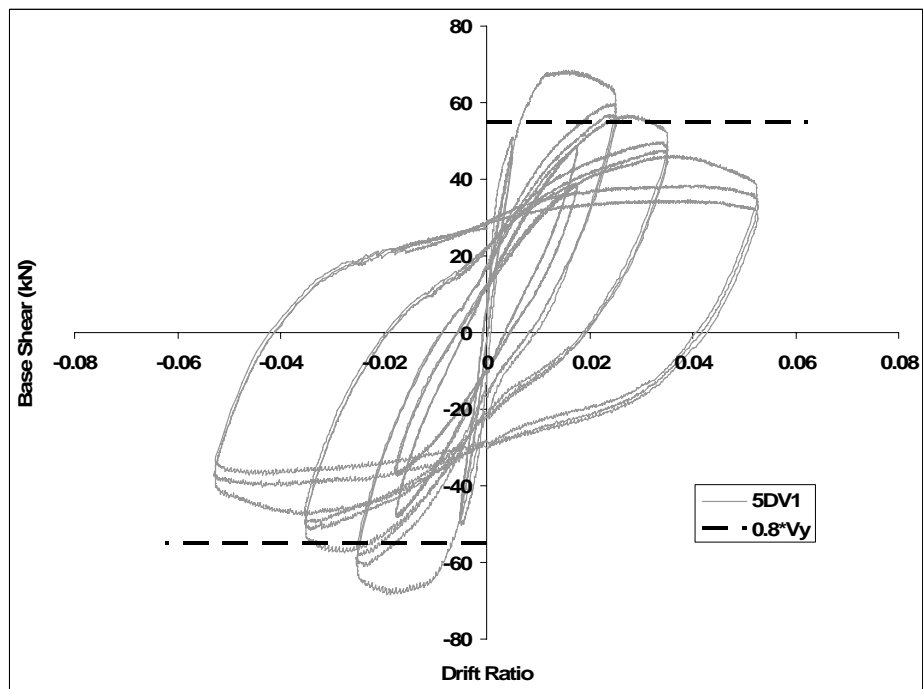
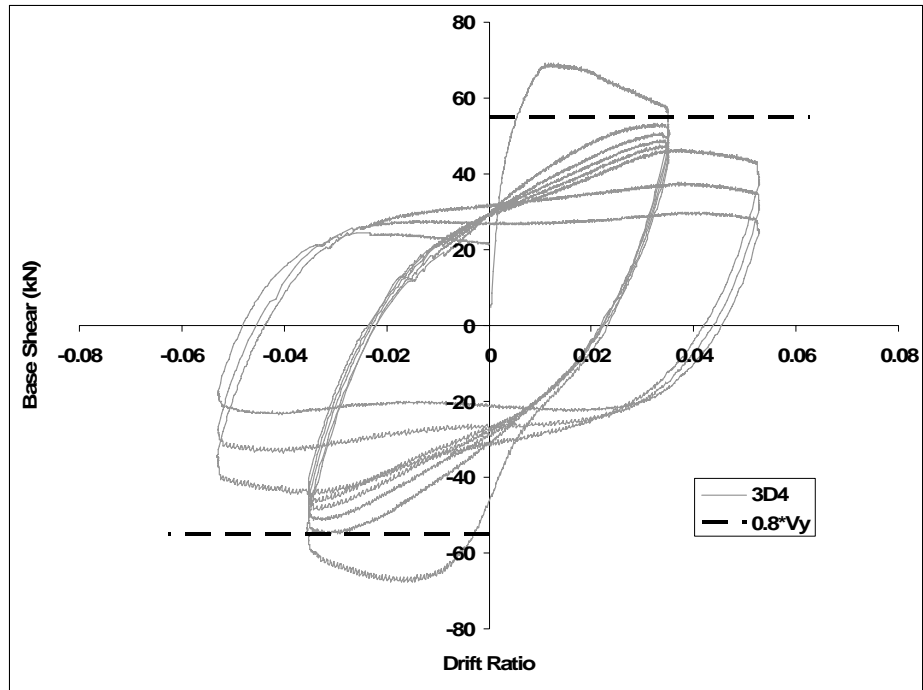


Figure 5.16 (cont'd) Experimental responses of Type-2 column specimens in terms of base shear-drift ratios

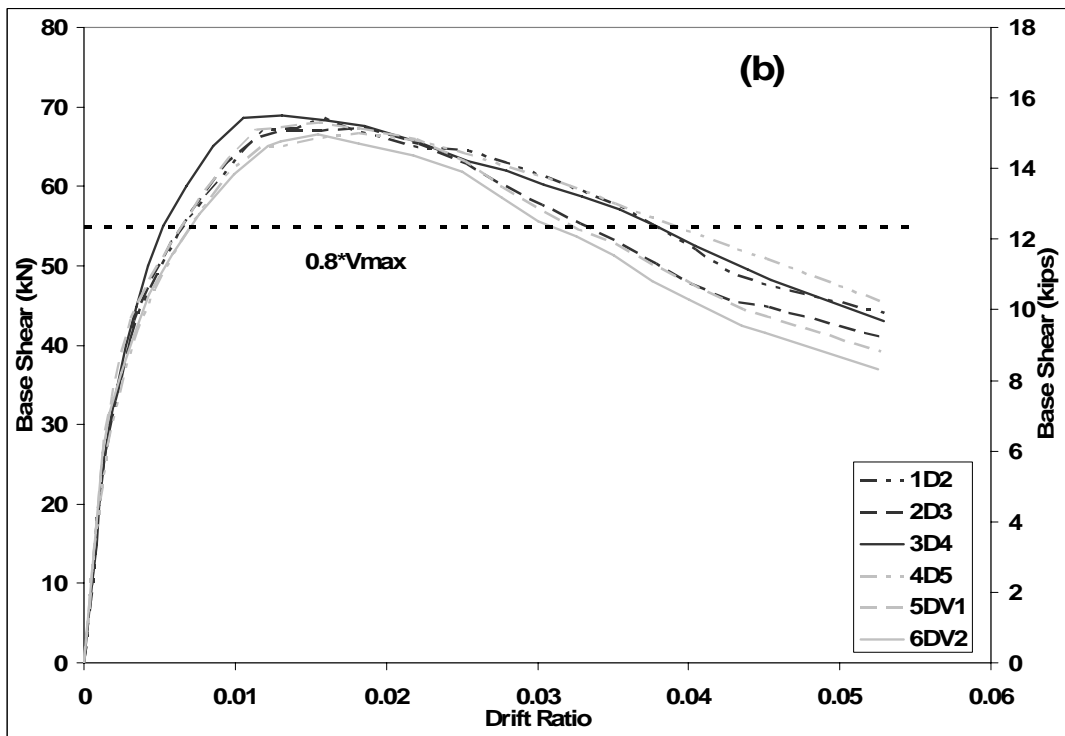
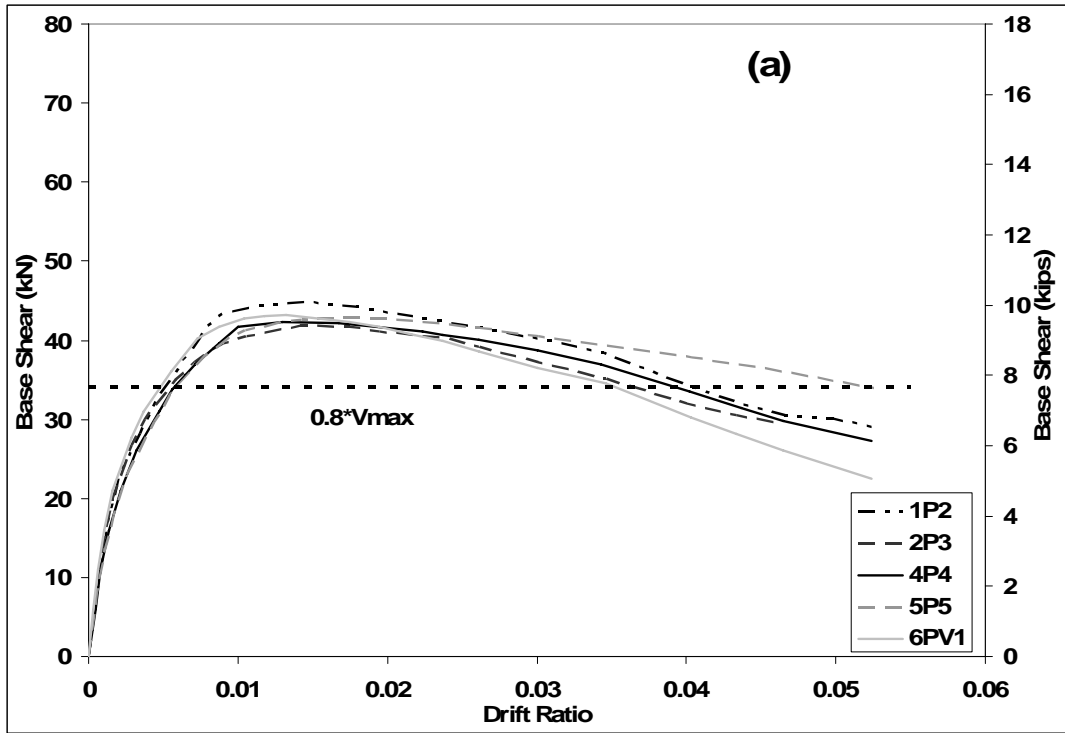


Figure 5.17 Envelope curves for positive base shear-drift ratio cycles of (a) Type-1 and (b) Type-2 column specimens

#### 5.4 The Effect of Displacement History on Target Displacement Demand

The column specimens reported in Chapter 4 can be considered as cantilever structures carrying an assigned mass, which possess the lateral force (base shear) versus lateral drift relationship as obtained from the experiments. These relationships are presented in Figures 5.15 and 5.16 for the Type-1 and Type-2 specimens, respectively. The applied lateral load measurements are corrected for the P- $\Delta$  effect caused by geometric nonlinearity of the loading system. 80% level of the yield lateral force level is also marked for each specimen on each figure. The specimen 3P3\_N04 is excluded from the group because of its relatively high axial load ratio compared to the other members. Specimens 4D5 and 5P5 subjected to large displacement reversals at the initial cycles are also excluded from this evaluation where it is not possible to investigate the effect of displacement history with their monotonic-like loading protocols. The lateral force-lateral drift envelopes for the first positive cycles of the Type-1 and Type-2 specimens are also obtained and shown in Figure 5.17.a and 5.17.b respectively. These envelopes are connecting the peaks of the first positive cycles in each stage of constant displacement cycles.

It is observed from Figure 5.17 that all specimens in Type-1 and Type-2 categories exhibit similar envelopes until they fall below the 80%  $V_{max}$  level, regardless of the cyclic displacement histories they are enveloping. The lateral strength of all specimens falls below 80% of  $V_{max}$  approximately at the same drift ratio of 0.035, or at the column drift of 70 mm.

If the average envelope curves in Figure 5.17 are considered as the capacity curves for the column structures, then the target drift demands of each column structure can be calculated through equivalent linearization procedure. The average envelope curves are replaced by bi-linear capacity curves shown in Figure 5.18.a by employing the equal energy approach. The capacity curves for the Type-1 and Type-2 column structures possess similar ductility ratios of 5.2 and 4.9 at the drift ratio of 0.035, and similar post yield stiffness ratios of -0.043 and -0.048, respectively. A mass producing an initial elastic period of  $T_0 = 0.3$  second is

assigned to each column, and the earthquake excitation is defined by the 5% damped design spectrum shown in Figure 5.18.b.

Two different approaches for equivalent linearization are employed comparatively. The first one is the improved procedure proposed in FEMA 440 (2005) where effective period and effective damping are calculated iteratively from the empirical equations based on strength degrading model, whereas they are directly calculated from the experimental data (Base shear-top displacements) in the second approach. The iterative solution for effective damping and effective period in the first (FEMA 440) approach converged at ductility ratios of 4.1 and 3.7 for the Type-1 and Type-2 specimens, respectively. Effective damping in the second approach is based on the first experimental cycles with drift amplitudes of 0.035. However if target drift calculated from equivalent linearization is different from 0.035, then a correction procedure is introduced for effective damping. Dissipated energy at this displacement cycle is scaled according to the ratio of calculated target drift to 0.035.

It is assumed that each column structure reaches its target drift after completing a past displacement history at lower drift values as given in Table 3.4. Hence effective damping reflects the effect of displacement history on target drift demand in the second approach. The results of the first (analytical: FEMA 440) and the second (experimental) equivalent linearization approaches are summarized in Table 5.2.

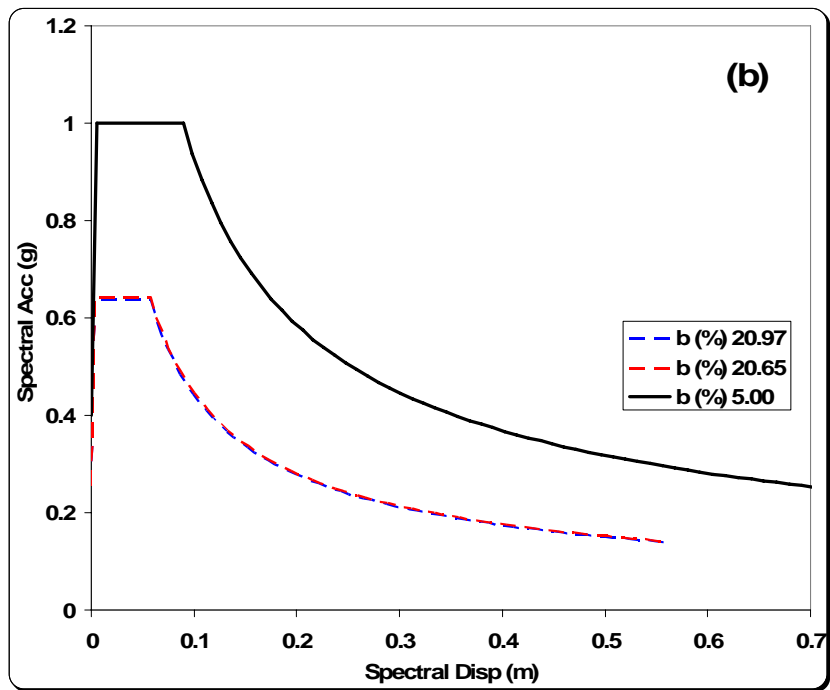
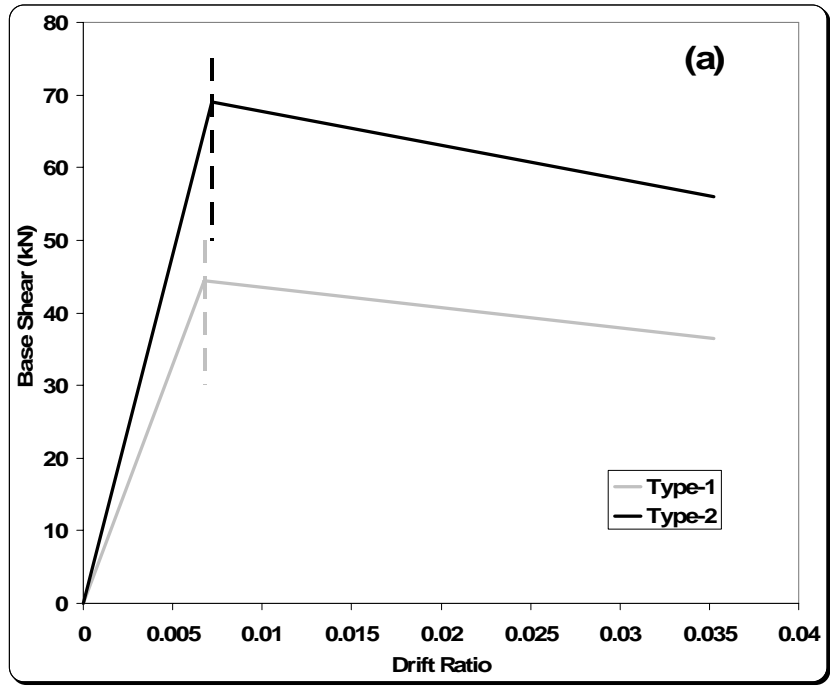


Figure 5.18 (a) Bi-linear capacity curves for Type-1 and Type-2 specimens, (b) design spectrum

Table 5.2 Target drift ratios calculated with equivalent linearization

	Specimen	Experimental			FEMA – 440		
		$\beta_{eff}$ (%)	$T_{eff} / T_0$	Target Drift	$\beta_{eff}$ (%)	$T_{eff} / T_0$	Target Drift
Type -1	<b>1P2</b>	26.73	2.51	0.034	20.97	1.77	0.027
	<b>2P3</b>	18.90	2.61	0.041			
	<b>4P4</b>	32.96	2.53	0.031			
	<b>6PV1</b>	25.48	2.64	0.037			
Type -2	<b>1D2</b>	24.50	2.46	0.034	20.65	1.70	0.026
	<b>2D3</b>	22.49	2.55	0.037			
	<b>3D4</b>	33.86	2.43	0.029			
	<b>5DV1</b>	23.76	2.55	0.036			
	<b>6DV2</b>	23.69	2.60	0.037			

The column structures 4P4 and 3D4 attain the target drift amplitudes of 0.031 and 0.029 in their first displacement cycles during testing with in-cycle degradation, however they do not exhibit any cyclic degradation due to displacement history effects. Accordingly they possess the highest effective damping values which lead to the lowest target drift ratios of the experimental approach for the Type-1 and Type-2 specimens. Target drift ratios for the other columns are higher, reflecting reduced effective damping due to cyclic degradation in energy dissipation capacity. FEMA 440 approach on the other hand does not properly reflect the effect of displacement history. Effective damping and effective period values obtained from the strength degrading model of FEMA 440 for the tested column structures lead to unconservative estimation of the target drift ratios compared to the experimental values. The target drift ratios obtained with the experimental approach for the column structures that undergo severe inelastic displacement cycles before reaching the maximum drift are 40% larger on average than those obtained with the FEMA 440 approach. The stiffness degrading model employed in the FEMA 440 approach perhaps do not properly represent the experimental in-cycle and cyclic degradation behavior of the columns presented herein.

## **5.5 Limitations of Test Results and Their Implications**

The test results presented herein have two limitations. First, lateral loading is uniaxial and second, axial load is constant. In 1989, Saatcioglu and Ozcebe (1989) investigated the effect of bidirectional loading cycles on strength and stiffness deterioration of reinforced concrete column members concluding that the degradation can be severe. Bousias et al. (1995) also observed strong coupling between two bending directions which produced considerable reduction in strength and stiffness compared to uniaxially tested columns. Galal and Ghobarah (2003) analytically investigated the effect of axial load variation and biaxial bending on lateral deformation of columns by using plasticity theory. They concluded that cycling of axial load causes reduction in strength and energy dissipation capacity. Therefore biaxial bending and cyclic axial load patterns result in softer columns with lower stiffness and smaller effective damping compared to columns under uniaxial bending and constant axial load. This phenomenon eventually leads to larger displacement demands under strong ground motions with long effective duration.

## **CHAPTER 6**

### **ENERGY DISSIPATION CHARACTERISTICS OF RC COLUMNS UNDER LOW CYCLE FATIGUE LOADING**

#### **6.1 General**

The effect of low-cycle fatigue loading on the hysteretic response, energy dissipation and strength degradation characteristics of reinforced concrete columns are investigated in this chapter. A total number of 22 column specimens from three different experimental programs were selected to form a database for evaluating the low cycle fatigue characteristics of reinforced concrete columns. Ten of them were selected from the tests conducted on column specimens during the reported thesis study (Acun and Sucuoğlu 2010; Type-1 and Type-2), and the remaining twelve were taken from the PEER structural performance database (Berry et al., 2004) tested under imposed constant amplitude displacement cycles (Pujol 2002, Wight and Sozen 1975). The cross section and material properties of each test specimen with their associated codes are presented in Table 6.1. All specimens were tested under at least five constant-amplitude displacement cycles at the drift and ductility ratios given in the last two columns of Table 6.1. Hysteretic response envelopes, cyclic energy dissipation and cyclic flexural strength degradation characteristics of these columns are investigated in view of the imposed low-cycle displacement patterns.

The specimens selected for establishing the database are first classified with respect to their failure modes based on the parameters employed in performance-

based seismic assessment practice (ASCE /SEI 41, Eurocode 8, TDY 2007). These parameters are the shear span ratio ( $a/d$ ), shear demand to shear strength ratio ( $V/V_n$ ) and normalized shear stress  $V/b_w.d\sqrt{f_c}$ . All of these parameters have indicated a clear distinction of failure modes, which is flexure dominant for the Acun and Sucuoğlu Type-1 and Type-2 specimens, and flexure-shear for the Pujol and Wight and Sozen specimens. These failure modes were also verified by the researchers themselves in their reports based on the observed behavior of tested specimens. Typical base moment-chord rotation hysteretic response samples from each group of specimens in Table 6.1 exhibiting both modes of failure are presented in Figure 6.1

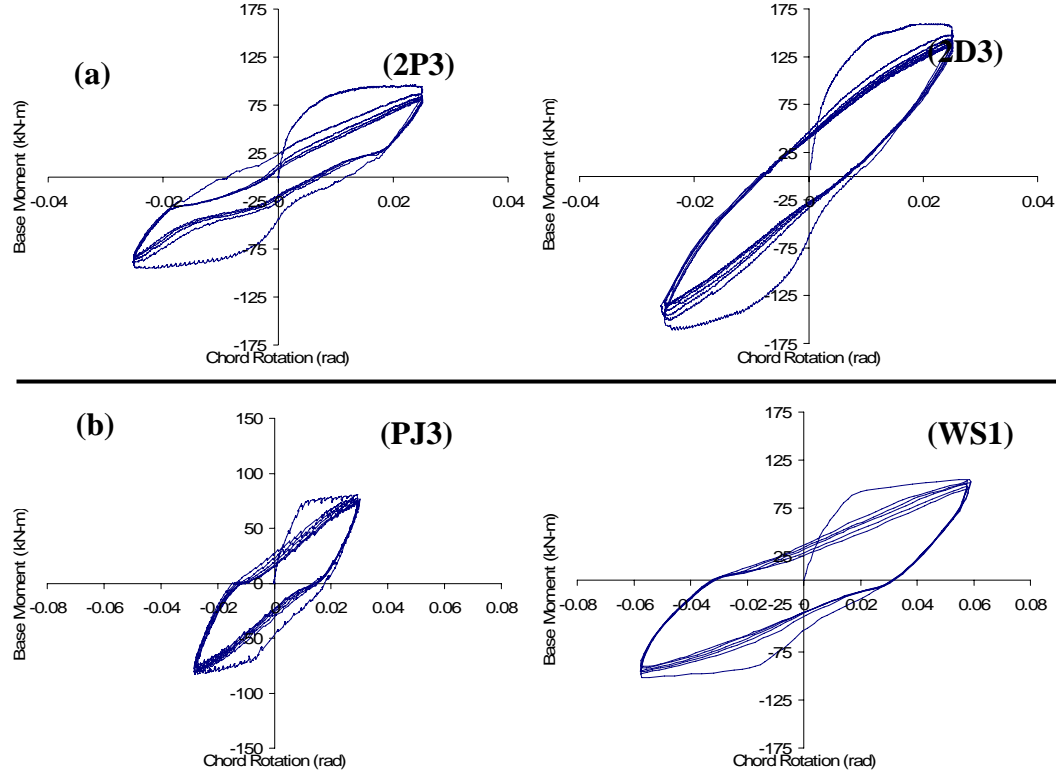


Figure 6.1 Moment-rotation response of column specimens with, (a) flexure (Type-1 and Type-2), (b) shear-flexure (Pujol, Wight and Sozen) failure modes

Table 6.1 Reinforced concrete column specimen database

No	Name	Code	$b_w$	$d$	$f_c$	$f_y$	$f_w$	$a/d$	$V$	$V/b_w d \sqrt{f_c}$	$V/V_n$	$N$	$N/F_c A_g$	$\rho_l$	$\rho_t$	$\delta$ (1st cycle)	$\mu_\theta$
			(mm)	(mm)	(MPa)	(MPa)	(MPa)		(kN)			(kN)		(%)	(%)	(%)	
1	Pujol, No. 10-2-3N	PJ1	152	254	33.7	453	411	2.70	112.0	0.498	0.884	134	0.08	2.45	0.545	2.00	2.27
2	Pujol, No. 10-2-3S	PJ2	152	254	33.7	453	411	2.70	112.0	0.498	0.884	134	0.08	2.45	0.545	2.00	2.27
3	Pujol, No. 10-3-1.5N	PJ3	152	254	32.1	453	411	2.70	111.0	0.506	0.521	134	0.09	2.45	1.094	3.00	3.46
4	Pujol, No. 10-3-1.5S	PJ4	152	254	32.1	453	411	2.70	111.0	0.506	0.521	134	0.09	2.45	1.094	3.00	3.46
5	Pujol, No. 10-3-2.25N	PJ7	152	254	27.4	453	411	2.70	112.0	0.553	0.738	134	0.10	2.45	0.727	3.00	3.30
6	Pujol, No. 10-3-2.25S	PJ8	152	254	27.4	453	411	2.70	112.0	0.553	0.738	134	0.10	2.45	0.727	3.00	3.30
7	Pujol, No. 10-2-2.25N	PJ11	152	254	34.9	453	411	2.70	114.0	0.499	0.729	134	0.08	2.45	0.727	2.00	2.46
8	Pujol, No. 10-2-2.25S	PJ12	152	254	34.9	453	411	2.70	114.0	0.499	0.729	134	0.08	2.45	0.727	2.00	2.46
9	Wight & Sozen,40.147-E	WS1	152	254	33.5	496	317	3.45	119.8	0.536	0.571	178	0.12	2.40	1.465	5.75	4.00
10	Wight & Sozen,40.147-W	WS2	152	254	33.5	496	317	3.45	120.5	0.539	0.571	178	0.12	2.40	1.465	5.75	4.00
11	Wight & Sozen,40.092-E	WS3	152	254	35.5	496	317	3.45	115.5	0.502	0.720	178	0.11	2.40	0.916	5.75	4.00
12	Wight & Sozen,40.092-W	WS4	152	254	35.5	496	317	3.45	113.0	0.491	0.720	178	0.11	2.40	0.916	5.75	4.00
13	Acun & Sucuoglu Type-1	1P2	350	315	13.5	315	368	6.35	42.4	0.105	0.317	340	0.21	1.00	0.261	1.75	1.91
14	Acun & Sucuoglu Type-1	2P3	350	315	12.2	315	368	6.35	42.4	0.110	0.317	302	0.20	1.00	0.261	2.50	2.72
15	Acun & Sucuoglu Type-1	3P3_N04	350	315	13.1	315	368	6.35	45.0	0.113	0.336	640	0.40	1.00	0.261	2.50	2.22
16	Acun & Sucuoglu Type-1	4P4	350	315	12.4	315	368	6.35	42.4	0.109	0.317	308	0.20	1.00	0.261	3.50	3.81
17	Acun & Sucuoglu Type-1	5P5	350	315	11.4	315	368	6.35	42.4	0.114	0.317	300	0.21	1.00	0.261	5.25	5.72
18	Acun & Sucuoglu Type-1	7P3_U	350	315	13.2	315	368	6.35	42.4	0.106	0.317	322	0.20	1.00	0.261	2.50	N.A.
19	Acun & Sucuoglu Type-2	1D2	350	315	25.8	454	469	6.35	68.5	0.122	0.192	638	0.20	1.00	0.615	1.75	1.43
20	Acun & Sucuoglu Type-2	2D3	350	315	25.9	454	469	6.35	68.5	0.122	0.192	632	0.20	1.00	0.615	2.50	2.05
21	Acun & Sucuoglu Type-2	3D4	350	315	27.6	454	469	6.35	68.5	0.118	0.192	674	0.20	1.00	0.615	3.50	2.87
22	Acun & Sucuoglu Type-2	4D5	350	315	24.6	454	469	6.35	68.5	0.125	0.192	610	0.20	1.00	0.615	5.25	4.30

## 6.2 Capacity Curves

Base moment - chord rotation capacity curves of the column specimens with identical cross section and material properties, but tested under different displacement amplitudes are constructed from their first positive cycles for a comparative evaluation.

The associated capacity curves of Type-1 specimens are given in Figure 6.2. The specimens 3P3\_N0.4 and 7P3\_U are also included in the figure in order to observe the effect of axial load and bond strength on the capacity of these specimens. Since all members of Type-1 group except 3P3\_N0.4 and 7P3\_U were tested under the same axial load ratio and have identical cross section properties, envelope curves of these specimens form a group. Specimen 3P3\_N0.4 displays a higher moment capacity as a consequence of its relatively high axial load ratio. On the other hand Specimen 3P3\_U displays a sudden stiffness decrease at the first cracking of concrete since only one crack develops at its base due to the broken bond between concrete and longitudinal bars. However the specimen reaches the same moment capacity level at about a drift ratio of 2 percent.

Capacity curves of Type-2 specimens are shown in Figure 6.3. All Type-2 specimens are identical in their material and cross section properties as well as in their axial load ratio of 20%, accordingly the capacity curves for these specimens exhibit small dispersion.

It is observed from Figures 6.2 and 6.3 that similar specimens exhibit almost identical capacity curves, which indicates that they represent a well controlled sample group. This case is also observed on the capacity curves of Pujol (2002) and Wight and Sozen (1975) specimens that are shown in Figures 6.4.a and 6.4.b, respectively.

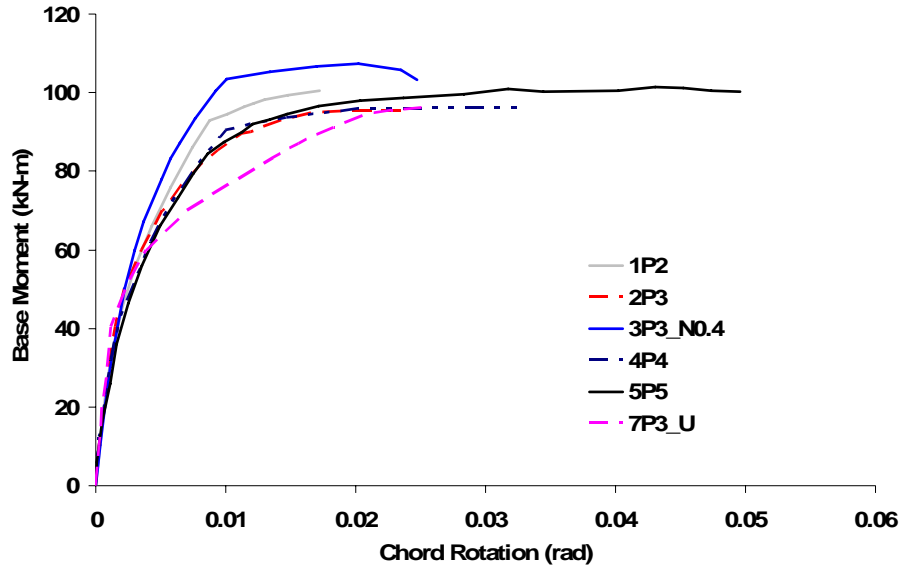


Figure 6.2 Base moment-chord rotation capacity curves of Type-1 specimens

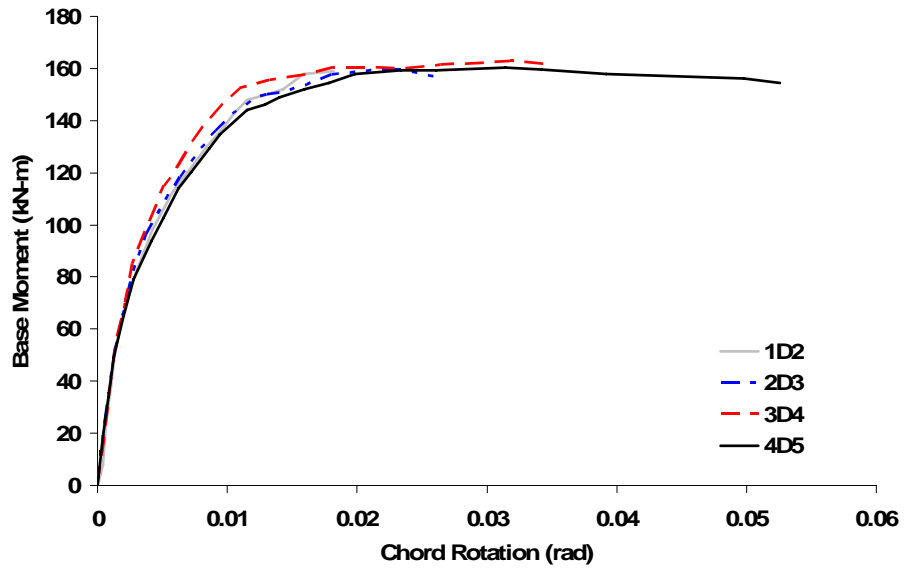


Figure 6.3 Base moment-chord rotation capacity curves of Type-2 specimens

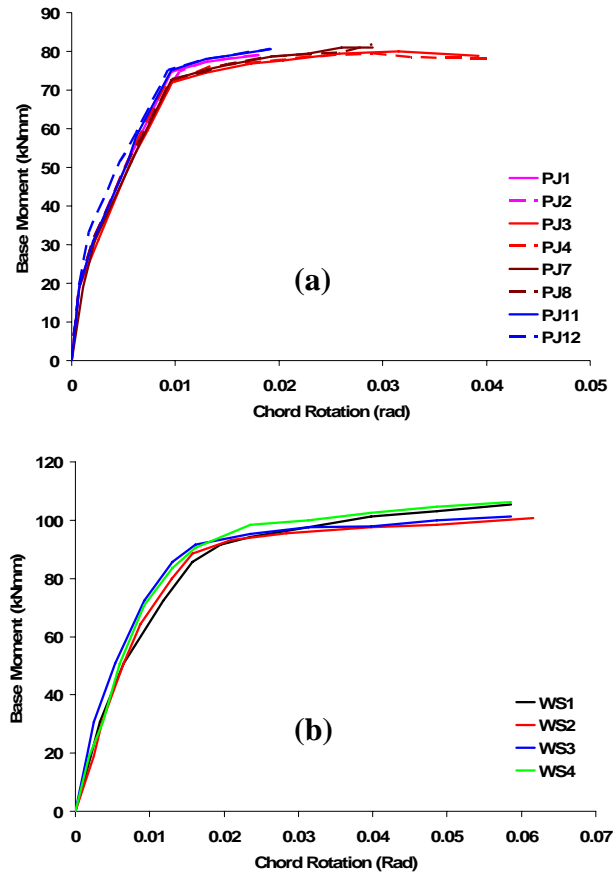


Figure 6.4 Base moment-chord rotation capacity curves of, (a) Pujol (2002) and (b) Wight and Sozen (1975) specimens

### 6.3 Cumulative Cyclic Energy Dissipation Characteristics

Cumulative energy dissipation characteristics are investigated separately for each specimen in the compiled data set. Accumulation of dissipated energy with the number of imposed displacement cycles are presented in Figures 6.5 and 6.6 for the Type-1 and Type-2 columns respectively. Similar relations are shown in Figures 6.7.a and 6.7.b for the Pujol and Wight and Sozen specimens respectively, for all constant displacement amplitudes. It is evident that the rate of dissipated energy accumulation is dependent on the imposed constant displacement amplitude. Energy dissipation rate increases with the amplitude of the displacement cycle, as expected.

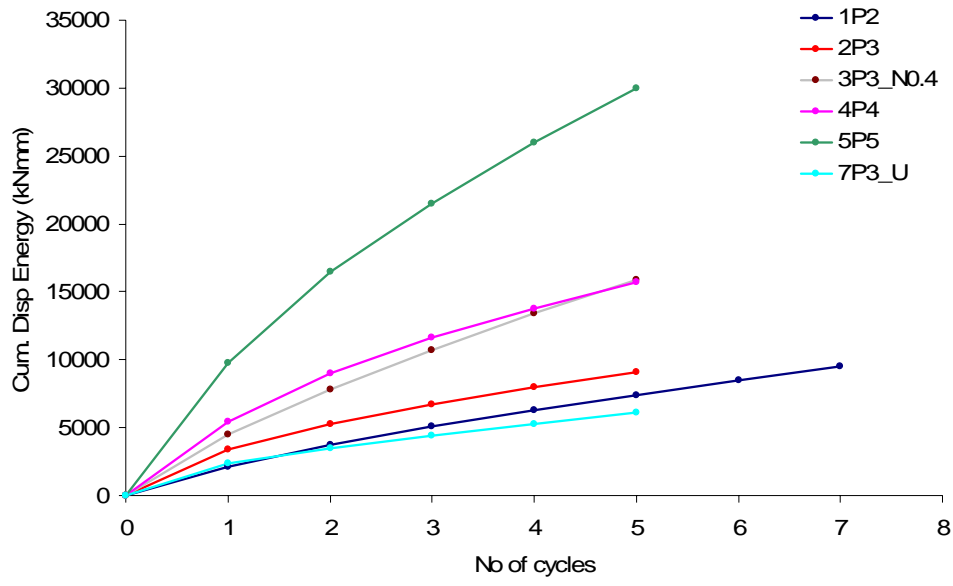


Figure 6.5 Dissipated energy accumulation of Type-1 specimens with the number of cycles

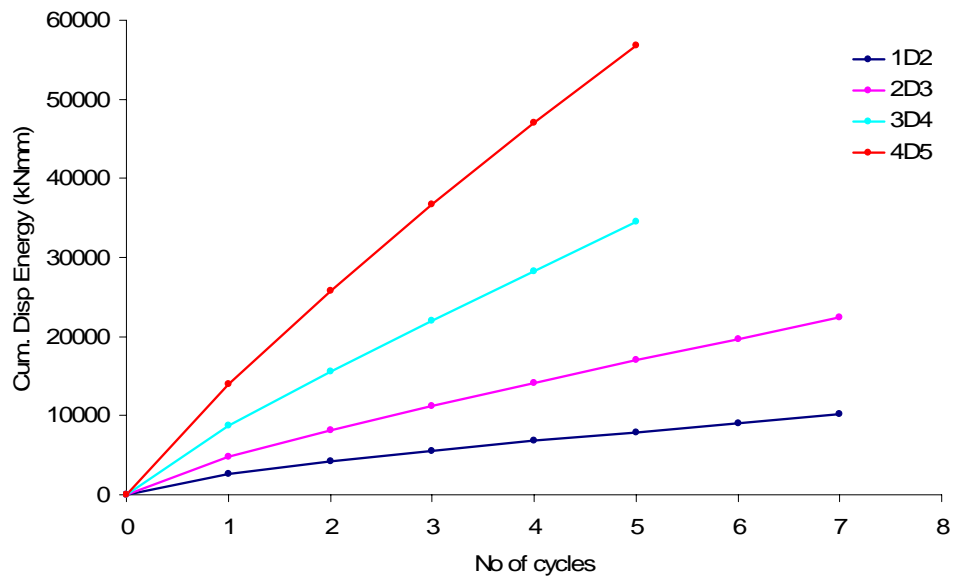


Figure 6.6 Dissipated energy accumulation of Type-2 specimens with the number of cycles

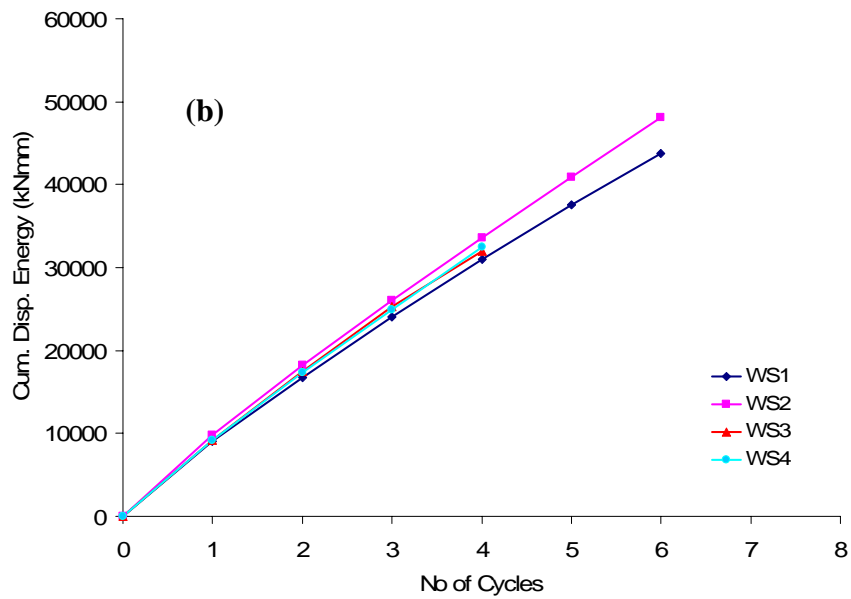
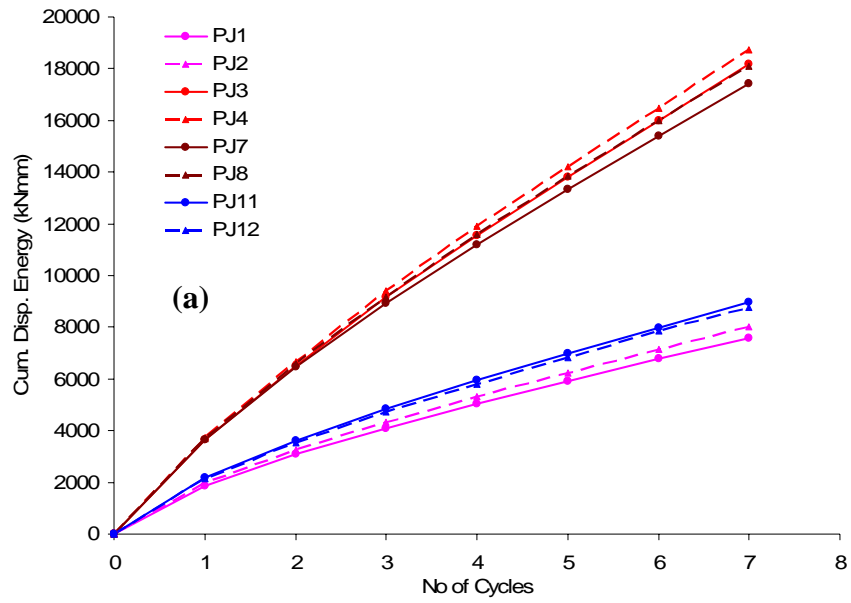


Figure 6.7 Cumulative dissipated energy curves for, (a) Pujol and (b) Wight and Sozen specimens

## 6.4 Normalized Cyclic Energy Dissipation Characteristics

The normalized cyclic energy dissipation for each specimen in the column database can be obtained by normalizing the hysteretic energy dissipated at each individual cycle either with respect to the energy dissipated at the first full cycle by the considered specimen, or with respect to the dissipated energy at the consecutive second full cycle. It should be noted that the first full cycle represents the unique, unsymmetrical response of the virgin specimen whereas the second full cycle represents the general, symmetrical response of the damaged specimen.

Dissipated energy is calculated from the base moment-chord rotation hysteresis curves presented in Chapter 5 for the Type-1 and Type-2 specimens, and from the data provided at “Peer Structural Performance Database” by converting the force-displacement histories into moment-chord rotation hysteresis for Pujol (2002) and Wight and Sozen (1975) column specimens. A force-based cycle definition is used where the area enclosed at each full cycle is defined in between two zero-moment crossing points as shown in Figure 6.8 for a typical specimen. The specimens 3P3\_N0.4 and 7P3\_U are excluded from the group because they are evaluated separately.

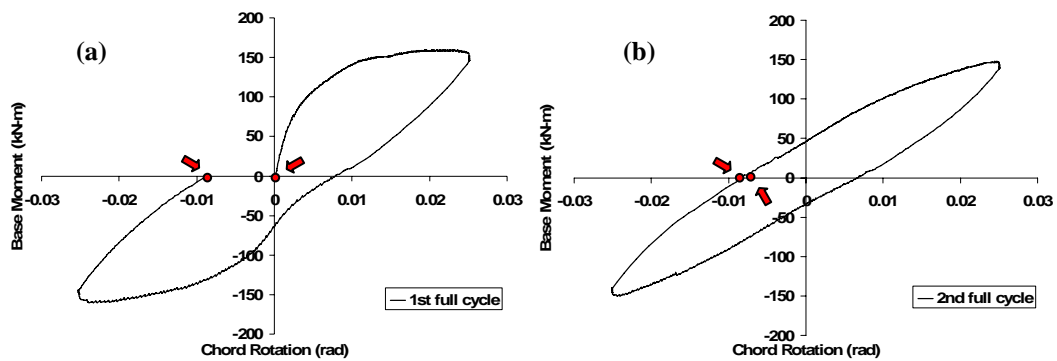


Figure 6.8 Force-based cycle definition for, (a) 1<sup>st</sup> full cycle, (b) 2<sup>nd</sup> full cycle

### 6.4.1 Normalization with respect to the 1<sup>st</sup> Full Cycle

The first full cycle in the hysteretic response of reinforced concrete column specimens under constant amplitude loadings is a unique cycle due to its unsymmetrical shape in the positive and negative loading directions. Although this unsymmetrical nature introduces a difficulty in the normalization process, variation in the energy dissipation capacity of reinforced concrete columns can be represented by normalizing the dissipated energy at each cycle with respect to this first special cycle. Figures 6.9 and 6.10 show the variation of normalized dissipated energy with the number of cycles for the Type-1 and Type-2 specimens, respectively.

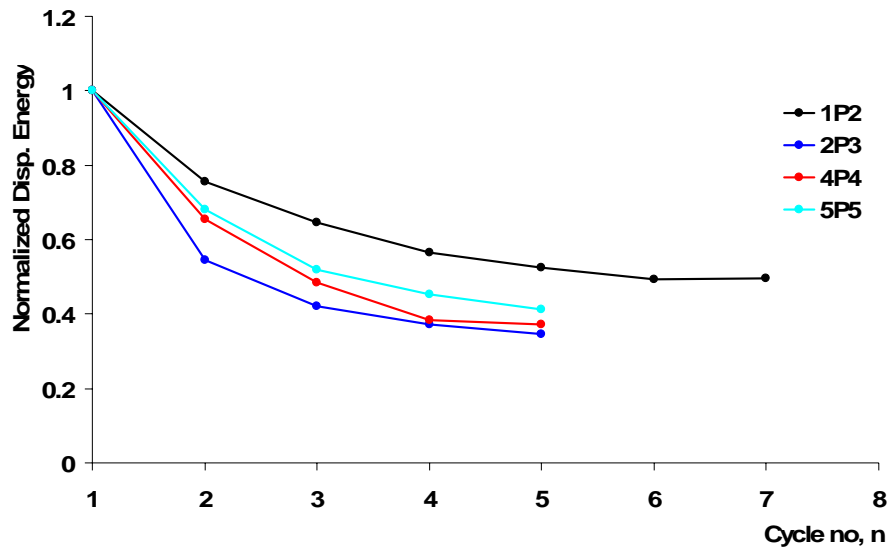


Figure 6.9 Variation of cyclic dissipated energy, normalized with respect to the 1<sup>st</sup> full cycle, with the number of cycles: Type-1 specimens

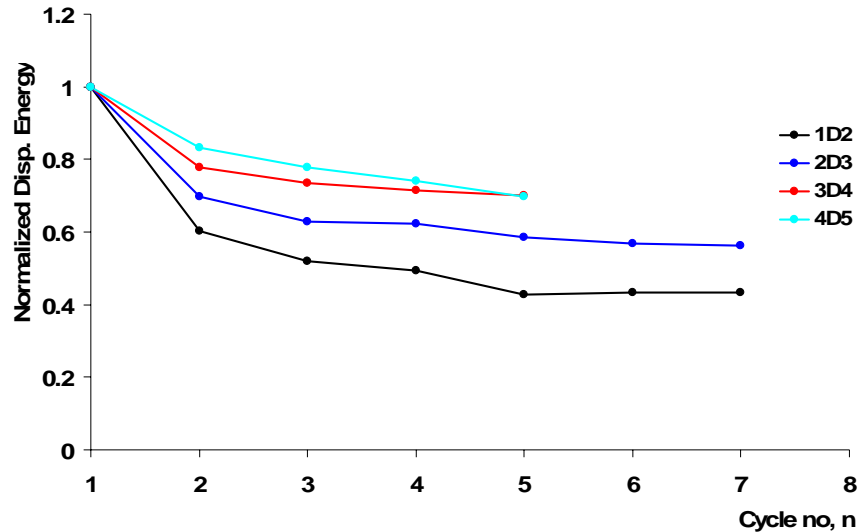


Figure 6.10 Variation of cyclic dissipated energy, normalized with respect to the 1<sup>st</sup> full cycle, with the number of cycles: Type-2 specimens

An exponential decay can be observed in the normalized dissipated cyclic energy with the number of constant-amplitude cycles for both types of flexural specimens from the above figures. Although the scatter in the normalized dissipated energy curves is weak for both Type-1 and Type-2 columns, it is indicating an amplitude dependency. Although there is no systematic amplitude dependency in Figure 6.9 for the Type-1 non-conforming specimens with plain bars, the normalized cyclic energy dissipation varies more systematically with displacement amplitude in Figure 6.10 for the Type-2 conforming specimens with deformed bars.

For Pujol specimens, it can also be observed that the normalized dissipated energy curves are forming separate bundles for the two groups of specimens tested under two different amplitudes of loadings as shown in Figure 6.11.

Since the amplitude of imposed displacements is identical for all Wight and Sozen test specimens, it is not possible to evaluate the amplitude dependency of cyclic energy dissipation. Decay in cyclic energy dissipation with the number of cycles similar to the other cases is observed in Figure 6.12, with a small dispersion of normalized dissipated energy.

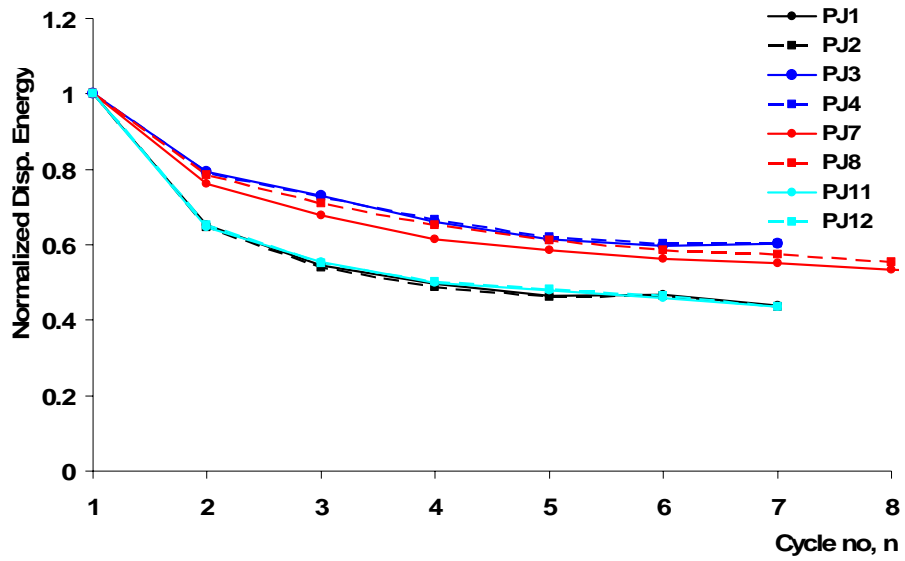


Figure 6.11 Variation of cyclic dissipated energy, normalized with respect to the 1<sup>st</sup> full cycle, with the number of cycles: Pujol specimens

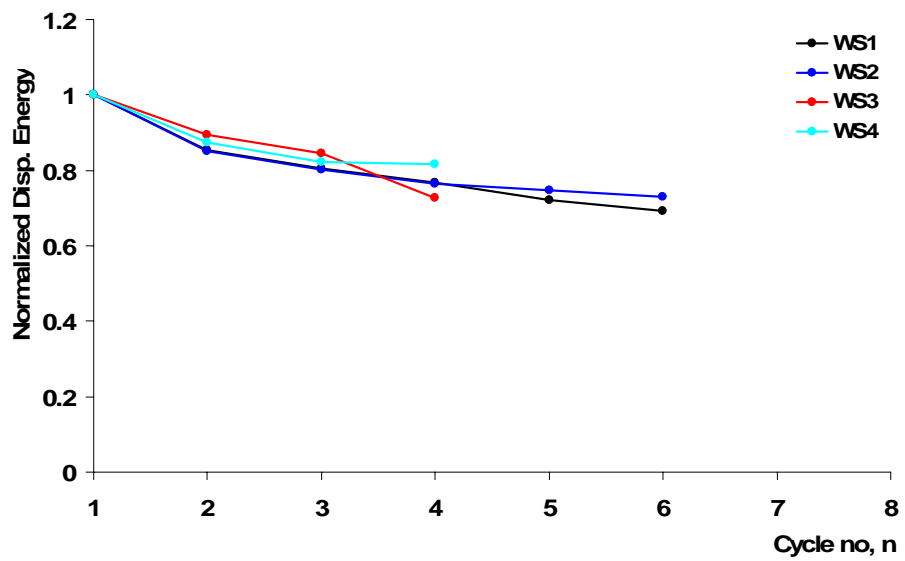


Figure 6.12 Variation of cyclic dissipated energy, normalized with respect to the 1<sup>st</sup> full cycle, with the number of cycles: Wight and Sozen specimens

### 6.4.2 Normalization with respect to the 2<sup>nd</sup> Full Cycle

The most significant change in cyclic energy dissipation occurs between the first and second cycles for all specimens as observed from Figures 6.9-6.12. This is due to the special unsymmetrical form of the first virgin cycle, which turns into the generic symmetrical elliptical loops by the second cycle. Accordingly, if the cyclic energy dissipated by each test specimen is normalized at each individual cycle with respect to the energy dissipated at the associated second cycle, amplitude dependency in cyclic energy dissipation almost disappears after the second cycle as shown in Figures 6.13 to 6.16 for all types of specimens. This can be considered as an advantage in predicting the cyclic energy dissipation under constant-amplitude low cycle fatigue loading.

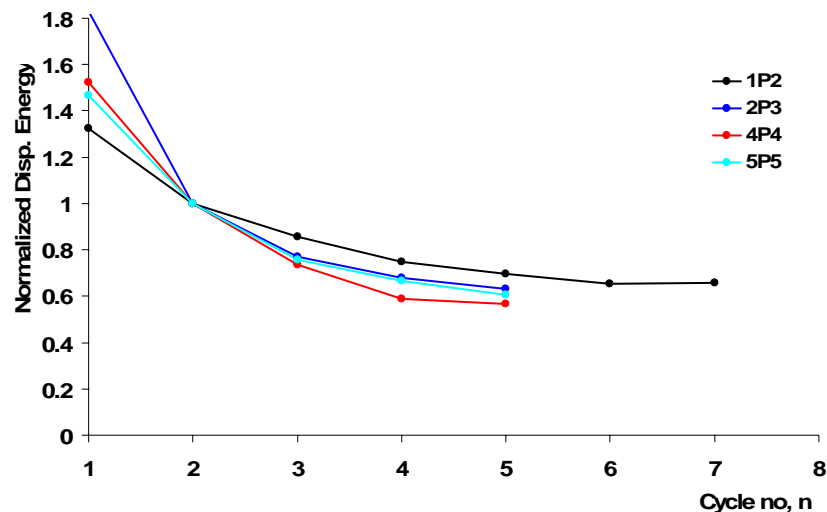


Figure 6.13 Variation of cyclic dissipated energy, normalized with respect to the 2<sup>nd</sup> full cycle, with the number of cycles: Type-1 specimens

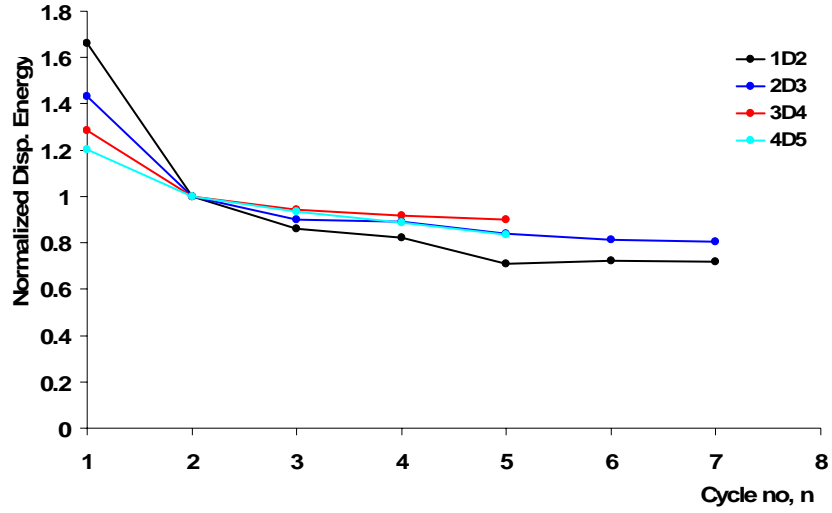


Figure 6.14 Variation of cyclic dissipated energy, normalized with respect to the 2<sup>nd</sup> full cycle, with the number of cycles: Type-2 specimens

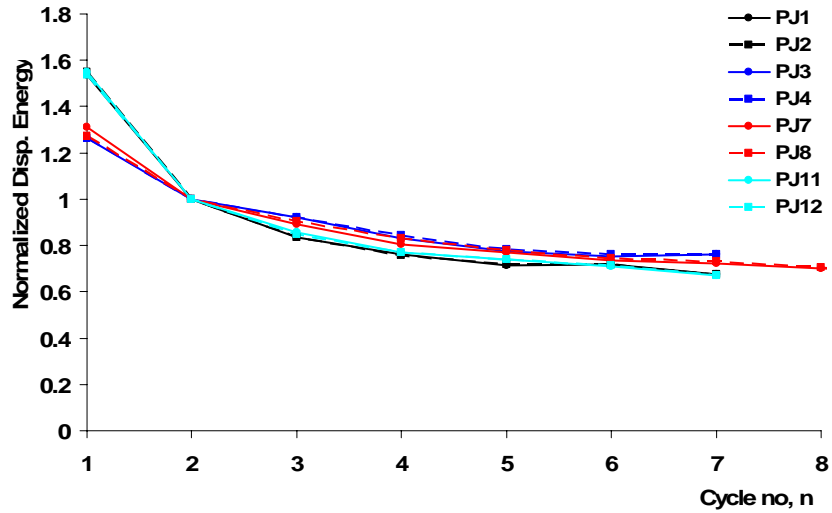


Figure 6.15 Variation of cyclic dissipated energy, normalized with respect to the 2<sup>nd</sup> full cycle, with the number of cycles: Pujol specimens

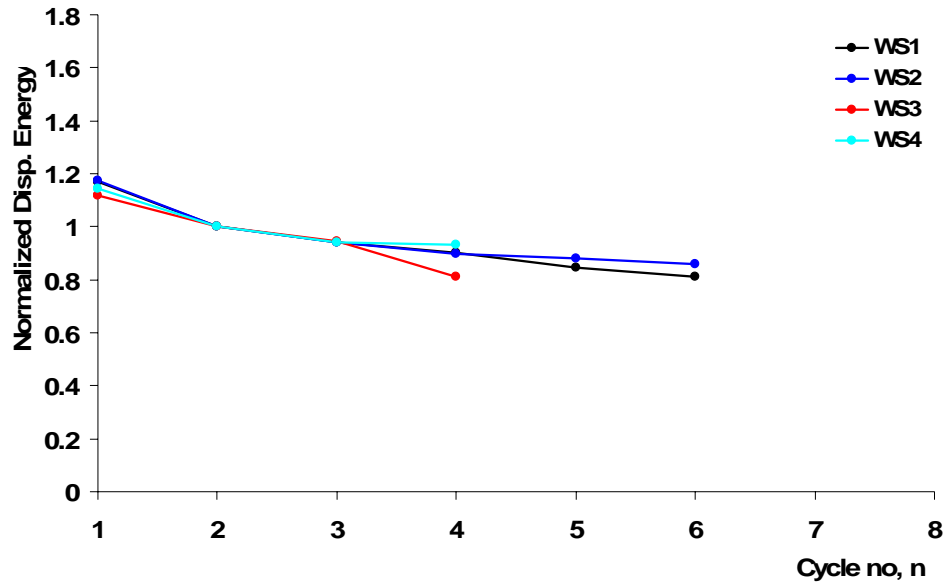


Figure 6.16 Variation of cyclic dissipated energy, normalized with respect to the 2<sup>nd</sup> full cycle, with the number of cycles: Wight and Sozen specimens

Shape-stable hysteretic response for constant amplitude cyclic loading indeed starts with the second full cycle as observed in Figure 6.1. An exponentially decaying form can be postulated for the variation of dissipated cyclic energy, normalized with respect to the second cycle, as a function of the number of cycles. It can be observed from Figures 6.13-6.16 that normalized cyclic energy is almost independent from the displacement amplitude of cyclic loading after the second cycle whereas it depends on the displacement amplitude in the first cycle.

### 6.5 Prediction of Cyclic Energy Dissipation in Low-Cycle Fatigue

A two-parameter low-cycle fatigue model was proposed for quantifying the deterioration characteristics of structural systems (Erberik and Sucuoğlu, 2004; Sucuoğlu and Erberik, 2004). This model is adopted herein in order to estimate the relationship between the cyclic energy dissipation, normalized with respect to the

energy dissipated at the second cycle, and the number of constant-amplitude displacement cycles by the second cycle ( $n = 2-N$ ) in the form of an exponential function as given in Equation 6.1.

$$\bar{E}_{h,n} = \alpha + (1 - \alpha) e^{\beta(2-n)} ; n = 2 - N \quad (6.1)$$

Here,  $\bar{E}_{h,n}$  is the normalized dissipated energy at cycle  $n$  ( $n = 2, 3, 4 \dots$ ), and  $\alpha$  and  $\beta$  are the two fatigue parameters. The first parameter  $\alpha$  is related to the residual capacity in cyclic energy dissipation at large values of  $n$ , and the second parameter  $\beta$  is related to the rate of deterioration in cyclic energy dissipation. A system with  $\alpha = 0$  loses all of its energy dissipation capacity whereas a system with  $\alpha = 1$  always retains its energy dissipation capacity in low cycle fatigue. Takeda hysteresis model (Takeda et al, 1970) corresponds to  $\alpha = 1$  in terms of cyclic energy dissipation since the constant amplitude cycles repeat themselves after the second cycle.

A typical r/c system that exhibits exponential decay in normalized energy dissipation capacity by the second full cycle is depicted in Figure 6.17.

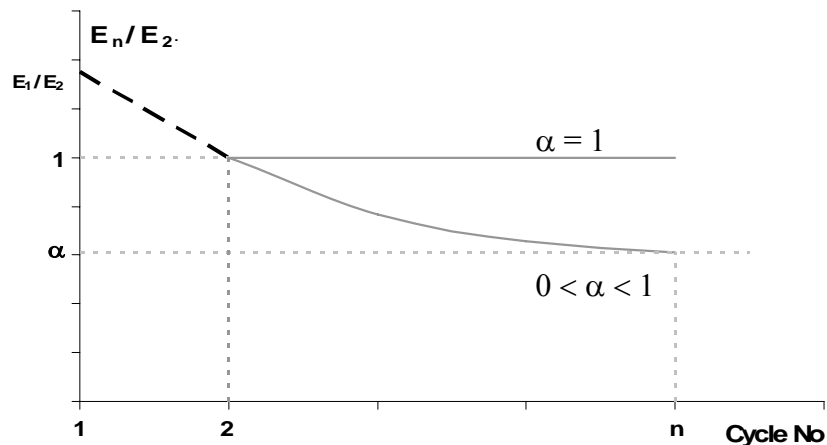


Figure 6.17 A representative exponential decay in normalized energy dissipation capacity after the second cycle for a typical r/c component

Since the dissipated cyclic energy is normalized with respect to the second cycle, the ratio of energy dissipated at the first cycle to the energy dissipated at the second cycle,  $E_1/E_2$  appears as a crucial entity to be discussed. Successful analytical predictions for the first cycle of reinforced concrete components exist in literature (Clough and Johnston, Takeda, Q-hyst). Obtaining  $E_1$  from such models and predicting  $E_2$  from the  $E_1/E_2$  model proposed herein is sufficient for determining the energy dissipated in the following low cycle fatigue cycles from Equation 6.1. Several parameters that may affect the  $E_1/E_2$  ratio and their correlations are presented and evaluated in the following section.

The compiled database of reinforced concrete column specimens can be interpreted in two distinct groups in view of their failure modes as mentioned before: flexure dominant and flexure-shear modes. Investigation of the parameters affecting the  $E_1/E_2$  ratio and the energy dissipation characteristics under low cycle fatigue is carried out by considering these two sub-groups of specimens separately.

The  $E_1/E_2$  ratio for all column specimens are calculated from test results and presented in Table 6.2. Furthermore, an exponential function with the formulation given in Equation 6.1 is fitted to the normalized dissipated energy curves obtained from the test results for each specimen, and the parameters representing low cycle fatigue characteristics ( $\alpha$  and  $\beta$ ) are determined by regression, accordingly. The estimated values of  $\alpha$  and  $\beta$  are also given in Table 6.2.

### **6.5.1 Dissipated Energy Ratio, $E_1/E_2$**

$E_1/E_2$  ratio is evaluated separately for the two groups of specimens with flexure dominant or flexure-shear failure modes.

#### Specimens with flexure dominant failure mode:

Although both Type-1 and Type-2 specimens have the same failure modes, they are interpreted as two separate sub-groups since their energy dissipation characteristics are different due to the differences in their concrete and

reinforcement properties. However concrete strength and reinforcement details are identical for all specimens in each sub-group, accordingly the influence of these parameters on the  $E_1/E_2$  ratio cannot be observed.

Table 6.2 Energy dissipation characteristics of specimens under low-cycle fatigue

No	Failure Mode	Name	Code	$E_1/E_2$	$\alpha$	$\beta$
1	Flexure-Shear	Pujol, No. 10-2-3N	PJ1	1.535	0.68	0.70
2		Pujol, No. 10-2-3S	PJ2	1.550	0.68	0.71
3		Pujol, No. 10-3-1.5N	PJ3	1.262	0.71	0.42
4		Pujol, No. 10-3-1.5S	PJ4	1.265	0.71	0.39
5		Pujol, No. 10-3-2.25N	PJ7	1.311	0.69	0.47
6		Pujol, No. 10-3-2.25S	PJ8	1.273	0.67	0.37
7		Pujol, No. 10-2-2.25N	PJ11	1.547	0.66	0.53
8		Pujol, No. 10-2-2.25S	PJ12	1.537	0.67	0.57
9		Wight & Sozen,40.147-E	WS1	1.171	0.78	0.30
10		Wight & Sozen,40.147-W	WS2	1.175	0.77	0.29
11		Wight & Sozen,40.092-E	WS3	1.118	N.A	N.A
12		Wight & Sozen,40.092-W	WS4	1.144	N.A	N.A
13	Flexure	Acun & Sucuoglu Type-1	1P2	1.325	0.62	0.52
14		Acun & Sucuoglu Type-1	2P3	1.830	0.61	0.87
15		Acun & Sucuoglu Type-1	3P3_N04	1.357	0.59	0.32
16		Acun & Sucuoglu Type-1	4P4	1.525	0.52	0.84
17		Acun & Sucuoglu Type-1	5P5	1.466	0.57	0.80
18		Acun & Sucuoglu Type-1	7P3_U	2.096	0.69	0.87
19		Acun & Sucuoglu Type-2	1D2	1.660	0.68	0.54
20		Acun & Sucuoglu Type-2	2D3	1.431	0.83	0.69
21		Acun & Sucuoglu Type-2	3D4	1.285	0.89	0.68
22		Acun & Sucuoglu Type-2	4D5	1.201	0.83	0.62

*Type-1 Specimens (Non-conforming)*

The average value of  $E_1/E_2$  is 1.515 for four columns with an axial load ratio of 0.2, whereas it is calculated as 1.357 for the specimen with a high axial load ratio

of 0.4. Apparently, axial load ratio has a significant influence on the  $E_1/E_2$  ratio. However it is not possible to quantify this influence with a single datum.

Another parameter that affects the  $E_1/E_2$  ratio is ductility. The variation of  $E_1/E_2$  with rotational ductility is presented in Figure 6.18. The column specimen 1P2 appears as an outlier perhaps due to its low rotational ductility.

*Type-2 Specimens (Conforming)*

Since the axial load ratio is constant for all of these test specimens, the only variable is ductility. The variation of  $E_1/E_2$  with rotational ductility for Type-2 specimens is also presented in Figure 6.18.

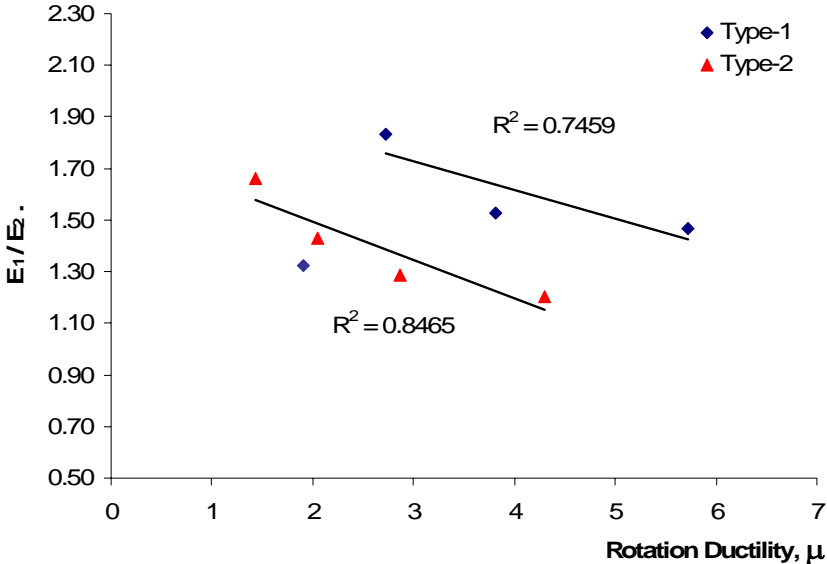


Figure 6.18 Correlation of  $E_1/E_2$  with ductility for test specimens with flexure dominant failure mode

Linear regressions for the variation of  $E_1/E_2$  ratio with rotational ductility are given in Figure 6.18 for Type-1 and Type-2 column specimens. It is interesting to

note that the energy dissipated in the second cycle tends to approach to that in the first cycle as rotation ductility increases.

Specimens with flexure-shear failure mode:

All test specimens with flexure-shear failure mode were tested under the same axial load ratio, hence it is not possible to evaluate the influence of axial load ratio on the  $E_1/E_2$  ratio.

Transverse reinforcement ratio is an effective parameter on the  $E_1/E_2$  ratio for reinforced concrete columns with flexure-shear mode. It is shown in Figure 6.19 that  $E_1/E_2$  ratio decreases with transverse reinforcement ratio in the  $\rho_t$  range of 0.5% to 1.5%, although the trend is not very strong.

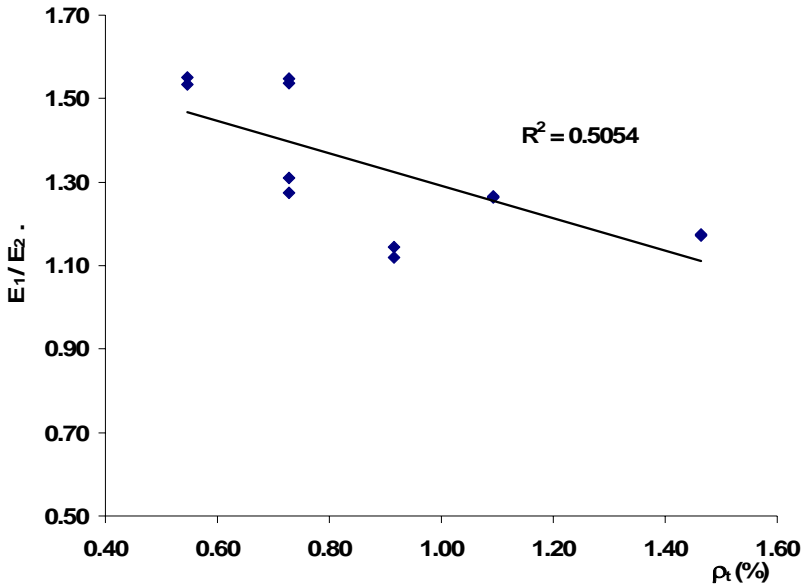


Figure 6.19 Correlation of  $E_1/E_2$  with confinement ratio for test specimens with flexure-shear failure mode

The shear ratio  $V/V_n$  is in the range of 0.5 to 0.9 for these columns. As the shear force  $V$  approaches the nominal shear strength  $V_n$ , degradation in energy dissipation capacity in the second cycle increases as presented in Figure 6.20. However there is a weak trend between  $E_1/E_2$  and  $V/V_n$ .

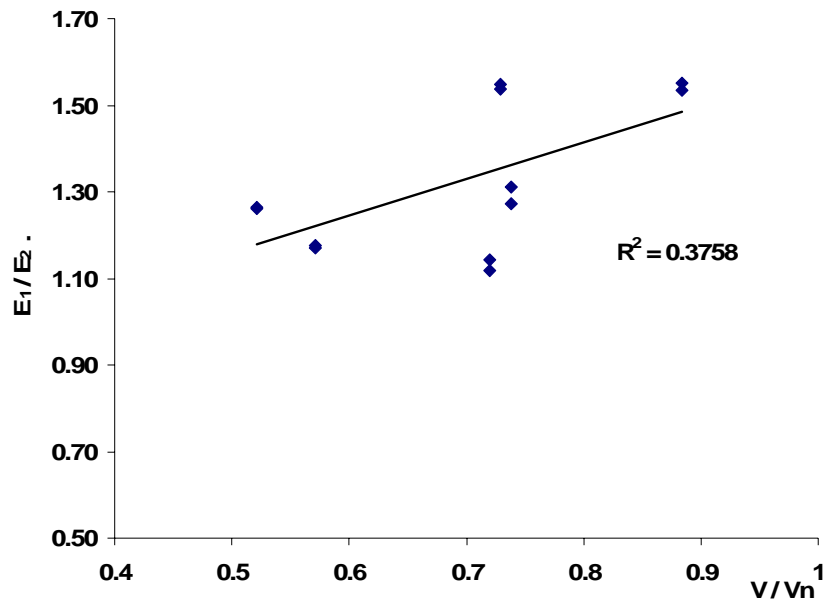


Figure 6.20 Correlation of  $E_1/E_2$  with shear ratio for test specimens with flexure-shear failure mode

On the other hand,  $E_1/E_2$  ratio has a clear trend with rotation ductility which can be observed from Figure 6.21 for column specimens with flexure-shear failure, similar to those with flexure dominant failure mode. A linear trendline is given in Figure 6.21 for the range of rotational ductility values in the dataset between  $\mu = 1.5$  and  $\mu = 4$ .

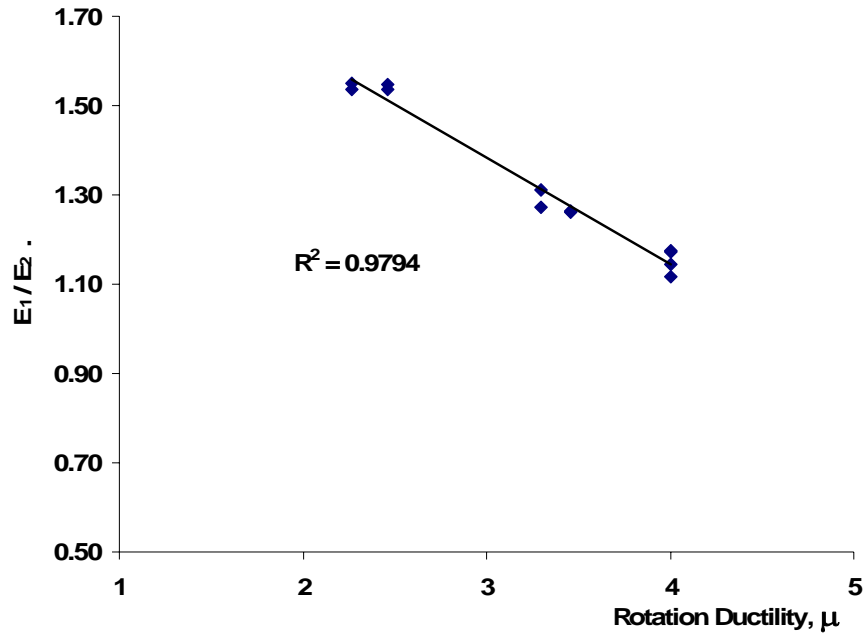


Figure 6.21 Variation of  $E_1/E_2$  with rotation ductility for test specimens with flexure-shear failure mode

### 6.5.1.1 Low Cycle Fatigue Parameter, $\alpha$

$\alpha$  is defined in Figure 6.17 as the residual capacity in normalized cyclic energy dissipation when the number of cycles approaches infinity. Correlation of  $\alpha$  with rotation ductility, shear ratio and transverse reinforcement ratio are discussed in the following paragraphs for subgroups of specimens with flexure dominant and flexure-shear failure modes.

#### Specimens with flexure dominant failure mode

The variation of  $\alpha$  can only be searched for rotation ductility since all other parameters are constant within each sub-group of Type 1 and Type-2 specimens.

*Type-1 Specimens (Non-conforming)*

It can be easily seen from Figure 6.22 that  $\alpha$  does not vary with rotation ductility for non-conforming specimens. The average value is 0.578 with a standard deviation of 0.045 and a coefficient of variation of 0.08.

*Type-2 Specimens (Conforming)*

Similar to Type-1 specimens,  $\alpha$  is almost constant for the Type-2 specimens with an average value of 0.849, standard deviation of 0.034 and coefficient of variation of 0.04. It should be noted that the specimen 1D2 is not included in this analysis since it seems to be an outlier most probably due to its low ductility ratio. The trend for  $\alpha$  with rotation ductility for conforming specimens is also given in Figure 6.22.

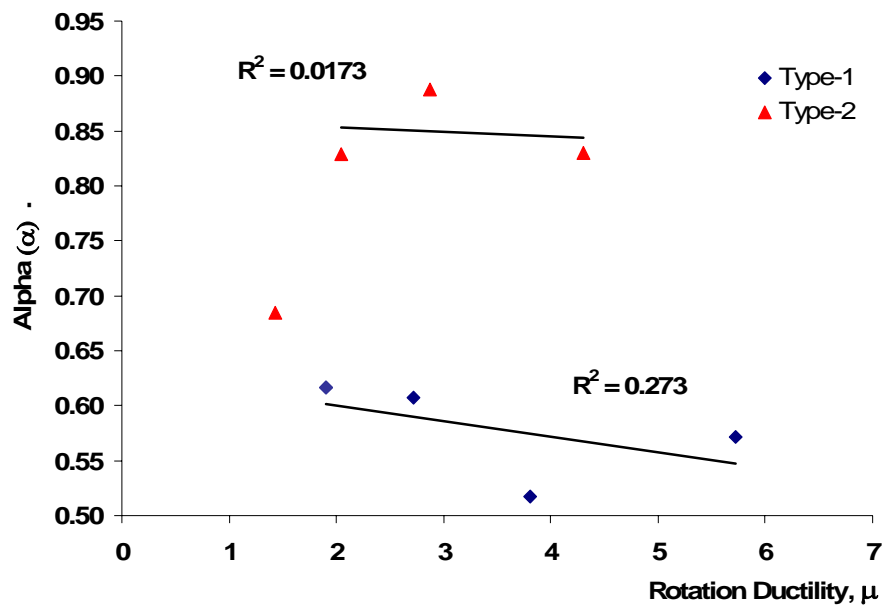


Figure 6.22 Correlation of  $\alpha$  with ductility for test specimens with flexure dominant failure mode

Specimens with flexure-shear failure mode:

Figure 6.23 indicates a clear trend for  $\alpha$  with the increase in transverse reinforcement ratio for test specimens with flexure-shear failure mode. This is due to improvement of cyclic response with the increase in the transverse reinforcement ratio which apparently leads to smaller values of  $\alpha$ , indicating larger residual energy dissipation capacity, hence reduced low-cycle fatigue deterioration in the energy dissipation capacity.

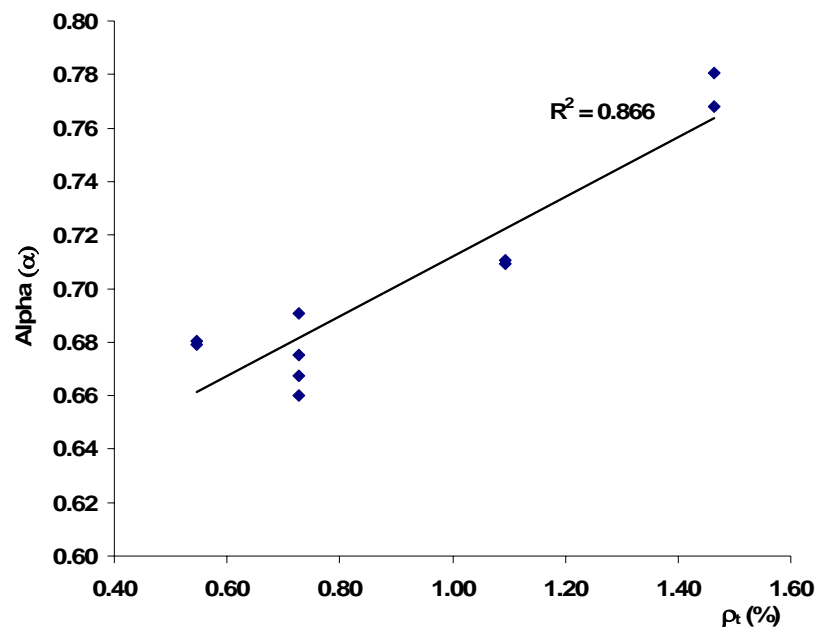


Figure 6.23 Correlation of  $\alpha$  with confinement ratio for test specimens with flexure-shear failure mode

There is a weak correlation between  $\alpha$  and shear ratio for flexure-shear specimens.  $\alpha$  decreases with increase in shear ratio as expected, since the increase in shear ratio indicates shifting of failure mode from flexure-shear to shear which leads to severe degradation in cyclic energy dissipation capacity. Figure 6.24 shows

the correlation of  $\alpha$  with shear ratio for test specimens with flexure-shear failure mode. Figures 6.23 and 6.24 are somehow correlated, because increase in the transverse reinforcement ratio in Figure 6.23 leads to increase in the nominal shear capacity  $V_n$  and accordingly reduction of the  $V/V_n$  ratio in Figure 6.24.

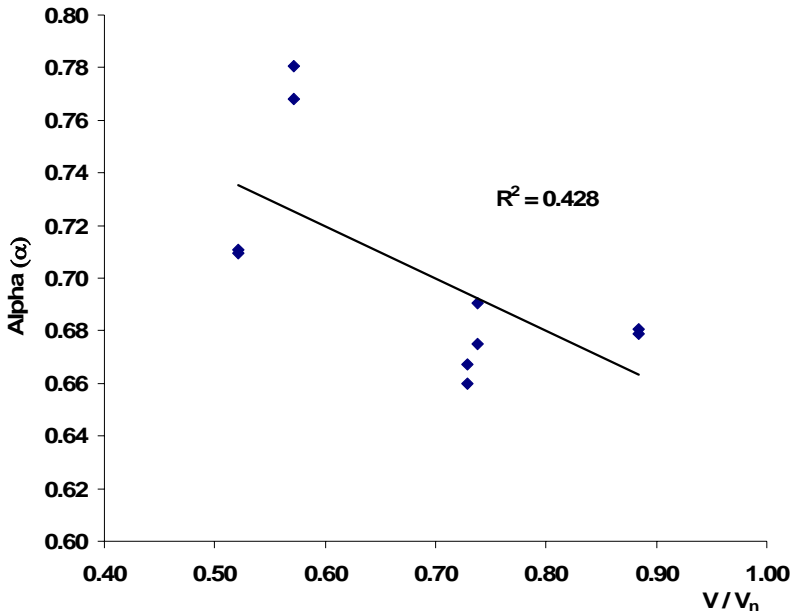


Figure 6.24 Correlation of  $\alpha$  with shear ratio for test specimens with flexure-shear failure mode

Contrary to the test specimens with flexure dominant failure mode, the estimated  $\alpha$  values for specimens with flexure-shear failure mode exhibit a significant trend with rotation ductility. Increase in  $\alpha$  with the increase in rotation ductility implies dependency of cyclic energy dissipation capacity with the amplitude of low-cycle fatigue loading. The correlation between  $\alpha$  and rotation ductility for the specimens with flexure-shear failure mode is shown in Figure 6.25.

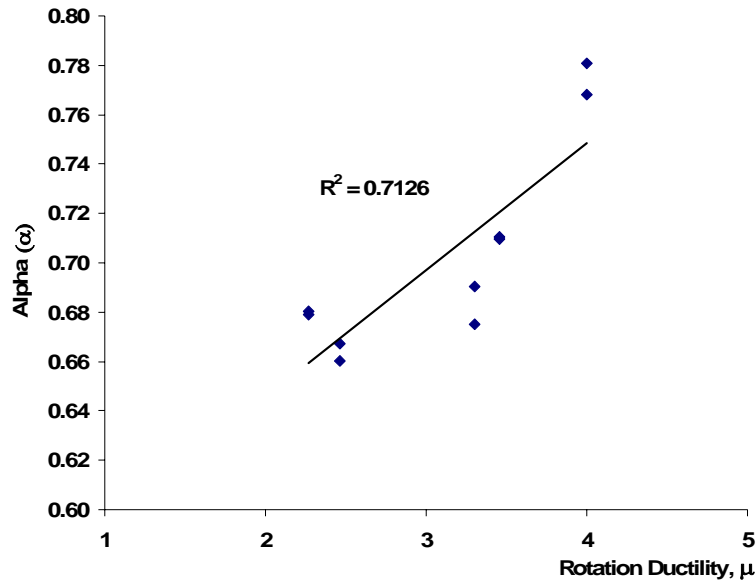


Figure 6.25 Correlation of  $\alpha$  with ductility for test specimens with flexure-shear failure mode

### 6.5.1.2 Low Cycle Fatigue Parameter, $\beta$

The rate of deterioration in cyclic energy dissipation capacity after the second cycle is defined by the parameter  $\beta$  in the proposed exponential formulation for low-cycle fatigue behavior of reinforced concrete column specimens, i.e. Equation 6.1. Similar to the other characteristic of low-cycle fatigue, correlations between  $\beta$  and the transverse reinforcement ratio, shear ratio and rotational ductility are discussed separately in the following paragraphs for sub-groups of specimens with flexure dominant and flexure-shear failure modes.

#### Specimens with flexure dominant failure mode:

Rotation ductility is the only variable parameter within each sub-group of Type 1 and Type-2 specimens. Hence the variation of  $\beta$  can only be searched for rotation ductility, similar to  $\alpha$ .

The rate of deterioration in energy dissipation capacity is insensitive to the change in rotation ductility for both Type 1 and Type-2 specimens as shown in Figure 6.26. The average value of  $\beta$  is calculated as 0.838 with a standard deviation of 0.035 and a coefficient of variation of 0.04 for Type-1 specimens. For Type-2 specimens, the average value of  $\beta$  is calculated as 0.663 with a standard deviation of 0.037 and a coefficient of variation of 0.056.

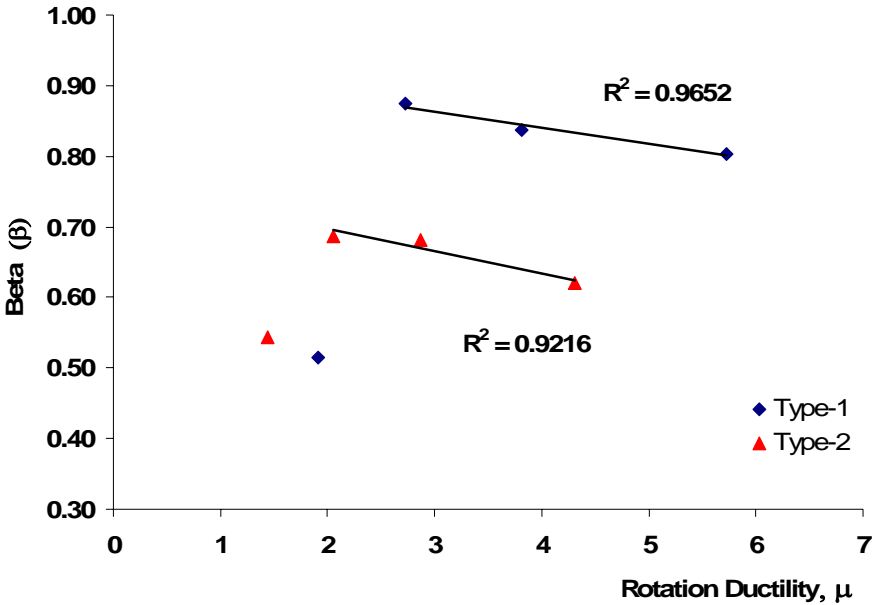


Figure 6.26 Variation of  $\beta$  with rotation ductility for test specimens with flexure dominant failure mode

Specimens with flexure-shear failure mode:

The low-cycle fatigue parameter  $\beta$  is sensitive to the transverse reinforcement ratio, shear ratio and ductility ratio for the specimens with flexure-shear mode.

The variation of  $\beta$  with the transverse reinforcement ratio is shown in Figure 6.27. The rate of deterioration in energy dissipation capacity decreases significantly

with the increase in transverse reinforcement ratio in flexure-shear specimens. A transverse reinforcement ratio that is twice of the minimum value of 0.6 % reduces the rate of deterioration to half of that for the minimum transverse reinforcement ratio.

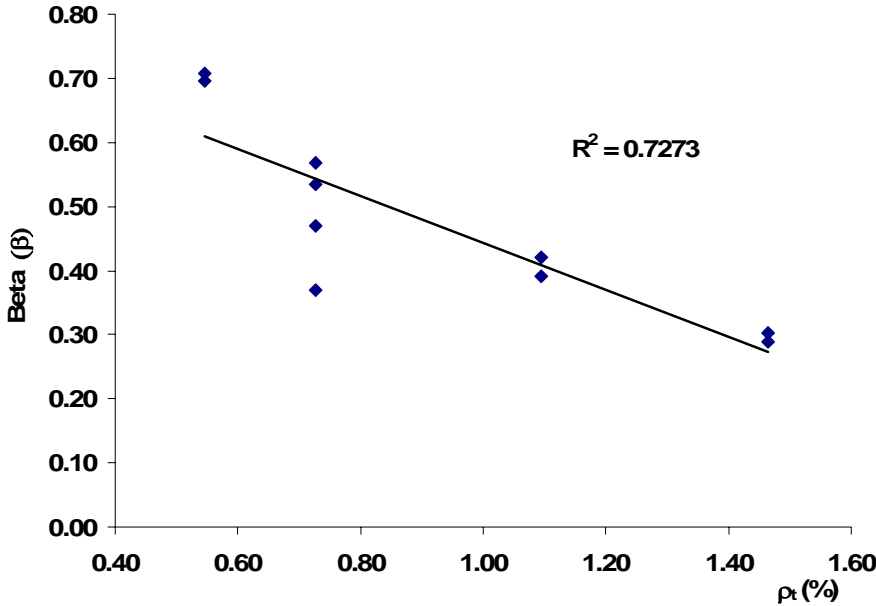


Figure 6.27 Correlation of  $\beta$  with confinement ratio for test specimens with flexure-shear failure mode

Similarly,  $\beta$  tends to increase with the increase in  $V/V_n$  ratio which is observed in Figure 6.28. Figures 6.27 and 6.28 are in fact providing similar information because increase in the transverse reinforcement ratio in Figure 6.27 leads to increase in the nominal shear capacity  $V_n$  in Figure 6.28, accordingly reduction in the  $V/V_n$  ratio.

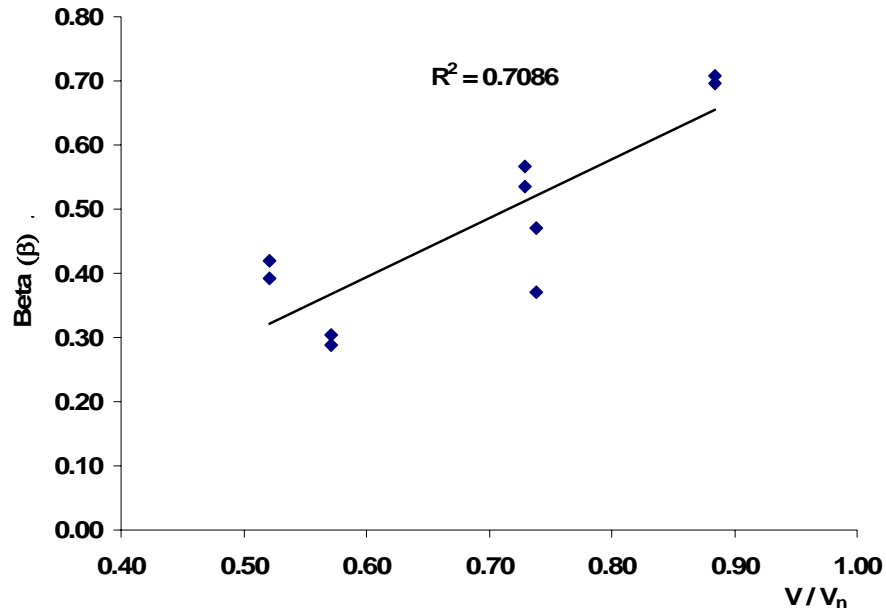


Figure 6.28 Correlation of  $\beta$  with shear ratio for test specimens with flexure-shear failure mode

Within the range of  $\mu=2$  to  $\mu=4$ ,  $\beta$  displays a decreasing trend with the increase in rotation ductility, indicating an amplitude dependency for  $\beta$ . This trend can be observed in Figure 6.29. When this trend in  $\beta$  is interpreted along with the variation of  $\alpha$  with rotational ductility, it can be concluded that as rotation ductility increases, residual normalized cyclic energy dissipation capacity increases and the rate of deterioration in the energy dissipation capacity reduces for reinforced concrete column specimens with flexure-shear failure mode.

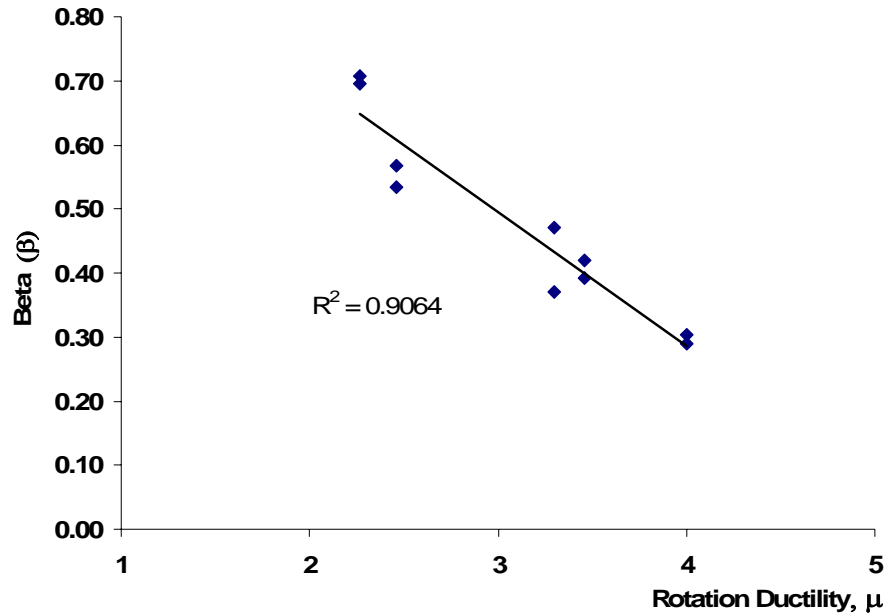


Figure 6.29 Correlation of  $\beta$  with rotation ductility for column specimens with flexure-shear failure mode

## 6.6 The Effect of Axial Load on Energy Dissipation Capacity

Specimens 2P3 and 3P3\_N0.4 were identical in their properties, and they were subjected to identical low cycle fatigue displacement cycles. The only difference was the axial load ratio, which was 20% in 2P3 and 40% in 3P3\_N0.4. The cumulative hysteretic energy dissipation and normalized cyclic energy dissipation with respect to the first full cycle and with respect to the second full cycle for these two specimens are compared in Figure 6.30. Higher ratio of axial load has a positive effect on energy dissipation capacity because it is both increasing the flexural strength (see Figure 6.2) and limiting the opening of cracks which in turn leads to reduced pinching.

Only one pair of test specimens is perhaps insufficient for determining the effect of axial load on the energy dissipation capacity of columns.

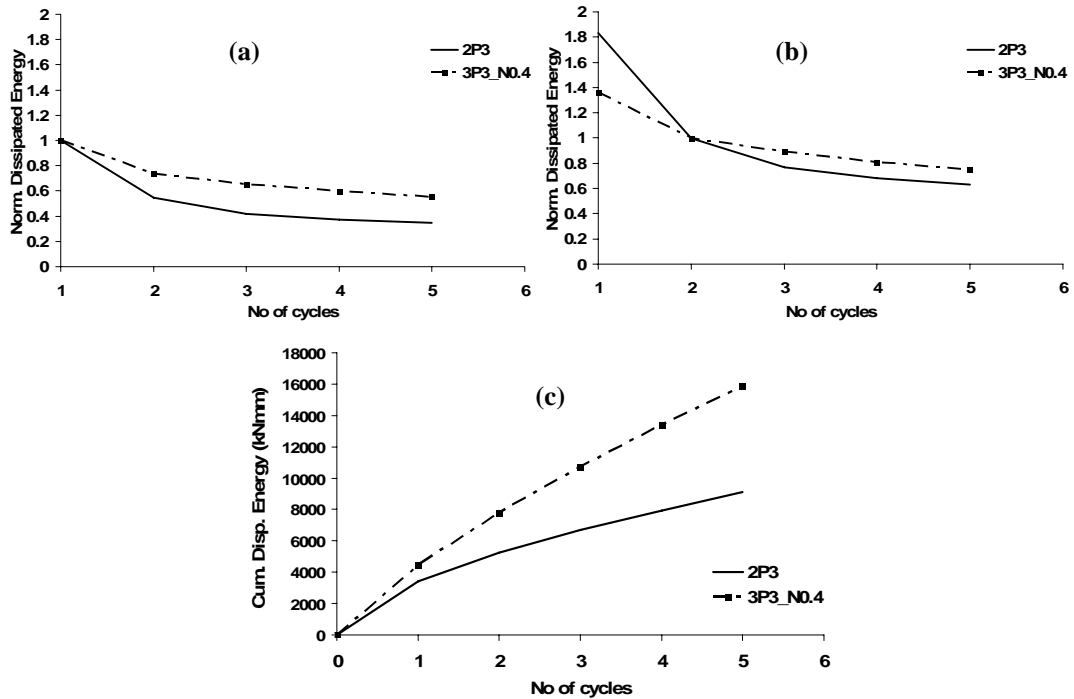


Figure 6.30 Comparison of the cyclic energy dissipation capacities of two companion columns with different axial load levels. Normalized energy dissipation, (a) w.r.to 1<sup>st</sup> full cycle, (b) w.r.to 2<sup>nd</sup> full cycle and (c) Cumulative energy dissipation

## 6.7 The Effect of Bond Strength on Energy Dissipation Capacity

The cumulative hysteretic energy dissipation and normalized cyclic energy dissipation capacity of the two companion specimens 2P3 and 7P3\_U are compared in Figure 6.31. It is interesting to observe that the normalized cyclic energy dissipation characteristics, either with respect to first full cycle or with respect to second full cycle of the two specimens, are very similar. This is an indication that the bond strength of plain reinforcement under low cycle fatigue loading reduces significantly in the plastic hinge region after the first inelastic cycle, and seemingly becomes similar to the unbounded specimen.

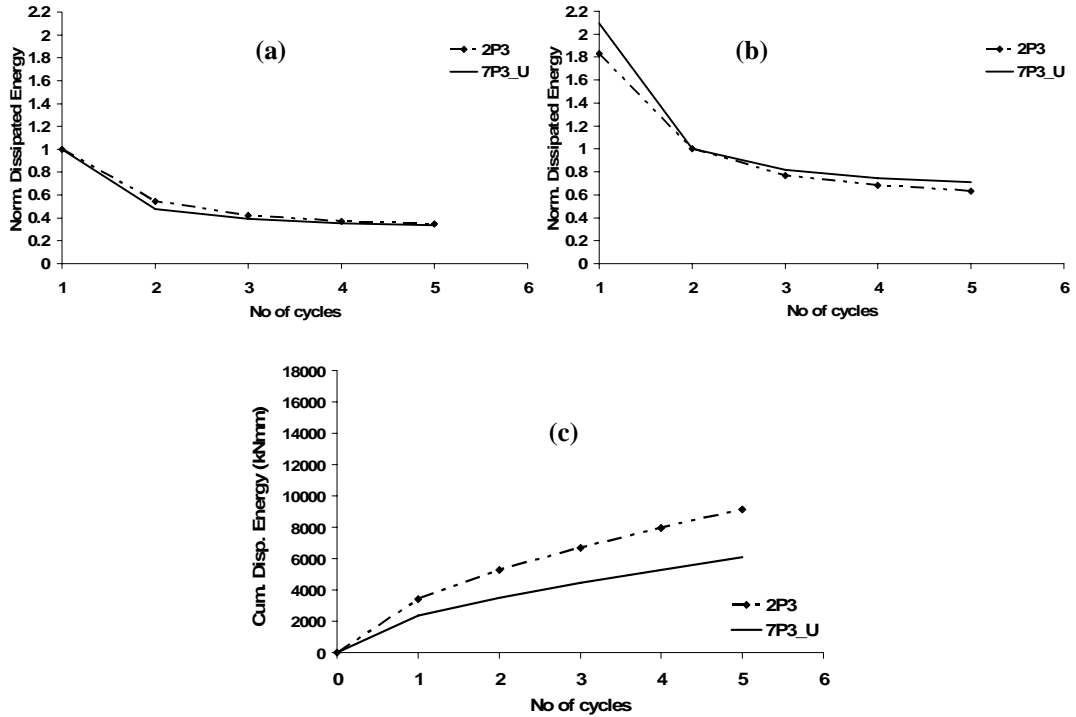


Figure 6.31 Comparison of the cyclic energy dissipation capacities of two companion columns with different bond strength. Normalized energy dissipation, (a) w.r.to the 1<sup>st</sup> full cycle, (b) w.r.to the 2<sup>nd</sup> full cycle and (c) Cumulative energy dissipation

## 6.8 Strength Degradation Under Low Cycle Fatigue Loading

Flexural strength capacities of the test specimens are also normalized similar to the normalized energy dissipation. Base moment values attained at the target displacement amplitudes in the positive and negative directions in each cycle are averaged, and then normalized with respect to the corresponding base moment value of the first full cycle. It should be noted that these moment values are not necessarily the maximum moment values attained in the cycle. Figure 6.32 depicts the moment values employed for calculating the normalized strength of a typical column specimen.

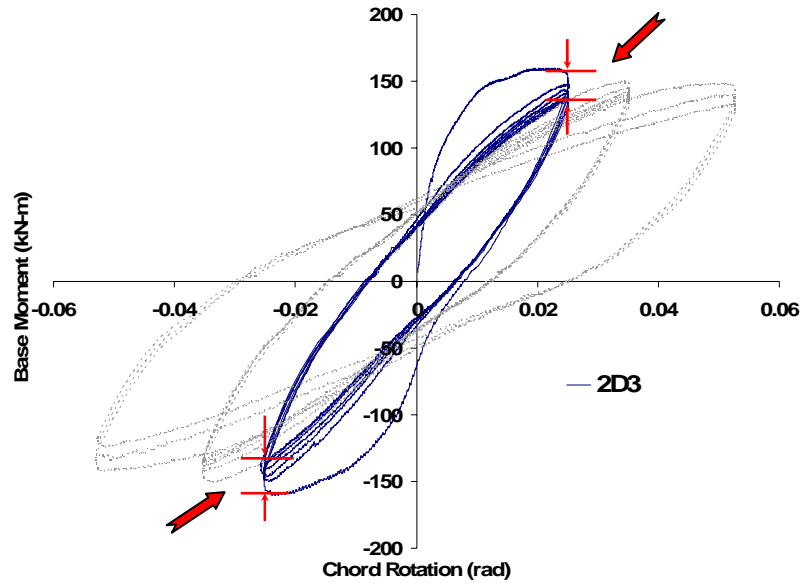


Figure 6.32 Cyclic strength degradation in low-cycle fatigue

The relationship between the normalized cyclic strength and cycle number for Type-1 and Type-2 specimens, and Pujol (2002) and Wight and Sozen (1975) specimens subjected to constant-amplitude low-cycle displacement cycles are shown in Figures 6.33 to 6.36, respectively. It is observed from Figures 6.33 and 6.34 that strength degradation under cyclic displacements occurs in all specimens, including the specimens 1P2 and 1D2 which are subjected to displacements slightly above their yield displacement. However the scatter in normalized strength variation with the number of constant-amplitude displacement cycles is small. There is a decreasing trend in the normalized strength similar to the normalized dissipated energy.

One outlier is specimen 5P5. The amplitude of imposed displacement corresponding to 5.25% drift ratio for specimen 5P5 seems beyond its displacement capacity under repeated displacement cycles as observed from Figure 5.5. The nominal flexural moment capacity attained in the first cycle falls at a high rate in the following cycles, leading to a typical low cycle fatigue failure. This specimen indicates the importance of displacement history in determining the displacement performance limits of reinforced concrete members.

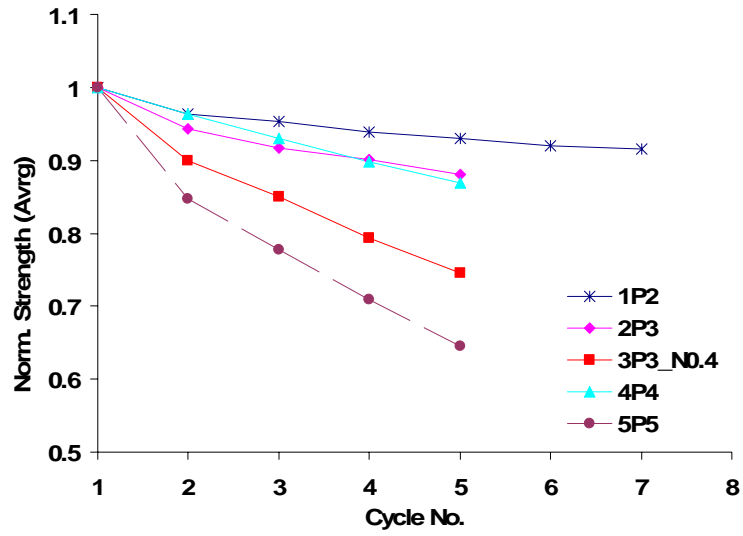


Figure 6.33 Normalized strength degradation with the number of cycles in Type-1 specimens

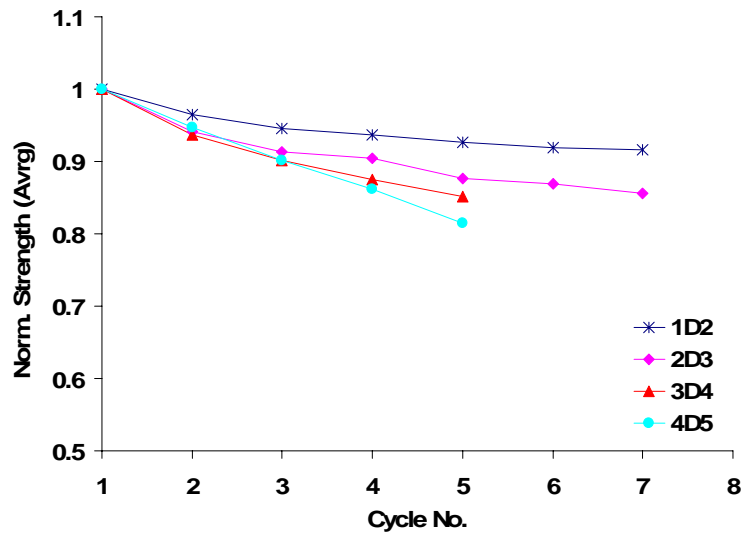


Figure 6.34 Normalized strength degradation with the number of cycles in Type-2 specimens

For Pujol specimens, deterioration in strength is less severe compared to Type-1 or Type-2 specimens although the normalized strength values are quite close to each other. The trend is more likely to be linear than exponential which is different from the case for Type-1 and Type-2 specimens. The amplitudes of imposed displacement for tested specimens are moderate (drift ratio of either 2% or 3%) so that the influence of amplitude is not as noticeable as Type-1 and Type-2 specimens. Even though they are classified as specimens with flexure-shear failure mode, the cyclic strength degradation even at their seventh cycle is still not greater than 10%. High concrete strength ( $f_c \cong 33$  MPa), large ratio of transverse reinforcement, relatively low axial load ratio ( $N/A_g.f_c = 0.1$ ) and moderate amplitudes of imposed displacement ( $\delta = 2 - 3$  %) are perhaps the reasons for having stable response with small decays in cyclic strength. Normalized strength degradation curves for Pujol specimens are shown in Figure 6.35.

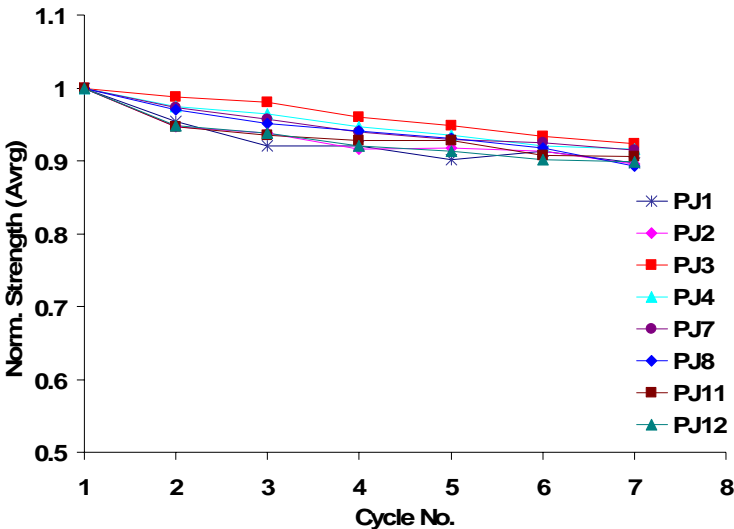


Figure 6.35 Normalized strength degradation with the number of cycles in Pujol specimens

Similar to Pujol specimens, a linear decay in normalized cyclic strength was observed in Wight and Sozen specimens WS1 and WS2. Although the amplitude of imposed displacements were quite high ( $\delta = 5.75\%$ ) the deterioration in cyclic strength is still less than 10% at sixth cycle for these specimens. The reason for maintaining their strength capacity is their high transverse reinforcement ratio ( $\rho_t = 1.5\%$ ) and relatively low axial load ratio ( $N/A_g f_c = 0.1$ ) even if the failure mode of these specimens are flexure-shear. However, the cyclic strength deterioration is more severe for WS3 and WS4 specimens mostly because of their rather less transverse reinforcement ratio as they were reported to fail in shear failure mode after 4 cycles of displacement with drift ratio of 5.75%.

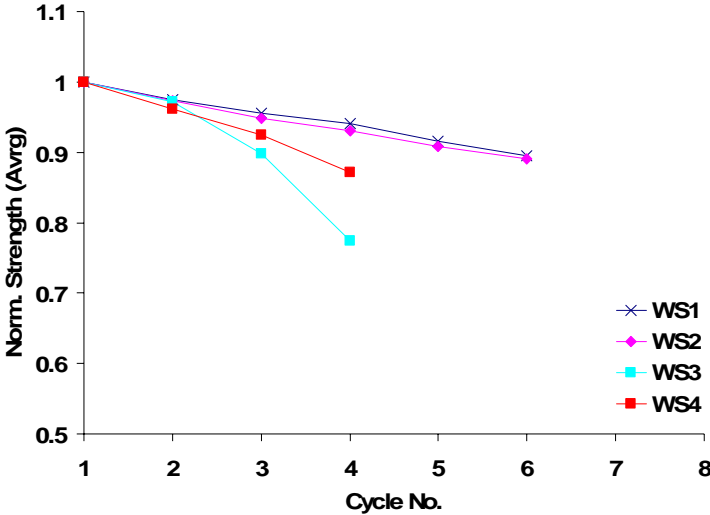


Figure 6.36 Normalized strength degradation with the number of cycles in Wight and Sozen specimens

**6.8.1 The Effect of Axial Load on Strength Degradation**

The normalized strength degradation curves of the specimens 2P3 and 3P3\_N0.4 are compared in Figure 6.37. The only difference between these two

specimens during testing was the axial load ratio, which was 20% in 2P3 and 40% in 3P3\_N0.4. The effect of axial load level on strength degradation is significant in both type of non-conforming and conforming columns. This is perhaps due to strength degradation in concrete fibers under cyclic uniaxial compression, which leads to shifting of the neutral axis toward the section centerline, hence reduce moment arm and flexural strength consequently. This issue deserves further attention with additional testing.

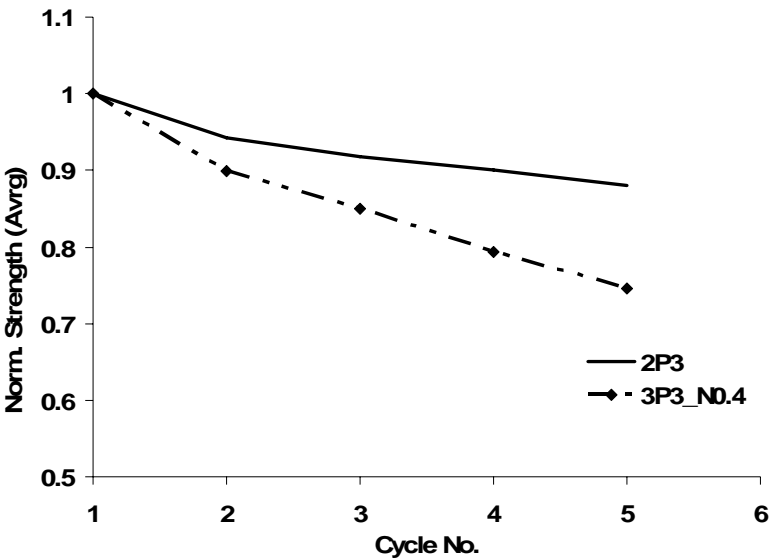


Figure 6.37 Comparison of the normalized cyclic strength degradation of two companion columns with different axial load levels.

**6.8.2 The Effect of Bond Strength on Strength Degradation**

The normalized strength degradation curves of the two companion specimens 2P3 and 7P3\_U are compared in Figure 6.38. These two specimens are different only in bond strength where the bond between concrete and longitudinal reinforcement was prevented along the column height for Specimens 7P3\_U.

The effect of bond strength on strength degradation seems not significant from Figure 6.38.

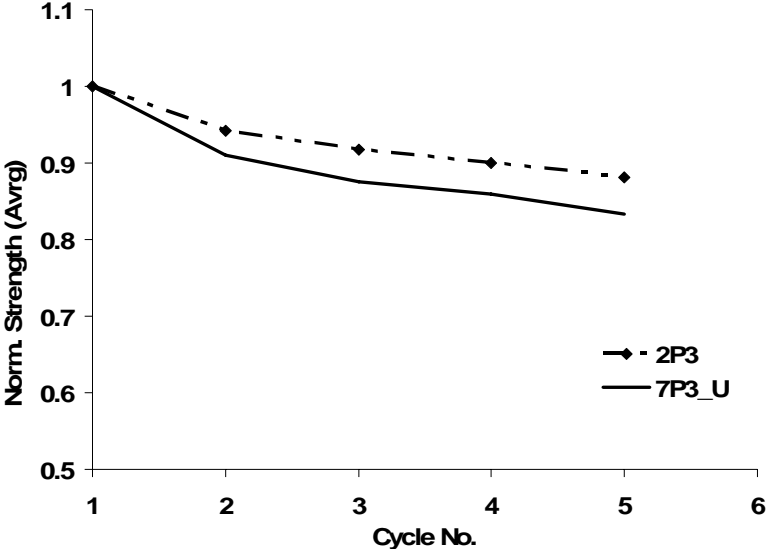


Figure 6.38 Comparison of the normalized cyclic strength degradation of two companion columns with different bond strength.

## **CHAPTER 7**

### **ENERGY-BASED HYSTERESIS MODEL FOR REINFORCED CONCRETE MEMBERS IN FLEXURE**

#### **7.1 General**

Reinforced concrete structures designed for ductile seismic response are expected to have the capability of experiencing inelastic deformations at their structural components for absorbing and dissipating the energy imparted by seismic excitations. In general, it is accepted that inelastic deformations develop and concentrate at certain critical regions of reinforced concrete structures. These critical regions are usually the ends of beams and columns and the beam-column joints where maximum flexural demands occur.

The main objective of this chapter is to propose a hysteretic response model in order to represent the inelastic moment-rotation (curvature) response of column members in flexure. The model accounts for the deterioration in strength and energy dissipation capacity under cyclic reversals. For this purpose, the information gathered from the conducted experiments on code conforming and non-conforming column specimens which were presented in detail in the previous chapters is utilized. Many hysteresis models with either simple or complicated path characteristics have already been proposed by several researchers in literature. They are the elasto-plastic, bilinear, stiffness degrading, and stiffness and strength degrading models (Clough and Johnston, 1966; Takeda et al., 1970; Kanaan and Powell, 1973; Saiidi and Sözen, 1979; Park et al., 1987; Özcebe and Saatcioglu,

1989; Sucuoğlu and Erberik, 2004). The proposed hysteresis model differs from these former ones with its unique characteristics such as its combined quadratic and piecewise linear cycle definition, and its long term memory on cumulative dissipated energy. It is thought that the cumulative dissipated energy history of any typical reinforced concrete column member under variable-amplitude loading can be represented by the composition of dissipated energies of the same member under constant-amplitude loadings through a conversion in terms of equivalent number of constant-amplitude cycles. Therefore, once the response of any column member under constant-amplitude loading has been identified, then its response under variable-amplitude loading can be predicted by employing the proposed energy-based hysteresis model. The proposed analytical model also takes into account cyclic strength deterioration by a simple cycle-based rule.

## **7.2 Influence of Displacement History on Energy Dissipation**

The dependency of cyclic energy dissipation characteristics on displacement history can simply be tested by imposing a number of displacement cycles with similar amplitudes on pairs of specimens where the amplitude patterns are arranged in different sequences.

Two Type 1 specimens 4P4 and 5P5 were subjected to the same amplitudes of displacement cycles, but with different sequences, in order to observe the effect of displacement history on energy dissipation characteristics. Although the observed rate of dissipated energy accumulation in these two specimens were quite different due to the different sequences of imposed displacements, both specimens dissipated nearly the same amount of energy cumulatively at the end of tests, which is an indication of path independency in terms of cumulative dissipated energy. The same tendency was also observed in the pair of Type-2 specimens 3D4 and 4D5 where the imposed displacement protocols are identical to their Type-1 specimen pairs although the last two cycles of specimen 3D4 displacement protocol was not completed due to a problem experienced with the loading system. Finally, the last

pair of Type-2 specimens 5DV1 and 6DV2 are employed for the path independency test by ignoring the first three linear elastic small displacement cycles imposed on them which evidently dissipated very small amount of energy. The following nine displacement cycles imposed on this pair have the same amplitudes, but arranged in different sequences. Specimens 5DV1 and 6DV2 dissipated almost the same amount of energy at the end of the 12<sup>th</sup> displacement cycle.

The associated displacement histories and dissipated energy accumulation for the three pairs of specimens are presented in Figure 7.1. The missing last two cycles of 3D4 are extrapolated in terms of dissipated energy.

There are two important corollaries derived from the comparisons shown in Figure 7.1 regarding the hysteretic energy dissipation of reinforced concrete members:

1. Amplitude dependency:

The rate of cyclic energy dissipation depends on the displacement amplitude, however dissipation rate decreases with the number of cycles repeated at this amplitude.

2. Path independency:

The sequence of displacement cycles with different amplitudes does not influence the total dissipated energy.

### **7.3 Dissipated Energy Predictions for Constant Amplitude Loading**

The procedure for predicting the energy dissipated under constant-amplitude cyclic loading is explained in this section. Starting with the prediction of dissipated energy at the first unique inelastic cycle (Cycle-1), the ductility dependent relation between the dissipated energies in first and second cycles is derived for both code conforming and non-conforming specimens. Introducing these quantities into the normalized dissipated energy relations, dissipated energy histories of column members are obtained under the following constant-amplitude displacement cycles.

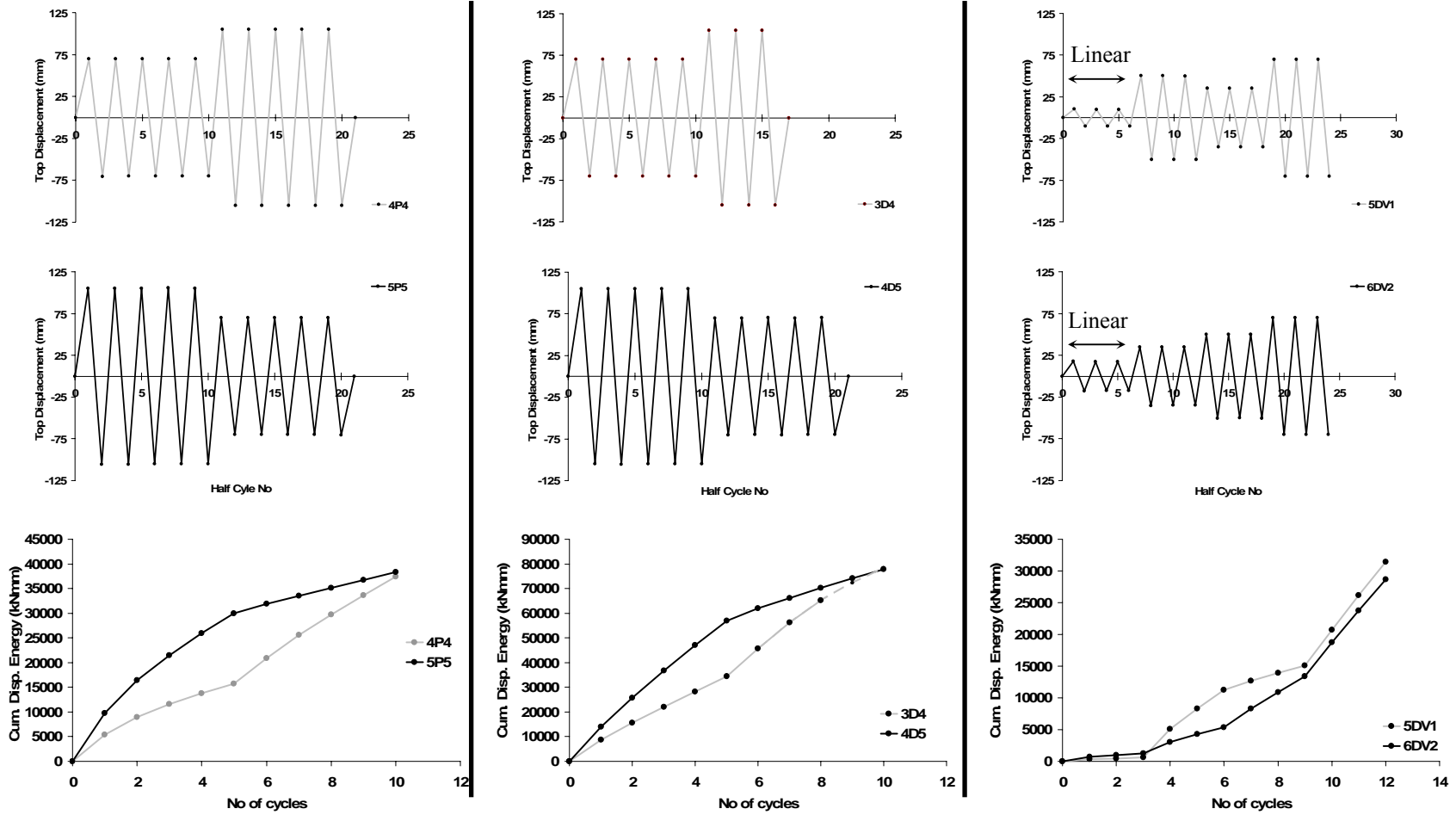


Figure 7.1 Effect of the sequence of imposed displacements on the energy dissipation characteristic of column specimens in flexure

### **7.3.1 Prediction of Cycle-1**

A modified version of Takeda (1970) model is used for calculating analytically the dissipated energy at the first full cycle of a constant-amplitude loading. As it is defined in the original model, a tri-linear curve with specified cracking and yielding points was used to construct the primary curve. Strain hardening was also considered for both types of column members, accordingly. Unloading branch stiffness which is considered as amplitude depended is calculated by using the formulation proposed by Takeda with an exponential coefficient of 0.4. It is assumed that the unloading curve ends at the point where the load reaches zero, and from this point on reloading starts.

The coordinates of cracking and yielding points on primary curve were calculated by moment-curvature analysis of column member sections with given cross-sectional and material properties. The analytical modified Takeda model versus experimental first cycle moment-chord rotation comparisons are presented in Section 7.5 for each specimen tested under constant amplitude loading. Although the modified Takeda model is mainly a piecewise linear sectional model, its predictions of dissipated energy at the first full cycle when compared to the actual dissipated energy values of test specimens under moderate axial load ratio were found to be quite successful as shown in Figure 7.2. For specimen 3P3\_N0.4 where the axial load level is 0.4, the prediction of the model for dissipated energy at the first cycle is less accurate.

### **7.3.2 Prediction of Energy Dissipation in Cycle-2**

It was shown in Section 6.5 of Chapter 6 that the ratio of dissipated energies in the first and second full cycles strongly depend on the ductility ratio for reinforced column specimens considered in this study. The analytical expressions representing this dependency for Type-1 and for Type-2 column specimens are given in Equation 7.1 and 7.2, respectively, with reference to Figure 6.18.

$$\text{Type-1 : } E_2 = E_1 \cdot [0.042 \cdot \mu_\theta + 0.46] \quad (7.1)$$

$$\text{Type-2 : } E_2 = E_1 \cdot [0.077 \cdot \mu_\theta + 0.52] \quad (7.2)$$

where  $\mu_\theta$  is the rotational ductility,  $E_1$  and  $E_2$  are the dissipated energies at 1<sup>st</sup> and 2<sup>nd</sup> full cycles, respectively.

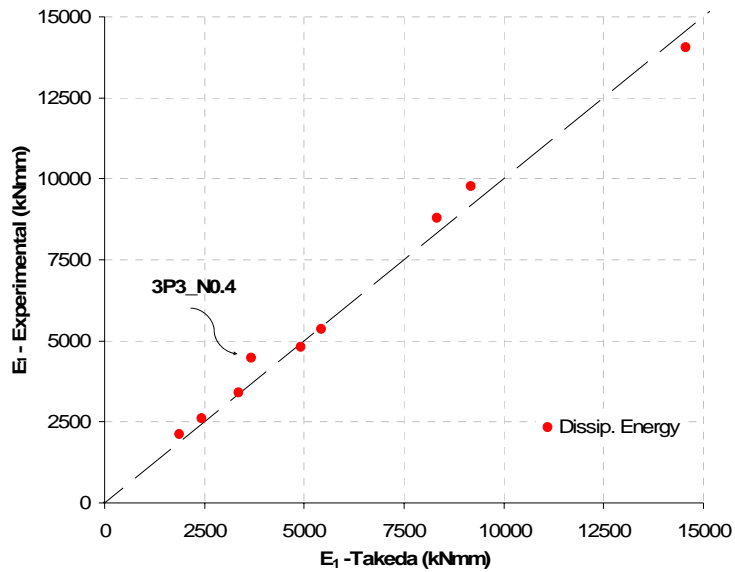


Figure 7.2 Correlation of actual dissipated energy with predicted dissipated energy at the first full cycle

Energy dissipated by the test specimens under constant amplitude loading and the predicted values in the first two cycles are given in Table 7.1. Specimen 1P2 seems to be the outlier of its group.

### 7.3.3 Prediction of Dissipated Energy in the Consecutive Cycles

Predictions of dissipated cyclic energy, normalized with respect to the energy dissipated in the second cycle, are presented in Figure 7.3.a and 7.3.b for

Type-1 and Type-2 specimens, respectively. As it was explained in detail in Chapter 6, the normalized cyclic energy dissipation relations for reinforced concrete columns in flexure can successfully be represented by an exponentially decaying function with two characteristic variables ( $\alpha$  and  $\beta$ ) in the cycles following the second cycle.

Table 7.1 Dissipated energy in the 1<sup>st</sup> and 2<sup>nd</sup> full cycles

		$E_1$	$E_1$	$\frac{E_1 (pred)}{E_1 (exp)}$	$E_2$	$E_2$	$\frac{E_2 (pred)}{E_2 (exp)}$
		<i>Experimental</i>	<i>Predicted</i>		<i>Experimental</i>	<i>Predicted</i>	
		(kNmm)	(kNmm)		(kNmm)	(kNmm)	
<b>Type - 1</b>	<b>1P2</b>	2123	1871	0.88	1602	1010	0.63
	<b>2P3</b>	3399	3363	0.99	1857	1931	1.04
	<b>4P4</b>	5344	5425	1.02	3532	3363	0.95
	<b>5P5</b>	9780	9178	0.94	6672	6427	0.96
<b>Type - 2</b>	<b>1D2</b>	2594	2437	0.94	1563	1536	0.98
	<b>2D3</b>	4799	4908	1.02	3353	3327	0.99
	<b>3D4</b>	8777	8331	0.95	6829	6172	0.90
	<b>4D5</b>	14046	14533	1.04	11684	12391	1.06

With the already-estimated values of  $E_1/E_2$  ratio in hand for Type-1 and Type-2 test specimens, dissipated energy curves normalized with respect to the second cycle energy can be obtained by substituting the average values of  $\alpha$  (0.58 for Type-1 and 0.85 for Type-2 specimens) and  $\beta$  (0.84 for Type-1 and 0.66 for Type-2 specimens) into Equation 6.1. It should be noted that the normalized dissipated energy curve is unique for each individual specimen after the second cycle, indicating that the amplitude dependency disappears after this cycle. Once they are constructed, the absolute dissipated energy curve can be obtained by

scaling it with the estimated value of dissipated energy at the second full cycle. The predicted energy dissipation curves for a selected pair of specimens (2P3, 2D3) are plotted along with the experimentally observed dissipated energy values of these specimens in Figure 7.4.

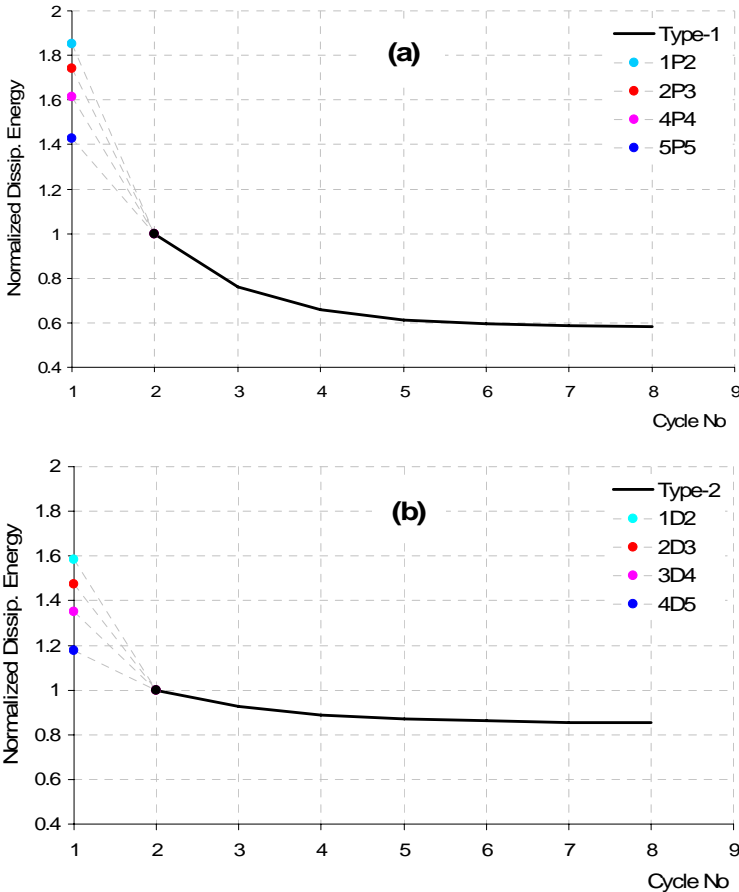


Figure 7.3 Normalized dissipated energy curves for (a) Type-1 and (b) Type-2 specimens

For comparison, dissipated cyclic energies of the two specimens predicted by modified Takeda model are also plotted in the same figure. Considering that the success of prediction depends solely on the successful estimation of dissipated

energies at the first and second full cycles, the proposed procedure for predicting the cyclic energy dissipation of typical reinforced concrete members yielded quite successful results. The modified Takeda model results in significant overestimation of dissipated energy for these test specimens since it does not account for any cyclic loss of dissipation capacity.

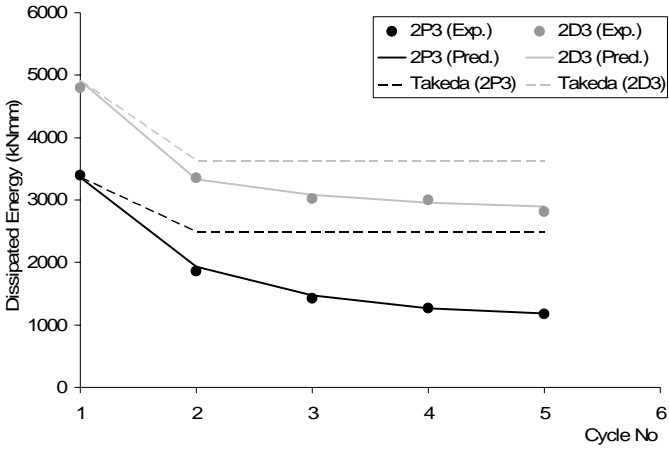


Figure 7.4 Comparison of experimental and predicted dissipated energies for typical Type-1 and Type-2 specimens

**7.4 Strength Deterioration under Constant Amplitude Loadings**

Observations on strength deterioration for Type-1 and Type-2 specimens at maximum attained displacement values from the constant-amplitude stages of loading protocols showed that normalized strength degradation has a small scatter in its decreasing trend for both types of specimens. Although, it is well known that strength deterioration under cyclic loading for reinforced concrete members is a complex phenomenon, strength degradation behavior for both type of specimens can be represented with a simple linear analytical expression by considering only the number of experienced cycles as given in Equation 7.3.

$$F_n = F_1 \cdot [1 - a \cdot (n - 1)] \quad (7.3)$$

Here,  $n$  is the cycle number,  $F_1$  is the strength at the first experienced cycle,  $F_n$  is the deteriorated strength at the  $n$ 'th cycle and  $a$  is a coefficient with a mean value of 0.03.

It can be observed from the comparisons shown in Figure 7.5.a and 7.5.b that the proposed strength degradation relation and the actual deterioration for Type-1 and Type-2 column members fit reasonably well in spite of its simplicity. The slope parameter  $a$  is weakly amplitude dependent, however this dependence is ignored for brevity.

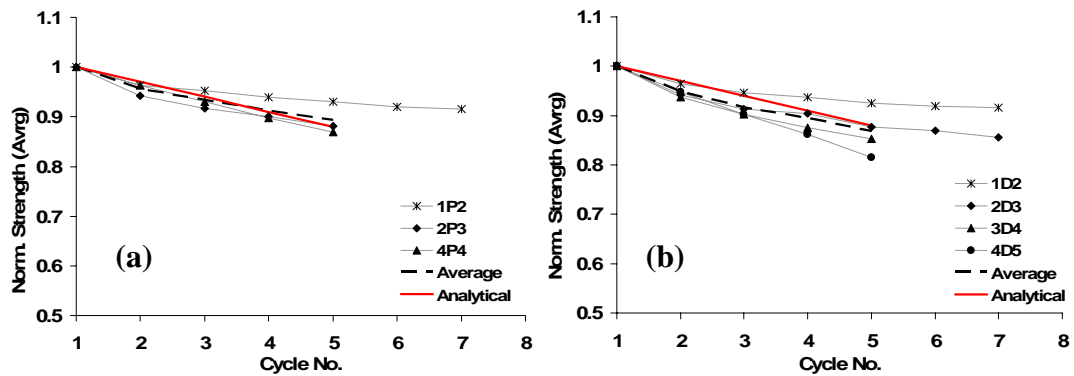


Figure 7.5 Normalized strength degradation for, (a) Type-1 and (b) Type-2 column members

## 7.5 Construction of Constant-Amplitude Hysteresis Cycles

A constant-displacement cycle of moment-rotation hysteresis can be constructed with the knowledge of the constant-displacement amplitude, strength degradation at the  $n$ 'th cycle, and the amount of energy to be dissipated during this cycle. More specifically, if the unloading branch is defined with a straight line as in the modified Takeda model, it then remains to define the expression for the

reloading branch. This reloading curve is bounded with points **A** and **B** shown in Figure 7.6 where point **A** is the intercept of the unloading branch with the rotation axis, and **B** is the deteriorated strength at the  $n$ 'th cycle. Furthermore, the area enclosed by the half-cycle **ABA'** should be equal to half of the dissipated cyclic energy obtained from Equation 6.1 for cycle number  $n$ . These three conditions facilitate a quadratic form for the reloading branch, where the three coefficients of the quadratic form are obtained from Equation 7.4.

$$\underline{C}.\underline{a} = \underline{F} \quad (7.4)$$

In Equation 7.4,  $\underline{a}$  is the unknown coefficients of the quadratic reloading hysteresis curve,  $\underline{C}$  and  $\underline{F}$  are functions of strength, rotation amplitude and energy dissipated at the  $n$ 'th cycle. The quadratic equations implemented in Equation 7.4 are presented in Equations 7.5.a, 7.5.b and 7.5.c with the values corresponding to three boundary conditions.

$$f(\theta_{i-1}) = a_0 + a_1\theta_{i-1} + a_2\theta_{i-1}^2 = 0 \quad (7.5.a)$$

$$f(\theta_n) = a_0 + a_1\theta_n + a_2\theta_n^2 = M_n \quad (7.5.b)$$

$$\int_{\theta_{i-1}}^{\theta_n} f(\theta).d\theta = \int_{\theta_{i-1}}^{\theta_n} (a_0 + a_1\theta + a_2\theta^2).d\theta = E_n^h + \frac{(\theta_n - \theta_{i-1}).M_n}{2} \quad (7.5.c)$$

Here  $\theta_{i-1}$ ,  $\theta_n$  and  $\theta_i$  are the rotation values indicated in Figure 7.6,  $E_n^h$  is half of the energy dissipated at the  $n$ 'th half cycle and  $M_n$  is the strength attained at this half-cycle. A representative sketch of an analytical cycle with a quadratic loading branch and a linear unloading branch is shown in Figure 7.6.

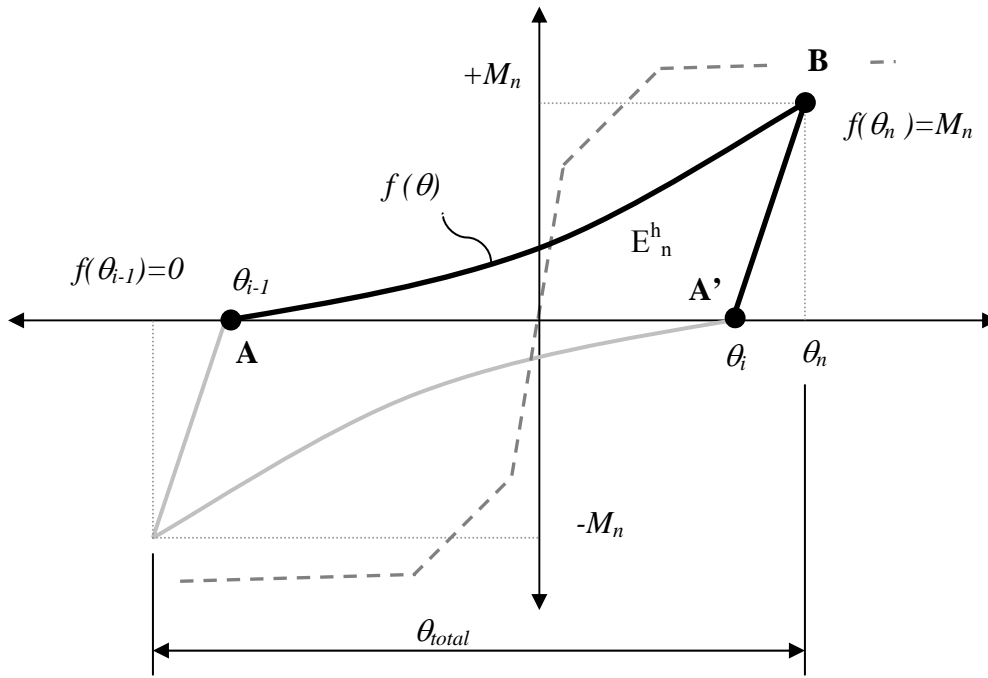


Figure 7.6 A representative analytical cycle with boundary conditions

Equating the dissipated energy of any typical analytical cycle with the energy predicted from the proposed cyclic energy dissipation relations and imposing the unloading boundary condition **A** and the strength boundary condition **B**, hysteresis loops for constant-amplitude loading can be constructed as summarized herein. For the unloading branch, the amplitude dependent formulation proposed by Takeda was utilized. The stiffness of the unloading branch was also modified with the deterioration in strength, forming a locus of intercepts on the rotation axis.

Cycle-by-cycle matches on the experimental loops of Type-1 (2P3, 4P4, 5P5) and Type-2 (1D2, 2D3, 3D4, 4D5) constant-amplitude specimens are presented in Figures 7.7 - 7.13 for the first five cycles of the constant amplitude loading sequences. Modified Takeda model predictions for these cycles are also depicted on the same graphs for comparison. The specimen 1P2 is not included in the analytical prediction since it was considered as an outlier in the test data set due to the discrete nature of its normalized energy dissipation in the Type-1 set.

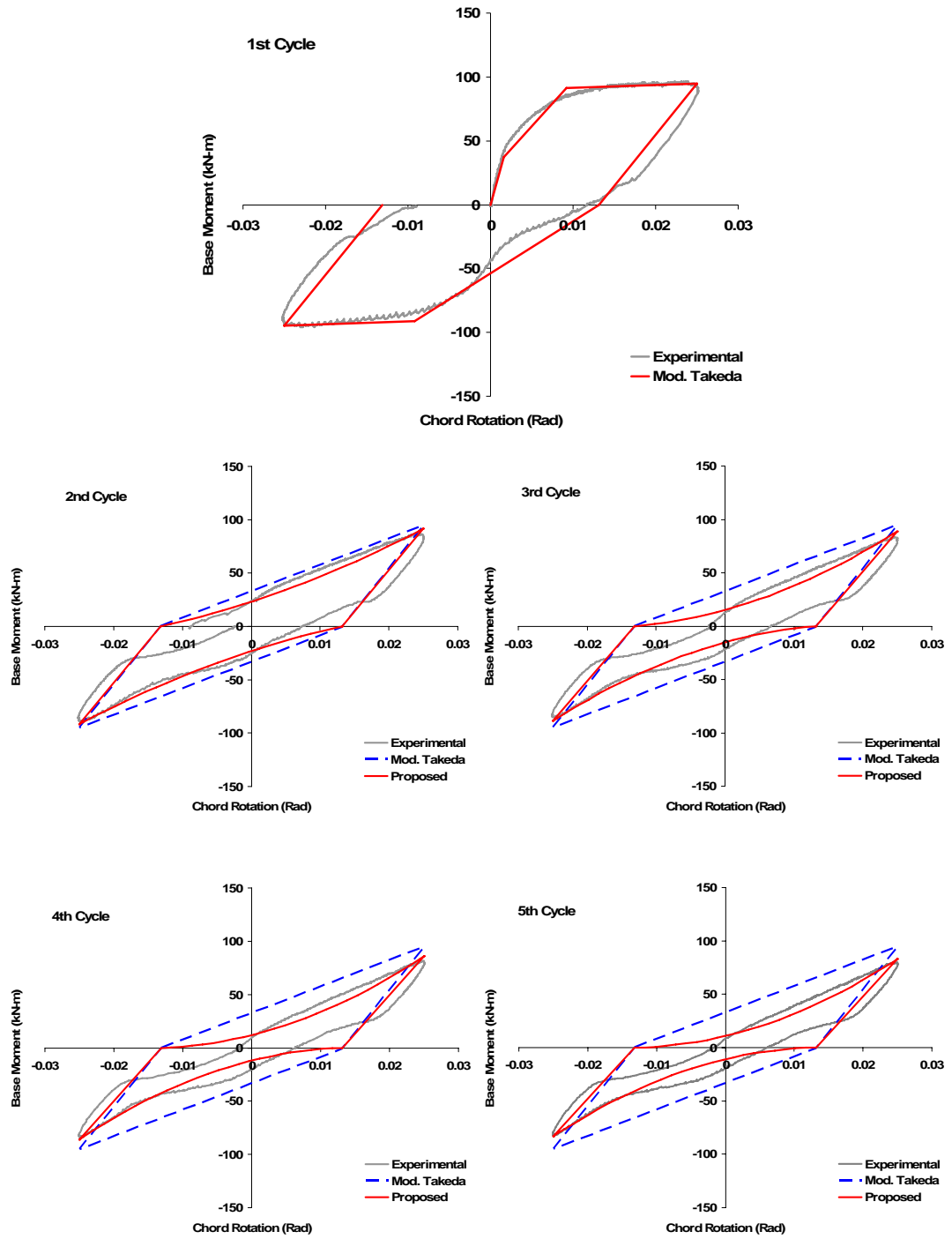


Figure 7.7 Predicted and observed responses of Specimen 2P3 for first five cycles

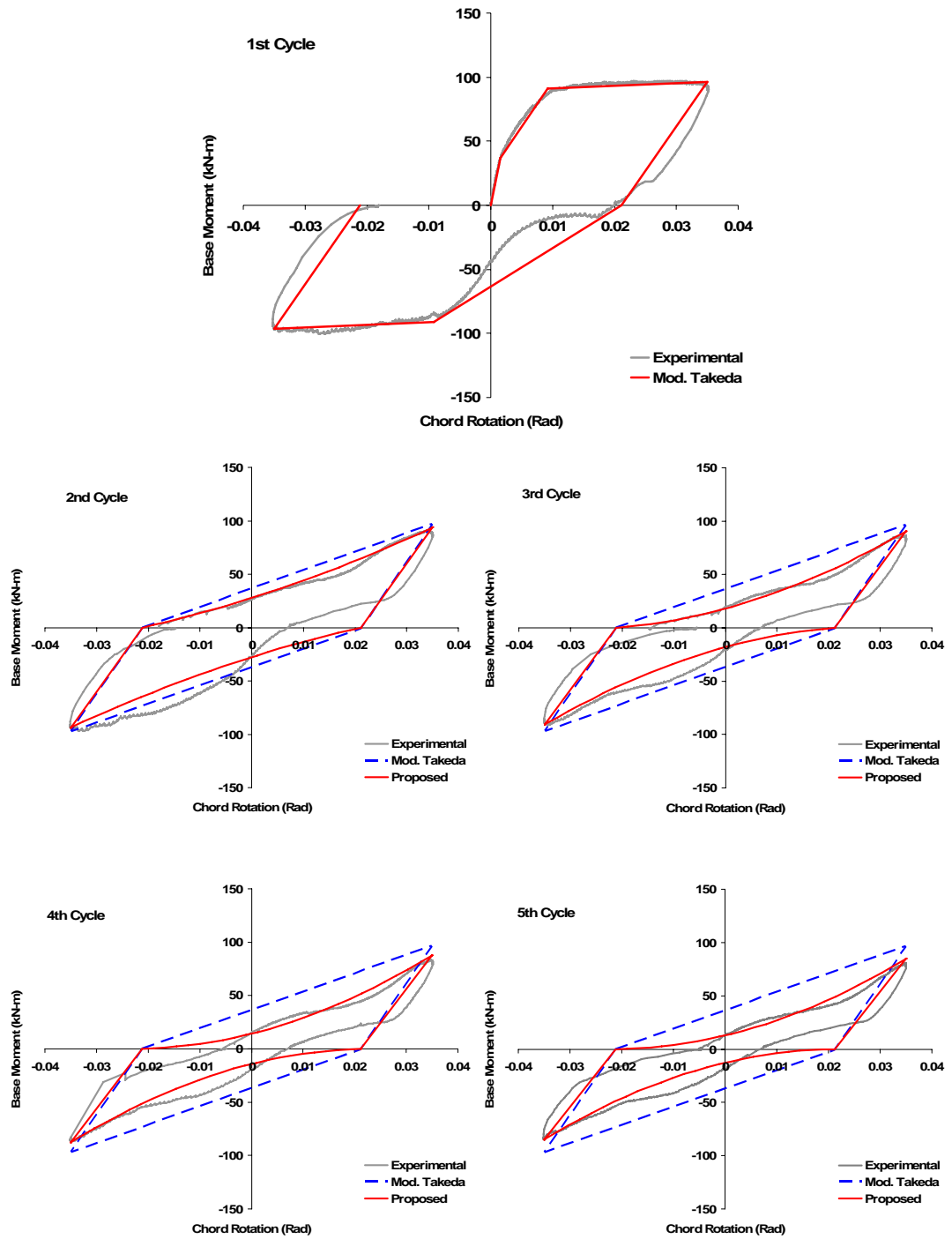


Figure 7.8 Predicted and observed responses of Specimen 4P4 for first five cycles

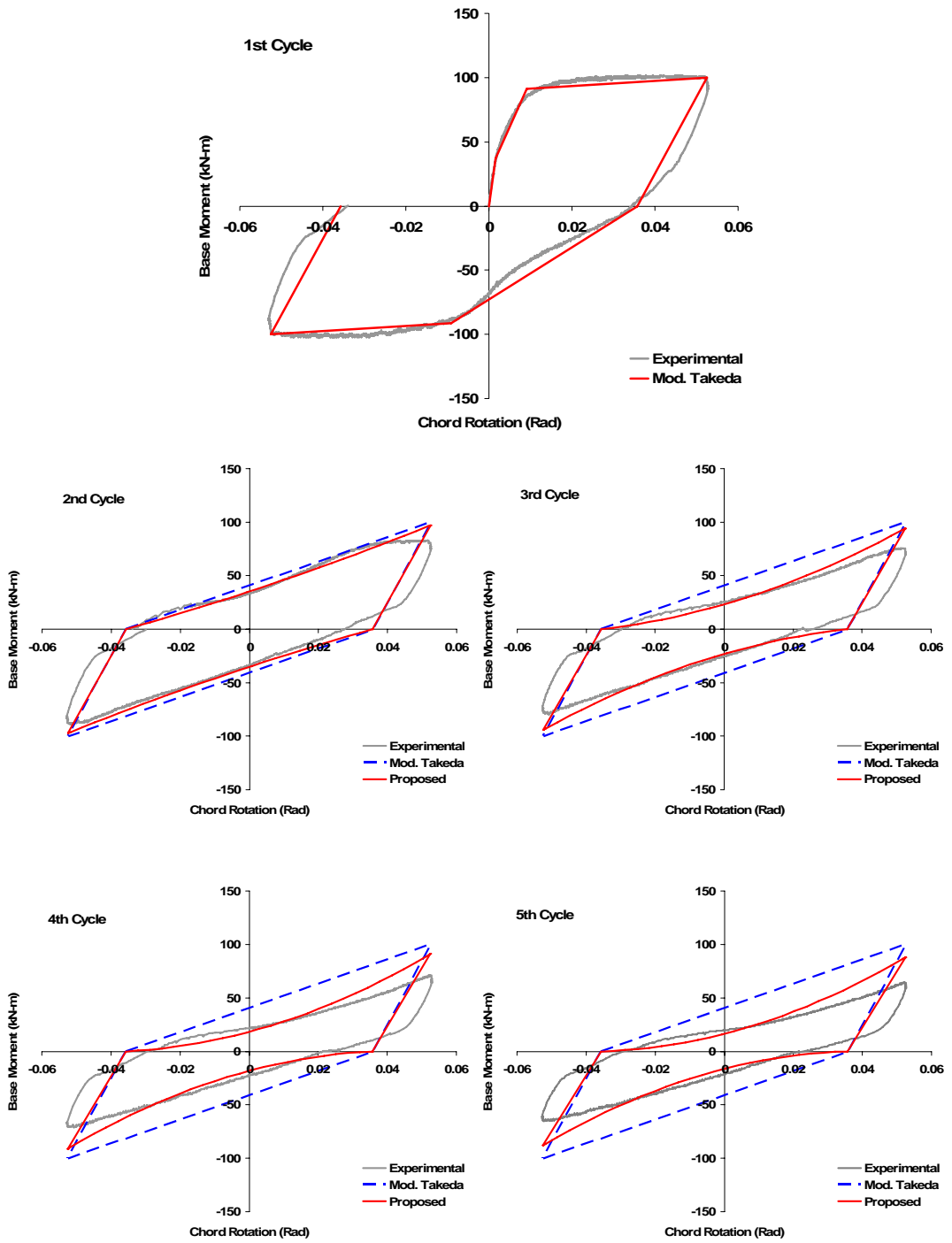


Figure 7.9 Predicted and observed responses of Specimen 5P5 for first five cycles

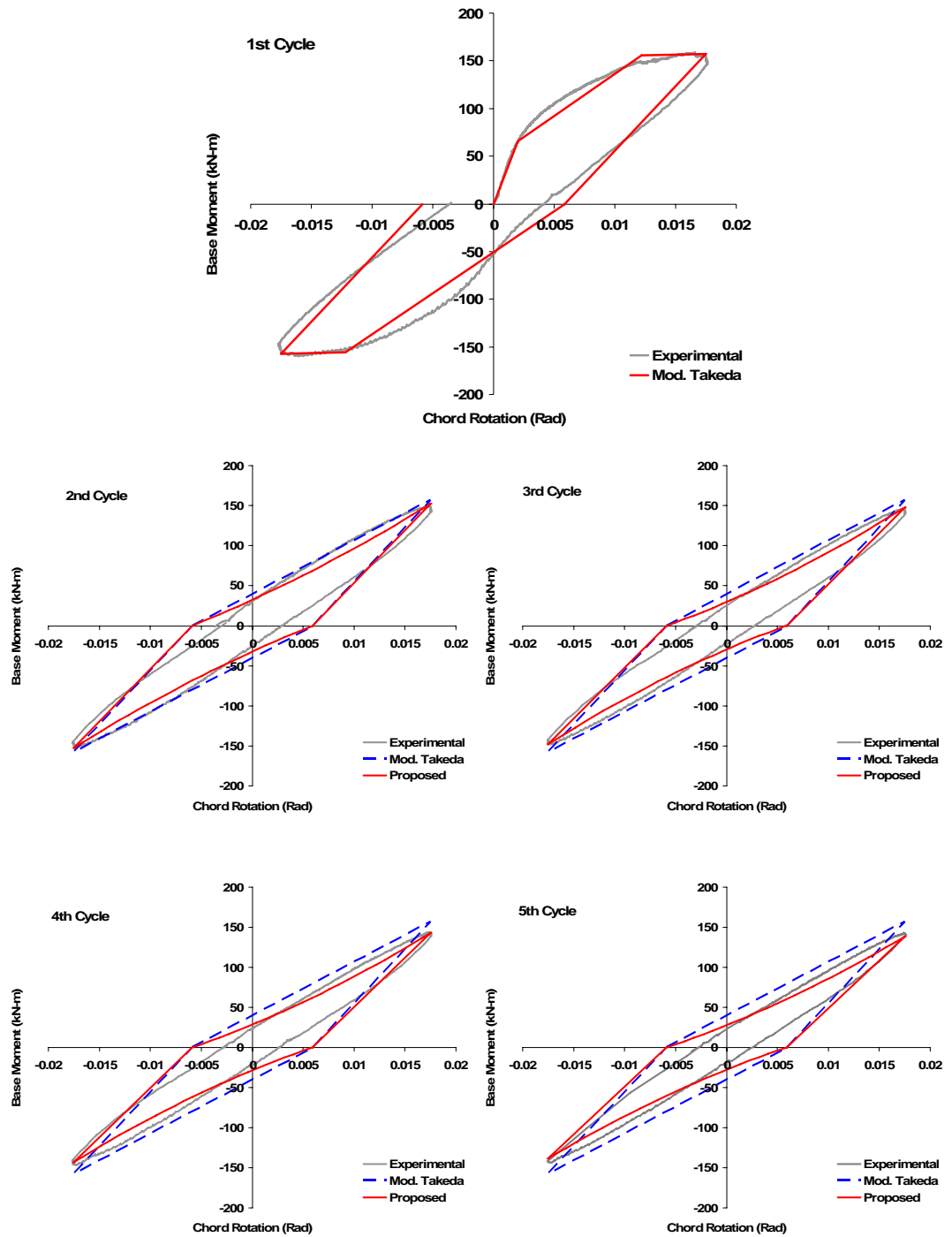


Figure 7.10 Predicted and observed responses of Specimen 1D2 for first five cycles

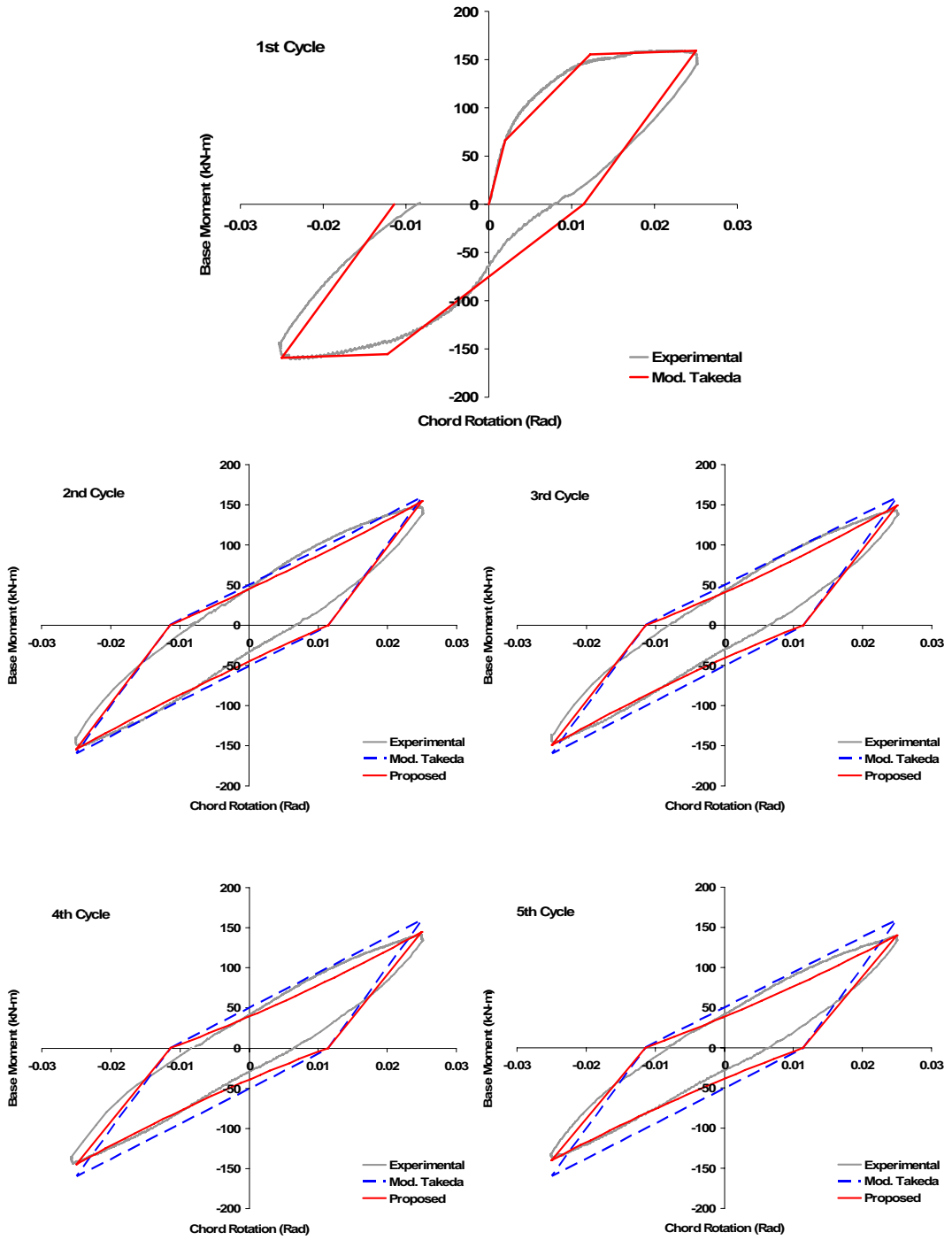


Figure 7.11 Predicted and observed responses of Specimen 2D3 for first five cycles

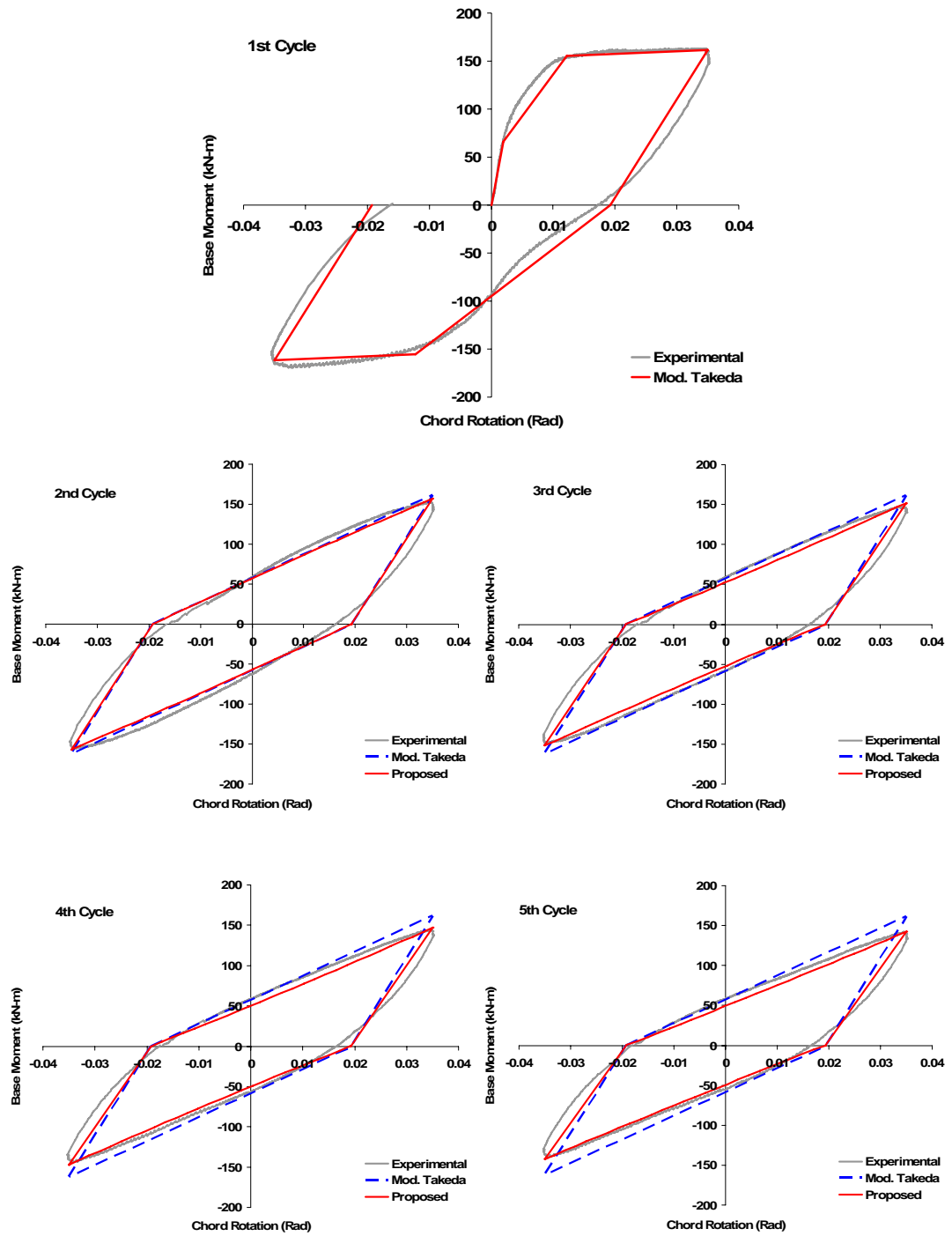


Figure 7.12 Predicted and observed responses of Specimen 3D4 for first five cycles

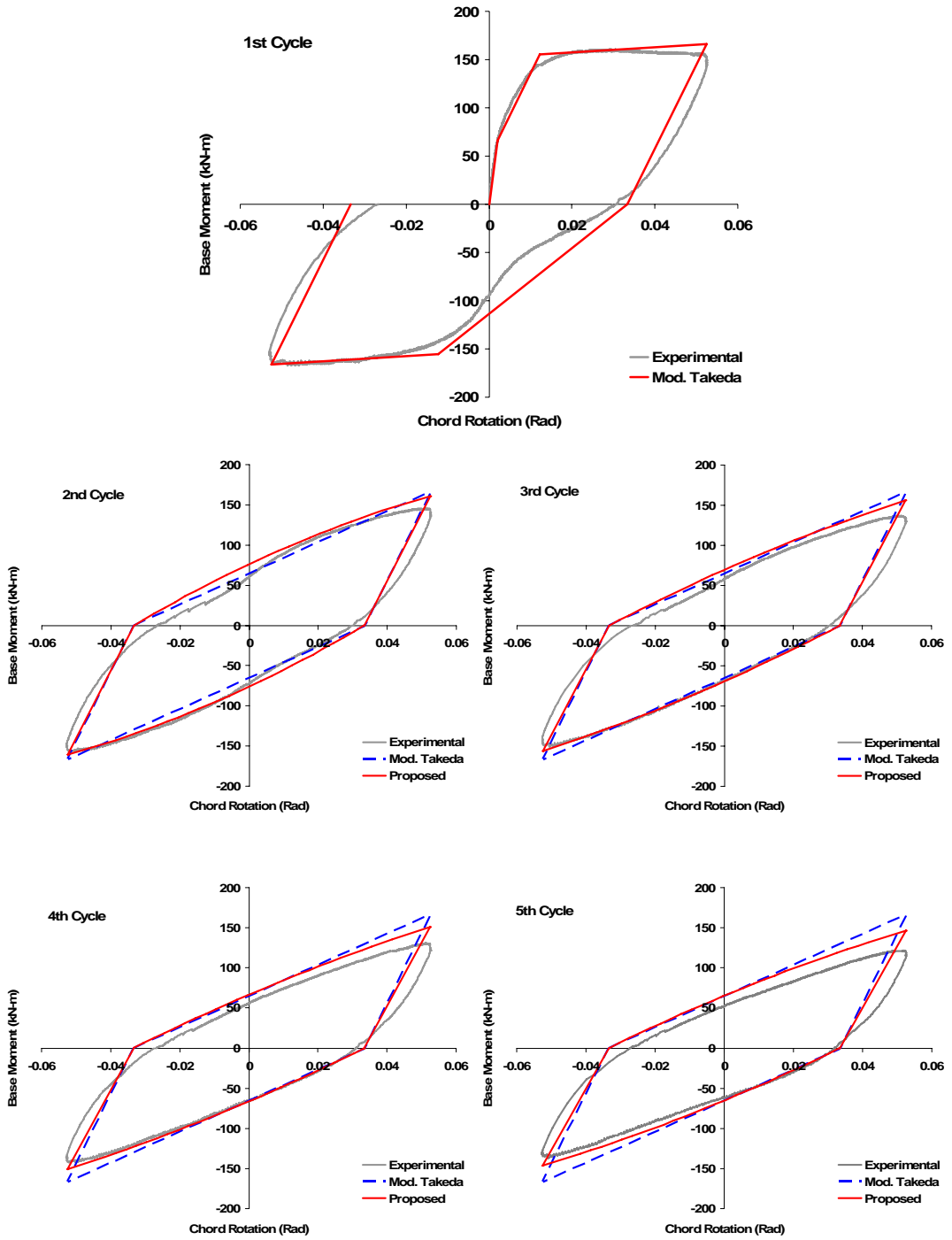


Figure 7.13 Predicted and observed response of Specimen 4D5 for first five cycles

## 7.6 Direct Prediction of Cumulative Dissipated Energy for Variable-Amplitude Displacement Cycles

Cumulative hysteretic energy dissipated by the column specimens tested under variable-amplitude displacement cycles (6PV1, 5DV1 and 6DV2) is predicted herein, either directly from the constant-amplitude test results, or by using the analytical procedure proposed in the previous section for estimating cyclic energy dissipation under constant-amplitude loading. An equivalent number of cycles ( $n_{eq}$ ) definition is employed for the prediction process, which was defined earlier by Sucuoğlu and Erberik (2004). At any stage of variable-amplitude loading, the cumulative dissipated energy up to that stage was expressed as the energy dissipated under constant-amplitude loading with an equivalent number of cycles, where the ductility of constant cycles was equal to the ductility of the following half-cycle of the variable-amplitude loading. Energy dissipated during the following cycle is then predicted from either experimental or analytical cumulative dissipated energy history of that constant-amplitude loading at the equivalent cycle number of “ $n_{eq}+1$ ”. It should be noted that the ductility definition utilized herein is the rotation ductility, which is the ratio of  $\theta_{total}$  to  $\theta_{yield}$  as given in Equation 7.5.

$$\mu_{\theta} = \frac{\theta_{total}/2}{\theta_{yield}} \quad (7.5)$$

Here,  $\theta_{total}$  is the absolute total rotation of the full cycle shown in Figure 7.6, and  $\theta_{yield}$  is the yield rotation.

Cumulative dissipated energy under variable-amplitude displacements imposed on test specimens 6PV1, 5DV1 and 6DV2 are predicted directly from the constant-amplitude test results, and from its analytical companion given in the previous section. The comparative results are presented in Figures 7.14.a, b and c, respectively for the three test specimens. Although the predictions for Type-2 variable-amplitude specimens 5DV1 and 6DV2 are quite successful, the predicted

cumulative energy at for Type-1 specimen 6PV1 possesses 20% error on average. It is apparent that the proposed prediction procedure is very successful for code-conforming column specimens.

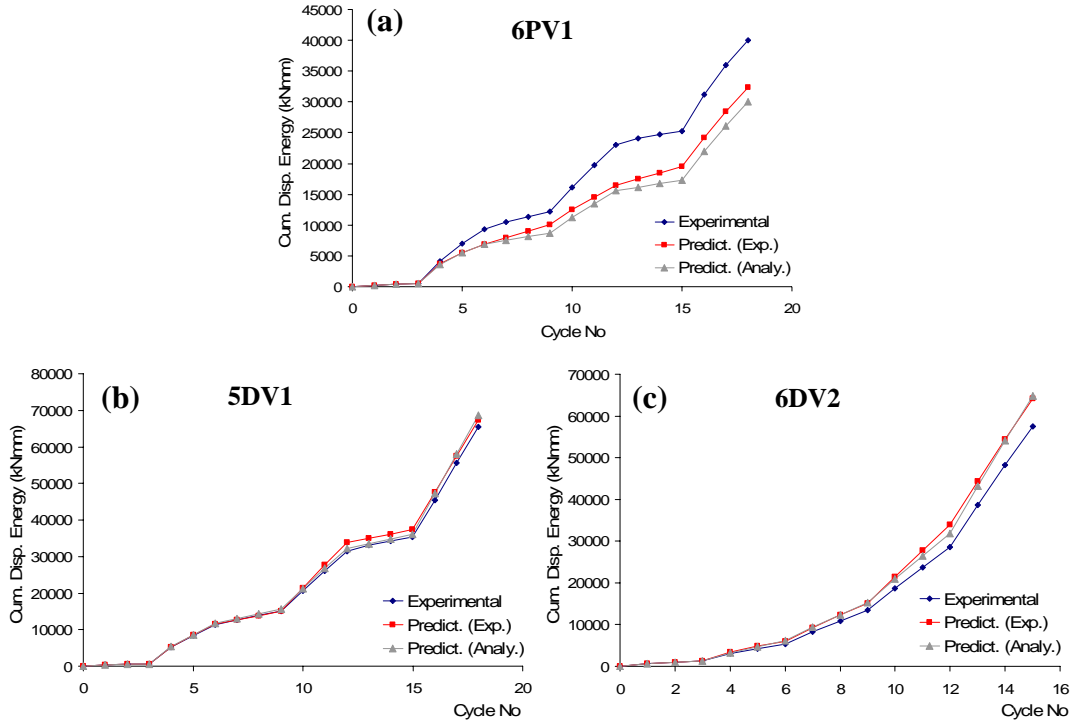


Figure 7.14 Cumulative dissipated energy predictions for variable-amplitude loadings of, (a) 6PV1, (b) 5DV1 and (c) 6DV2

### 7.7 Moment-Rotation Model for Reinforced Concrete Column Sections in Flexure

General rules and characteristics of an energy-based hysteresis model for moment-rotation response of reinforced concrete column members in flexure are explained in this section. Derived from the well-known Takeda (1970) hysteresis model, the proposed model is mainly a composition of piece-wise linear and quadratic hysteresis paths representing cyclic response with deterioration in

strength. The details of prediction process and general rules for constructing the analytical hysteretic response are explained in detail and comparisons with the actual experimental results are presented in the following sections. Similar rules and features introduced earlier for constant-amplitude hysteresis prediction such as strength deterioration, amplitude dependent unloading stiffness, equivalent number of cycle definition and quadratic formulation for loading branch are also applicable exactly in the way they were defined for constant-amplitude loading.

### **7.7.1 Rules for Constructing the Hysteresis Model**

Since the analytical hysteresis model is defined by piece-wise linear and quadratic hysteresis curves for unloading and reloading hysteresis paths respectively, it is not convenient to state the rules for constructing the model for all possible response cases all at once. To cope with that, rules for the proposed model are defined for some discrete phases. However, it should be noted that the hysteretic response will be defined by a composition of these phases, accordingly the rules will be utilized wherever they are applicable.

An envelope curve (i.e. primary curve for Takeda model) will be followed at some stages of response which can be defined simply by just assuming a constant yielding plateau or by defining a negative/positive post yield stiffness (strain hardening or softening). Cycle-1 defined in constant-amplitude loading is the envelope curve of the hysteresis model for a constant amplitude loading.

#### Phase 1: Before First Cracking

Loading and unloading take place on a linear path with a slope of  $k_{cr}$  which is equal to the ratio of moment to rotation at first cracking calculated from moment-curvature analysis. No energy dissipation occurs.

### Phase 2: Before First Yielding

This is the phase where moment exceeds the cracking moment but do not reach the yielding. Rules of Phase-1 apply herein as well. Loading takes place on envelope curve up to yielding and unloading occurs with a slope where it shoots to the cracking moment in other direction. If unloading occurs after cracking takes place in this direction, then unloading continues on the path that shoots to the cracking point in the other direction till it reaches the zero-moment level, and then continues hereafter by shooting to the maximum experienced moment on the envelope curve. This phase is depicted with its rules defined on a generic hysteresis in Figure 7.15.

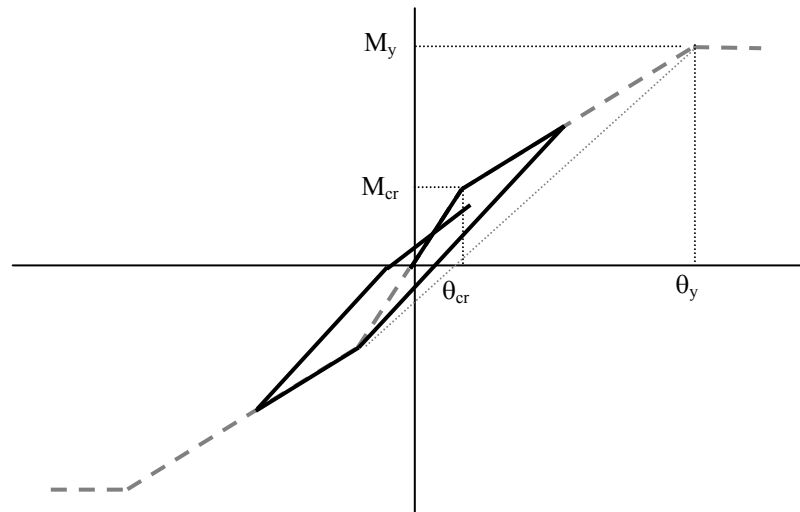


Figure 7.15 Phase-2 of analytical hysteresis model

### Phase 3: After First Yielding

In this phase, moment reaches yielding in one direction and inelastic deformations start to take place. Rules of Phase-2 apply herein as well. Envelope curve is followed up to the point where unloading starts. From this point, unloading takes place till it reaches to zero-force level with a slope  $k_r$ , which depends on the

amplitude of deformation experienced. This slope is calculated by the formulation proposed by Takeda et al. (1970). Shooting to the yield point in the other direction, reloading branch continues till yielding and follows the envelope curve afterwards. If unloading occurs at any point on the reloading branch before yielding, it takes place with a slope of  $k_y$  which is also defined by the Takeda model as “*the slope of line joining the yield point in one direction to the cracking point in other direction*”. This phase actually represents the Cycle-1 of constant-amplitude loadings if the deformations attained in both loading directions are equal. Phase 3 is presented schematically in Figure 7.16

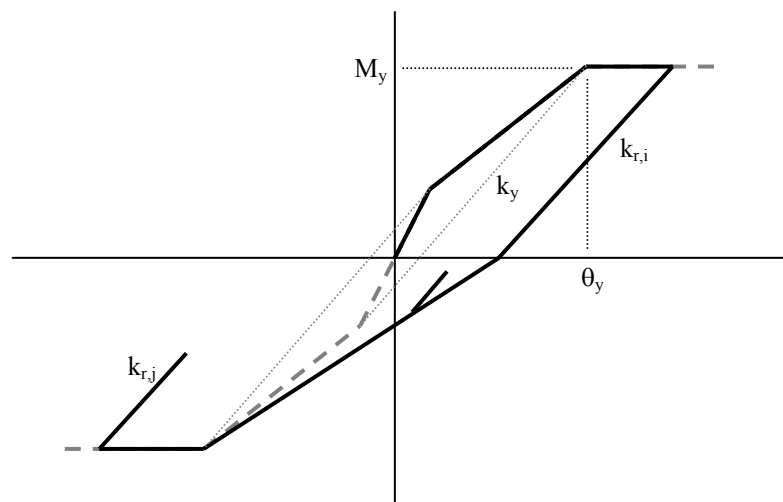


Figure 7.16 Phase-3 of analytical hysteresis model

#### Phase 4: General Inelastic Response

This is the phase defined for hysteretic response after yielding occurs in any direction of loading at least once. Rules of Phase-3 apply herein as well. In this phase, reloading branches are defined by a quadratic formulation according to the boundary conditions of each corresponding cycle. The quadratic formulation for loading branch was explained in detail in the former sections. After experiencing

the first inelastic cycle, reloading branch shoots to the deteriorated strength value of the cycle with maximum deformation attained in that direction formerly. At this stage, quadratic expression of the reloading branch is determined by employing the predicted dissipated energy value of the coming cycle with the known boundary conditions.

On the way to the aimed point of deteriorated strength at the maximum attained deformation;

- If unloading occurs before reaching the strength value, unloading branch follows a linear path with the same slope of unloading branch at the shooted strength value. Dissipated energy of this cycle is then calculated accordingly and the cumulative energy value is modified.
- If unloading occurs at exactly the point when it reaches the shooted strength point, unloading branch follows a linear path with a slope calculated by modifying the slope of non-deteriorated cycle with the same displacement amplitude so that a locus of intercepts forms on zero-moment axis.
- If it does not unload till the value shot, it continues on the same path defined by extrapolating the quadratic function of the loading branch until it reaches the envelope curve. Continuing on the envelope curve, it reaches the point where it unloads. The slope of unloading curve is calculated by the amplitude dependent formulation of Takeda model as it was done for the former cycles. Dissipated energy of this cycle is calculated and the cumulative dissipated value is modified accordingly.

A representation of the general inelastic response phase is illustrated in Figure 7.17 schematically for a constant yield plateau for the post yielding stage.

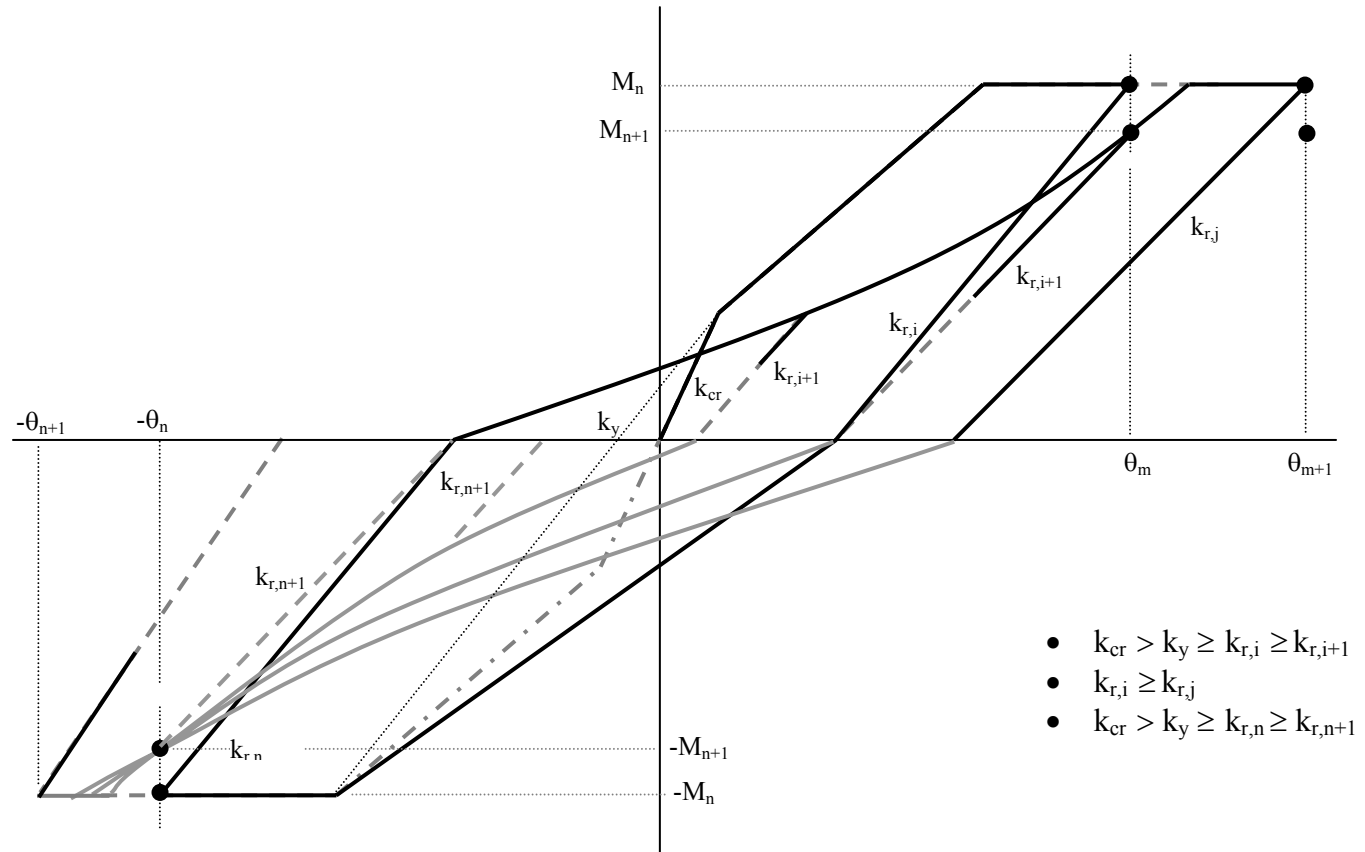


Figure 7.17 Rules for the unloading and reloading branches of proposed moment-rotation hysteresis model

### 7.7.2 Hysteretic Response Prediction of R/C Column Sections under Variable-Amplitude Loading

The envelope curves for the analytical response predictions of Type-1 and Type-2 specimens are derived from the experimental envelope curves which are shown in Figures 7.18.a and 7.18.b. A constant plateau is assumed for Type-2 specimens 5DV1 and 6DV2 whereas a softening post yielding branch is assumed for the Type-1 specimen 6PV1 while constructing their hysteresis models.

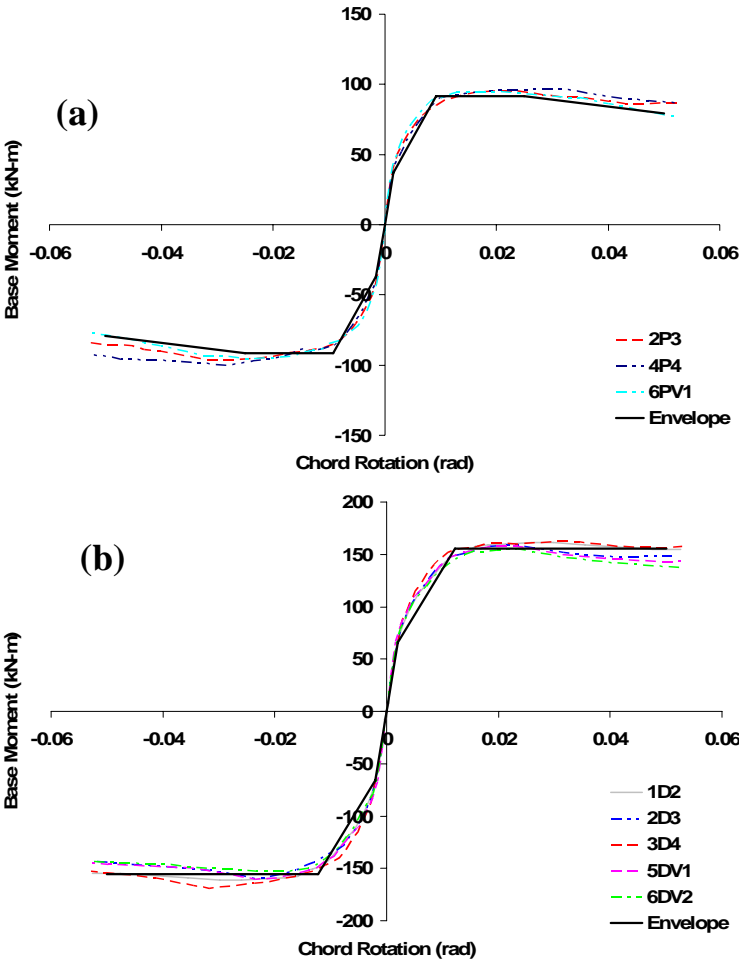


Figure 7.18 Envelope curves proposed for estimation of hysteretic response of (a) Type-1 specimens and (b) Type-2 specimens

The experimental responses of column specimens tested under variable amplitude loadings and their responses predicted by the proposed model are compared in order to verify the validity of the proposed model. Observed and predicted base moment-chord rotation responses of test specimens 6PV1, 5DV1 and 6DV2 are presented in Figures 7.19.a, 7.20.a and 7.21.a, respectively. Cumulative dissipated energy histories of these specimens measured from the experiment and calculated from the proposed model are also shown in Figures 7.19.b, 7.20.b and 7.21.b.

Considering that the main aim of the proposed model is not to obtain a perfect cycle-by-cycle match of the experimental response, it can be concluded that the predictions for moment-rotation response hysteresis is satisfactory for non-conforming Type-1 specimen, and reasonably well for conforming Type-2 specimens. Implicit considerations of the pinching behaviour, simplified representation of unloading and strength degradation and inherent discrepancies in response of reinforced concrete column members, especially for non-conforming ones, are thought to be the main sources of error.

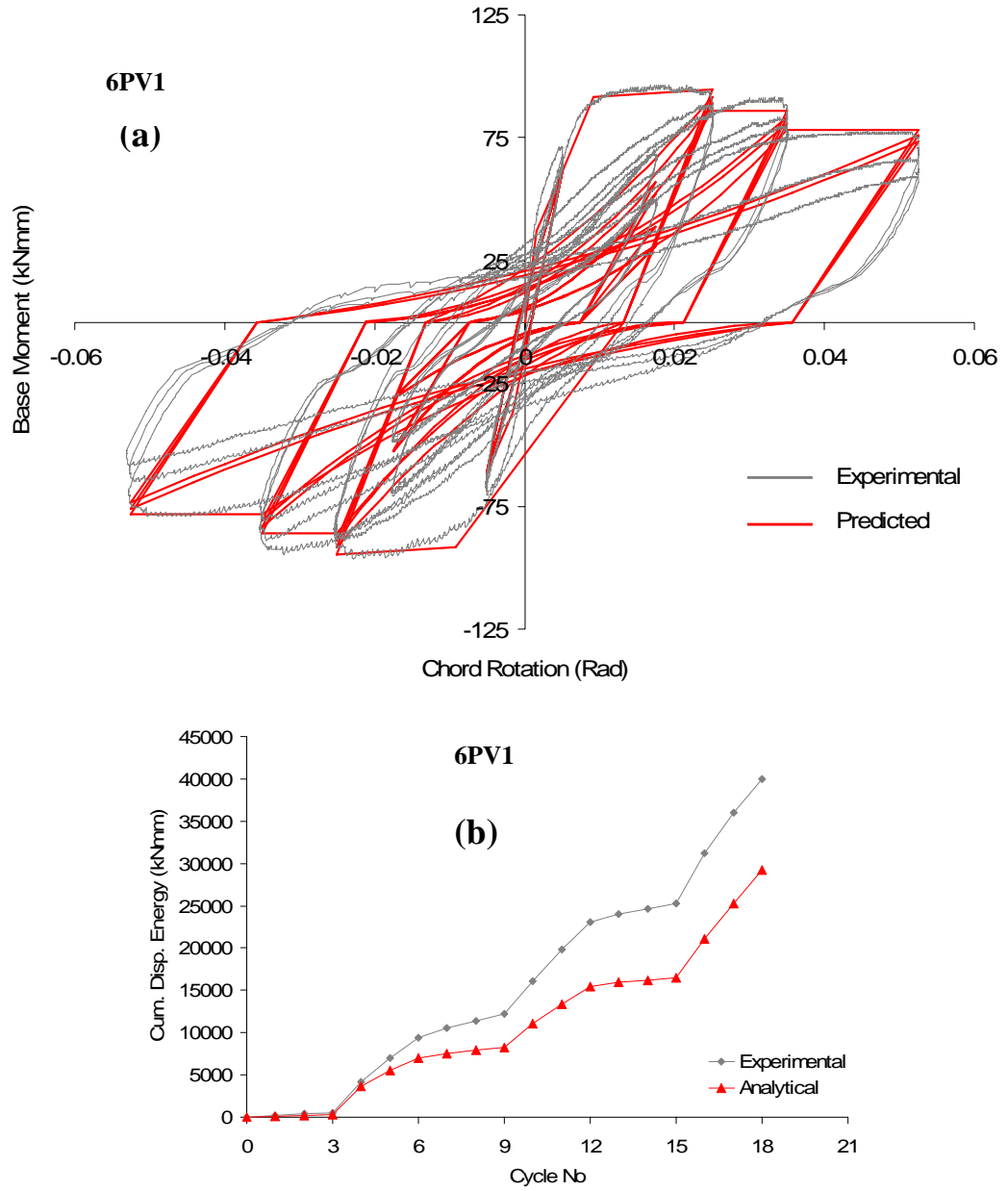


Figure 7.19 (a) Experimental and predicted response and (b) cumulative dissipated energy histories of specimen 6PV1

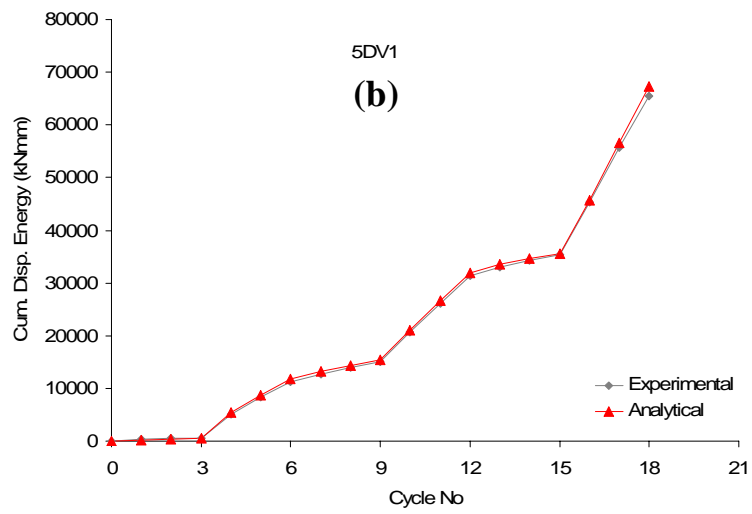
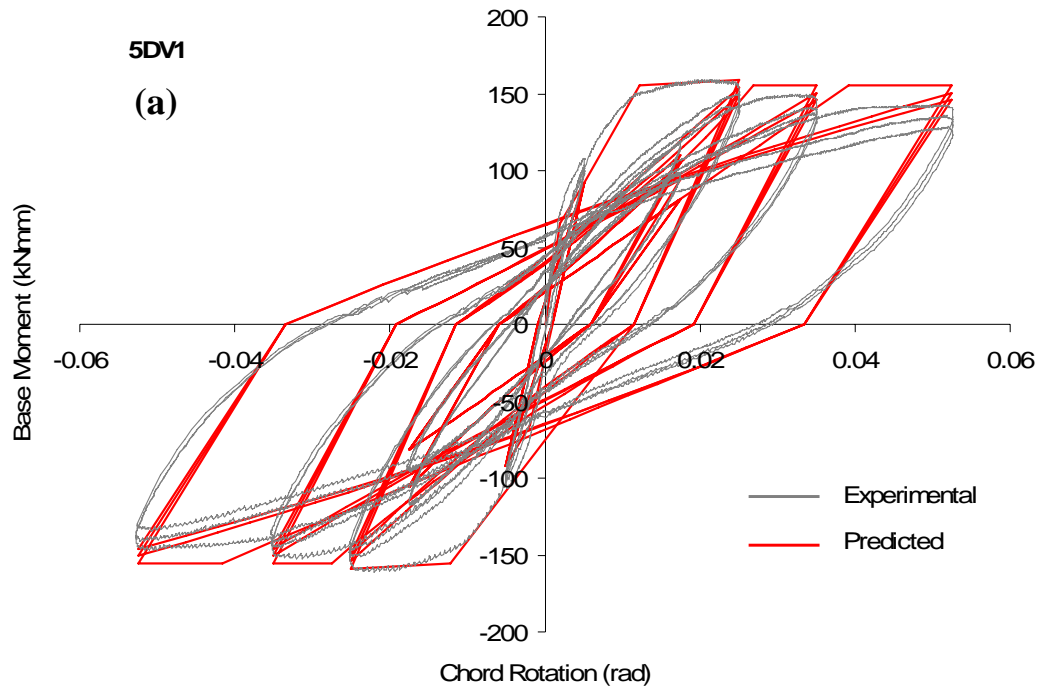


Figure 7.20 (a) Experimental and predicted response and (b) cumulative dissipated energy histories of specimen 5DV1

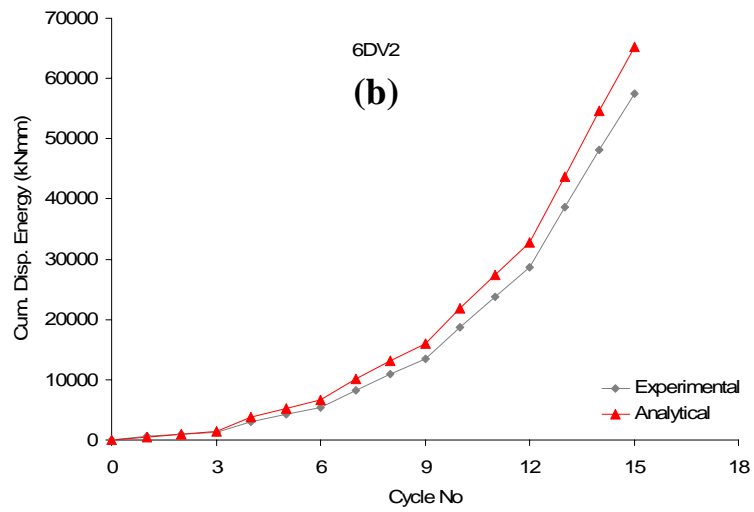
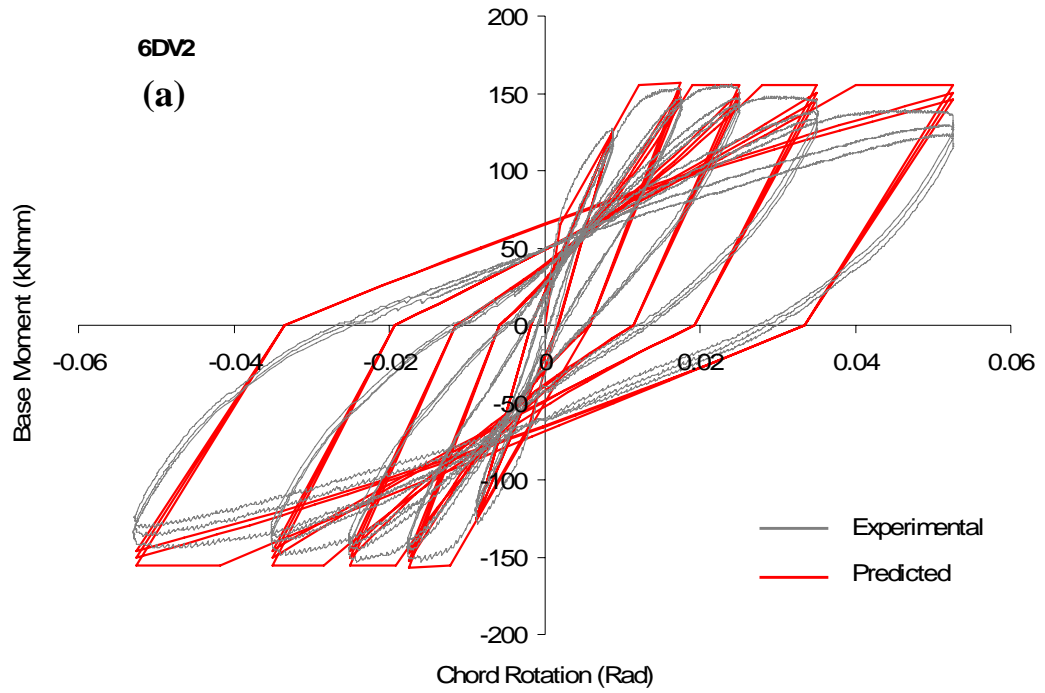


Figure 7.21 (a) Experimental and predicted response and (b) cumulative dissipated energy histories of specimen 6DV2

## CHAPTER 8

### SUMMARY AND CONCLUSIONS

#### 8.1 Summary

Twelve full scale column specimens designed for pure flexure failure were tested in this study under repeated cyclic displacement histories. Two typical column designs were employed in the tests where the first set of specimens (Type-1) represent sub-standard columns and the second set of specimens (Type-2) represent columns conforming to the modern concrete design codes, respectively. Axial load ratio was 0.20 in all specimens except one. The main variable in the experiments was the imposed displacement histories. The effects of axial load ratio and bond strength between longitudinal reinforcements and concrete on member response are also investigated.

The performance limit states proposed by current seismic codes ASCE/SEI 41-Update, Eurocode 8 and TDY 2007 for reinforced concrete columns was evaluated by comparing them with the test results in terms of observed rotations at the plastic hinge regions. Modeling criteria of ASCE/SEI 41-Update for nonlinear static assessment procedure was also applied and discussed for the assessment of lateral force-displacement behavior of reinforced concrete column members.

Degradation in cyclic energy dissipation capacity, deterioration in strength and hysteretic response characteristics of a selected set of reinforced concrete column members with flexure dominant and flexure-shear failure modes were

investigated under low-cycle fatigue loading. Dependency of energy dissipation capacity and strength to the number of displacement cycles is established.

An energy-based hysteresis model for a realistic representation of the inelastic moment-rotation response of reinforced concrete column members in flexure was proposed and calibrated by using the results of column specimens tested under constant-amplitude loadings. Subsequently, proposed model is verified by comparing the estimated response with the actual response of column specimens tested under variable-amplitude loadings.

## **8.2 Conclusions**

Based on the conducted experiments on reinforced concrete column members and analytical research employed for performance assessment by using energy based procedures, the following conclusions can be drawn.

- Imposed displacement amplitude affects the rate of cyclic energy dissipation. Moreover, the dissipation rate decreases with the number of cycles repeated at the same amplitude.
- Cumulative dissipated energy at the end of a displacement protocol imposed on a column member seemed to be not influenced from the change in sequence of displacement cycles with different amplitudes for the same number of cycles, which is an indication of path independency.
- Experimental results revealed that deterioration in energy dissipation capacity and flexural cyclic strength are significant even for reinforced concrete members detailed and constructed according to modern design codes. Knowing this fact, it can be stated that inelastic response of reinforced concrete columns can only be represented by models which take into account the load path dependent degrading behavior of these members.

- The amplitude of imposed displacement is found to be influencing the dissipated energy only in the first virgin inelastic cycle. Accordingly, the ratio of dissipated energies in this first special cycle to the second cycle of a reinforced concrete column specimen under low-cycle fatigue loading is amplitude dependent. The second and the proceeding hysteresis cycles under this constant-amplitude loading are so-called “shape-stable” since the degradation in normalized energy dissipation capacity for these shape-stable cycles is not necessarily amplitude dependent.
- For both code conforming and non-conforming specimens, the decay in normalized cyclic dissipated energy under low-cycle fatigue loading is observed as exponential after the first special inelastic cycle. Both types of specimens possess unique exponential decay functions with characteristic functional variables depending on their sectional and material properties, independent however from the amplitude of imposed displacement history. Once the relation between the properties of a column member and the characteristic decay variables are identified, cyclic energy dissipation for this type of column members can be predicted by estimating the dissipated energy at the first virgin inelastic cycle.
- For the axial load ratios considered in this study, higher ratio of axial load has a positive effect on the energy dissipation capacity of a column specimen under low-cycle fatigue loading since it is both increasing the flexural strength and limit the opening of cracks which in turn leads to a reduction in pinching. Higher axial load increases cyclic strength deterioration however.
- The normalized cyclic energy dissipation characteristics of Type-1 specimens with proper bond provided and with reduced bond are very

similar. This is an indication that the bond strength of plain reinforcement under cyclic loading reduces significantly in the plastic hinge region after the first inelastic cycle.

- The effect of displacement history has a significant effect on the target drift demands of reinforced concrete structures under severe earthquake ground motions. Realistic models simulating the degradation behavior of columns under severe displacement histories are required for accurate calculation of drift demands for both static pushover analysis and nonlinear time history analysis.
- Displacement based performance limit states proposed by Eurocode 8, ASCE/SEI 41-Update and TDY 2007 were found quite close for the yielding limit state for both code-conforming and non-conforming columns. However, their estimations for other higher limit states are quite different from each other. In the light of observed experimental behavior and the gathered information from test results, it can be stated that the limit state predictions of Eurocode 8 and TDY 2007 in terms of plastic rotations are confirmed by test results although they can still be accepted as conservative. On the other hand, the limit states proposed by ASCE/SEI 41-Update seem to be very conservative for both types of code conforming and non-conforming column specimens.
- Energy-based hysteresis models can be used effectively in predicting the hysteretic response of reinforced concrete columns under low-cycle fatigue. Moreover, the inelastic moment-rotation response of column specimens under variable amplitude loadings can also be predicted by extending the findings of constant-amplitude loadings with proper conversions by employing cumulative dissipated energy. The proposed analytical model predicts the inelastic moment-rotation response of non-conforming columns

in flexure satisfactorily and the response of code-conforming columns designed for flexure reasonably well.

## REFERENCES

Acun B. and Sucuoğlu H., 2010, “Performance of R/C Columns Designed for Flexure Under Severe Displacement Cycles”, ACI Structural Journal, ACI, No 107-S3, (in press)

Akiyama H., 1985, “Earthquake Resistant Limit State Design of Buildings”, University of Tokyo Press, Tokyo, Japan.

ASCE/SEI 41, 2007, “Seismic Rehabilitation of Existing Buildings,” American Society of Civil Engineers, Reston, VA, USA.

Balazs G., 1991, “Fatigue of bond”, ACI Materials Journal, ACI, No88-M64, pp.620-629

Bechtoula H., Kono S. and Watanabe F., 2005, “Experimental and Analytical Investigations of Seismic Performance of Cantilever Reinforced Concrete Columns Under Varying Transverse and Axial Loads”. Journal of Asian Architecture and Building Engineering, Vol. 4, No. 2 pp.467-474.

Berry M., Parrish M. and Eberhard M., 2004, “PEER Structural Performance Database User’s Manual (Version 1.0)”, Report No. EEC-9701568, Pacific Earthquake Engineering Research Center, University of California, Berkeley, USA.

Bousias S.N., Verzeletti G., Fardis M.N. and Guitierrez E., 1995, “Load-Path Effects in Column Biaxial Bending with Axial Force”, Journal of Structural Engineering, ASCE, V.121, No.5, pp. 596-605.

Bruneau M. and Wang N., 1996, "Some aspects of energy methods for the inelastic seismic response of ductile SDOF structures", *Engineering Structures*, Elsevier, Vol.18, No.1, pp. 1-12.

Bruneau M. and Wang N., 1996, "Normalized energy-based methods to predict the seismic ductile response of SDOF structures", *Engineering Structures*, Elsevier, Vol.18, No:1, pp. 13-28.

Chai Y.H., Romstad K.M. and Bird S.M., 1995, "Energy Based Linear Damage Model for High Intensity Loading", *Journal of Structural Engineering*, ASCE, Vol. 121, No. 5, pp. 857-864

Clough R.W. and Johnston S.B., 1966, "Effect of Stiffness Degradation on Earthquake Ductility Requirements", *Proceedings, Second Japan National Conference on Earthquake Engineering*, pp. 227-232.

Comite Europeen de Normalisation, 2005, "European Standard EN 1998-3 Eurocode 8: Design of Structures for Earthquake Resistance – Part 3: Assessment and Retrofitting of Buildings," Brussels, Belgium.

Comite Euro-International Du Beton (CEB), 1982, "Bond Action and Bond Behavior of Reinforcement", *Bulletin D'Information*, No:151, pp.109-126.

Decanini L.D. and Mollaioli F., 2001, "An Energy-based Methodology for the Assessment of Seismic Demand", *Soil Dynamics and Earthquake Engineering*, Vol. 9, No:5, pp 113-137.

Eligehausen R., Popov E. and Bertero V., 1983, "Local Bond Stress-Slip Relationships of Deformed Bars Under Generalized Excitations", UCB/EERC-83/23, *Earthquake Engineering Research Center*, Univ. of California, Berkeley, 169 p.

Elwood K.J., and Moehle J.P., 2006, "Idealised Backbone Model For Existing Reinforced Concrete Columns and Comparisons With FEMA 356 Criteria." *Struct. Design Tall Spec. Build.*, Vol 15, pp. 553-569.

Elwood J.K., Matamoros A.B., Wallace J.W., Lehman D.E., Heintz J.A., Mitchell A.D., Moore M.A., Valley M.T., Lowes M.T., Comartin C.D. and Moehle J.P., 2007, "Update to ASCE/SEI 41 Concrete Provisions," *Earthquake Spectra*, V. 23, No. 3, pp. 493-523.

Erberik M.A. and Sucuoğlu H., 2004, "Seismic Energy Dissipation in Deteriorating Systems Through Low-Cycle Fatigue", *Journal of Earthquake Eng. and Str. Dynamics*, Vol. 33, pp.49-67

Ergüner K., 2009, "Analytical Examination of Performance Limits for Shear Critical Reinforced Concrete Columns", Master Thesis, METU, Ankara, Turkey.

Ersoy U. and Özcebe G., 2001, "Betonarme", Evrim Yayınevi, 775 pages

Fajfar P. and Gaspersic P., 1996, "The N2 method for the Seismic Damage Analysis of RC Buildings", *Journal of Earthquake Eng. and Str. Dynamics*, Vol. 25, pp.31-46

Fajfar P., Vidic T. and Fischinger M., 1990, "A measure of earthquake motion capacity to damage medium-period structures", *Soil Dynamics and Earthquake Engineering*, Vol. 9, No.5, pp 236-242.

Fardis M.N. and Kosmopoulos A., 2007, "Practical Implementation of Seismic Assessment Method in Eurocode 8 – Part 3, with Linear or Nonlinear Analysis and Deformation-Based Verification Using Empirical Chord Rotation Capacity Expressions," Sixth National Conference on Earthquake Engineering, Istanbul, Turkey.

FEMA 356, 2000, "Prestandard and Commentary for the Seismic Rehabilitation of Buildings", American Society of Civil Engineers (ASCE), Washington, D.C., USA

FEMA 440, 2005, "Improvement of Nonlinear Static Seismic Analysis Procedures," Applied Technology Council (ATC-55 Project), Redwood City, California, USA.

FEMA P440A, 2009, "Effects of Strength and Stiffness Degradation on Seismic Response", (ATC), Washington D.C., USA

Galal K.E. and Ghobarah A., 2003, "Flexural and Shear Hysteretic Behaviour of Reinforced Concrete Columns with Variable Axial Load," *Engineering Structures*, V.25, pp. 1353-1367.

Housner G.W., 1956. "Limit Design of Structures to Resist Earthquakes", *Proceedings, 1st World Conference on Earthquake Engineering, Berkeley, C.A.*, pp.1-11

Ibarra F.L., Medina R.A. and Krawinkler H., 2005, "Hysteretic Models that incorporate strength and stiffness deterioration", *Journal of Earthquake Eng. and Str. Dynamics*, Vol. 34, pp.1489-1511

Ismail M.A.F. and Jirsa J.O., 1972, "Bond Deterioration in reinforced Concrete Subjected to Low Cycle Loads", *ACI Journal, Proceedings V. 69*, pp.334-343.

Iwasaki T., Kawashima K., Hasegawa K., Koyama T. and Yoshida T., 1987, "Effect of Number of Loading Cycles and Loading Velocity of Reinforced Concrete Bridge Piers" 19<sup>th</sup> Joint Meeting of the US-Japan Panel on Wind and Seismic Effects, *UJNR, Tsukuba*, pp. 225-238

Kanaan A. and Powell G.H., 1973, "DRAIN-2D: A General Purpose Computer Program for Dynamic Analysis of Inelastic Plane Structures", *UCB-EERC Report No. 73/6*, University of California, Berkeley, CA.

Ismail M.A.F. and Jirsa J.O., 1972, "Bond Deterioration in Reinforced Concrete Subjected to Low Cycle Loads", *ACI Journal, Proceedings V.69*, pp.334-343.

Karsan I.D. and Jirsa J.O., 1969, "Behaviour of Concrete under Compressive Loadings", *Journal of the Structural Division, ASCE*, Vol. 95 ST-12, pp. 2543-2563

Kemp E.L. and Wilhelm W.J., 1979, "Investigation of the Parameters Influencing Bond Cracking", *ACI Journal, Proceedings V.76, No.1*, pp.47-72.

King D.J., Priestley M.J.N. and Park R., 1986, "Computer Programs for Concrete Column Design", *Research Report 86/12*, Department of Civil Engineering, University of Canterbury, New Zealand.

Kuwamura H. and Galambos T.V., 1989, "Earthquake Load for Structural Reliability", Journal of Structural Engineering, ASCE, Vol. 115, pp.1446-1462

Kwak H.G. and Kim S.P., 2001, "Nonlinear Analysis of RC Beam Subject to Cyclic Loading", Journal of Structural Engineering, ASCE, Vol. 127, No.12, pp.1436-1444

Leelataviwat S., Goel S.C. and Stojadinovic B., 2002, "Energy-based Seismic Design of Structures using Yield Mechanism and Target Drift", Journal of Structural Engineering, ASCE, Vol. 128, No.8, pp. 1046-1054.

Leger P. and Dussault S., 1992, "Seismic-Energy Dissipation in MDOF Structures", Journal of Structural Engineering, ASCE, Vol. 118, No.5, pp. 1251-1269.

Lin I.J. and Hawkins N.M., 1982, "Anchorage of Reinforcing Bars for Reversed Cyclic Loading", Report SM 82-1, Department of Civil Engineering, Univ. of Washington, Seattle, USA.

Lynn A.C., Moehle J.P., Mahin S.A. and Holmes W.T., 1996, "Seismic Evaluation of Existing Reinforced Concrete Columns," Earthquake Spectra, V. 21, No. 4, pp. 715-739.

Mander J.B., Priestley M.J.N and Park R., 1988, "Theoretical Stress-Strain Model for Confined Concrete", Journal of Structural Engineering, ASCE, Vol. 114, No.8, p. 1804-1849

Manfredi G., 2001, "Evaluation of Seismic Energy Demand", Journal of Earthquake Eng. and Str. Dynamics, Vol. 30, pp.485-499.

MathWorks Inc., 2002, MATLAB - Version 6.5.

McCabe S.L. and Hall W.J., 1989, "Assessment of Seismic Structural Damage", Journal of Structural Engineering, ASCE, Vol. 115, No.5, pp. 2166-2183.

Miner M.A., 1945, "Cumulative Damage in Fatigue", Journal of Applied Mechanics, Vol. 67, pp. 159-164

Ministry of Public Works and Settlement, 1998, ‘Turkish Earthquake Code: Specifications for the Buildings to be Constructed in Disaster Areas’, Ankara, Turkey.

Montejo L.A and Kowalsky M.J., 2007, “Set of Codes for the Analysis of Reinforced Concrete Members”, Report No IS-07-01, Constructed Facilities Laboratory, North Carolina State University, Raleigh, NC, pp.1-41

Mostaghel N., 1998, “Analytical Description of Pinching, Degrading Hysteretic Systems” Rep. No. UT-CE/ST-98-102, Univ. of Toledo, Ohio, USA

Ozcebe G. and Saatcioglu M., 1989, “Hysteretic Shear Model for Reinforced Concrete Members”, Journal of Structural Division, ASCE, Vol.115, No.1, pp. 132-148.

Palmgren A., 1924,“The Service Life of Ball Bearings“ Zeitschrift des Vereines Deutscher Ingenieure, 68, 14, pp 339-341.

Park Y.J. and Ang A.H., 1985, “Mechanistic Seismic Damage Analysis of Reinforced Concrete” Journal of Structural Engineering, ASCE, Vol. 111, No. 4, pp.722-739

Park Y.J., Reinhorn A.M. and Kunnath S.K., 1987, “IDARC: Inelastic Damage Analysis of Reinforced Concrete Frame – Shear Wall Structures”, Technical Report NCEER-87-0008, State University of New York at Buffalo.

Perus I. and Fajfar P., 2007, “Prediction of the Force-Drift Envelope for RC Columns in Flexure by the CAE Method”, Journal of Earthquake Eng. and Str. Dynamics, Vol. 36, pp.2345-2363

Pujol S., 2002, “Drift Capacity of Reinforced Concrete Columns Subjected to Displacement Reversals”, PhD Thesis, Purdue University, West Lafayette, Ind, USA, 311 p.

Pujol S., Sozen M.A. and Ramirez J.A., 2006, “Displacement History Effects on Drift Capacity of Reinforced Concrete Columns,” ACI Structural Journal, V.103, No. 2, pp. 253-262.

Priestley M.J.N., Calvi G.M. and Kowalsky M.J., 2007, "Displacement-Based Seismic Design of Structures," IUSS Press, Fondazione EUCENTRE, Pavia, 720 p.

Quasalem H., Kabeyasawa T. and Tasai A., 2004, "Evaluation of Axial Deformation Capacity at Axial Load Collapse of Reinforced Concrete Columns," 13<sup>th</sup> World Conference on Earthquake Engineering, Vancouver, British Columbia, Canada.

Roufaiel M.S.L. and Meyer C., 1987, "Analytical Modeling of Hysteretic Behavior of R/C Frames", Journal of Structural Division, ASCE, Vol.113, No.3, pp. 429-444.

Saatcioglu M. and Ozcebe G., 1989, "Response of Reinforced Concrete Columns to Simulated Seismic Loading", ACI Structural Journal, V.86, No. 1, pp. 3-12.

Saiidi M. and Sozen M.A., 1979, "Simple and Complex Models for Nonlinear Seismic Response of R/C Structures", Structural Research Series 465, Civil Engineering Studies, University of Illinois, Urbana, IL.

Sezen H. and Moehle J.P., 2006, "Seismic Tests of Concrete Columns with Light Transverse Reinforcement," ACI Structural Journal, V.103, No. 6, pp. 842-849.

Shen J. and Akbas B., 1999, "Seismic Energy Demand in Steel Moment Frames", Journal of Earthquake Engineering, Imperial College Press, Vol. 3, No.4, pp. 519-559.

Sinha B.P., Grestle K.H. and Tulin L.G., 1964, "Stress-Strain Relations for Concrete under Cyclic Loading", Journal of American Concrete Institute, Vol. 61, No.2, pp. 195-211.

Sivaselvan M.V. and Reinhorn A.M., 1999, "Hysteretic Models for Cyclic Behavior of Deteriorating Inelastic Structures", Technical Report MCEER-99-0018, State University of New York at Buffalo.

Sivaselvan M. and Reinhorn A., 2000, "Hysteretic Models for Deteriorating Inelastic Structures", Journal of Engineering Mechanics, Vol. 126., No.6, pp. 633-640

Soretz S. and Holzenbein H., 1979, "Influence of Rib Dimensions on Reinforcing Bars on Bond and Bendability", ACI Journal, Proceedings V. 76, No.1, pp. 111-128  
Stojadinovic B. and Thewalt C.R., 1996, "Energy Balanced Hysteresis Models", Paper No. 1734, Eleventh World Conference on Earthquake Engineering, Acapulco, Mexico.

Sucuoğlu H. and Erberik M.A., 2004, "Energy-based Hysteresis and Damage Models for Deteriorating Systems", Journal of Earthquake Eng. and Str. Dynamics, Vol. 33, pp.69-88

Takeda T., Sozen M.A. and Nielsen N.N., 1970, "Reinforce Concrete Response to Simulated Earthquakes", Journal of Structural Division, ASCE, Vol.96, No.ST-12, pp. 2557-2573.

Taylor A.W., El-Bahy A., Stone W.C. and Kunnath S.K., 1996, "Effect of Load Path on Damage to Concrete Bridge Piers", Wind and Seismic Effects, U.S./Japan Cooperative Program in Natural Resources Panel on Wind and Seismic Effects, Gaithersburg, pp.149-158

Tembulkar J.M. and Nau J.M., 1987, "Inelastic Modelling and Seismic Energy Dissipation", Journal of Structural Engineering, ASCE, Vol. 113, No. 6, pp. 1373-1377

Turkish Standard Institute, 2000, 'TS-500 Requirements for Design and Construction of Reinforced Concrete Structures', Ankara, Turkey.

Uang C. and Bertero V.V., 1990, "Evaluation of Seismic Energy in Structures", Journal of Earthquake Eng. and Str. Dynamics, Vol. 19, pp.77-90

Verderame G.M., Fabbrocino G. and Manfredi G., 2008, "Seismic Response of RC Columns with Smooth Reinforcement. Part II: Cyclic Tests," Engineering Structures, V.30, pp. 2289-2300.

Wight J.K. and Sozen M.A., 1975, "Strength Decay of Columns under Shear Reversals", Journal of the Str. Div., ASCE, Vol.101, No.ST5, pp.1053-1065

Yoshimura M., Takaine Y. and Nakamura T., 2004, “ Axial Collapse of Reinforced Concrete Columns”, 13<sup>th</sup> World Conference on Earthquake Engineering, Vancouver, B. Columbia, Canada.

Youssef M. and Ghobarah A., 1999, “Strength Deterioration Due to Bond Slip and Concrete Crushing in Modeling of Reinforced Concrete Members”, ACI Structural Journal, ACI, No. 96-S105, pp.956-964.

Zahrah T.F. and Hall W.J., 1984, “Earthquake Energy Absorption in SDOF Structures”, Journal of Structural Engineering, ASCE, Vol. 110, No. 8, pp.1757-1772.

## APPENDIX A

### DESIGN OF REFERENCE COLUMN IN 4-STORY BUILDING FRAME

Details of analysis and design for the reference column specimen are presented in this section. Plan view of the building considered and elevation view for the frame where the selected column to be designed are presented in Figure A.1 and Figure A.2.

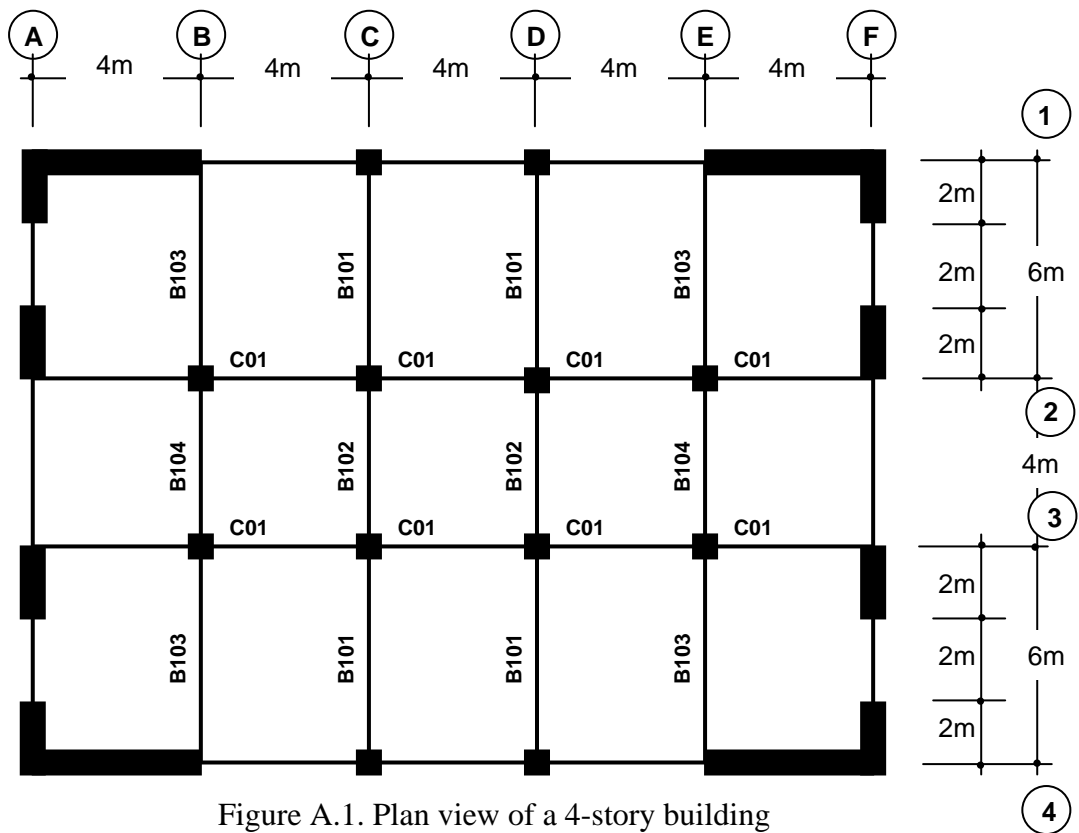


Figure A.1. Plan view of a 4-story building

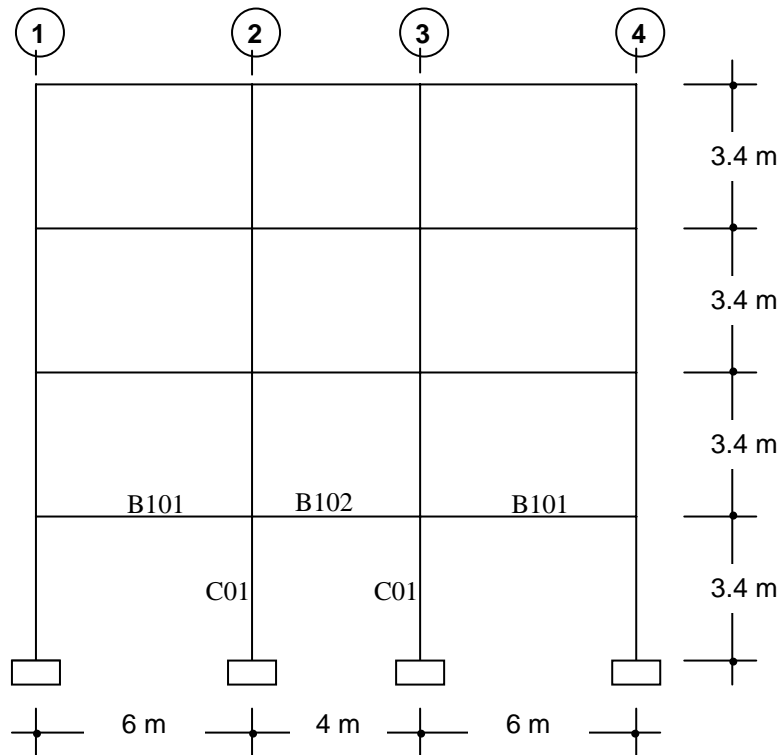


Figure A.2. Elevation view of frame C-C

Material Properties : C13 and St 37 ( $f_y=330$  MPa) for Type-1 Columns  
C25 and St 53 ( $f_y=420$  MPa) for Type-2 Columns

Slab Thickness: 120 mm

Estimated Loads:

Exterior Beams : Dead Load:15 kN/m Live Load: 5 kN/m

Interior Beams : Dead Load:10 kN/m Live Load: 3 kN/m

Load Combinations:

E1 →  $1G + 1Q + 1E$   
S1 →  $1.4G + 1.6Q$  (All beams loaded)  
S2 →  $1.4G + 1.6Q$  (Only interior beams loaded)  
S3 →  $1.4G + 1.6Q$  (Only exterior beams loaded)

Preliminary Design for Columns:

It was assumed that the uniformly distributed load on floor slabs and the dead/live load averages are about 10 kN/m<sup>2</sup>.

Tributary area of column C01;

$$4 * \left( \frac{6}{2} + \frac{4}{2} \right) = 20m^2$$

Load on tributary area;      10\*20=200 kN

At ground level columns, the axial load will be;

$$4 \text{ stories} \rightarrow N_d = 4 * 200 = 800 \text{ kN}$$

Minimum dimensions for columns (TEC);

$$A_c \geq \frac{N_d}{0.5 * f_{ck}} > 75 * 10^3 \text{ mm}^2$$
$$\frac{800}{0.5 * 0.013} = 123 * 10^3 \text{ mm}^2 > 75 * 10^3 \text{ mm}^2$$

Column dimensions were selected as 350\*350 mm.

Preliminary Design for Beams:

Using the estimated loads, design load for beams;

$$P_d \cong 1.4g + 1.6q = 1.4 * 15 + 1.6 * 5 = 29 \text{ kN/m}$$

Maximum design moment will be;

$$M_{d \max} \cong \frac{1}{9} * P_d * l^2 = \frac{1}{9} * 29 * \left( \frac{4+6}{2} \right)^2 = 80.6 \text{ kNm}$$

Design shear;

$$V_d \cong P_d * \frac{l_n}{2} = 29 * \frac{(6-0.35)}{2} = 81.93 \text{ kN}$$

- For Type-1 Specimens: C13 and St37  $\rightarrow K_l = 530 \text{ mm}^2/\text{kN}$

For flexure;  $b_w * d^2 \leq M_d * K_l$   
 $b_w * d^2 \leq 80.6 * 10^3 * 530 \rightarrow b_w = 250 \text{ mm} , d = 450 \text{ mm}$

For shear;  $b_w * d \cong \frac{0.9 * V_d}{f_{ctd}}$   
 $b_w * d \cong \frac{0.9 * 81.93}{1.0} \rightarrow b_w = 250 \text{ mm} , d = 295 \text{ mm}$

- For Type-2 Specimens: C25 and St53  $\rightarrow K_l = 291 \text{ mm}^2/\text{kN}$

For flexure;  $b_w * d^2 \leq M_d * K_l$   
 $b_w * d^2 \leq 80.6 * 10^3 * 291 \rightarrow b_w = 250 \text{ mm} , d = 305 \text{ mm}$

For shear;  $b_w * d \cong \frac{0.9 * V_d}{f_{ctd}}$   
 $b_w * d \cong \frac{0.9 * 81.93}{1.0} \rightarrow b_w = 250 \text{ mm} , d = 295 \text{ mm}$

Beam dimensions were selected as 250\*450 mm. (d=415 mm)

Assigning the dimensions estimated in preliminary design for all beams and all columns, the frame shown in Figure A.3 was analysed under different loading conditions and internal forces calculated for column C01 were tabulated in Table A.1.

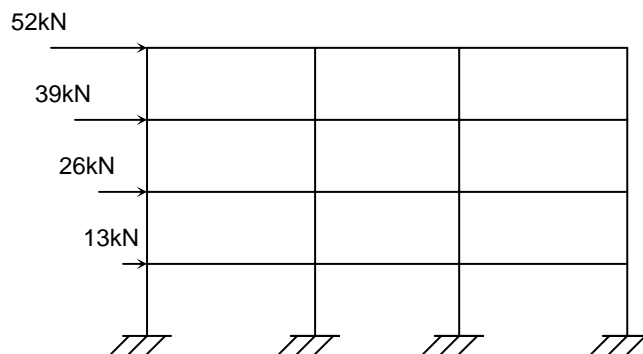


Figure A.3. Analysed planar frame

Table A.1. Design forces for column C01

	COLUMN C01		
Load Combinations	Nd (kN)	Max Vd (kN)	Md <sub>i</sub> (kN-m)
E1	-385.0 (-313.1)	43.2 (31.9)	79.0 (67.8)
A1	-505.5	8.1	18.5
A2	-408.3	5.0	11.5
A3	-446.5	8.9	20.2

Column C01 for Type-1 Specimen

Considering the earthquake loading, for minimum axial load (N=313 kN), column moment capacity will be;

$$M_r = 92.7 \text{ kN-m (Table A.2)}$$

(calculated by computer program "COLUMN DESIGN" Ersoy and Ozcebe, 2002 )

Use minimum long. reinf. ratio  $\rho_l = 0.01$

Long reinf. 8 $\phi$ 14

Clean height of column  $\longrightarrow$   $l_n = 3.00 \text{ m}$

$$\text{Shear capacity, } V_e = \frac{92.7 + 92.7}{3} = 61.8 \text{ kN (symmetric longitudinal reinf.)}$$

Omitting the concrete contribution;

$$\frac{A_{sw}}{s} = \frac{61.8}{0.330 * 315} = 0.595$$

$\phi 8$  stirrup }  
 $2\phi 8$  cross-tie }  $A_{sw} = 150 \text{ mm}^2$

$$s = \frac{150}{0.595} = 252\text{mm} \quad \text{use max.}$$

$$\text{max } s_o = 12 \cdot \phi_1 = 168 \text{ mm}$$

use  $\phi 8/165$  mm for unconfined region

use  $\phi 8/100$  mm for confined region

Since Type-1 Specimens represent the defective columns,  $\phi 8/165$  mm will be used for all along the column without any confined region.

### Column C01 Type-2 Specimen

Considering the earthquake loading, for minimum axial load ( $N=313$  kN), column moment capacity will be;

$$M_r = 118.2 \text{ kN-m (Table A.3)}$$

(calculated by computer program "COLUMN DESIGN" Ersoy and Ozcebe, 2002)

Use minimum long. reinf. ratio  $\rho_1 = 0.01$

Long reinf.  $8\phi 14$

Clean height of column  $\longrightarrow$   $l_n = 3.00 \text{ m}$

$$\text{Shear capacity, } V_e = \frac{118.2 + 118.2}{3} = 78.8 \text{ kN} \quad (\text{symmetric longitudinal reinf.})$$

Omitting the concrete contribution;

$$\frac{A_{sw}}{s} = \frac{78.8}{0.420 \cdot 315} = 0.595$$

$$\left. \begin{array}{l} \phi 8 \text{ stirrup} \\ 2\phi 8 \text{ cross-tie} \end{array} \right\} A_{sw} = 150 \text{ mm}^2$$

$$s = \frac{150}{0.595} = 252mm \text{ use min.}$$

$$\max s_o = 12 \cdot \phi_1 = 168 \text{ mm}$$

use  $\phi 8/165$  mm for unconfined region

use  $\phi 8/70$  mm for confined region

**Table A.2 Column Design- Type-1 Columns**

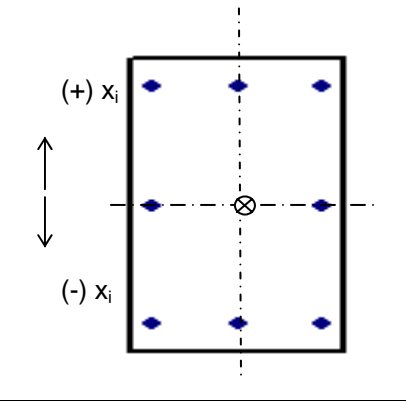
Design Values	
$N_d$	$M_d^{(*)}$
(kN)	(kN.m)
313.0	79.0

Reinforcement Layout		
$d'$	No of bars (ds)	$\lambda^{(**)}$
(mm)	$2 \leq ds \leq 6$	
35	3	0.25

Reinforcement		
Layer	Area ( $A_{Si}$ )	Dist. To Centroid ( $x_j$ )
	(mm <sup>2</sup> )	(mm)
1-)Top	459	140
2) Bottom	459	-140
3) Mid 1	306	0
4) Mid 2	0	0
5) Mid 3	0	0
6) Mid 4	0	0

Concrete	
$f_{ck}$	$\gamma_{mc}$
(MPa)	
13	1.00

Steel	
$f_{yk}$	$\gamma_{ms}$
(MPa)	
330	1.00



Cross section	
Depth (b)	Height (h)
(mm)	(mm)
350	350

$N_d =$	313.0
$M_r =$	92.7

**Table A.3 Column Design- Type-2 Columns**

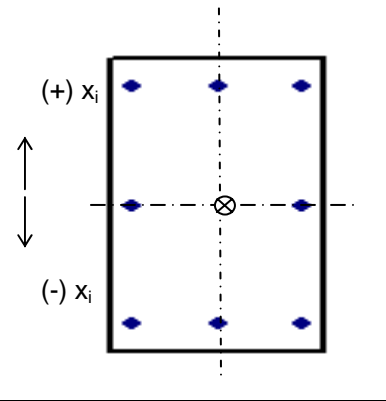
Design Values	
$N_d$	$M_d^{(*)}$
(kN)	(kN.m)
313.0	79.0

Reinforcement Layout		
$d'$	No of bars (ds)	$\lambda^{(**)}$
(mm)	$2 \leq ds \leq 6$	
35	3	0.25

Reinforcement		
Layer	Area ( $A_{Si}$ ) (mm <sup>2</sup> )	Dist. To Centroid ( $x_j$ ) (mm)
1-)Top	459	140
2) Bottom	459	-140
3) Mid 1	306	0
4) Mid 2	0	0
5) Mid 3	0	0
6) Mid 4	0	0

Concrete	
$f_{ck}$ (MPa)	$\gamma_{mc}$
25	1.00

Steel	
$f_{yk}$ (MPa)	$\gamma_{ms}$
420	1.00



Cross section	
Depth (b) (mm)	Height (h) (mm)
350	350

$N_d =$	313.0
$M_r =$	118.2

## **CURRICULUM VITAE**

### **PERSONAL INFORMATION**

Name : Bora ACUN  
Birth Date : 11/10/1977  
Birth Place : Ankara / TURKEY  
Citizenship : Republic of Turkey  
Phone : +90 (312) 2105464  
Fax : +90 (312) 2101193  
e-mail : boraacun@gmail.com

### **EDUCATION**

2002 - 2009 Ph.D., Civil Engineering, METU (CGPA: 3.57/4.00)  
1999 - 2002 MS, Civil Engineering, ITU (CGPA: 3.68/4.00)  
1995 - 1999 BS, Civil Engineering, Çukurova Univ. (CGPA: 3.47/4.00)  
1989 - 1995 Adana Anatolian High School  
1988 - 1989 Kars Anatolian High School

### **EMPLOYMENT RECORD**

2002 - 2010: Research Assistant, Dept. of Civil Eng., METU

### **COMPUTER SKILLS**

#### **Computer Programming Languages**

MATLAB, Mathcad, Visual Basic, C++ , Fortran

#### **Software Related to Earthquake Engineering and Structural Analysis**

SAP2000, ANSYS, Drain-2DX, SeismoStruct, SeismoSignal, AutoCAD, NONLIN

## **Other Software**

Microsoft Office Applications, Web Design Tools

## **SCIENTIFIC PUBLICATIONS**

### **International Refereed Journals**

1. **Acun B.** and Sucuođlu H., 2010, “Performance of R/C Columns Designed for Flexure Under Severe Displacement Cycles”, ACI Structural Journal, ACI, No 107-S3, (in press)

### **International Conference Proceedings**

- 1 Erberik M.A., **Acun B.**, 2005, “An Energy-based Softening Index for Seismic Performance Evaluation of Reinforced Concrete Column Members“, Earthquake Engineering in the 21st Century, Skopje, Macedonia
- 2 **Acun B.**, Sucuoglu H., 2006, “Strengthening Of Masonry Infill Walls In Reinforced Concrete Frames With Wire Mesh Reinforcement“, 8th U.S. National Conference on EQ. Eng., California, USA
- 3 **Acun B.**, Sucuoglu H., 2007. “Seismic Response of RC Columns with Strength Deterioration“, 9th Canadian National Conference on EQ. Eng., Ottawa, Canada

### **National Conference Proceedings**

- 1 **Acun B.**, Sucuođlu H., 2005, “Tuđla Dolgu Duvarlı Çerçevelerin Hasır Donatı ile Güçlendirilmesi “, Deprem Sempozyumu, Kocaeli, Türkiye (in Turkish).
- 2 **Acun B.**, Sucuođlu H., 2007, “Betonarme Kolonların Enerji Esaslı Yöntemlerle Performans Deđerlendirmesi”, Altıncı Ulusal Deprem Mühendisliđi Kongresi (6UDMK), İstanbul, Türkiye (in Turkish)

## **SUPPORT/AWARDS/HONOURS**

- 1999** Graduated 1<sup>st</sup> rank in the department and 4<sup>th</sup> rank in the Faculty of Engineering at Çukurova University

## **NON-PROFESSIONAL ACTIVITIES / AMATEUR HOBBIES**

Ballroom dancer (Salsa), Electro guitar player (IBANEZ), Member of the Research Assistant's Basketball team (Power Forward), Amateur photographer (Voigtlander Vito CD), Motorcycle rider (Keeway ARN 150 cc), Goal keeper (JRC-Stagieries Floorball team),